UNIVERSITY OF LIVERPOOL

Identification of drug resistance mechanisms induced in response to KRAS therapeutics

Hannah Rose Warren

Thesis submitted in accordance with the requirements of the University of Liverpool for the degree of Doctor in Philosophy

September 2021

Abstract

KRAS is one of the most frequently mutated oncogenes in cancer and exhibits high prevalence in pancreatic, colon and lung cancers. The development of effective KRAS therapeutics has been challenging and only in recent years have promising targeted KRAS inhibitors been developed, including those that specifically target the oncogenic KRAS-G12C mutant commonly found in non-small cell lung cancer (NSCLC). As with most targeted therapeutics, it is almost inevitable that resistance will develop and limit the clinical efficacy of these new targeted drugs. Therefore, understanding the molecular mechanisms of resistance associated with KRAS inhibitors is important for developing improved treatment options, including combination strategies.

In this study different KRAS inhibitors were used to create a novel panel of NSCLC resistant cell lines, enabling multiple comparisons of acquired resistance mechanisms to be carried out. Surprisingly evidence of pathway rewiring to all KRAS inhibitors emerged within days of inhibitor treatment. Transcriptomic and proteomic approaches were used to interrogate resistance mechanisms associated with both acute and chronic treatments. Consistent up-regulation of receptor tyrosine kinases, RAS-GEFs as well as DNA damage repair and cell cycle signalling pathways were observed across resistant cells.

Screening of 25 inhibitors targeting the pathways of these potential resistance mechanisms identified 15 inhibitors that showed differential sensitivities across the panel of resistant cells, with 3 inhibitors effective across all. This included the broad CDK inhibitor flavopiridol and two inhibitors of mTOR. To improve therapeutic potential, additional vertical and horizontal inhibitor combinations were evaluated. Additional promising strategies to re-sensitise cells with acquired resistance to KRAS-G12C inhibition included a combination of EGFR and mTOR inhibition. This strongly decreased cell viability and downstream pERK and pAKT signalling. Alternatively, the synergistic combination of FGFR1 and MEK inhibition was also able to re-sensitise cells resistant to pan-KRAS inhibition, though this was not as effective as mTORi. Evaluation of inhibitor combinations in naïve parental cells identified a number of combinations which slowed the emergence of resistance. Treatment with flavopiridol and combinations targeting EGFR with mTOR or SHP2 inhibition were particularly effective alongside all KRAS inhibitors.

These results demonstrate a wider understanding of resistance to KRAS therapeutics and present potential clinical significance through effective combination strategies that maximise the efficacy of KRAS inhibition and slow the emergence of resistance.

Table of contents

List of Figures

List of Tables

List of Appendixes

List of Abbreviations

ASO	Antisense Oligonucleotide
ATM	Ataxia telangiectasia mutated
ATP	Adenosine trisphosphate
ATR	Ataxia telangiectasia and Rad3-related protein
BAD	BCL-X_1/BCL-2 associated death promoter
BCA	Bicinchoninic acid
BCL	B-cell lymphoma
CDC	Cell division control
CDK	Cyclin-dependent kinase
CDKi	CDK inhibition
CRC	Colorectal cancer
Ct	Cycle threshold
CTRL	Control
DEG	Differentially expressed gene
DMSO	Dimethyl sulphoxide
DNA	Deoxyribonucleic acid
DSG	Desmoglein
DUSP	Dual-specificity phosphatase
E2F	E2 transcription factor
EDTA	Ethylenediaminetetraacetic acid
EGFR	Epidermal growth factor receptor
EGFRi	EGFR inhibition
EGFR/ERBB2i	Dual EGFR/ERBB2 inhibition
EMT	Epithelial-to-mesenchymal transition
ERBB2	Erb-b2 receptor tyrosine kinase 2 (also known as HER2)
ERBB2i	ERBB2 inhibition
ERK	Extracellular signal regulated kinase
FBS	Fetal bovine serum

4E-BP1	Eukaryotic translation initiation factor 4E-binding protein 1
FGFR	Fibroblast growth factor receptor
FGFRi	FGFR inhibition
FOXO	Forkhead box O
FPKM	Fragments per kilobase million
FTase	Farnesyltransferase
FTI	Farnesyltransferase inhibitors
GAP	Guanosine triphosphatase activating protein
GDP	Guanosine disphosphate
GEF	Guanine exchange factor
GGTase	Geranylgeranyltransferase I
GO	Gene ontology
GTP	Guanosine triphosphate
GTPase	Guanosine triphosphatase
GPCR	G-protein coupled receptor
GRB2	Growth factor receptor-bound protein 2
GSK3	Glycogen synthase kinase 3
H358-A	H358 acutely treated cells
H358-R	H358 chronically treated resistant cells
Hr	Hour
HER2	Human epidermal growth factor receptor 2
HER3	Human epidermal growth factor receptor 3
HRAS	Harvey rat sarcoma viral oncogene homolog
HVR	Hypervariable region
IC50	50% maximal inhibitory concentration
IC90	90% maximal inhibitory concentration
ICMT	Isoprenylcysteine carboxylmethyltransferate
IGFR	Insulin-like growth factor receptor
INSR	Insulin receptor
KEGG	Kyoto Encyclopedia of Genes and Genomes
KRAS	Kirsten-rat sarcoma
KRASi	KRAS inhibition

MAPK	Mitogen-activated protein kinase
MDM2	Mouse double minute 2 homolog
MEK	Mitogen-activated protein kinase/extracellular signal-regulated kinase
MEKi	MEK inhibition
MES	2-(*N*-morpholino)ethanesulfonic acid
MOPS	3-(*N*-morpholino)propanesulfonic acid
mRNA	Messenger RNA
mTOR	Mechanistic target of rapamycin
mTORi	mTOR inhibition
mTORC	Mechanistic target of rapamycin complex
NF1	Neurofibromin 1
NFκB	Nuclear factor-κB
nM	Nanomolar
NRAS	Neuroblastoma RAS viral oncogene homolog
NSCLC	Non-small cell lung cancer
p-	Phospho-
PARP	Poly (ADP-ribose) polymerase
PBS	Phosphate-buffered saline
PCR	Polymerase chain reaction
PDE6δ	Phosphodiesterase 6δ
PDGFR	Platelet-derived growth factor receptor
PDX	Patient-derived xenograft
PH	Pleckstrin homology
PI3K	Phosphoinositide-3-kinase
PIP_2	Phosphatidylinositol-4,5-bisphosphate
PIP_3	Phosphatidylinositol-3,4,5-trisphosphate
PTEN	Phosphatase and tensin homolog
RAC1	Ras-related C3 botulinum toxin substrate 1
RAF	Rapidly accelerated fibrosarcoma
RAL	Ras Like
RAL-GDS	RAL guanine nucleotide dissociation stimulator
RAL-GEF	RAL guanine exchange factor
R-ARS	H358 ARS1620-treated resistant cells

RAS-GRP	RAS guanyl nucleotide-releasing protein
R-ASO	H358 AZD4785-treated resistant cells
RCE1	Ras converting enzyme 1
R-DMSO	H358 DMSO resistant cells
RGL	Ral Guanine Nucleotide Dissociation Stimulator Like
RHEB	Ras homolog enriched in brain
RIPA	Radioimmunoprecipitation assay
RNA	Ribonucleic acid
RNA-seq	RNA sequencing
RPPA	Reverse phase protein array
R-Sel	H358 selumetinib-treated resistant cells
RTK	Receptor tyrosine kinase
RT-qPCR	Quantitative reverse transcription *PCR*
S-IIP	Switch II pocket
SCLC	Small-cell lung cancer
SDS-PAGE	Sodium dodecyl sulphate polyacrylamide gel electrophoresis
SEM	Standard error of mean
SH2	Src Homology 2
SH3	Src Homology 3
SHP2	Src homology region 2 domain-containing phosphatase-2
SHP2i	SHP2 inhibtion
SOS	Son of sevenless
SW-I	Switch I
SW-II	Switch II
TC	Tissue culture
TBS	Tris-buffered saline
TBST	Tris-buffered saline with tween
TF	Transcription factor
TJP	Tight junction protein
TSC	Tuberous Sclerosis Complex
μl	Microlitre
μM	Micromolar

VIM	Vimentin
v/v	Volume/volume
v/w	Volume/weight
WT	Wildtype
YAP1	Yes-associated protein 1
ZEB1	Zinc finger E-box binding homeobox 1

Acknowledgements

Firstly, I would like to express my sincere gratitude to my supervisor Professor Ian Prior. I am extremely grateful for his dedicated support, guidance, enthusiasm and encouragement throughout the duration of my PhD. I also wish to thank my co-supervisor Professor Judy Coulson for her helpful advice, feedback and guidance with this research project. I would like to gratefully acknowledge the Wellcome Trust for the funding received towards my PhD and for the opportunity to peruse research in this exciting field.

I am also grateful to collaborators at AstraZeneca (Cambridge, UK) who despite not funding this research, provided reagents and supervision. I would like to thank Dr Sarah Ross, for her invaluable advice, guidance and knowledge of RAS drug discovery, and for enabling me the opportunity to undertake a placement at AstraZeneca's Oncology labs in Cambridge. Thanks also to Dr Paul Smith for sharing his expertise and innovative suggestions.

I would like to extend my thanks to all of my colleagues in the Prior lab and 5th Floor Nuffield labs with whom it was a pleasure to work alongside and for their help and advice. I'm grateful to have met and worked alongside you.

I am incredibly thankful to Charlotte, Zoe, Sophie, Rachel, Hannah and Beth for their long-standing friendships and support over the past decade. I would also like to thank Norah for the fun memories living in Liverpool, always keeping me in good spirits and generous friendship. I'm grateful also to Joanna for the fun coffee breaks and for her wonderful friendship.

I am enormously thankful to my family for their unconditional love and unwavering support, and to Richard for being a wonderful partner and for always being there for me. Finally, a heartfelt thanks goes to my parents for always believing in me – I couldn't have done it without you!

Chapter 1

Introduction

1.1 Cancer

Cancer is a complex disease caused by the acquisition of key genetic alterations which drive unregulated cell survival and proliferation. During tumorigenesis cancer cells overcome the normal control mechanisms for cell growth and acquire the ability to divide indefinitely whilst evading cell death signals. The process is characterised by the accumulation of genetic or epigenetic mutations in proto-oncogenes, tumour suppressor genes and DNA repair genes. Over time cancer cells become better equipped to survive and proliferate in the hostile tumour microenvironment with adaptive advantages such as the ability to tolerate hypoxic conditions, metabolic alterations and evasion of immune responses. As tumours grow, they stimulate angiogenesis to supply oxygen and nutrients via the formation of new blood vessels, which eventually enables malignant cancer cells to invade beyond normal tissue boundaries and metastasise to other sites around the body; this stage is generally associated with poor prognosis.

1.1.1 The hallmarks of cancer

The complexity of cancer is highlighted by the fact there are more than 100 distinct types of cancer and diverse sets of risk factors. Typically tumours are classified according to their tissue of orgin, however the Pan Cancer Atlas – the largest and most comprehensive cross-cancer study to date, analysed and re-characterised 33 different types of cancer from over 10,000 patient tumour samples according to their molecular profiles [1]. The results of the study highlighted that 28 distinct molecular subtypes were identified across the

different cancers studied and the majority of these clusters contained different histological tumour types [1]. This highlighted that cancers originating from the same tissue can have very different genetic profiles. During the course of tumorigenesis solid tumours become more heterogeneous, with the tumour encompassing subpopulations of cells harbouring a range of distinct mutations and molecular signatures [2]. This spatial and temporal intra-tumour heterogeneity can enable cancer cells to adapt to the changing tumour microenvironment [3]. As a result, tumorigenesis is referred to as an evolutionary process. In two landmark papers, Hanahan and Weinburg proposed that the complexity of cancer could be defined by eight underlying capabilities shared by all human cancers that enable cells to progress towards a neoplastic state [4, 5]. These were termed the hallmarks of cancer and include self-sufficiency in growth signals, insensitivity to growth-inhibitory signals, evasion of cell death, limitless replicative potential, sustained angiogenesis, tissue invasion and metastasis, reprogramming of energy metabolism and evading immune destruction. Additionally, two final characteristics underpinning these hallmarks were identified; genome instability and inflammation [5].

1.1.2 Oncogene addiction

Cancer cells exhibit extensive genome instability and are driven by the progressive accumulation of many mutations and epigenetic alterations that activate a variety of oncogenic functions and can evolve over an extended period of time [6]. Analysis of Pan Cancer Data identified a total of 299 different cancer driver genes of which 116 occured across two or more different cancer types [7]. Despite this, evidence from preclinical studies and application of targeted therapeutics has shown that cancer cell survival can often be dependent on one or relatively few key genetic ‘driver’ events and inactivation of these oncogenes can inhibit cancer cell growth [8]. This phenomenon was termed ‘oncogene addiction’. Clinical evidence for oncogene addiction is widely recognised from the impressive clinical responses and therapeutic efficacy of targeted agents in patients [9]. One of the earliest examples of this is the antibody trastuzumab, which targets the HER2 receptor, and shows

clinical success in HER-2 positive breast cancer patients [10]. Furthermore clinical responses with imatinib, which targets the protein kinase fusion BCR-ABL responsible for the majority of chronic myeloid leukaemia, demonstrated remarkable effectiveness and drastically improved patient survival [11]. In NSCLC patients with EGFR activating mutations, treatment with targeted EGFR inhibitors gefitinib and erlotinib also improves survival rates [12, 13], as does treatment with BRAF inhibitors such as vemurafenib for BRAF-mutant melanoma [14]. Such findings provide strong rationale for targeted anti-cancer therapies and significant efforts have been made to develop inhibitors that target specific driver oncogenes.

1.2 The RAS signalling pathway

The RAS family of proto-oncogenes are important intracellular signalling proteins involved in signal transduction pathways regulating numerous cellular processes including cell survival, cell growth, differentiation, proliferation, migration and apoptosis. RAS proteins were one of the earliest oncogenes described and were originally identified from studies investigating sarcoma-inducing retroviruses in rats [15, 16]. Later RAS oncogenes were identified within the human genome and were found to transform normal human cells into tumours [17-19]. Since these early discoveries, intensive research efforts in RAS structure, biochemistry and biology helped to further elucidate its importance and contribution to many human cancers. Notably mutations in RAS genes are one of the most common events driving tumorigenesis and overall occur in up to 20% of human cancers [20, 21]. As a result, RAS is a major target for drug discovery.

1.2.1 RAS structure

RAS proteins are small GTPases which act as molecular switches downstream of receptor tyrosine kinases (RTKs) and play a key regulatory role in cytoplasmic signalling networks controlling cellular processes. All human cells express three RAS isoforms: HRAS, KRAS (comprising two alternative splice variants KRAS4A and KRAS4B) and NRAS which are encoded by

separate genes. Despite RAS isoforms sharing approximately 82-90% primary amino acid sequence identity they have overlapping yet distinct functions [22, 23]. The N-terminus exhibits the highest sequence similarity across isoforms and contains the G-domain (aa 1-165) which is involved in GTP binding and hydrolysis [23] (Figure 1.1). Within this domain are switch I (aa 30-38) and switch II (aa 59-76) regions which undergo major conformational changes upon nucleotide exchange and subsequently reveals an effector binding site [24-26]. Thr-35 and Gly-60 are crucial residues for GTP binding and form hydrogen bonds with the γ-phosphate, which is subsequently released upon GTP hydrolysis allowing the switch regions to return to a GDP-bound conformation using a spring-loaded mechanism [27]. The allosteric lobe (aa 87-166) shares approximately 82% sequence similarity across the RAS isoforms and has been suggested to contribute to membrane interactions, as well as containing hotspots for protein-ligand interactions [28, 29]. In contrast, the hypervariable region (HVR) at the C-terminus is poorly conserved and contains the membrane anchor sequence and terminal CAAX motif. Ras isoforms display different post-translational lipid modifications at this region, thus directing differential Ras trafficking and subcellular localisation [30-34]. All four Ras isoforms are prenylated at the CAAX cysteine residue with the addition of a farnesyl lipid via a thioether linkage catalysed by farnesyltransferase (FTase) [35, 36]. The remaining AAX residues are subsequently cleaved by Ras converting enzyme 1 (Rce1) and the carboxyl group on the cysteine is methylesterified by isoprenylcysteine carboxylmethyltransferase (ICMT) [37]. In addition both KRAS and NRAS isoforms can undergo alternative prenylation by geranylgeranyltransferase I (GGTase I) in the presence of FTase inhibitors [38]. The membrane association of Ras also requires a second localisation signal from palmitoylation of an additional C-terminal cysteine upstream of the CAAX motif, with the exception of KRAS4B which lacks a second cysteine residue and therefore isn't palmitoylated [36, 39]. Alternatively, KRAS4B has a polylysine region which creates electrostatic interactions with the phospholipid head groups of the plasma membrane [40]. Consequently, these interactions promote Ras isoforms to associate with distinct signalling nanoclusters that

are suggested to mediate preferential coupling to effector signalling pathways [41, 42].

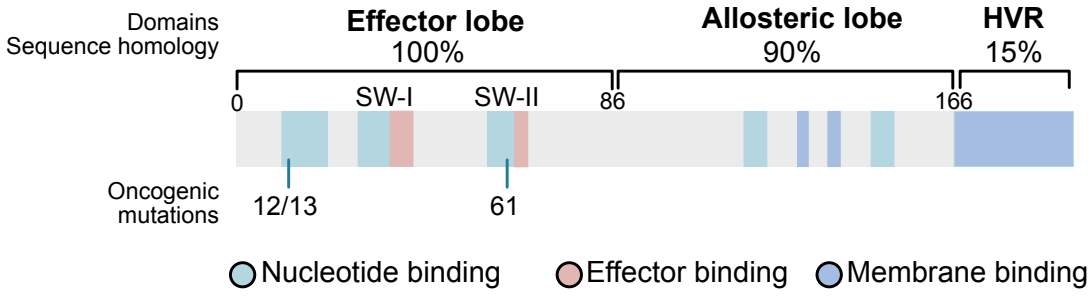

Figure 1.1: RAS protein structure and homology across isoforms

The RAS G-domain includes the effector and allosteric lobes and encompasses the switch I (SW-I) and switch II (SW-II) regions. The main area of RAS isoform sequence divergence is in the hypervariable region (HVR) which encodes the majority of membrane binding motifs. The key oncogenic mutations at codons 12, 13 and 61 are highlighted in nucleotide binding regions and mutations result in enhanced GTP binding.

1.2.2 RAS signalling

RAS proteins are regulated by a wide range of cell surface receptors which upon stimulation switch RAS from an inactive GDP-bound to an active GTP-bound state [43, 44]. The nucleotide binding state of RAS is tightly regulated by guanine nucleotide exchange factors (GEFs) which promote GDP dissociation and GTP binding, along with GTPase-activating proteins (GAPs) which catalyse GTP hydrolysis [45]. The activation state of RAS is determined by the balance of these proteins. Once activated, GTP-bound RAS interacts with a variety of downstream effectors, for instance RAF proteins, phosphoinositide 3-kinase (PI3K), RAL guanine nucleotide dissociation stimulator (RAL-GDS), phospholipase C and Tiam1 to name a few. These effectors interact via RAS-binding (RBD) or Ras-association (RA) domains which promote effector recruitment to the plasma membrane and subsequently facilitates pathway activation [46].

1.2.2.1 Signalling upstream of RAS

RAS can be activated by several cell surface receptor types including receptor tyrosine kinases (RTKs) and G-protein coupled receptors (GPCRs) which activate RAS through the stimulation of exchange factors [47]. Signal transduction between RTKs and RAS is mediated by adaptor proteins such as GRB2 which contain a SH2 domain that binds to the phosphorylated tyrosine sites on activated RTKs [48]. Through SH3 domains GRB2 can bind to the SOS-family RAS-GEFs, SOS1 and SOS2, which are recruited to the plasma membrane where RAS is localised and facilitate nucleotide exchange on RAS [49, 50]. SOS1/2 promotes dissociation of bound GDP from RAS, enabling GTP to bind and activate it. The mechanism of RTK mediated SOS-activation of RAS has been well characterised, yet other families of RAS-GEFs that are controlled under different conditions can also be involved in the activation of RAS [51]. For example, enhanced calcium influx as a result of GPCR stimulation can also activate the RAS-GRF family of RAS-GEFs, via calcium-dependent calmodulin association [52, 53]. Additionally, phospholipase C activation and diacylglycerol (DAG) production can directly activate the RAS-GRP family of RAS-GEFs and recruit them to the plasma membrane [54]. Consequently, the diversity of RAS-GEFs enables RAS to become activated by a varied collection of stimuli. On the other hand, this activation is counteracted by RAS-GAPs which rapidly inactivate RAS following its activation. There are 14 predicted RAS-GAPs with the most documented examples including p120 and NF1 [55]. Conversely the loss of RAS-GAP activity, such as the loss of NF1, is associated with activated RAS signalling and tumour development which is consistent with tumour suppressor characteristics [56-58].

1.2.2.2 RAS effectors

Once in its active GTP-bound state, RAS interacts with and activates several effectors of distinct signalling cascades controlling cell proliferation, survival and other cell behaviours. The signal transduction and pathway components of the major RAS effector pathways are described below.

The RAS-RAF-MEK-ERK pathway

Once activated, RAS binds to and recruits three closely related RAF proteins – CRAF, BRAF and ARAF, from the cytosol to the plasma membrane [59] (Figure 1.2). The three isoforms share a common structure and three conserved regions (CR). In the N-terminus, the CR1 contains a RAS binding domain (RBD) and cysteine-rich domain required for RAS interaction and membrane recruitment [60]. CR2 contains important Ser/Thr phosphorylation sites involved in the negative regulation of RAS binding and RAF activation [61]. Whereas CR3 located in the C-terminus contains the kinase domain and activation segment featuring phosphorylation sites important for kinase activation [60]. In an inactive state, RAF exists in a closed conformation where the N-terminal region interacts with the kinase domain, obstructing the catalytic site [62]. These inhibitory interactions are thought to be further stabilised by the binding of scaffold protein 14-3-3 to phosphorylated S259 and S621 sites located in the N-terminus and C-terminus respectively [63]. Although the process of RAF activation is not fully understood, it is thought that upon RTK activation, the RBD of RAF binds to the effector loop of activated RAS-GTP and the cysteine rich domain also forms additional interactions with the farnesyl groups on the C-terminus of RAS [62, 64]. RAS binding also promotes the dephosphorylation of 14-3-3 inhibitory binding sites which is mediated by protein phosphatase-1 (PP1) and protein phosphatase-2A (PP2A) [65]. The subsequent release of 14-3-3 from RAF induces its transition into an open kinase formation [60, 63, 66]. Consequently, RAS binding promotes RAF translocation to the plasma membrane, which promotes RAF interaction with additional kinases such as SRC kinases and casein kinase 2 (CK2), which phosphorylate key activating sites in the negatively charged N-region up-stream of the RAF kinase domain [62]. This region differs slightly between the RAF isoforms allowing divergent regulation and consists of four amino acid residues (SSYY, residues 338-341 in CRAF and SSDD, residues 446-449 in BRAF). In BRAF, the N-region exhibits a constitutive negative charge due to the aspartic acid residues, and this promotes a higher basal kinase activity compared to the other RAF isoforms [67]. In addition, RAF dimerisation has emerged as an important activation

event [68], with BRAF-CRAF heterodimers predominating in RAS signalling which possess higher kinase activity compared to their respective homodimers [69, 70]. It was also identified that catalytically impaired oncogenic BRAF mutants could still promote downstream ERK1/2 signalling through transactivation of CRAF [71, 72]. This phenomenon has also been found to be crucial for the paradoxical ability of RAF inhibitors to induce RAF dimerisation and ERK signalling [73] (also discussed in section 1.3.3.1). In addition 14-3-3 proteins bound to phosphorylated S621 on CRAF and S729 on BRAF are also thought to be involved in RAF dimerisation by providing a scaffold for their interaction [70, 72].

In turn activated RAF kinase phosphorylates and activates mitogen-activated protein kinase kinases 1 and 2 (also known as MEK1 and MEK2), which subsequently phosphorylate and activate the MAPKs ERK1 and ERK2 [74]. MEK1 and MEK2 are the only known activators of ERK1/2, and function to direct multiple upstream signals to induce ERK1/2 activation [75]. This three-tiered signalling system promotes substantial signal amplification, with phosphorylation of Thr and Tyr residues, T202/Y204 in ERK1 and T183/Y185 in ERK 2, stimulating a 1000-fold activation of kinase activity [76]. ERK1/2 are proline-directed kinases which catalyse the phosphorylation of substrates containing a PxS/TP sequence, with the proline directly after the phosphorylation site is a consistent determinant of ERK1/2 substrates [77]. Activated ERK1/2 has a wide substrate specificity with thousands of cytoplasmic and nuclear substrates estimated, although incomplete knowledge and validation of ERK targets and their effects under different biological contexts remains a challenge. Additional substrate specificity is also determined through separate functional ERK1/2 docking domains (known as the D-domain and F-domain) that are found independently or together within ERK1/2 substrates [78, 79]. The D-domain contains the motif DEJL, whereas the F-domain (also known as DEF) is characterised by the motif FxFP [80]. These docking domains bind to distinct recruitment sites within ERK1/2 called the D-site or F-site which are spatially distinct from the catalytic site [80].

Many substrates among signalling molecules are often low abundance, have transient interactions and regulation of their subcellular localisation as well as involvement in complex feedback and crosstalk pathways. Several studies using phosphoproteomics and analog-sensitive kinases have helped to identify many additional novel ERK1/2 substrates [81-83]. Typically these include transcription factors and additional kinases which are involved in a number of cellular processes related to cancer development including cell survival, proliferation, cell cycle progression, metabolism, cell migration and adhesion [84].

ERK activation is however tightly regulated through additional feedback controls providing a precise level of signalling depending on the cellular context. ERK1/2 can phosphorylate MEK1 at Thr292, preventing its dimerisation to MEK2 which decreases MEK1/2 kinase activity [85]. In addition, activated ERK1/2 can also phosphorylate specific S/TP sites on RAF proteins (S151, T401, S570 and T753) to inhibit their interaction with RAS and disrupt RAF dimerisation [76, 86, 87]. However this negative feedback loop is ineffective against specific BRAF-mutants such as BRAF-V600E which do not require RAS signalling or RAF dimerisation for activation [62]. Another upstream feedback target includes the RAS-GEF SOS1, where ERK1/2 phosphorylation inhibits SOS1 interaction with GRB2, downregulating activation from RAS [88-90]. ERK1/2 feedback controls also include transcriptional induction of dual-specificity phosphatases (DUSPs) and sprouty (SPRY) proteins. DUSPs inactivate ERK1/2 by dephosphorylating the conserved Thr/Tyr motif within the ERK1/2 catalytic domain [91, 92]. On the other hand, SPRY proteins bind to and inhibit GRB2 as well as inhibiting the RAF catalytic domain [93, 94]. Overall the relationship between high signal amplification and negative feedback control mechanisms, enables dynamic regulation of this signalling pathway. However, it is also one of the most dysregulated in human cancers and is a major mediator of RAS-induced

oncogenesis. Many cancers exhibit dysregulated MAPK pathway activation as well as increased dependency upon its signalling [95].

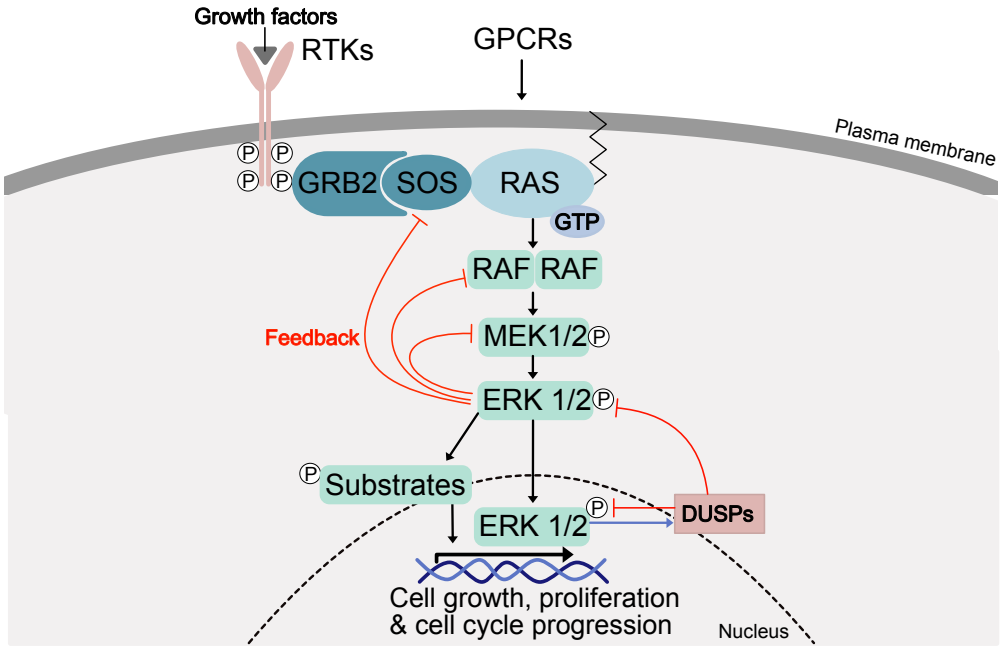

Figure 1.2: Overview of the RAS-RAF-MEK-ERK signalling pathway

Growth factor binding to receptor tyrosine kinases (RTKs) causes autophosphorylation of specific tyrosine residues which associate with adaptor proteins such as GRB2. Subsequent recruitment of RAS-GEFs such as SOS1/2 to the plasma membrane activate RAS by promoting nucleotide exchange and GTP binding. Activated RAS binds to RAF kinases and promotes their activation through dimerisation. In turn, active RAF kinases phosphorylate MEK1/2 kinases which then phosphorylate and activate ERK1/2. Activated ERK1/2 phosphorylates many cytoplasmic and nuclear substrates which control a wide variety of cellular processes including proliferation and cell survival. ERK1/2 activity is also regulated by several negative feedback controls, including inhibitory phosphorylation of RAF, MEK1/2 and SOS1/2. ERK1/2 also induces transcriptional upregulation of DUSPs which inhibit ERK1/2 activity in both the cytoplasm and nucleus, thus negatively regulating RAS activity.

The PI3K pathway

Another signalling pathway that RAS can interact directly with is the PI3K pathway, which plays an important role in cell growth, proliferation and survival (Figure 1.3). Phosphatidylinositol 3-kinase (PI3K) are a family of important lipid kinases that deliver signals in the PI3K/AKT pathway. Inactive PI3Kα is a stable heterodimer which consists of a regulatory p85α subunit and a catalytic p110α subunit [96]. RAS directly binds to the catalytic subunit of type I PI3Ks

and promotes its recruitment to the plasma membrane leading to its activation [97]. Here PI3K phosphorylates phosphatidylinositol-4,5-bisphosphate (PIP_2) to phosphatidylinositol-3,4,5-trisphosphate (PIP_3) which propagates intracellular signalling by directly binding to a number of proteins with pleckstrin homology (PH) domains, such as the kinases phosphoinositide-dependent kinase 1 (PDK1) and AKT (also known as PKB) [98]. This association with PIP_3 at the plasma membrane facilitates the phosphorylation and activation of AKT by PDK1 [99]. On the other hand, PIP_3 signalling is regulated by the tumour suppressor phosphatase and tensin homolog (PTEN) which dephosphorylates PIP_3 and converts it back to PIP_2, reducing PIP_3-dependent signalling [100].

One way in which the PI3K pathway promotes cell growth and survival is from AKT phosphorylation and subsequent inhibition of the proapoptotic protein BAD [101, 102]. Phosphorylation creates a binding site for 14-3-3 proteins and prevents BAD from binding to Bcl-2 and Bcl-X_L, promoting cell survival. In addition, AKT can also phosphorylate MDM2, which antagonises p53-mediated apoptosis [103]. Another target of AKT is glycogen synthase kinase 3 (GSK3) which is inhibited upon phosphorylation by AKT and as a result pathways usually repressed by GSK3 become activated [104]. For example, GSK3 inhibition allows accumulation of cyclin D1 and thus promotes cell cycle progression [105]. GSK3 inhibition also activates glycogen synthase, contributing to increased glycogen synthesis [106]. AKT can also phosphorylate TSC2, inhibiting the RHEB GTPase activity of the TSC1-TSC2 complex, enabling accumulation of active RHEB which in turn activates the mechanistic target of rapamycin (mTOR) [107, 108]. Activation of mTOR mediates increased protein synthesis via phosphorylation and activation of p70 S6 kinase and 4E-BP1 [109].

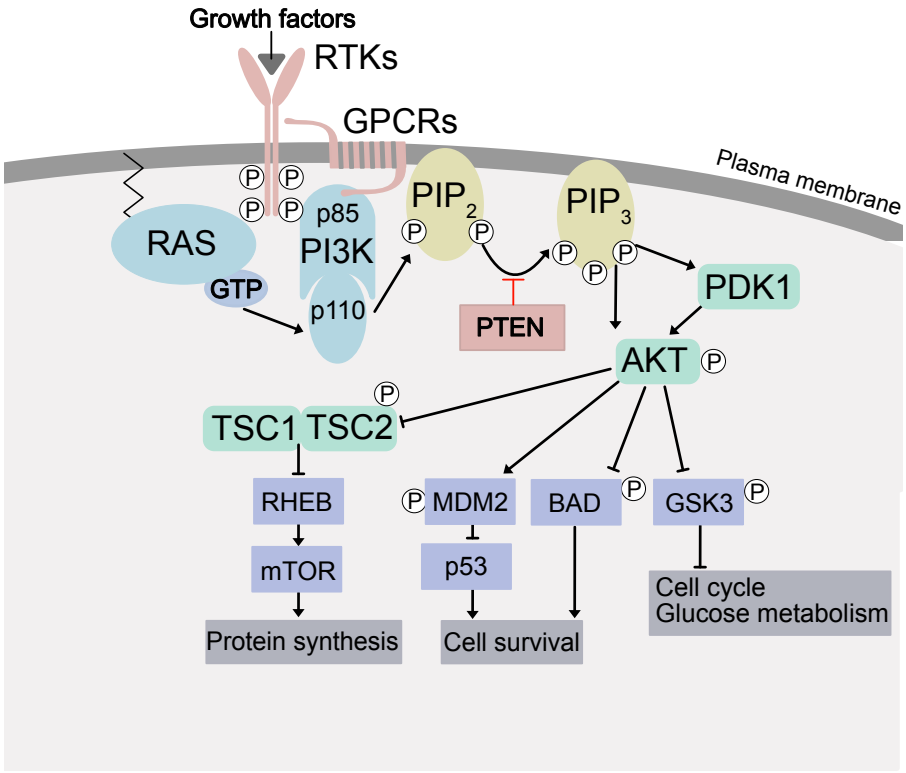

Figure 1.3: Overview of the PI3K signalling pathway

PI3K is activated by receptor tyrosine kinases (RTKs), G-protein-coupled receptors (GPCRs) as well as activated RAS. At the plasma membrane PI3K phosphorylates phosphatidylinositol-4,5-bisphosphate (PIP_2) to phosphatidylinositol-3,4,5-trisphosphate (PIP_3) which then recruits and activates PDK1 and AKT kinases. Active AKT inhibits TSC2 activity through direct phosphorylation, driving activation of mechanistic target of rapamycin (mTOR) and increased protein synthesis. AKT also phosphorylates downstream effectors MDM2 and BAD leading to increased cell survival. Additionally, AKT also inhibits GSK3, increasing cell cycle progression and glucose metabolism.

The RAL-GDS pathway

A third major RAS effector pathway involves the RAS-related RAL proteins; RALA and RALB (Figure 1.4). These small GTPases also cycle between an active GTP-bound and inactive GDP-bound state. Activated RAS recruits RAL exchange factors (RAL-GEFs), such as RAL-GDS, to the plasma membrane and promotes the formation of active RAL-GTP [110]. Three additional RAL-GEFs have been identified and named RAS-GDS-like (RGL1, RGL2 and RGL3) [111]. RAL-GTPases interact with a range of effectors involved in regulation of membrane trafficking, actin cytoskeleton, migration and invasion.

For example, RAL-GTP binds RAL-binding protein 1 (RAL-BP1) which regulates actin cytoskeleton organisation through its regulation of CDC42 and RAC1 [111]. RAL-GTP also binds to Sec5 and Exo84 subunits of the exocyst - a molecular tether that is recruited for plasma membrane exocytosis [112]. This interaction has also been shown to regulate macroautophagy which is involved in cellular adaptation to nutrient restriction [113]. Activated RAL can also regulate gene expression through activation of the transcription factors NFκB [114] and FOXO4 [115] amongst others. Overall there is growing evidence that aberrant RAL activation occurs in human cancers [116, 117], and has been shown to promote tumour invasiveness and metastasis [118].

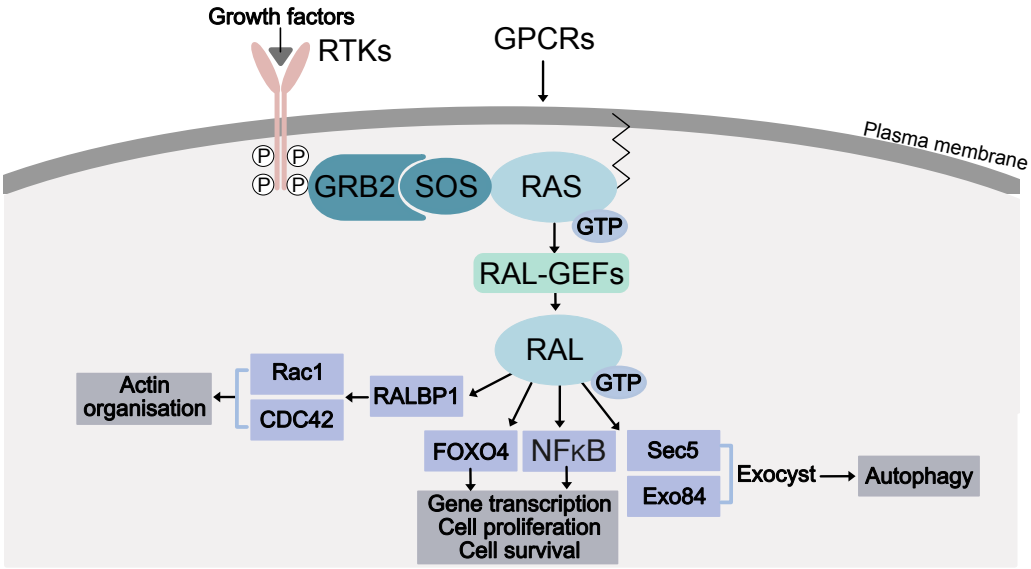

Figure 1.4: Overview of the RAL-GDS pathway

Activated RAS recruits RAL-GEFs, such as RAL-GDS and RGL1-3, promoting RAL nucleotide exchange to generate active RAL-GTP. Activated RAL interacts which a variety of downstream effectors involved in promoting actin organisation, gene transcription, cell proliferation and survival and autophagy.

1.2.3 RAS mutations

Of the RAS isoforms, KRAS is the most frequently mutated isoform (69%), followed by NRAS (22%) and HRAS (9%) [119] . These mutations typically occur at one of three mutational hotspots located at codons G12, G13 and Q61, which subsequently favour GTP binding. These mutations decrease RAS intrinsic GTPase activity and have been shown to impair the normal GTP-hydrolysis by RAS-GAPs, resulting in accumulation of active GTP-bound RAS and subsequent signalling to downstream effectors [21]. Despite these mutations being activating, they possess differences in their oncogenic potential [120-124]. For example, analysis of commonly occurring KRAS mutations (G12A, G12C, G12D, G12R, G12V, G13D, Q61L, and Q61H) highlighted differences in nucleotide exchange, GTP hydrolysis and RAF affinity [123]. Cell-based studies have also identified differences in transforming phenotypes between KRAS G12 and G13 mutations, with G12 mutations exhibiting resistance to apoptosis and favouring anchorage independent growth [125], as well as differential metabolic reprogramming, protein trafficking and kinase signalling [126].

RAS isoforms also exhibit distinct associations with particular tumour types as well as differences in the mutational frequency at these mutation hotspots [21]. For example, pancreatic ductal adenocarcinomas, lung adenocarcinomas and colorectal adenocarcinomas are greatly associated with mutated KRAS [127]. In contrast, NRAS is predominantly mutated in cutaneous melanoma and haemopoietic cancers, whilst HRAS mutations are primarily linked to head and neck squamous cell carcinomas. Additional complexity arises as each isoform shows bias towards specific codon mutations; G12 mutations predominant in KRAS (81%), Q61 mutations are the most frequent mutation in NRAS (62%), whereas HRAS mutations are more evenly split between codons G12, G13 and Q61 (26%:23%:38%) [119].

In addition to mutation frequency across isoforms, specific mutations can also be linked to certain mutagen exposure, with NSCLC representing a key example. In non-smokers, the majority of KRAS G12 mutations are caused by

a G-to-A transition resulting in an amino acid change from glycine to aspartic acid (G12D mutation). However, in smokers G-to-T transversions predominate producing a cysteine at codon 12. This specific G12C mutation is associated with DNA adduct formation [74]. According to Cancer Research UK approximately 35,600 deaths occur every year due to lung cancer, which is still the most common cancer related death in the UK [128] and tobacco smoking remains the greatest single cause accounting for 72% of cases [129]. Approximately 15-25% of lung adenocarcinomas contain mutations in KRAS [130] and of these 65% have G12C mutations [131].

The explanation for these varying RAS mutation frequencies observed in human cancers remains poorly understood, and it is likely that many factors are involved such as differences in RAS effectors, RAS expression levels, epistatic interactions, isoform structural differences and cellular context [119]. Overall it suggests that some RAS variants are able to achieve an optimum level of RAS signalling, whereas others may conduct too little or too much RAS signalling to effectively drive tumorigenesis under certain conditions.

1.2.4 Additional RAS pathway mutations

Activating mutations in RTKs and RAS effector genes such as BRAF and PIK3CA are also common occurrences in human tumours, further highlighting the importance of Ras signalling pathways in driving tumour growth [127].

Upstream of RAS, RTKs such as EGFR, ERBB2 (HER2) and MET are often abnormally activated in many human cancers, particularly lung and breast cancers through genomic amplification, gain of function mutations, chromosomal rearrangements and autocrine activation [132]. In NSCLC, the most common EGFR mutations are small in-frame deletions located in exon 19 or an L858R point mutation in exon 21 both situated within the tyrosine kinase domain [133]. This results in constitutive activation of the receptor as well as downstream signalling pathways. Notably EGFR mutations and KRAS mutations appear to be mutually exclusive, although KRAS mutation can confer resistance to EGFR inhibitors [134].

BRAF is also frequently mutated in approximately 7% of human cancers, particularly in melanomas, thyroid and colorectal cancers, whereas mutations in CRAF and ARAF are exceptionally rare [135, 136]. The majority of BRAF mutations occur in the kinase domain, in particular the activation loop or phosphate binding loop regions, of which the most common encodes a V600E mutation [135, 136]. This gain-of-function mutation increases kinase activity 500-fold compared to BRAF-WT cells and produces a BRAF kinase capable of signalling as a monomer [71, 136]. Similarly, BRAF V600E and KRAS mutations also appear to be mutually exclusive, and concomitant mutations in both proteins are extremely rare [136, 137]. This suggests that activating mutations in either of these proteins has comparable effects on tumorigenesis [137]. Additional BRAF mutations include gene fusions and in-frame deletions which promote constitutively activated BRAF-mutants capable of dimerisation independent of RAS activation [138].

Unlike RAS and RAF, MEK activating mutations are found at a much lower prevalence in the cancer genome, making it an attractive therapeutic target for cancers with aberrant RAS-ERK1/2 signalling [139]. The majority of MEK mutations cluster in the N-terminal negative regulatory region and N-terminal kinase domain [75], highlighting that some MEK mutations not only increase kinase activity but also modulate MEK regulation such as dephosphorylation [140].

Alternatively, the PI3K pathway can be activated by amplification or mutation of the PI3KCA gene, encoding the PI3K p110α subunit, which occurs at high frequency in many common human cancers [141]. Furthermore, the tumour suppressor PTEN, which dephosphorylates PIP_3 and thus terminates PIP_3-dependent downstream signalling, is also commonly mutated. Loss of PTEN function can occur through gene mutation, deletion, transcriptional silencing or protein instability, resulting in constitutive activation of the PI3K pathway [142].

1.3 Targeting RAS

Since the discovery over 30 years ago that RAS genes are frequently mutated within a large variety of tumours, the RAS GTPase family and associated signalling pathways have presented attractive targets for cancer therapeutics and significant efforts have been committed to inhibiting RAS [139]. However direct pharmacological inhibition of RAS has been a major challenge, primarily due to a small inaccessible GTP binding pocket which exhibits intrinsically high affinity for GTP, thus rendering displacement by small molecules a difficult task. Consequently, major strategies of RAS inhibition have focused on indirect inhibition through blocking post-translational modification, localisation and signalling cascades (Figure 1.5).

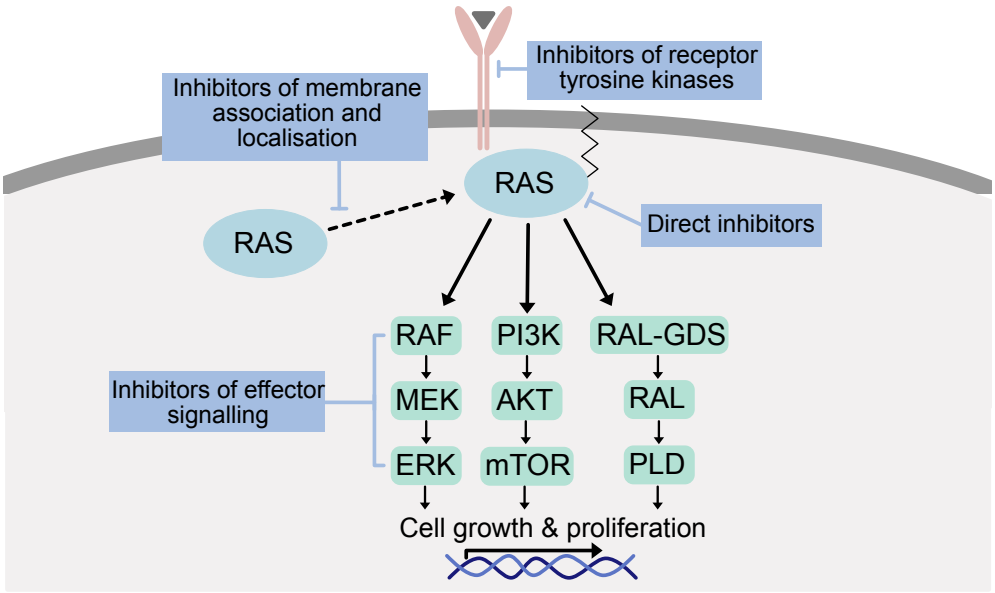

Figure 1.5: Approaches of targeting mutant RAS

Strategies for anti-RAS drug development include direct inhibition of RAS, inhibition of upstream receptor tyrosine kinases, inhibition of enzymes that promote RAS membrane association and localisation at the plasma membrane and inhibition of RAS downstream effector signalling, particularly signalling through RAF and PI3K.

1.3.1 RAS Localisation inhibitors

Given the essential requirement for RAS signalling at the plasma membrane, early efforts to target RAS involved disrupting its membrane localisation through inhibition of the FTase responsible for membrane-targeting prenylation of the C-terminal CAAX motif [39]. Despite FTase inhibitors (FTIs) demonstrating promising anti-tumour effects in preclinical *in vitro* and *in vivo* studies [143], they failed to show anti-tumour activity in tumours harbouring KRAS and NRAS mutations [144]. The underlying basis for this lack of efficacy is due to the alternative prenylation of KRAS and NRAS by GGTase I in the presence of FTase inhibition, which also supports membrane association and promotes oncogenic signalling [38, 145]. However, several FTIs including lonafarnib and tipifarnib have progressed into clinical trials for HRAS-driven tumours [146, 147]. Alternatively, combination approaches of FTase and GGTase inhibitors present toxicity challenges due to the finding that more than 100 other proteins are also targets of these enzymes [148]. Despite this concern, studies with genetic mouse models have supported the anti-tumour effects of GGTase inhibitors [149, 150]. Approaches targeting the two other RAS processing enzymes, RCE1 and ICMT also generate similar toxicity concerns from affecting other additional substrates. In a study using KRAS-G12D mutant pancreatic mouse models, ablation of ICMT was demonstrated to instead accelerate pancreatic neoplasia [151]. More recently, targeting palmitoylation and depalmitoylation has also been considered as an alternative approach to destabilising NRAS and HRAS membrane association [152, 153]. Additional approaches have entailed disrupting RAS from binding to chaperone proteins and so preventing its subsequent trafficking to the plasma membrane. An example includes targeting of phosphodiesterase-6δ (PDE6δ) which can bind to both farnesylated and geranylgeranylated proteins, although not to those that are also palmitoylated [154, 155]. As a result, PDE6δ inhibition selectively effects KRAS trafficking compared to HRAS. Alternatively, other studies have investigated existing inhibitors which disrupt RAS nanoclustering at the plasma membrane and promote RAS mis-localisation. These include fendiline an L-type calcium channel blocker [156],

staurosporines which inhibit phosphatidylserine trafficking [157] and metformin [158, 159].

1.3.2 Inhibitors targeting upstream of RAS

Over the past two decades, inhibitors of growth factor receptor tyrosine kinases have represented a large group of targeted drugs which have been used clinically for cancer treatment. They typically target either the receptor-ligand interaction such as monoclonal antibody inhibitors or they target the receptor kinase domain and competitively inhibit ATP binding sites [160]. Overall this prevents subsequent phosphorylation and activation of downstream signalling cascades. EGFR and ERBB2 receptors in particular have an important role in the activation of RAS pathways and are able to stimulate RAS via GRB2 and SOS interactions. In NSCLC EGFR inhibitors such as gefitinib and erlotinib show robust efficacy in EGFR-mutant tumours, however their effectiveness can often be limited by the development of resistance [161]. The protein tyrosine phosphatase SHP2 (PTPN11) is an important mediator of signal transduction from RTKs, particularly in mutant KRAS-driven cancers [162, 163]. The development of SHP2 inhibitors provides an alternative strategy to prevent the activation of RAS. The SHP2 inhibitor SHP099 alone or in combination with MEK inhibition demonstrated effective inhibition of downstream ERK signalling in some RAS-mutant preclinical models [164]. Several combinations of SHP2 inhibitors with direct RAS inhibitors are also being explored [165]. Efforts have also been in the development of RAS-GEF inhibitors such as BI 1701963 (Boehringer Ingelheim) which selectively inhibits RAS-SOS1 interactions and thereby hinders the formation of active GTP-bound KRAS. Phase I clinical trials are being conducted as a monotherapy and in combination with a MEK inhibitor (NCT04111458). Overall these agents offer the potential to switch off all RAS mutants by hitting targets at the beginning of the signal cascade.

1.3.3 Inhibitors of RAS effector pathways

In RAS driven cancers, the downstream RAF/MEK/ERK and PI3K/AKT/mTOR signalling cascades become aberrantly activated and the inhibition of these

pathway nodes have presented attractive targets. However due to multiple points of crosstalk and negative feedback loops, single agent inhibition has not been successful clinically and thus combinational inhibition has been the primary treatment strategy to overcome potential resistance mechanisms [166].

1.3.3.1 BRAF inhibitors

Despite RAF functioning as a key downstream effector of RAS, pharmacological inhibition of BRAF by ATP-competitive inhibitors in RAS-mutant and RAS/RAF-WT tumours unexpectedly enhanced downstream ERK1/2 signalling and enhanced tumour growth [167, 168]. In these cells, inhibitor binding promoted RAF dimerisation and transactivation of CRAF in RAF heterodimers and homodimers, consequently leading to increased pathway signalling via CRAF [167]. Clinical studies also confirmed these findings with the development of RAF-inhibitor induced keratoacanthomas and cutaneous squamous cell carcinomas in patients with mutant RAS [169]. Nethertheless, several BRAF inhibitors including vemurafenib and dabrafenib have been clinically approved specifically for the treatment of BRAF-mutant metastatic melanoma [14, 170]. In these patients, single agent BRAF inhibitor treatment significantly improved overall and progression-free survival compared to standard chemotherapy, although the development of acquired resistance often limits their responsiveness. The development of pan-RAF inhibitors such as Belvarafenib may prove to be more effective for the treatment of both BRAF and RAS mutant tumours [171].

1.3.3.2 MEK inhibitors

The majority of MEK1/2 inhibitors act as non-ATP competitive inhibitors binding to a novel allosteric binding pocket adjacent to the ATP binding site [172]. As a result, this enables higher specificity of MEK1/2 inhibitors compared to ATP competitive inhibitors. In the presence of allosteric inhibitors, MEK1/2 adopts an inactive conformation where the ERK1/2 activation loop becomes displaced and causes disruption of the catalytic domains in the ERK1/2 binding site [172]. As observed with BRAF inhibitors, MEK inhibitors

are most effective in tumours which exhibit strong dependency upon ERK1/2 signalling such as those with BRAF-V600E mutations [173, 174]. Three MEK1/2 inhibitors, trametinib, cobimetinib and binimetinib have been approved for the treatment of BRAF-mutant metastatic melanoma, as single agents or combined with BRAF inhibitors [175-177]. In KRAS-mutant cancers, multiple phase I and phase II clinical trials have been conducted with the MEK1/2 inhibitor selumetinib, both as a single and combined agent [178]. Despite showing initial promise in the phase II SELECT-1 clinical trial in combination with docetaxel in KRAS-mutant NSCLCs, the subsequent phase III trial determined that the addition of selumetinib was not clinically effective [179, 180]. In RAS-mutant tumours MEK inhibitors induce pathway feedback loops by relieving ERK-dependent negative feedback loops resulting in RAF activation and therefore display variable sensitivity to MEK inhibition [173]. The MEK inhibitor GDC-0623 which blocks MEK activation by RAF underwent clinical evaluation but was later discontinued [181, 182]. Due to complex feedback reactivation, targeting multiple nodes within the MAPK pathway has also been explored through combined RAF and MEK inhibition in studies with KRAS-mutant cancer cell lines [183, 184]. Increased GTP-RAS and RAF dimerisation in KRAS-mutants was suggested to enhance the synergy of this therapeutic combination [184]. As a result, two clinical trials are currently investigating this combination in KRAS-mutant tumours (NCT03284502, NCT02974725).

1.3.3.3 ERK inhibitors

In order to overcome some of the difficulties faced with RAF and MEK inhibitors, inhibitors of the downstream kinase ERK represent an alternative approach to overcome reactivation of the MAPK pathway. In comparison to the upstream RAF and MEK inhibitors, the development and clinical progression of selective ERK1/2 inhibitors has lagged behind with no ERK inhibitors yet clinically approved [185]. Several are under clinical investigation, though results from early clinical trials for KRAS-mutant tumours have been largely disappointing. Similar to MEK inhibitors, ERK inhibitors prevent ERK feedback phosphorylation of RAF, subsequently leading to enhanced MEK signalling [127]. In phase I trials, the ERK1/2 inhibitor MK-8353 showed no

anti-tumour effects on KRAS-mutant cancers as monotherapy, although some responses were observed in patients with BRAF-mutant tumours [186]. As a result of lower response rates, clinical trials are currently taking place combining MK-8353 with MEK inhibition (NCT03745989) as well as with the immunotherapeutic agent pembrolizumab (NCT02972034). A preclinical study combining the ERK1/2 dual inhibitor GDC-0994 with MEK inhibition showed promising efficacy in KRAS-mutant lung and pancreatic tumour mouse models, with MAPK pathway suppression greater than with either single agent alone [187]. However, in a phase I clinical trial the combination was not tolerated and the trial was terminated [188]. On the other hand, the reversible ATP competitive ERK1/2 inhibitor ulixertinib has shown promising clinical evidence in NRAS-mutant and BRAF-mutant tumours [189], and is also undergoing further clinical trials in combination with CDK inhibition (NCT03454035) and as part of the MATCH precision medicine cancer treatment clinical trial for BRAF non-V600 mutation tumours (NCT02465060). In a recent preclinical study, the combined inhibition of RAF and ERK was found to be more synergistic and effective at supressing ERK signalling in KRAS-mutant cells than combined ERK/MEK inhibition or MEK/RAF inhibition [190]. This RAF/ERK inhibitory combination also decreased ERK feedback signalling [190]. As part of an ongoing clinical trial (NCT02974725) this combination is being clinically investigated using a pan-RAF inhibitor in combination with the ERK1/2 inhibitor LTT462.

1.3.3.4 PI3K pathway inhibitors

Several PI3K inhibitors have also been developed, including dual PI3K and mTOR inhibitors, and many of these are undergoing preclinical development and clinical evaluation. Early preclinical mouse studies highlighted that PI3K signalling is required for RAS-driven tumourgenesis [191, 192]. As observed with other inhibitors of RAS effector pathways, they showed limited efficacy as monotherapies in KRAS-driven tumours, although preclinical studies suggested combined inhibition of PI3K and MEK would be efficacious [193-195]. However translation of these findings into clinical trials demonstrated the challenges of overlapping monotherapy toxicities and demonstrated low

response rates and little efficacy at tolerable drug doses [196, 197]. Several AKT inhibitors are also undergoing clinical evaluation, as both monotherapies and as combinative therapeutics, although currently no AKT inhibitors have yet been approved for cancer treatments [198]. As observed with PI3K-MAPK inhibition, the combination of AKT and MEK inhibitors in phase I/II trials has indicated poor tolerability and limited efficacy in patients with advanced solid tumours including those with RAS or BRAF mutations [199-201]. Additionally, mTOR and dual mTOR/PI3K inhibitors combined with MEK inhibition also failed to provide efficacy at acceptable drug tolerable doses [202, 203].

1.3.4 Direct RAS inhibitors

Despite decades of research, only in recent years with advances in drug discovery approaches and technology have direct RAS inhibitors been developed, including the discovery of small molecules that selectively bind to the KRAS-G12C mutant most frequently present in NSCLC tumours [204]. A variety of high throughput strategies have been used to identify such compounds including screening strategies to assess the disruption of GEF interaction and effector binding [205, 206]. These molecules irreversibly bind to the reactive thiol group of the mutated cysteine at position 12 and therefore do not inhibit KRAS-WT or other mutated forms. Inhibitor binding occupies a switch-II pocket only accessible when GDP is bound which disrupts the adjacent switch I and switch II regions and promotes a shift in nucleotide affinities of KRAS-G12C to favour GDP over GTP [204, 207]. Consequently, this leads to an accumulation of mutant RAS in the inactive state and impairs binding to downstream RAF. Following the success and further development of initial compounds, two KRAS-G12C inhibitors AMG-510 (Amgen) and MRTX849 (Mirati Therapeutics) have entered into clinical trials to treat KRAS-G12C cancers and show promising early results in NSCLC [208, 209]. Currently KRAS-G12C inhibitors are the only targetable mutant specific KRAS inhibitors which have entered the clinic, however there is emerging evidence that other KRAS mutants might one day be druggable. For example therapeutic peptides targeting KRAS-G12D have been developed as well as

pan-mutant KRAS macromolecule degraders, although currently these strategies are limited therapeutically by suitable delivery systems [210, 211].

Another approach of direct RAS inhibition is targeting RAS expression using antisense oligonucleotides (ASOs). These are short strands of deoxyribonucleotides that are complementary to mRNA sequences. This therapeutic approach therefore enables the development of highly specific and selective inhibitors according to gene sequence information and offers the potential to target molecules that have previously been difficult to inhibit by conventional drugs [212]. Upon binding to mRNA, ASOs downregulate their molecular target by inducing RNase H endonuclease activity to cleave the DNA-RNA duplex thus reducing target gene translation [213]. ASOs can also prevent translation by steric hindrance of ribosomal activity, reducing mRNA stability and inhibition of mRNA splicing [213]. Improvements in ASO pharmacology and chemistry have enhanced compound stability and potency [214]. Examples of ASOs targeting RAS include ISIS-2503 (Isis Pharmaceuticals) targeting HRAS mRNA and AZD4785 (Ionis 651987) targeting KRAS mRNA [215, 216]. Despite demonstrating safety and tolerability in phase I/II clinical trials, both compounds have since failed to progress and enter the clinic as a cancer treatment.

1.4 Mechanisms of resistance to targeted therapeutics

The development of targeted therapeutics has undoubtably transformed the treatment of many cancers and improved overall prognosis of cancer patients, such as EGFR-mutant NSCLC treated with EGFR inhibitors, BRAF-mutant melanomas treated with BRAF inhibitors and HER2-amplified breast cancer treated with HER2 inhibitors. However, despite initially responding to treatment, most patients treated with targeted therapies acquire resistance to these agents. As targeted therapies for RAS-mutant tumours are developing and undergoing clinical evaluation, understanding potential resistance mechanisms is becoming important for improving these treatments. Drug resistance can be classified as intrinsic, existing before treatment, or as

acquired where resistance develops following drug treatment among patients whom were initially responsive [217, 218]. Adaptive resistance to KRAS-G12C inhibitors AMG-510 and MRTX849 has been observed in early preclinical models [219, 220] and overcoming this could be an important step for improving treatment efficacy.

1.4.1 Intrinsic resistance to RAS inhibitors

The heterogeneity of tumours can promote intrinsic resistance to develop, whereby alternative non-targeted genetic mutations exist within some tumour cells, such as other RAS mutations [221, 222], creating subpopulations which are resistant to allele-specific or RAS isoform-specific inhibitors. This heterogeneity severely limits the success of targeted therapeutics by selecting for and promoting the outgrowth of resistant cancer cells. Pre-existing mutations in RAS which increase nucleotide exchange (Y40A, N116H, A146V) or alternatively impair GTPase activity (A59G, Y64A) could also reduce the interaction of current KRAS-G12C inhibitors which bind to GDP-KRAS [223]. As well as alternative mutations within tumours, differing dependencies of tumours for KRAS signalling could also promote intrinsic resistance to KRAS inhibitors [224], for example those that may not rely primarily on ERK signalling for cell viability. For example, even complete knockout of the *KRAS* gene using CRISPR genome editing enabled a subset of KRAS-mutant cell models to survive [225]. At present there is little evidence of what de novo mutations may arise and cause resistance to KRAS inhibitors, though ongoing clinical responses will help to clarify this.

1.4.2 Adaptive resistance to RAS inhibitors

Acquired resistance mechanisms that have been previously observed for other inhibitors targeting the MAPK pathway, such as EGFR, BRAF and MEK inhibitors, may provide some insight into potential acquired resistance mechanisms associated with direct KRAS inhibitors (summarised in Table 1.1). These can be broadly categorised into secondary alterations of the

target, reactivation of signalling pathways and phenotypic transformation [226].

1.4.2.1 Alteration of the target

The use of targeted inhibitors can select for the emergence of mutations within the primary drug target, often abrogating drug binding or enhancing oncogenic signalling. For example, as observed in 50-60% of EGFR-mutant NSCLC, the gatekeeper T790M mutation within the EGFR kinase domain can arise following EGFR inhibitor treatment, which enhances ATP affinity and subsequently kinase activity despite the presence of inhibitor [227, 228]. Furthermore, the majority of mutations that confer resistance to MEK inhibition occur in its allosteric drug binding pocket which provides approximately 100-fold resistance to MEK inhibition [229, 230]. As such alternative oncogenic KRAS-G12 mutations, such as G12D or G12V, could be expected to occur with targeted KRAS-G12C inhibitors [185]. Alternatively, in BRAF-V600E mutant melanoma, amplification of BRAF-V600E itself was identified as a mechanism of resistance to BRAF inhibitors [231, 232]. Elevated signalling from the CRAF isoform was also identified as an acquired resistance mechanism to BRAF inhibition [233]. Subsequently amplification of *KRAS*, or alternatively *HRAS* or *NRAS* could drive RAS dimerization and activation in the presence of RAS inhibitors.

1.4.2.2 Alternative signalling pathways

To maintain cell homeostasis, cell signalling pathways are regulated by a finely controlled network of protein interactions, feedback mechanisms and crosstalk within signalling networks [234]. Mechanisms of feedback control help to precisely tune signalling outcomes through post-translational modifications such as phosphorylation that alter protein activity [235, 236]. While these mechanisms help cells to survive under dynamic physiological conditions, they can also enable cancer cells to adapt to pharmacological pathway perturbations. Drug resistance can evolve through dynamic re-wiring of cell signalling networks to circumvent the initial drug blockade [237]. This adaptive

response can occur extremely quickly following treatment, promoting cell adaptation and continued cell survival in the presence of drug through parallel activation of alternative signalling pathways that are not targeted by the drug. The majority of acquired resistance mechanisms to MAPK pathway inhibitors promote recovery of the MAPK pathway through rebounded ERK1/2 activation. In EGFR-mutant lung cancer the amplification of alternative EGFR-family receptors such as *MET* and *HER2* have been identified [227, 238, 239]. Similarly, in BRAF-mutant tumours this can be achieved by activating mutations in *NRAS* and *MEK1/2* [229, 232, 240-242], as well as inactivating mutations in *CDKN2A* [243]. In addition, amplification of the upstream oncogene BRAF-V600E was observed in CRC and melanoma cell lines resistant to MEK inhibitors [242, 244, 245], as well as amplification of mutant KRAS in KRAS-mutant CRC cell lines resistant to selumetinib [244]. In addition loss of *NF1,* resulting in reduced RAS-GAP protein neurofibromin and thus increased RAS activity, has also been identified as a mechanism of resistance to targeted inhibitors in both BRAF-mutant and EGFR-mutant tumours [246, 247].

In addition to increased MAPK pathway signalling, cancer cells can activate alternative signalling pathways such as the PI3K pathway to bypass signalling in response to targeted MAPK pathway inhibitors. For example in BRAF-mutant tumours the overexpression of upstream receptor PDGFRβ was associated with lower reactivation of the MAPK signalling pathway, and instead promoted activation of other signalling pathways for cell survival [240]. Mutations in *AKT1/3* and *PTEN* were identified in BRAF-mutant melanoma resistant to BRAF inhibition [243], whilst loss of *PTEN* contributed to resistance to targeted EGFR inhibition in EGFR-mutant NSCLC [248]. As a result, reactivation of MAPK or PI3K signalling pathways can undertake numerous mechanisms of resistance through alteration of upstream signalling and downstream signalling, and subsequently similar resistance mechanisms are also likely to occur with targeted RAS inhibition.

Table 1.1: Known acquired resistance mechanisms to EGFR, BRAF and MEK targeted inhibitors

Category	Cancer type	Resistance Mechanism	Example	Studies
Resistance to EGFR inhibitors	NSCLC	Target Mutation	EGFR T790M substitution	[227, 249]
		Amplification	MET	[238]
			HER2	[227, 239]
		Down regulation Mutation	NF1	[246]
			BRAF	[250]
Resistance to BRAF inhibitors	Melanoma	Amplification	BRAF	[231, 232, 251]
			CRAF	[233]
			PDGFRβ	[240]
		Mutation	MEK1/2	[232, 241, 242, 251]
			NRAS	[232, 240, 243]
			AKT1/3	[243]
			CDKN2A	[243]
		Down regulation	NF1	[247]
			PTEN	[243]
	CRC	Mutation	MEK1/2	[252]
		Amplification	KRAS (WT)	[252]
			BRAF	[252]
Resistance to MEK inhibitors	Melanoma	Mutation	MEK1/2	[229]
		Amplification	BRAF	[242]
	CRC	Mutation	MEK1/2	[230]
		Amplification	BRAF	[244, 245]
			KRAS	[244]

1.4.2.3 Phenotypic transformation

Cancers may also acquire resistance through phenotypic transformation via epithelial-to-mesenchymal reprogramming. Several transcriptions factors, including ZEB1/2, TWIST1/2 and SNAI1/2 are involved in mediating gene expression and regulating epithelial-to-mesenchymal transition (EMT) which increases cell migration and invasiveness [253]. In NSCLC an EMT phenotype has been associated with resistance to EGFR inhibitors [254-256] and similarly in melanoma, resistance to BRAF inhibitors was associated with ZEB1-mediated phenotype switching [257]. It is suggested that EMT reprogramming may rewire the expression of RTKs promoting cells to activate alternative survival signalling pathways driving EMT-mediated drug resistance [258, 259]. For example, in KRAS-mutant NSCLC treated with MEK inhibitors, a mesenchymal phenotype activated the PI3K pathway independent of HER3 and instead FGFR1 was dominantly expressed, whilst cells with an epithelial phenotype activated the PI3K pathway in a HER3-dependent manner [258]. Alternatively in mesenchymal cells treated with AMG-510, PI3K activation was mediated by IGFR [259]. Histologic transformation, such as a switch from NSCLC to small-cell lung cancer (SCLC) has also been observed as a mechanism of resistance to EGFR inhibitors in patients with EGFR-mutant tumours [227, 260]. In these cases, the original *EGFR* driving mutation observed in the original NSCLC is also retained in the SCLC phenotype, indicating an evolutionary transformation of the original tumour cells to adopt the genetic features of SCLC, rather than its de novo development.

1.4.3 Emergence of resistance

Despite numerous mechanisms of drug resistance to targeted therapeutics being identified, the underlying emergence and evolution of these resistant cells remains unclear. One suggestion is that a small subpopulation of reversibly drug-tolerant cells emerges as an acute response to drug exposure [261]. These cells are able to maintain viability in the presence of the drug through epigenetic alterations and adopting a quiescent-like state [261]. They likely function as a transition state, actively supporting the development of

more permanent resistance mechanisms to be established, before culminating into fully drug-resistant cells [261]. From monitoring resistant clones over time, this process was observed during the development of acquired resistance caused by an EGFR-T790M mutation within initially EGFR-T790M negative drug-tolerant NSCLC cells [262].The emergence of drug-tolerant cells can be attributed to branched tumour evolution giving rise to subpopulations of cancer cells with varying treatment responsive phenotypes, with some bearing selective advantages [263]. When sudden selective pressures are imposed by therapeutics, this process is particularly evident. Whole exome-sequencing identified that diverse resistance mechanisms could emerge from a single drug-tolerant NSCLC clone treated with an EGFR inhibitor [264]. This branching evolutionary process is integral to underlying tumour heterogeneity.

1.5 Aims of this project

Recent advances in the development of direct KRAS inhibitors, including those that specifically target the KRAS-G12C mutation frequently observed in lung cancers, provides promising therapeutic strategies for KRAS-driven tumours. Although this development is hugely exciting and two KRAS-G12C inhibitors have already entered clinical trials with encouraging initial results [208, 219], drug resistance against these new inhibitors poses a significant challenge that may limit their clinical efficacy. Acquired resistance commonly emerges in response to other RAS pathway targeted therapeutics, and these mechanisms are likely to be seen with these new classes of direct RAS inhibitors. Therefore, understanding the molecular mechanisms involved in the survival of drug resistant cancer cells treated with KRAS inhibitors is critical for helping to develop improved treatment options. If critical signalling pathways involved can be predicted and targeted in patients, there is greater potential for delaying or preventing the emergence of resistance by using appropriate combination therapies. This will enable a more promising approach to personalised treatment for RAS-driven cancers.

Using a panel of KRAS-mutant and KRAS-WT NSCLC cell lines, alongside direct KRAS inhibitors with distinct inhibitory mechanisms and a MEK inhibitor with previously identified resistance, I had the following aims for this project:

- To validate the efficacy of direct KRAS inhibitors in a panel of NSCLC and to generate drug-resistant cell lines.
- To identify gene and protein signatures associated with emerging KRAS inhibitor resistance and to determine potential signalling pathways involved that could also be therapeutically targeted.
- To determine if there are differences in resistance mechanisms between different mechanisms of RAS pathway inhibition.
- To identify potential combination therapies that could delay or overcome the development of acquired resistance.

Chapter 2

Materials and Methods

2.1 Cell Biology

2.1.1 Cell biology reagents

The reagents used in the cell biology experiments are listed in Tables 2.1 - 2.5.

Table 2.1: Reagents used for cell biology

Reagent	Supplier	Catalogue number
RPMI 1640 Medium with Glutamax™	Thermo Fisher Scientific	61870036
Fetal Bovine Serum (FBS)	Thermo Fisher Scientific	10270
Trypsin-EDTA (0.5%)	Thermo Fisher Scientific	15400054
Phosphate buffered saline (PBS)	ThermoFisher Scientific	14200067
CellTitre-Glo ® 2.0 assay	Promega	G9242
CellTox™ Green	Promega	G8743
IncuCyte® Nuclight Rapid Red Reagent	Sartorius	4717
IncuCyte® Cytotox Green Reagent	Sartorius	4633
MOWIOL	Merck	475904
e-Myco™ PLUS Mycoplasma PCR Detection Kit	Boca Scientific	25237

Table 2.2: Details and characteristics of the lung cancer cell lines

Cell line	Source	Tissue	KRAS Mutation	KRAS Dependency
NCI-H358 [H358]	ATCC® CRL-5807™	NSCLC bronchioalveolar carcinoma metastasis	G12C	2D/3D
NCI-H1792 [H1792]	ATCC® CRL-5895™	Pleural effusion metastasis from lung adenocarcinoma	G12C	3D

NCI-H2030 [2030]	ATCC® CRL-5914™	Lymph node metastasis	G12C	2D (partial 3D)
NCI-H2122 [H2122]	ATCC® CRL-5985™ Obtained from AstraZeneca (Cambridge, UK)	Lymphoblastic pleural effusion NSCLC metastasis	G12C	2D (partial 3D)
SW 1573 [SW-1573]	ATCC® CRL-2170™	Epithelial alveolar carcinoma cells	G12C	3D
NCI-H1793 [H1793]	ATCC® CRL-5896™	Epithelial NSCLC adenocarcinoma cells	WT	-
NCI-H1437 [H1473]	ATCC® CRL-5872™ Obtained from AstraZeneca (Cambridge, UK)	NSCLC pleural effusion metastasis	WT	-

Table 2.3: Details of inhibitors used to treat cells.

Inhibitor	Target	Supplier	Catalogue number
Adavosertib	Wee1	Generon	HY-10993
ARS1620	KRAS-G12C	Generon	HY-U0041
AZD0156	ATM	Generon	HY-100016
AZD4547	FGFR1-4	Generon	HY-13330
AZD4785 (ASO)	KRAS	Ionis	n/a
AZD549148 (ASO CTRL)	n/a	AstraZeneca	n/a
AZD5438	CDK1, -2, -9	Generon	A11105
AZD8055	mTOR	Generon	A8214
AZ6813	KRAS-G12C	AstraZeneca	n/a
BAY-293	KRAS-SOS1	Generon	HY-114398
Berzosertib	ATR	Generon	HY-13902
BI-3406	KRAS-SOS1	Generon	HY-125817
Crenolanib	PDGFR	Generon	HY-13223
CP-673451	PDGFR	Generon	HY-12050
Deltarasin	KRAS	Tocris Bioscience	5424
Erlotinib	EGFR	Generon	HY-50896
Everolimus	mTORC1	Generon	HY-10218
Fendiline	KRAS	Santa-Cruz Biotechnology	SC-239988
Flavopiridol	CDK2, -4, -6	Generon	HY-10005
Gefitinib	EGFR	Generon	HY-50895
Infigratinib	FGFR1-4	Generon	HY-13311
Lapatinib	EGFR, ERBB2	Generon	HY-50898
Niraparib	PARP1/2	Generon	HY-10619
NVP-ADW742	IGF-1R, INSR	Generon	HY-10252
Olaparib	PARP1/2	Generon	HY-10162
Palbociclib	CDK4, -6	Generon	HY-50767A
Ribociclib	CDK4, -6	Generon	HY-15777
RMC-4550	SHP2	Generon	HY-116009
Roscovitine	CDK5, -2, cdc2	Generon	HY-30237
Sapanisertib	mTOR1/2	Generon	HY-13328
Selumetinib	MEK1/2	AstraZeneca	n/a
SHP099	SHP2	Generon	HY-100388
Talazoparib	PARP1/2	Generon	HY-16106

Table 2.4 Primary antibodies used for Immunofluorescence

Antibody	Species of origin	Blocking solution	Dilution	Supplier	Catalogue number
E-cadherin (24E10)	Rabbit	5% Marvel/TBST	1:1000	Cell Signalling	3195
N-cadherin	Mouse	5% Marvel/TBST	1:1000	BD Bioscience	610921

Table 2.5 Secondary antibodies used for Immunofluorescence

Antibody	Blocking solution	Dilution	Supplier	Catalogue number
Donkey anti-rabbit Alexa-Fluor™ 594	10% Goat serum/PBS	1:1000	Invitrogen	A21207
Donkey anti-mouse Alexa-Fluor™ 488	10% Goat serum/PBS	1:1000	Invitrogen	A21202

2.1.2 Cell culture

All cell cultures were grown in RPMI 1640 Medium supplemented with 10% fetal bovine serum (FBS). Cells were cultured at 37°C in a humidified incubator at 95% O_2 and 5% CO_2 and were routinely passaged at 80% confluency. For passaging, existing growth medium was aspirated, and the cells washed in room temperature (1X) Phosphate buffered saline (PBS). Cells were then incubated in 1.5ml of pre-warmed 0.5% (1X) trypsin-EDTA at 37°C for 2-4 minutes depending upon the cell line. Detached cells were then re-suspended in fresh pre-warmed growth medium and a 1:5 dilution transferred to a new T75 cell culture flask and cultured at 37°C in a humidified incubator.

2.1.2.1 Mycoplasma testing

All cell lines were tested for mycoplasma contamination. To prepare samples, $5x10^4$ cells were pelleted, washed twice in PBS and resuspended in 100μl of PBS. Samples were then heated for 10 minutes at 95°C, vortexed for 10 seconds and centrifuged at 13,000rpm for 2 minutes. An aliquot was then transferred to a fresh tube and used as PCR template. Samples were processed using the e-Myco™ PLUS Mycoplasma PCR Detection Kit.

2.1.2.2 Cell line storage

To preserve cells for long term storage, cells were trypsinised as above, resuspended in fresh RPMI 1640 medium and pelleted by centrifugation at 120g for 5 minutes. Existing growth medium was aspirated, and the pellet was resuspended in freezing medium (RPMI-1640 with 15% (v/v) FBS and 5% (v/v) DMSO). 1ml of cell suspension was added to each cryovial (Corning) and stored in an insulating freezing container at -80°C overnight. Cryovials were then transferred to liquid nitrogen for long term storage. When required cells were thawed at 37°C in a water bath, resuspended in growth medium and centrifuged as above to remove traces of DMSO. The cell pellet was then resuspended in fresh growth medium and cells transferred to a new T25 cell culture flask (Corning).

2.1.3 Inhibitor treatments

Small molecule inhibitors were dissolved in dimethyl sulfoxide (DMSO) to yield 30mM or 10mM stocks and stored at -80°C. Inhibitors were stable at -80°C for 6 months or -20°C for 1 month. Antisense oligonucleotides were dissolved in phosphate-buffered saline (PBS) to yield 10mM stocks and stored at 4°C with stability under these conditions beyond 1 year. Drug stocks were diluted in growth medium to provide a dosing solution that was applied to cells to yield the final drug concentration. Drug dilutions were prepared to ensure each well contained a final vehicle concentration of 0.1%. Growth medium containing vehicle-only (DMSO or PBS) was used as a control. Cells were treated in triplicates or otherwise stated, and incubated at 37°C at 95% O_2 and 5% CO_2 for the length of time indicated in experiments.

2.1.4 IncuCyte Analysis

For monitoring dose responses, cells were seeded in 96-well TC-treated plates (Corning, #3595) for 2D culture and 96-well cell repellent surface plates (Greiner Bio-One, #650979) for 3D culture. Cells were seeded at a density of 1000 cells per well in 100μl of RPMI-1640 with 10% FBS medium. Spheroid plates were incubated overnight in the IncuCyte S3 (Essen Bioscience) and

2D plates were incubated in the IncuCyte Zoom (Essen Bioscience), both at 37°C inside a humidified incubator at 95% O_2 and 5% CO_2. Cells were allowed to adhere or form spheroids overnight and the following day a 10-fold dilution series of indicated inhibitors were applied to give a final volume of 150µl per well. AZ6813 and Selumetinib were dosed using the HP D300e dispenser, whilst AZD4785 dilutions were dosed manually and cells were incubated in the IncuCyte for 7 days following treatment. Spheroid images were collected every 6 hours and 2D images every 4 hours. Spheroids were analysed using the IncuCyte S3 2018A software (Essen Bioscience) using the spheroid module, whereas 2D cells were analysed using the IncuCyte Zoom 2016A software (Essen Bioscience).

For monitoring inhibitor combination assays, H358-R cells were seeded in 384-well TC-treated plates (Corning, #3712) at a density of 2000 cells per well in 40µl of 10% FBS RPMI-1640 medium. Plates were incubated overnight in the IncuCyte S3 (Essen Bioscience) at 37°C inside a humidified incubator at 95% O_2 and 5% CO_2. The following day H358-R cells were treated with corresponding IC_{90} inhibitor concentrations, IncuCyte® Nuclight Rapid Red Reagent and IncuCyte® Cytotox Green Reagent. A 5-fold dilution series of combination inhibitors were applied, giving a final assay volume of 80µl. Cells were incubated in the IncuCyte for 4 days following treatment and images were collected every 6 hours. Cells were analysed using the IncuCyte S3 2020B software (Essen Bioscience).

For triple combination assays, H358 cells were seeded in 96-well TC-treated plates (Corning, #3595) at a density of 1000 cells per well in 100µl of 10% FBS RPMI-1640 medium. Plates were incubated overnight in the IncuCyte S3 (Essen Bioscience) at 37°C inside a humidified incubator at 95% O_2 and 5% CO_2. The following day H358 cells were dosed manually with inhibitor concentrations to give a final assay volume of 150µl. Cells were incubated in the IncuCyte for 14 days following treatment and were re-dosed with fresh media and inhibitors every 5 days. Images were collected every 6 hours. Cells were analysed using the IncuCyte S3 2020B software (Essen Bioscience).

2.1.5 Cell viability and cytotoxicity assays

Cells were seeded in 96-well black walled TC-treated plates (Corning, #3603) for 2D culture and 96-well black walled ultra-low attachment plates (Corning, #4515) for 3D culture. Cells were seeded at a density of 1000 cells per well in 60μl of 10% FBS RPMI-1640 medium. Cells were allowed to adhere or form spheroids overnight and the following day a 3-fold dilution series of indicated inhibitors were applied to give a final volume of 80μl per well. Cell cytotoxicity and cell viability were measured respectively using a multiplex of the CellTox™ Green assay and the CellTiter-Glo® 2.0 assay. A CellTox™Green (5X) reagent was prepared using a 1:200 dilution of CellTox™Green Dye to Assay Buffer. 20μl of CellTox™Green reagent was added to each well containing 80μl of medium. The plate was mixed on an orbital shaker at 300rpm for 1 minute and incubated for 15 minutes at room temperature. The fluorescence was measured at 485-500nm_{Ex}/520-530nm_{Em} using the GloMax® Plate Reader (Promega) with the built-in CellTox™Green Promega protocol. 100μl of CellTiter-Glo® reagent was then added to each well. For 2D cell cultures the plate was mixed on an orbital shaker at 300rpm for 2 minutes and incubated at room temperature for 10 minutes, whereas for 3D culture mixing was extended to 5 minutes followed by a 25-minute incubation. The luminescence was recorded using the GloMax® Plate Reader (Promega) with the built-in CellTitre-Glo® Promega protocol.

2.1.6 Generation of KRAS inhibitor resistant cell populations (H358-R)

H358 cells were seeded into T75 flasks (1 $x10^6$ cells per flask) and the following day the media was replaced with media supplemented with the indicated concentration of inhibitor. Resistant cell populations were generated using two dosing schedules determined from target engagement assays; a dose escalation starting from the IC_{50} concentration which is doubled at each passage and a constant IC_{90} high concentration. Media changes were carried out every 2-3 days for small molecule inhibitors and every 4-5 days for AZD4785 until the cells reached 80% confluency. The cells were then

trypsinised and re-seeded at the original density and aliquots of remaining cells were prepared for liquid nitrogen storage. IC_{50} dose escalations were continued until the IC_{90} concentration was achieved and cells were then maintained at this concentration (2.63 μmol/L AZ6813, 830 nmol/L ARS1620, 87 nmol/L Selumetinib, 2.34 μmol/L AZD4785). An additional flask where the dose was doubled to above the IC_{90} concentration was also established alongside. The development of emerging resistance was monitored by shifts in the cell viability dose responses treated with increasing drug concentrations (see cell viability and cytotoxicity assays).

2.1.7 Immunofluorescence

Cells were seeded onto sterile 22x22mm coverslips in a 6-well plate. Following treatment, the coverslips were washed twice in PBS and fixed using 4% paraformaldehyde (PFA) in PBS for 15 minutes at RT. The PFA was discarded and the cells washed twice again with PBS, followed by 50mM ammonium chloride for 10 minutes. The coverslips were again washed with PBS three times and then the cells were permeabilised with 0.2% (v/v) Triton X-100 in PBS for 5 minutes at RT. The coverslips were washed three times in PBS and then blocked in 10% (v/v) goat serum in PBS for 30 minutes. The primary antibodies were diluted in 10% (v/v) goat serum in PBS (see Table 2.4) and added to the cells for 1 hour at RT. Following three PBS washes, the cells were incubated with secondary antibodies diluted in 10% (v/v) goat serum in PBS for 20 minutes (see Table 2.5). The coverslips were washed with a final three PBS washes, followed once by MilliPore water, and then mounted onto slides using Mowiol containing DAPI (1:1000 ratio). The slides were left to dry overnight and then visualised on the Zeiss LSM 800 confocal microscope. Images were processed using FIJI software.

2.2 Transcriptomics

2.2.1 Transcriptomics reagents

The reagents used for transcriptomic experiments are listed in Tables 2.6 and 2.7.

Table 2.6: Reagents and kits used for transcriptomics

Reagent	Supplier	Catalogue number
SingleShot Cell Lysis Kit	Bio-Rad	1725080
iTaq Universal SYBR® Green One-Step Kit	Bio-Rad	1725151
RNeasy Mini Kit	Qiagen	74106
RNA 6000 Nano Kit	Agilent	5067-1511
TRIzol	Thermo Fisher Scientific	15596026
Phosphate buffered saline (PBS)	ThermoFisher Scientific	14200067

Table 2.7: qRT-PCR primer sequences

Primer	Sequence (5' – 3')
***KRAS* forward**	GATGTACCTATGGTCCTAGTAG
***KRAS* reverse**	CATCATCAACACCCTGTCTTG
***DUSP6* forward**	CGGAAATGGCGATCAGCAAG
***DUSP6* reverse**	TGTGCGACGACTCGTATAGC
***ACTIN* forward**	CACCTTCTACAATGAGCTGCGTGTG
***ACTIN* reverse**	ATAGCACAGCCTGGATAGCAACGTAC

2.2.2 Quantitative Reverse Transcription PCR (qRT-PCR)

Cells were seeded in 96 well TC-treated plates (Corning, #3595) at a density of 2000 cells per well in 60μl of 10% FBS RPMI-1640 medium. Cells were allowed to adhere overnight and the following day a 3-fold dilution series of indicated inhibitors were applied to give a final volume of 80μl per well. Cells treated with small molecule inhibitors were incubated for 24 hours and those treated with ASO were incubated for 72 hours. Cell lysates were prepared using the SingleShot Cell Lysis Kit. Existing culture medium was removed from each well and cells were washed in 125μl of room temperature PBS. 50μl of SingleShot Cell Lysis Buffer was added to each well and the plate was incubated at room temperature for 10 minutes. Cell lysates were transferred to a 96-well PCR plate, incubated at 37°C for 5 minutes followed by 75°C for

5 minutes and stored at -20°C until required. Cell lysates were used directly in a one-step RT-qPCR reaction using the iTaq Universal SYBR® Green One-Step Kit according to the manufacturer's instructions. Primers that were used are shown in Table 2.7. Reactions were carried out in triplicates with the following reaction mixture and reaction protocol shown in Table 2.8 and Table 2.9. Reactions were run on the CFX Connect™ Real-Time PCR Detection System (Bio-Rad). Gene expression was normalised to *ACTIN* housekeeping gene Ct values and quantified using the comparative Ct (-ΔΔCt) method.

Table 2.8: iTaq Universal SYBR® Green One-Step qRT-PCR reaction mixture

Reagents	Volume
iTaq Universal SYBR® Green reaction mix (2X)	10μl
iScript Reverse Transcriptase	0.25μl
Forward Primer (20μM)	0.3μl
Reverse Primer (20μM)	0.3μl
Cell lysate (RNA Template)	2μl
Water	7.15μl
Total Volume	20μl

Table 2.9: iTaq Universal SYBR® Green One-Step qRT-PCR protocol

Step	No. of cycles	Temperature	Time Duration
Reverse Transcription	1	50°C	10 min
Polymerase Activation and DNA Denaturation	1	95°C	1 min
Denaturation	X 39	95°C	10 sec
Annealing and Extension		60°C	30 sec
Melt	1	T_m gradient (60°C - 95°C) 0.5°C increment	2 – 5 sec per step

2.2.3 RNA-Sequencing

2.2.3.1 RNA extraction

Cells were trypsinised and resuspended in PBS. $2x10^5$ cells were pelleted and resuspended in 1ml TRIzol reagent. Cell lysates in TRIzol were stored at -80°C until required. Cells were thawed at room temperature, 200μl of

chloroform added and centrifuged at 12,000g for 15 minutes. The upper aqueous phase was removed and transferred to a fresh Eppendorf tube. An equal volume of 70% ethanol was added, and samples were immediately loaded onto a RNeasy Mini Spin Column and RNA extraction performed according to the manufacturer's instructions. RNA was eluted in 30μl of RNase free water. A Nanodrop 1000 spectrophotometer (Labtech) was used to assess RNA purity and concentration. RNA integrity was measured using the RNA 6000 Nano Kit according to the manufacturer's instructions and samples run on the Agilent 2100 Bioanalyzer.

2.2.3.2 RNA-Sequencing Quantification Library

RNA-sequencing was performed and bioinformatically analysed by BGI Tech Solutions (Hong Kong) using the Illumina-HiSeq2500/4000 platform. Sequencing reads which contained low-quality, adaptor polluted and high unknown base (N) reads were first filtered out. Clean reads were mapped to the reference genome using HISAT [265]. After genome mapping StringTie [266] was used to reconstruct transcripts and with genome annotation novel transcripts were identified using Cuffcompare. Novel transcripts were then merged with reference transcripts to achieve a complete reference. Clean reads were mapped using Bowtie2 [267] and gene expression levels calculated with RSEM [268]. Based on gene expression levels, possion distribution algorithms were used to detect differentially expressed genes (DEGs).

2.3 Protein biochemistry

2.3.1 Protein biochemistry reagents

The reagents used for protein biochemistry are listed in Tables 2.10 - 2.12.

Table 2.10: Reagents used for protein biochemistry

Reagent	Supplier	Catalogue number
BCA Protein Assay	Pierce Biotechnology	23225
Bovine IgG	Sigma Aldrich	I9640
Protease inhibitor cocktail	Sigma-Aldrich	P8340
PhosSTOP (protease inhibitor cocktail)	Roche-Sigma	4906837001
Tris-Acetate SDS running buffer	Invitrogen	LA0041
NuPAGE MOPS buffer	Invitrogen	NP0001-02
NuPAGE MES buffer	Invitrogen	NP0002-02
Amersham™ full range molecular weight rainbow marker	Sigma Aldrich	GERPN800E
Amersham™ Protran® 0.45µm nitrocellulose membrane	Sigma Aldrich	GE10600002
Ponceau-S	Sigma Aldrich	P7170

Table 2.11: Primary antibodies used for Western Blotting

Antibody	Species of origin	Blocking solution	Dilution	Supplier	Catalogue number
AKT	Rabbit	5% Marvel/TBST	1:1000	Cell Signalling	9272
p-AKT (T308)	Rabbit	5% Marvel/TBST	1:500	Cell Signalling	9275
p-AKT (S473)	Rabbit	5% Marvel/TBST	1:2000	Cell Signalling	4060
β-actin	Mouse	5% Marvel/TBST	1:10000	Proteintech	66009-1-Ig
DUSP6	Rabbit	5% Marvel/TBST	1:500	Abcam	ab76310
ERK1/2	Rabbit	5% Marvel/TBST	1:1000	Cell Signalling	4695
p-ERK1/2 (T202/Y204)	Rabbit	5% Marvel/TBST	1:2000	Cell Signalling	4370
H-Ras	Rabbit	5% Marvel/TBST	1:300	Santa Cruz	sc-520
K-Ras	Mouse	5% Marvel/TBST	1:1000	LifeSpan	LS-C175665-100
MEK1/2	Rabbit	5% Marvel/TBST	1:1000	Cell Signalling	9122
p-MEK1/2 (S217/221)	Rabbit	5% Marvel/TBST	1:1000	Cell Signalling	9154
N-Ras	Mouse	5% Marvel/TBST	1:300	Santa Cruz	sc-31
Ras	Rabbit	5% Marvel/TBST	1:1000	Abcam	ab52939

E-cadherin (24E10)	Rabbit	5% Marvel/TBST	1:1000	Cell Signalling	3195
N-cadherin	Mouse	5% Marvel/TBST	1:1000	BD Bioscience	610921
Vimentin	Rabbit	5% Marvel/TBST	1:1000	Cell Signalling	5741
PDGFRβ	Mouse	5% Marvel/TBST	1:1000	Cell Signalling	3175
p-PDGFRβ (Y771)	Rabbit	5% Marvel/TBST	1:1000	Cell Signalling	3173
FGFR1	Rabbit	5% Marvel/TBST	1:1000	Cell Signalling	9740
p-FGFR1 (Y653/654)	Rabbit	5% Marvel/TBST	1:1000	Cell Signalling	52928
EGFR	Rabbit	5% Marvel/TBST	1:1000	Cell Signalling	4267
p-EGFR (Y1068)	Rabbit	5% Marvel/TBST	1:1000	Cell Signalling	2234
ERBB2	Mouse	5% Marvel/TBST	1:1000	Cell Signalling	2248
p-ERBB2 (Y1221/1222)	Rabbit	5% Marvel/TBST	1:1000	Cell Signalling	2243

Table 2.12: Secondary antibodies used for Western Blotting

Antibody	Blocking solution	Dilution	Supplier	Catalogue number
IRDye®800CW Donkey anti-Mouse IgG	5% Marvel/TBST	1:15000	LI-COR	926-32212
IRDye®800CW Donkey anti-Rabbit IgG	5% Marvel/TBST	1:15000	LI-COR	926-32213
IRDye®680CW Donkey anti-Rabbit IgG	5% Marvel/TBST	1:15000	LI-COR	926-68023

2.3.2 Cell lysis

Cell lysis was performed on ice. The cell culture medium was removed, and the cells were washed twice with ice-cold PBS. Cells were lysed with RIPA buffer (10mM Tris pH7.5, 150mM NaCl, 1% sodium deoxycholate, 0.1% SDS, 1% Triton X-100) supplemented with protease inhibitor cocktail (1:250 ratio) (Sigma-Aldrich) and PhosSTOP phosphatase inhibitors (1:100 ratio) (Roche) for 10 minutes. Cells were scraped and the lysate collected. Lysates were then clarified by centrifugation at 13,000g for 20 minutes at 4°C to pellet insoluble material. The supernatant was transferred to a fresh tube.

2.3.3 Protein quantification and sample preparation

Protein concentration of cell lysates was measured using the Pierce™ BCA assay (Thermo Scientific) according to manufacturer's instructions. A standard curve using bovine IgG (Sigma-Aldrich) was carried out alongside triplicate repeats of sample lysates in a 96 well plate. The BCA reagents A and B were mixed (1:50 ratio) and added to the wells. After 30 minutes incubation at 37°C, the plate was read at OD_{562} using a Thermo Labsystems Multiskan spectrum plate reader. Samples were prepared for western blotting in 5X sample buffer (15% SDS, 321.5mM Tris-HCL pH6.8, 50% Gylcerol, 16% 2-Mercaptoethanol, 1.25% Bromophenol blue) and diluted in RIPA lysis buffer to the desired concentration. Samples were heated at 95°C for 5 minutes and stored at -20°C.

2.3.4 Western Blotting

2.3.4.1 SDS-PAGE

Equal concentrations of protein samples were resolved by SDS-PAGE. Samples were loaded into pre-cast NuPAGE® 4-12% Bis-Tris gels (Invitrogen) using a XCell Sure Lock gel tank (Thermo Fisher Scientific). Gels were typically ran with 1X MOPs SDS running buffer (Invitrogen), although 1X MES SDS running buffer (Invitrogen) was used to separate low molecular weight proteins. The Amersham™ full range molecular weight rainbow marker (Sigma-Aldrich) was ran alongside samples to measure molecular weight. The protein gels were initially ran at 100V until the samples had passed into the gel, then raised to 180V for approximately 1 hour.

2.3.4.2 Protein transfer and immunostaining

Proteins were transferred onto an Amersham™ Protran® 0.45μM pore size nitrocellulose membrane (Sigma) using a Genie blotter system (Idea Scientific). The transfer tanks were filled with transfer buffer (25mM Tris, 192mM glycine, 20% (v/v) methanol) and ran at 0.9A and 24V for 1 hour at RT. The quality of protein transfer was assessed by staining the nitrocellulose membrane with Ponceau-S (Sigma-Aldrich), and then washed multiple times

in PBS to remove the stain. Membranes were then blocked in 5% (w/v) powered milk in Tris-buffered saline with Tween (TBS-T)(10mM Tris pH 7.4, 150mM NaCl, 0.1% (v/v) Tween 20) for 1 hour and then probed with primary antibodies diluted in 5% milk TBS-T at 4°C overnight (see Table 2.11 for dilutions). Membranes were washed three times for 5 minutes with TBS-T to remove unbound antibody and then probed with IRDye® secondary antibodies in 5% milk TBS-T for at least an hour (Table 2.12). Following two 5-minute TBS-T washes and a final TBS (10mM Tris pH 7.4, 150mM NaCl) wash, the membranes were scanned on the LICOR Odyssey® CLx imaging system. Images were analysed using ImageStudio software.

2.3.5 Ras activity assay

Cells were seeded in 15cm dishes and allowed to adhere overnight. The following day cells were treated with inhibitors for the indicated amount of time. The Ras Activation Assay BioChem Kit (Cytoskeleton Inc, #BK008) was used to pull-down active GTP-bound RAS. As according to the manufacturer's instructions, cells ready to harvest were washed with ice-cold PBS, then lysed on ice with cells lysis buffer supplemented with protease inhibitor cocktail. Samples were clarified by centrifugation at 10,000rpm and lysates snap frozen and stored in liquid nitrogen until required. 20μl of lysate was saved for BCA protein quantification. Subsequently samples were equalised to give identical protein concentrations at 1mg/ml. For the pull-down assay, 200μg of cell lysate was added to 30μl of beads and incubated with rotation at 4°C for 1 hour. The beads were pelleted at 5000g at 4°C for 1 minute. The supernatant was removed, and the beads washed with wash buffer. Following centrifugation at 5000g at 4°C for 3 minutes, the supernatant was once again removed, and the beads resuspended in 20μl 2X Laemmli sample buffer and heated at 95°C for 2 minutes. Samples were then analysed by SDS-PAGE and Western Blot using the total sample eluate.

2.4 Proteomics

2.4.1 Reverse Phase Protein Array (RPPA)

Cells were trypsinised, centrifuged and the cell pellets washed twice with PBS. Remaining PBS was removed, and the dry cell pellets stored at -80°C until samples were submitted to the Functional Proteomics RPPA Core Facility at the MD Anderson Cancer Center in The University of Texas. Here samples were serially diluted two-fold for 5 dilutions and arrayed on nitrocellulose-coated slides to produce sample spots. Sample spots were then probed with 466 antibodies by a tyramide-based signal amplification approach and visualised by DAB colorimetric reaction to produce stained slides which were scanned on a Huron TissueScope scanner to generate 16-bit images. Sample spots were identified from the images and the densities quantified by Array-Pro Analyzer 6.3. Relative protein levels for each sample were determined by interpolating each dilution curve produced from the densities of the 5-dilution sample spots using SuperCurve_1.5.0 R script. The relative protein levels were designated as $\log_2$ values which were then normalised for protein loading and transformed to linear values.

Chapter 3

Validating targeted KRAS inhibitors

3.1 Introduction

Since the discovery that *RAS* genes are frequently mutated in a large variety of tumours, the RAS GTPase family have been considered attractive targets for cancer therapeutics and significant efforts have been committed to the development of targeted inhibitors [127, 269]. However direct inhibition of RAS has presented a major challenge, primarily due to a small inaccessible GTP binding pocket which exhibits intrinsically high affinity for GTP, making it difficult to design effective competitive inhibitors. Secondly the smooth protein surface has a lack of known allosteric regulatory sites and pockets that can be targeted [270]. Nevertheless, recent progress has been made in the development of covalent inhibitors that selectively bind to the KRAS-G12C mutant [204]. These compounds directly bind to the chemically reactive thiol group of Cys-12 and project into an adjacent allosteric pocket beneath the effector binding switch-II region. This switch-II pocket (S-IIP) is only accessible in the GDP-bound form of KRAS-G12C. Such compounds were found to impair RAS activity by blocking SOS-mediated nucleotide exchange and altering the relative affinity of KRAS to favour GDP binding, subsequently leading to the accumulation of RAS in its inactive GDP-bound state. This mechanism of action consequently blocks effector and regulatory protein interactions helping to reduce downstream KRAS signalling. Following the initial discovery by Shokat and colleagues, KRAS-G12C targeting compounds were further developed by several groups to improve cellular activity and potency within a drug candidate range [207, 271]. From these successes, pharmaceutical companies Mirati Therapeutics and Amgen have developed their own similar

KRAS-G12C compounds, MRTX849 and AMG 510, which are the first compounds to have entered phase I/II clinical trials for the treatment of KRAS-G12C mutant tumours [208, 209].

Although these compounds show promise, they only have the potential to treat a small subset of KRAS mutant tumours. Nucleic acid-based approaches which are designed according to the target protein gene sequence have the ability of targeting a wider array of RAS oncogenes and present an alternative strategy to small molecule inhibitors [272]. Antisense oligonucleotides (ASOs) are short single-stranded oligodeoxynucleotides that bind to and degrade target mRNA, leading to a reduction in target gene translation and reduced protein expression. Advances in ASO pharmacology and chemistry have yielded new generations of ASO compounds with improved stability and potency, resulting in the progress of ASO-based strategies into therapeutics [214]. For example AZD4785 (Ionis 651987) is an advanced chemistry ASO targeting the KRAS mRNA 3' untranslated region (UTR) and therefore reduces both wild-type and mutant KRAS expression [215]. In preclinical models, AZD4785 demonstrated productive uptake without the need for delivery agents, although anti-tumour responses varied between cell lines as a result of differences in KRAS dependency [215].

Other attempts to target oncogenic RAS include disrupting its cellular localisation given that RAS oncogenic activity is dependent upon its association at the plasma membrane. Farnesyl-transferase inhibitors (FTIs) were the first to be developed, inhibiting the post-translational addition of a farnesyl group onto the C-terminus of RAS required for its membrane association [273]. However, in phase III trials FTIs failed to elicit a clinical benefit for cancers with high frequency KRAS mutations, which was found to be due to alternative prenylation of KRAS4B and NRAS by geranylgeranyl transferase I (GGTase I) retaining membrane association under FTI treatment [38]. In recent years interest in targeting RAS membrane association has increased again following the identification of fendiline, an L-type calcium channel blocker which acts by non-specifically inhibiting acid sphingomyelinase and therefore reducing phosphatidylserine in the plasma

membrane [156, 274]. Another approach to disrupting RAS membrane association has been blocking the prenyl-binding protein phosphodiesterase 6δ (PDE6δ), which regulates RAS trafficking from recycling endosomes or the Golgi to the plasma membrane [155]. Deltarasin, a small molecule inhibitor which binds to the farnesyl-binding pocket of PDE6δ, results in impaired RAS trafficking to the plasma membrane which was shown to disrupt its cellular activity and reduce KRAS mutant tumour growth [275].

Currently the majority of anti-RAS strategies have focused on inhibiting RAS effector pathways as a mechanism of blocking RAS activity, which has led to the development of many selective and potent inhibitors of different RAS effector signalling cascades. At least 11 different classes of RAS effectors have been identified, although the nodes within the RAF-MEK-ERK mitogen activated protein kinase (MAPK) pathway and the PI3K-AKT-mTOR pathway have seen the greatest attention [139, 276]. However due to multiple points of crosstalk and negative feedback loops, single agent inhibition has not been successful clinically and thus combinatorial inhibition has been the primary treatment strategy to delay or overcome potential resistance mechanisms [166].

Despite decades of research, effective anti-RAS therapeutics have yet to successfully reach the clinic but renewed advances in RAS function, new therapeutic strategies and drug design give hope for RAS-directed therapies to be attainable in the not so distant future [269]. However as is the case with most targeted therapeutics, adaptive and acquired resistance is likely to emerge with new classes of direct RAS inhibitors, although this has not yet been formally tested. Decreased drug responsiveness and recurrence of cancer can be caused by pre-existing intrinsic resistance which is present before the administration of treatment or from acquired resistance generated following therapy [217, 218]. RAS effector signalling is highly complex and dynamic, and as is the case with many other RAS pathway inhibitors, compensatory rewiring of signalling and secondary genetic alterations often occur in response to pharmacological inhibition [139]. For example, the reactivation of downstream ERK1/2 signalling is common following both RAFi

and MEKi [75]. In colorectal cancer cells (CRC), acquired resistance to the MEK1/2 inhibitor selumetinib (AZD6244) was shown to develop by intrachromosomal amplification of the driving KRAS-G13D oncogene enabling cells to maintain ERK1/2 activity in the presence of inhibitor [244]. Furthermore, in both KRAS-mutant lung and colon cancer cells, intrinsic resistance to selumetinib was associated with strong PI3K-AKT pathway activation via increased expression and activation of the receptor tyrosine kinase (RTK) ERBB3 [277, 278]. The signalling networks involved in mutant RAS-driven cancers can also be activated by RAS-independent mechanisms such as activation of YAP1 via inactivation of the Hippo signalling pathway, providing an alternative route to cell proliferation and survival [279]. Such preclinical studies have established a strong rationale for multiple pathway inhibition and combinations of MEK and PI3K inhibitors show increased efficacy compared to monotherapy in KRAS-driven tumours [193].

In order to investigate the potential drug resistance mechanisms induced in response to KRAS therapeutics, a selection of direct KRAS inhibitors was validated. Included was AZ6813 (WO2015054572), the only KRAS-G12C inhibitor available at the time of starting, as well as the KRAS antisense oligonucleotide AZD4785 [215], fendiline [156] and deltarasin [275]. By using a variety of KRAS inhibitors, it is also possible to gain insight and compare differences in resistance mechanisms between different approaches of KRAS inhibition. In addition, the MEK1/2 inhibitor selumetinib (AZ6244) was included as part of this comparison in order to represent a clinically approved comparator with known resistance in KRAS mutant cells. This enables the identification of any overlap in KRAS inhibition with resistance associated with downstream MEK inhibition.

In order to understand the molecular mechanisms underlying nascent resistance, there is a need for relevant cancer models and experimental approaches to analyse and recapitulate drug sensitivities, and for *in vitro* and *in vivo* systems to predict clinically relevant resistance mechanisms [280]. Experimental approaches include target-based mutagenesis in cell lines, *in vivo* studies using xenografts or genetically engineered mice, as well as the

gold standard characterisation of patient tumour samples. Primarily one of the most common methods to study drug resistance involves the culturing of drug-sensitive cancer cell lines with the selected inhibitor for an extended period of time until resistant subpopulations that survive and proliferate in the presence of high drug concentrations emerge [281]. Comparison to parental cells enables the genetic and biochemical differences that account for resistance to be identified. Large numbers of cancer cell lines are available and ease of culture and suitability for high-throughput genomic and proteomic analysis makes them favourable models [280]. In order to study RAS therapeutics, additional considerations regarding the cell type and genetic context of cancer cell lines is important, due to the heterogeneity observed between RAS-mutant cancers. Within different cancer types there are striking differences in both the frequency of RAS mutations and the distribution of specific mutations [21].

Aims

In this study a panel of KRAS-G12C mutant and KRAS-WT non-small cell lung cancer (NSCLC) cell lines was used to determine the initial sensitivity to, and development of resistance against, our panel of KRAS targeted inhibitors. Lung cancer cell lines were chosen as a suitable model due to the fact that KRAS-G12C mutations account for 65% of KRAS-mutant lung adenocarcinomas [131]. The high frequency of KRAS-G12C mutations in lung cancer is linked to mutagen exposure from tobacco causing DNA adduct formation and a G-to-T transversion at this mutational hotspot [74]. To generate resistant cell lines two inhibitory doses, an IC50 escalating dose and a constant IC90 dose, will be used in parallel to compare the development of resistance. Following treatment, the surviving resistant cells can be compared to parental cells using cell viability assays to analyse changes in drug sensitivity [282].

Using these approaches, I aimed to:

- Validate the efficacy of a panel of direct RAS inhibitors in NSCLC cells
- Compare drug sensitivities between 2D and 3D cell culture
- Generate drug-resistant cell lines

3.2 Results

3.2.1 Down-regulation of DUSP6 and KRAS mRNA by KRAS inhibitors

Target validation is a crucial step in drug discovery and ensures that the interaction of inhibitors with their target biomolecules is specific and has potential therapeutic benefit. As a first step it was important to establish that the assembled panel of RAS targeted drugs directly engaged with their targets in NSCLC cells as predicted. The measure of substrates or biomarkers that are directly linked to the levels of target can be used as a measure of the level of target inhibition. KRAS mRNA expression was measured for the ASO inhibitor AZD4785 and DUSP6 mRNA expression was measured as a readout for changes in RAS-MAPK pathway activation that would indicate RAS or MEK inhibition. H358 cells (KRAS-G12C) were treated with small molecule inhibitors (AZ6813, deltarasin, fendiline and selumetinib) for 24 hours and with the ASO AZD4785 and a control ASO (CTRL ASO) for 72 hours to ensure maximal knock-down of KRAS mRNA and KRAS protein depletion. mRNA expression was analysed by quantitative reverse transcription polymerase chain reaction (qRT-PCR).

A dose dependent decrease in both KRAS and DUSP6 mRNA expression was observed in cells treated with AZD4785 (Figure 3.1A). This effect was not observed in cells treated with CTRL ASO, which does not bind to any target mRNA, highlighting the dose response is a specific effect of AZD4785 rather than general toxicity of adding increased concentrations of any ASO. The loss of KRAS mRNA expression also corresponded with reduced DUSP6 mRNA expression as expected and confirmed DUSP6 as a suitable choice of biomarker for measuring changes in RAS pathway activation in these cells.

The KRAS-G12C inhibitor AZ6813 also showed a dose dependent decrease in DUSP6 mRNA expression with increasing inhibitor concentration indicating good pathway inhibition and evidence of target engagement (Figure 3.1B). The MEK1/2 inhibitor selumetinib shows a similar albeit more potent dose

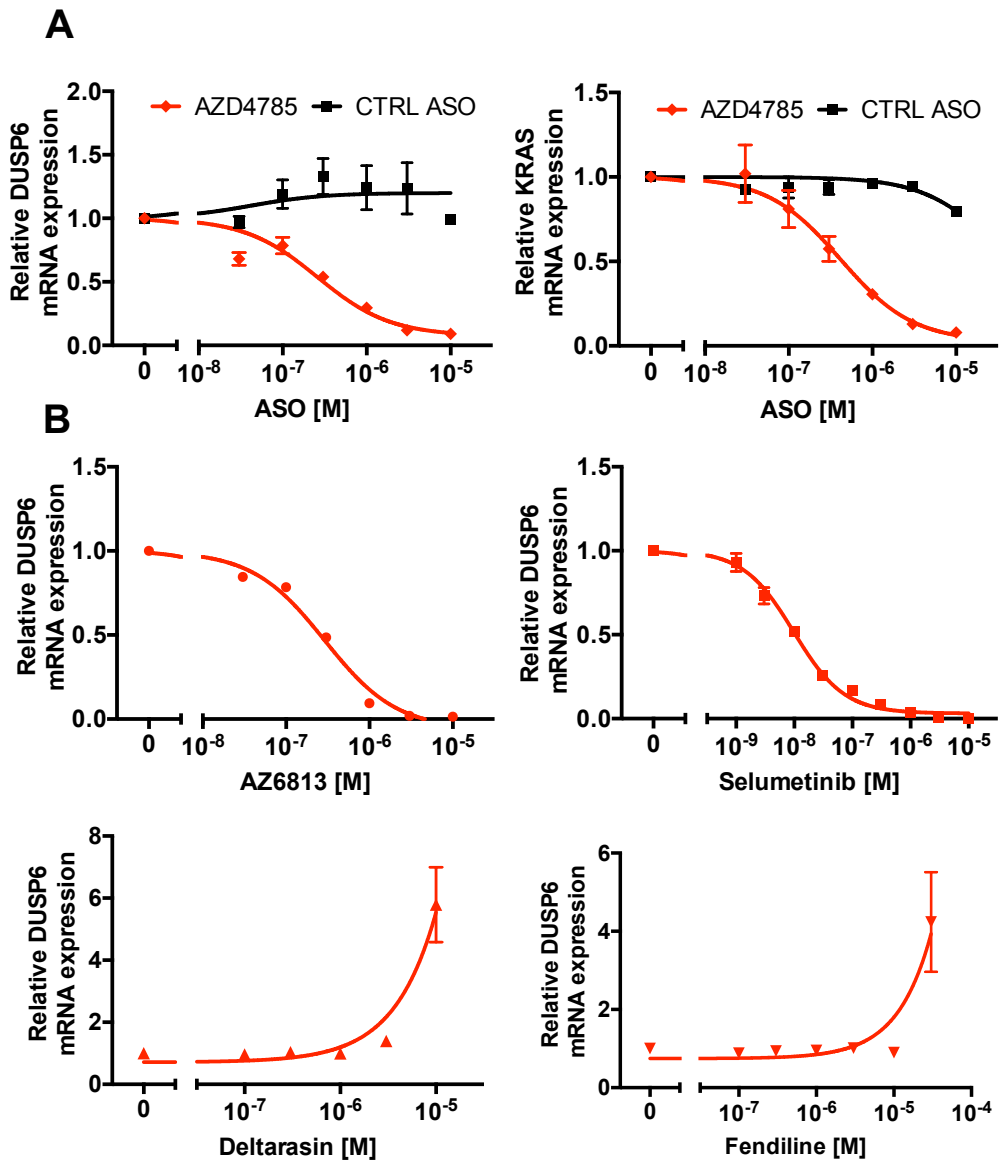

Figure 3.1: Down-regulation of *DUSP6* and *KRAS* mRNA by small molecule inhibitors and ASOs targeting KRAS.

H358 cells were seeded at 2000 cells/well and treated with a dose response of **(A)** ASOs (AZD4785 and CRTL ASO) for 72hrs and **(B)** small molecule inhibitors (AZ6813, selumetinib, Deltarasin and Fendiline) for 24hrs. Relative *DUSP6* and *KRAS* mRNA expression was measured by one-step quantitative reverse transcription PCR (RT-qPCR). Expression is relative to vehicle-only controls and normalised to *ACTIN* mRNA expression. Data shown is presented as means ±SEM from triplicate repeats of two independent experiments.

dependent decrease in DUSP6 mRNA expression. The fact that both AZD4785 and AZ6813 RAS inhibitors follow a similar trend to MEKi provides further confidence of upstream RAS target engagement and moving forward both the IC50 and IC90 concentrations calculated from this assay will be used to establish drug resistant cell lines. No change in DUSP6 mRNA expression was observed with increasing concentrations of deltarasin and fendiline and higher doses >10μM show an off-target effect represented by a dramatic increase of DUSP6 mRNA expression. As a result, fendiline and deltarasin were not included in any further experiments due to the lack of evidence for target engagement.

3.2.2 AZ6813, AZD4785 and selumetinib inhibit cell growth

Having observed good target engagement with three inhibitors (AZ6813, AZD4785 and selumetinib), dose responses in a panel of 7 NSCLC cell lines (see Table 2.2) were carried out in order to determine how effective these inhibitors are at preventing cell growth. Cells were cultured as both 2D and 3D spheroid cultures in order to compare the effect of the inhibitors between growth conditions and to observe any phenotypic issues that would hinder their suitability for making resistant cells. Changes in confluency and spheroid area were monitored using IncuCyte technology over 7 days following inhibitor treatment. A lower concentration range (1μM-0.01μM) was used for selumetinib due to the increased potency of this inhibitor previously observed.

From the 2D assay the majority of cell lines demonstrated a dose dependent inhibitory effect to the three inhibitors, with the exception of SW1573 which appeared particularly insensitive to KRAS-G12C inhibition (Figure 3.2). SW1573 cells also express PIK3CA-K111E; a gain of function mutation which may enable them to be KRAS-mutant independent [283]. However, a higher concentration of 10μM AZ6813 was shown to have a toxic effect on growth of all cell lines, including KRAS-WT cells. Cell confluency and morphology was also observed by microscopy (Figure 3.3). This further highlighted that all cell lines showed fewer cells and reduced confluency with inhibitor treatment compared to vehicle controls, particularly with selumetinib. H2122 cells grew

more slowly compared to the other KRAS-G12C cell lines and were also semi-adherent, making them less desirable to take forward for drug resistance studies.

Cells were then tested for their ability to form 3D spheroids *in vitro* using 96-well round bottom low attachment plates to facilitate cell-cell contact. When grown as spheroids distinct morphologies were also observed between cell lines (Figure 3.4). H358, H1792 and SW1573 cells formed tightly packed round spheroids, whereas H2122 and H2030 were loosely packed and did not form 3D structures, and KRAS-WT cell lines H1437 and H1793 formed spheroids with an irregular shape. Following treatment for 7 days, there were clear differences between vehicle controls (DMSO and PBS) and inhibitor treated cells (Figure 3.5). Firstly, the majority of cells showed a decrease in spheroid size following treatment with 1μM AZ6813 or selumetinib. In line with 2D cell culture, spheroids also appeared most sensitive to selumetinib with the exception of SW1573 cells, which showed reduced sensitivity to selumetinib and an increase in spheroid size. A similar effect is seen with AZD4785 treatment in KRAS-G12C cells in relation to the PBS control, however both KRAS-WT cell lines showed no inhibitory effect and SW1573 cells again showed little change. Furthermore there are often variations in drug responses between 2D and 3D spheroid cultures from differences in drug penetration and exposure, differences in morphology and altered gene and surface receptor expression [284]. This is highlighted by comparison of NSCLC KRAS-G12C cell lines which demonstrate differential sensitivities to RAS pathway inhibition when grown as 3D spheroids and 2D cell culture (Figure 3.6). Overall following the generation of spheroids with different KRAS-G12C cell lines, H358 cells were chosen as the most suitable for subsequent experiments due to their ability to form reproducible spheroids. Other cell lines, particularly H2122 and H2030 demonstrated a lack of cell-cell attachment rendering them unsuitable for spheroid drug resistance experiments.

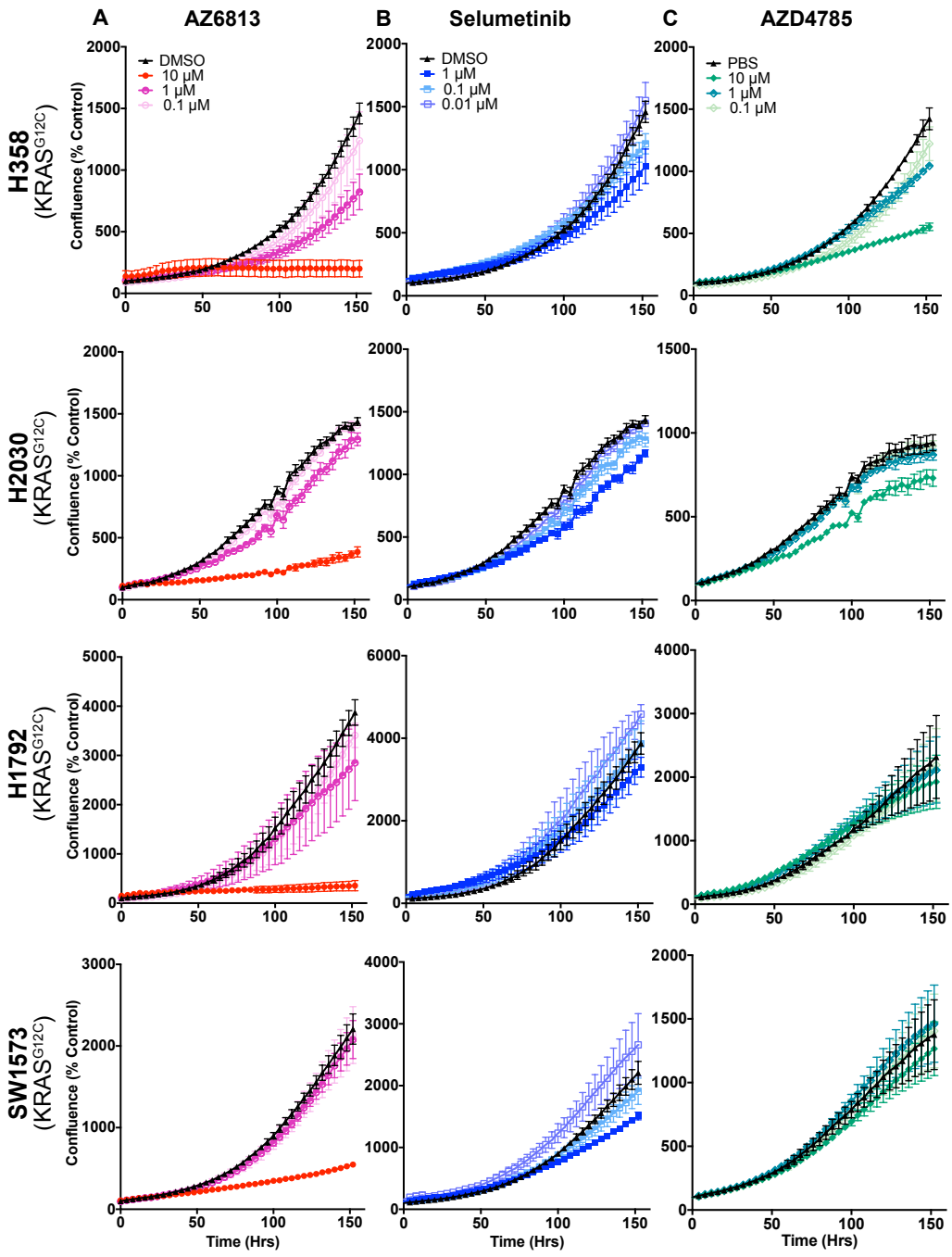

Figure 3.2: Cell confluency after 7 days treatment with small molecule inhibitors or AZD4785.

The growth of 2D cell cultures was measured using IncuCyte technology which monitored cell confluency (%) at 4-hour intervals over a period of 7 days. Cells were treated with concentrations of **(A)** AZ6813, **(B)** selumetinib and **(C)** AZD4785. Graphs are presented as mean percentages of vehicle controls (DMSO or PBS) SEM from duplicates of two independent experiments. Figure continued onto next page.

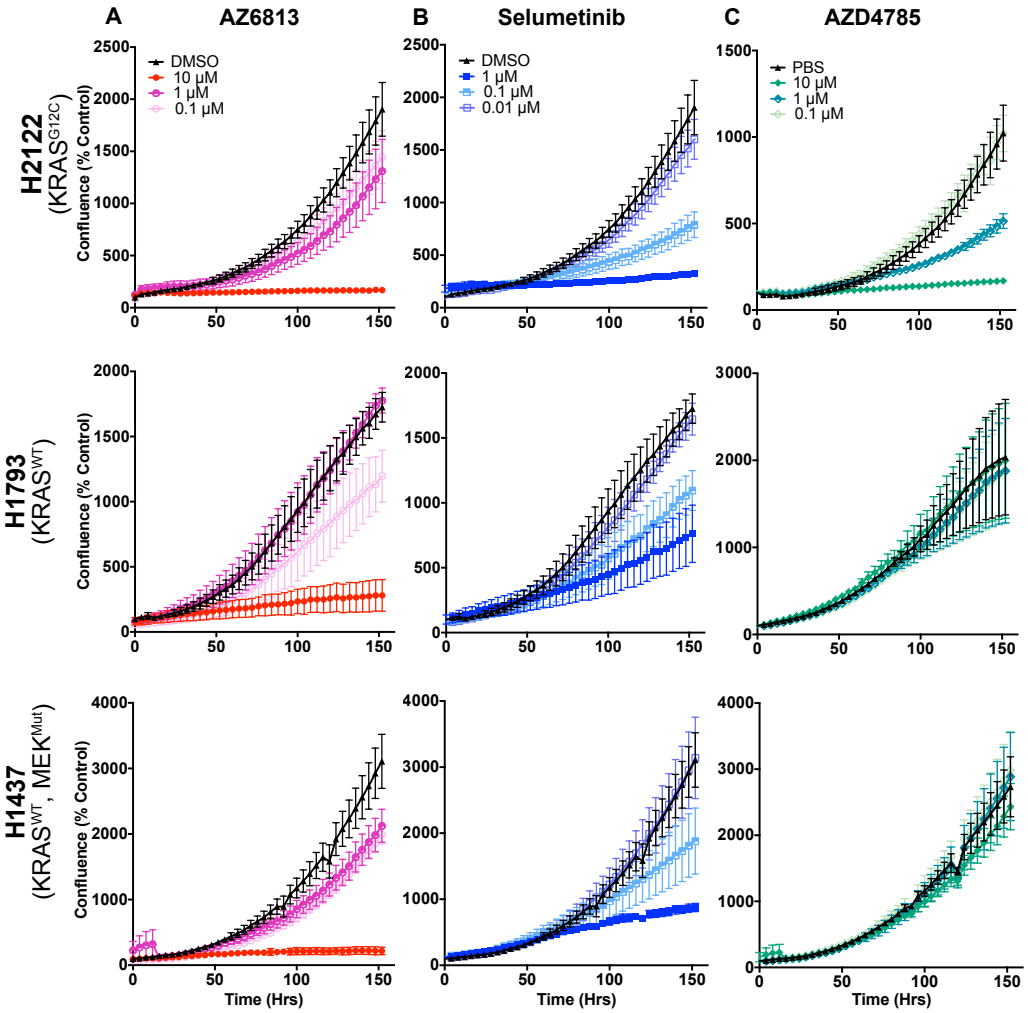
A
AZ6813
B
Selumetinib
C
AZD4785
H2122
(KRASG12C)
H1793
(KRASWT)
H1437
(KRASWT, MEKMut)
Confluence (% Control)
Time (Hrs)
DMSO
10 µM
1 µM
0.1 µM
0.01 µM
PBS

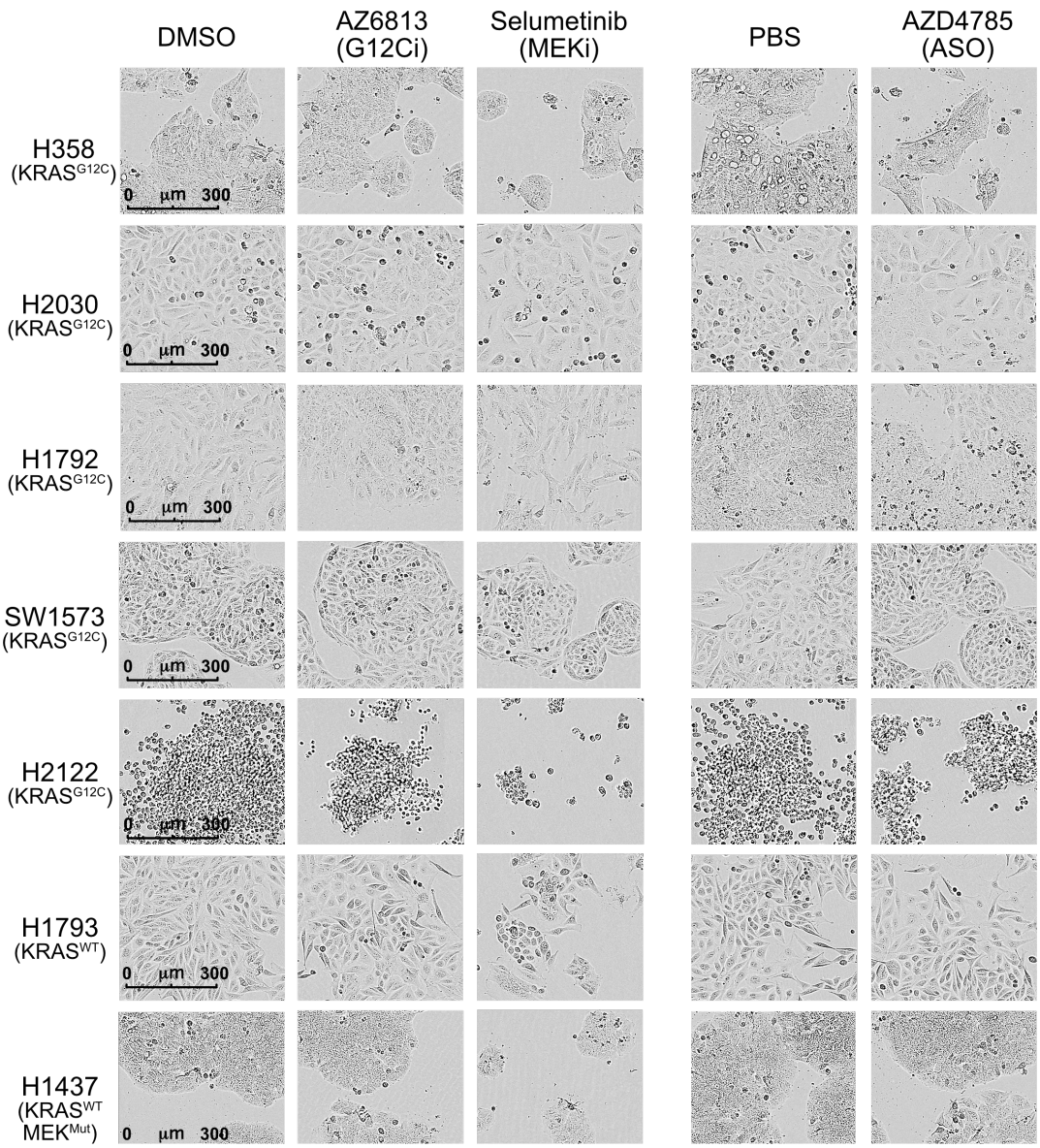

Figure 3.3: KRAS small molecule inhibitors and AZD4785 (ASO) reduce 2D cell confluency and alter cell morphology.

Cells were seeded in 96-well cell plates at 1000 cells/well and treated with a dose response of small molecule inhibitors and AZD4785. Images were taken on the IncuCyte Zoom following 7 days of treatment. A representative figure of two repeats is shown here from cells treated with 1uM AZ6813, 1uM selumetinib, 10uM AZD4785 and 0.1% DMSO/PBS controls.

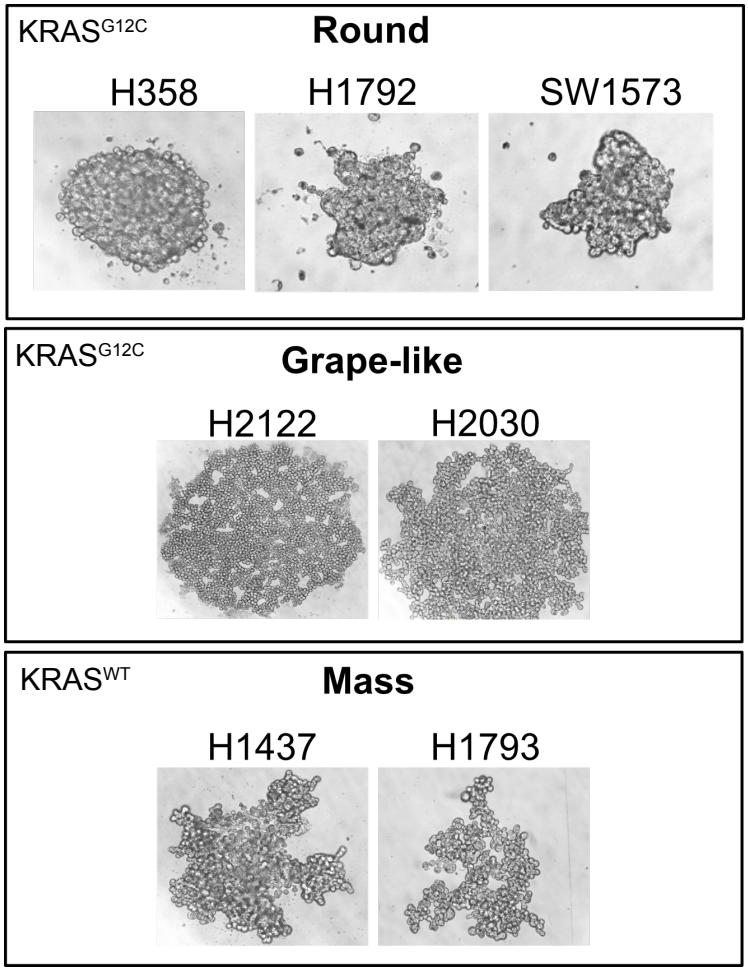

Figure 3.4: Differences in spheroid morphology between lung cancer cell lines.
Images represent 1000 cells seeded in 96-well cell repellent surface plates and incubated on the IncuCyte S3 for 24hrs. A representative figure from three independent experiments is shown here.

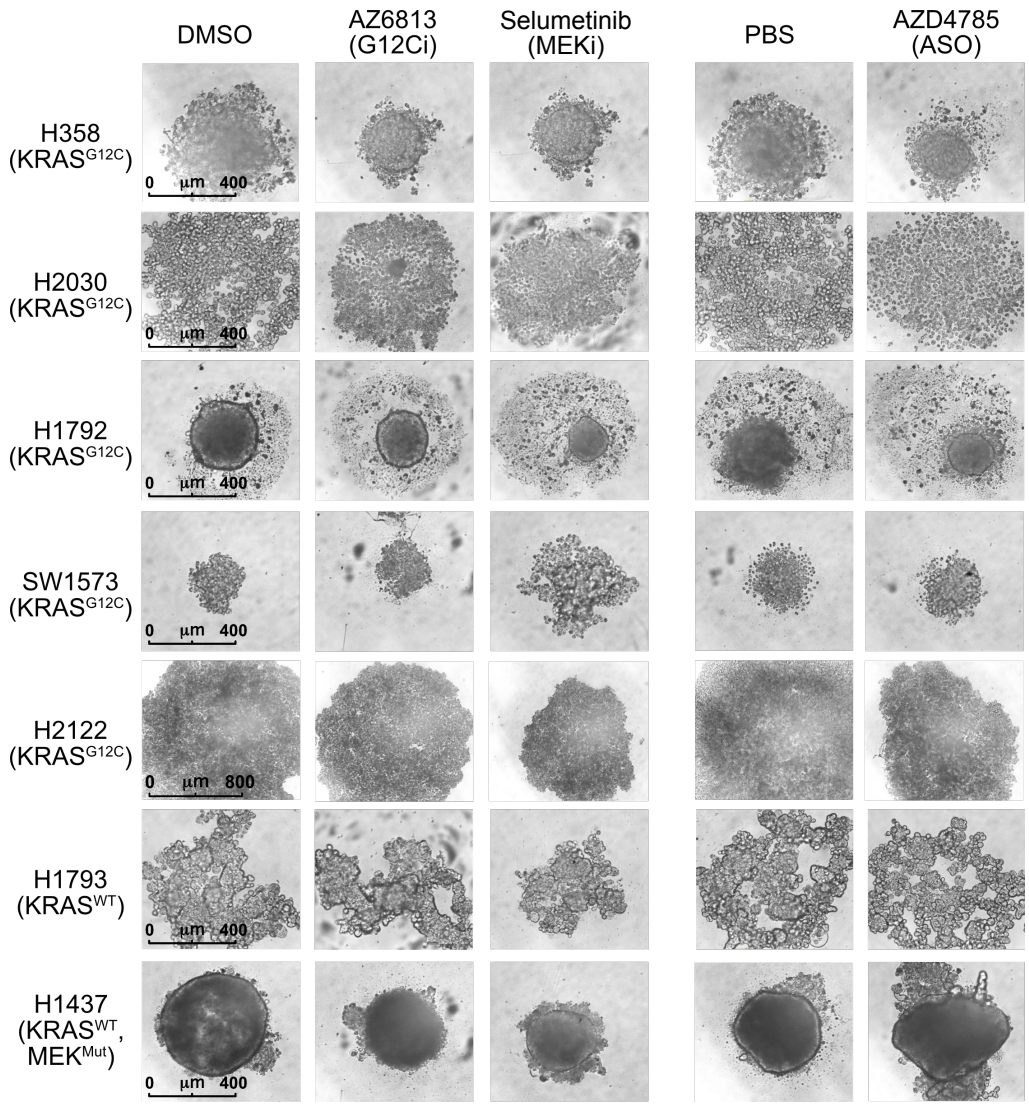

Figure 3.5: Effect of KRAS small molecule inhibitors and AZD4785 (ASO) on spheroid morphology.

Cells were seeded in 96-well cell repellent surface plates at 1000 cells/well and treated with a dose response of small molecule inhibitors and AZD4785 (ASO). Images were taken on the IncuCyte S3 following 7 days of treatment. A representative figure of three repeats is shown here from cells treated with 1uM AZ6813, 1uM selumetinib, 10uM AZD4785 and 0.1% DMSO/PBS controls.

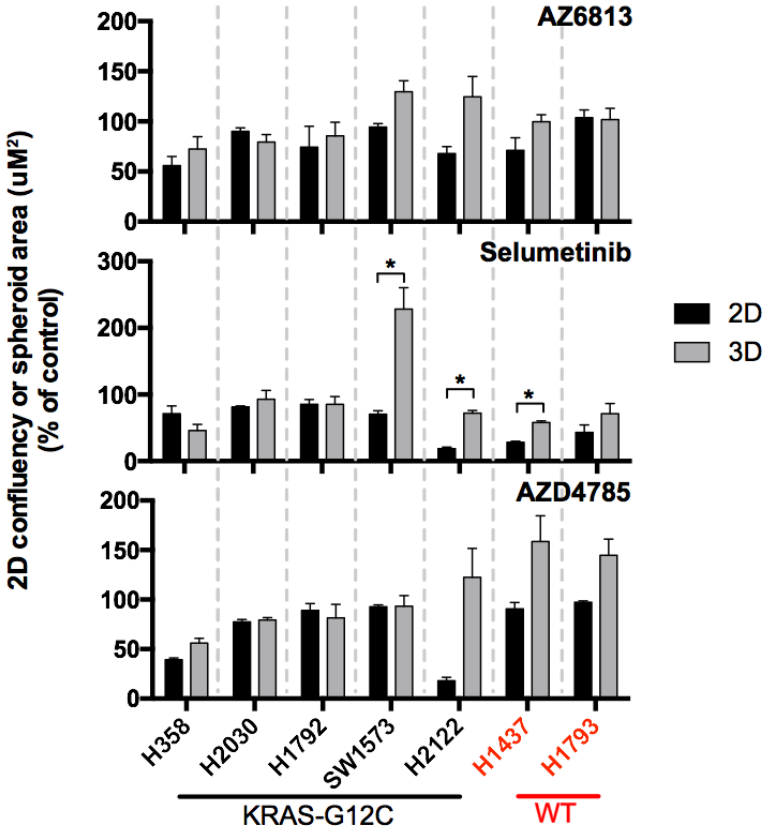

Figure 3.6: Comparison of 2D and 3D spheroid cell growth

NSCLC cell lines grown as 2D adherent monolayers or ultra-low adherent 3D spheroids following 7 days of drug treatment with 1uM AZ6813, 1uM selumetinib, 10uM AZD4785. Graphs are presented as mean percentages of vehicle controls (DMSO or PBS) SEM from duplicates of two-three independent experiments. Statistical analysis using multiple t-tests *p<0.05.

3.2.3 AZ6813, AZD4785 and selumetinib induce cell death

In order to determine whether inhibitors are specifically inducing cell death rather than causing general toxicity to cells, a multiplex of cell viability and cytotoxicity assays were performed on both 2D and 3D cultured H358 cells. The CellTiter-Glo assay (Promega) measures the amount of ATP present as an indicator of metabolically active cells correlating to the number of viable cells. Alternatively, the CellTox Green assay (Promega) binds to DNA of cells with impaired membrane integrity and thus measures cytotoxicity.

In 2D culture both AZ6813 and selumetinib show a similar dose-dependent decrease in cell viability coupled with no change in cytotoxicity at concentrations <10μM, indicating cell growth inhibition (Figure 3.7A). Only at concentrations ≥10μM did the inhibitors, particularly AZ6813, have a cytotoxic effect. AZD4785 also shows a gradual decline in cell viability at concentrations between 300nM and 10μM, however the CellTox Green assay proved incompatible for multiplexing with ASOs due to the assay directly binding to the oligonucleotide. In comparison, H358 spheroids showed greater sensitivity to both AZ6813 and selumetinib observed by the decrease in cell viability IC50 concentrations and increased cytotoxic effect at concentrations >1μM (Figure 3.7B). A shift towards increased sensitivity was also observed with AZD4785 but not with CRTL ASO, highlighting the specificity of this inhibitor.

Cell viability and cytotoxicity assays were then performed on additional lung cancer cell lines grown as spheroids, which are understood to demonstrate greater KRAS dependency when grown under these conditions (Table 2.2). In the KRAS-G12C mutated cell lines H1792 and H2122 all three inhibitors demonstrated good potency from a dose-dependent decrease in cell viability (Figure 3.8). This was also coupled with no change in cytotoxicity for small molecule inhibitors at concentrations <3μM. As seen previously with H358 cells, these other cell lines also showed greater sensitivity to selumetinib. H2030 cells also showed a decrease in viability with increasing inhibitor dose although demonstrated similar sensitivity to both AZ6813 and selumetinib. These cells also appeared less sensitive to AZD4785 in comparison. Corresponding with the previous spheroid Incucyte analysis in section 3.2.2, SW1573 cells also showed increasing viability with selumetinib concentrations ≤3μM, and similarly with AZ6813 and AZD4785 little or no change in viability was observed, highlighting that this cell line is particularly insensitive to these inhibitors. In comparison the control KRAS-WT cell line H1793 showed no change in cell viability and cytotoxicity, indicating the specific action of AZ6813 and selumetinib to induce cell death in mutated KRAS cell lines.

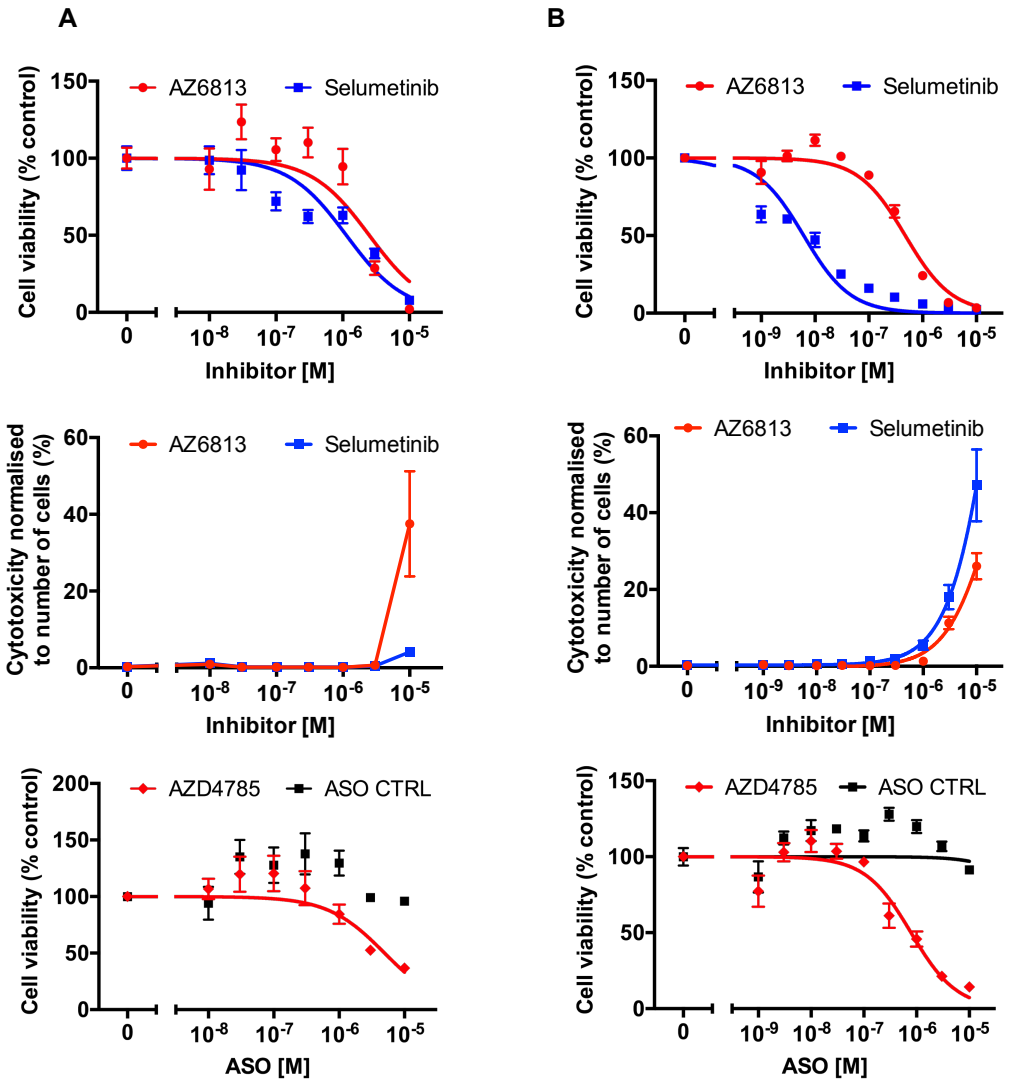

Figure 3.7: Spheroid H358 cells demonstrate greater sensitivity to KRAS inhibitors than 2D cultures.

H358 cells were seeded as **(A)** 2D cell cultures and **(B)** 3D spheroid cell cultures at 1000 cells/well and treated in triplicates with a dilution series of AZ6813, Selumetinib, AZD4785 and ASO CTRL. Cell viability and cytotoxicity were measured following 7 days of treatment. Graphs are presented as mean percentages of vehicle controls ±SEM from two-three independent experiments.

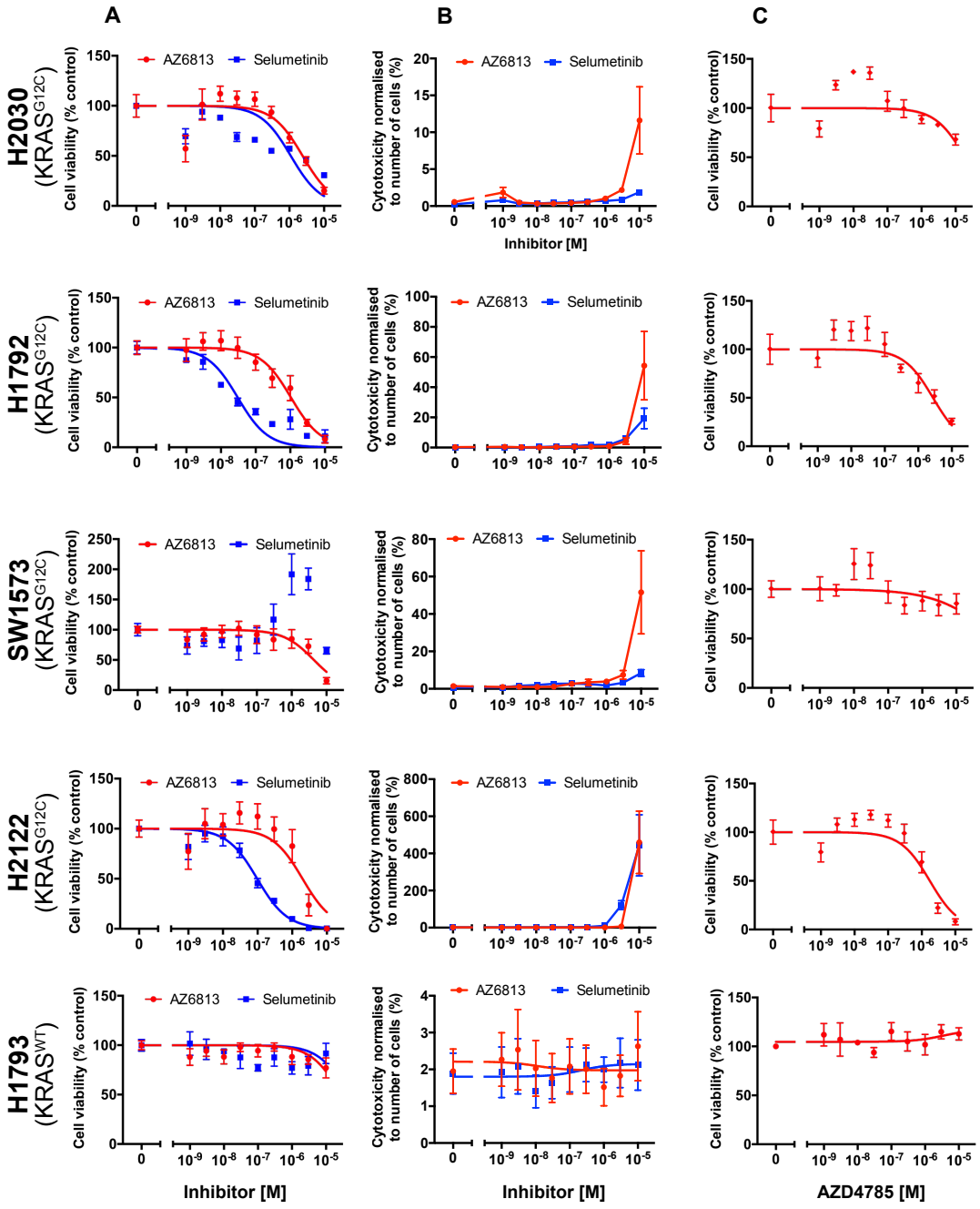

Figure 3.8: 3D spheroid dose responses of KRAS small molecule inhibitors or AZD4785 (ASO) in additional cell lines.

Cells were seeded as 3D cell cultures at 1000 cells/well and treated with concentrations of small molecule inhibitors and AZD4785. (A) Cell viability and (B) cytotoxicity of cells treated with AZ6813 and Selumetinib. (C) Cell viability of cells treated with AZD4785. Measurements were recorded following 7 days of treatment. Graphs are presented as mean percentages of vehicle controls ±SEM from triplicates of two independent experiments

3.2.4 ARS-1620 is a more potent KRAS-G12C inhibitor

Since the KRAS-G12C inhibitor AZ6813 demonstrated evidence of off-target toxicity from both the dose response in KRAS-WT cells lines (Figure 3.2) and increased cytotoxicity at concentrations ≥10μM across all cell lines (section 3.2.3), an additional KRAS-G12C inhibitor was validated. ARS1620 is a second-generation S-IIP binding KRAS-G12C small molecule inhibitor which has improved potency and pharmacological properties [271]. The addition of a fluorophenol hydrophobic binding moiety revealed an additional interaction to His-95 and a more favourable covalent interaction compared to prior compounds [271].

Firstly, ARS1620 showed a more potent down-regulation of DUSP6 mRNA expression in H358 cells (Figure 3.9) with a reduced IC50 concentration compared to the dose response observed previously with AZ6813 (Figure 3.1B). This indicated improved pathway inhibition and evidence of target engagement.

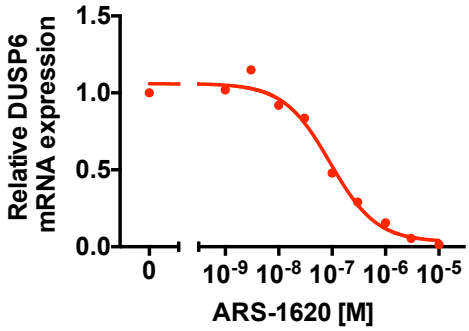

Figure 3.9: Down-regulation of *DUSP6* by ARS-1620.
H358 cells were seeded at 2000 cells/well and treated with a dose response of ARS-1620 for 24hrs. Relative *DUSP6* mRNA expression was measured by one-step quantitative reverse transcription PCR (RT-qPCR). Expression is relative to vehicle-only controls and normalised to *ACTIN* mRNA expression. Data shown are presented as means from triplicate repeats of two independent experiments.

ARS1620 also showed a greater decrease in cell viability with increasing concentration in 2D H358 cells, although toxicity was still observed at concentrations ≥10μM (Figure 3.10). Consistent with previous observations, spheroid H358 cells showed increased sensitivity to ARS1620 by a decrease in cell viability IC50 and increased cytotoxic effect at concentrations >1μM (Figure 3.10, Table 3.1). A dose response of ARS1620 was also carried out in KRAS-WT cell lines, H1793 and H1437, grown as both as 2D and 3D spheroid cultures (Figure 3.10). In both cell lines no effect of ARS1620 on cell viability and cytotoxicity was observed at concentrations <10 μM.

Going forward, the KRAS-G12C inhibitor ARS1620 was included in further experiments and despite displaying off-target toxicity, AZ6813 was still included as it enabled a comparison between two KRAS-G12C inhibitors with similar mechanisms of action but differing potencies.

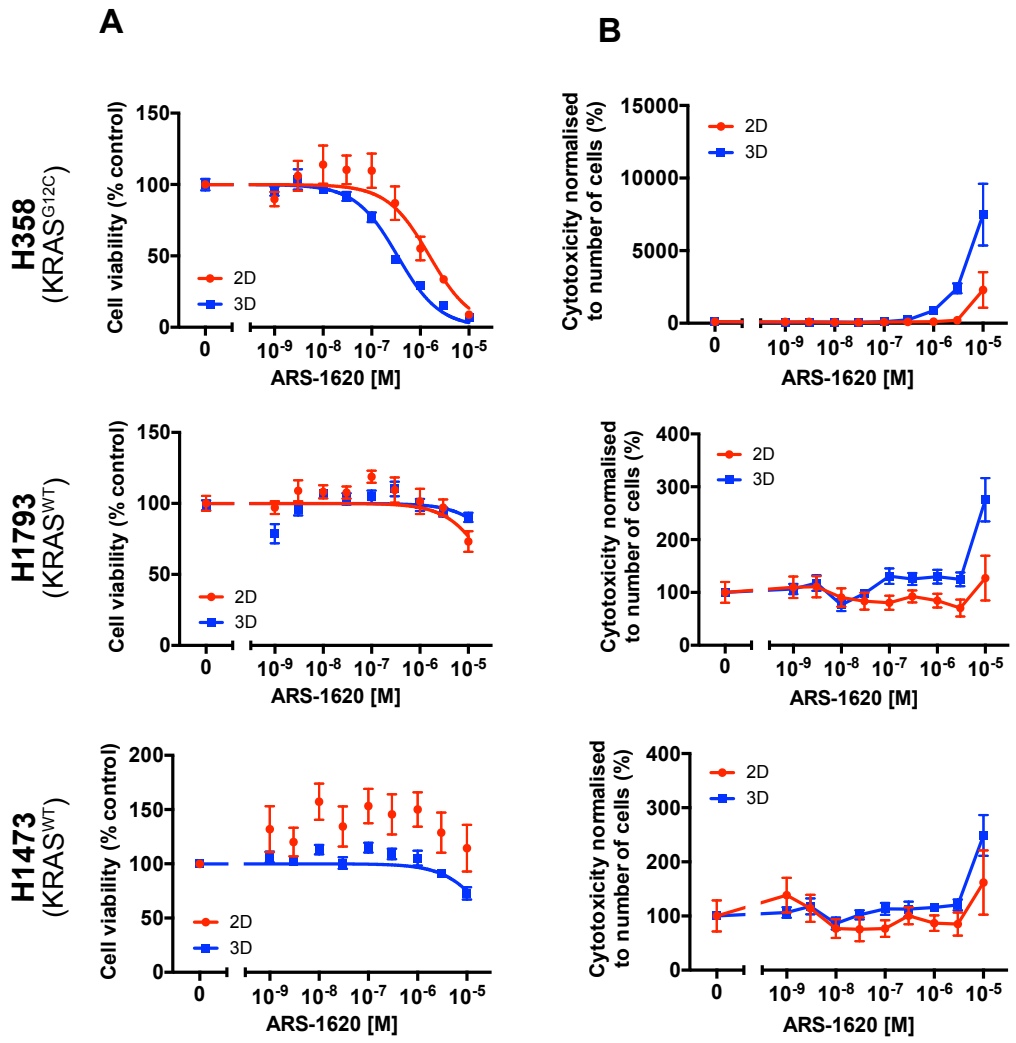

Figure 3.10: 2D versus 3D cell viability and cytotoxicity responses of ARS1620 in KRAS-G12C mutant and KRAS wild type cell lines.

H358, H1793 and H1437 cells were seeded as 2D cell cultures and 3D spheroid cell cultures at 1000 cells/well and treated in triplicates with a dilution series of ARS-1620. Cell viability **(A)** and cytotoxicity **(B)** were measured following 7 days of treatment. Graphs are presented as mean percentages of vehicle controls from triplicate repeats of two-three independent experiments.

3.2.5 Generation of resistant H358 cells

To identify an appropriate inhibitor concentration for treating cells to generate resistance, the IC50 and IC90 concentrations from the target engagement, 2D and 3D viability assays of H358 cells were compared (Table 3.1). H358 cells were chosen as a suitable cell line to start generating resistance due to their observed KRAS dependency in both a 2D and 3D context. Comparison between 2D and 3D viability assays showed the IC50 and IC90 of spheroids were approximately 4-fold, 5-fold and 6-fold less for ARS1620, AZ6813 and AZD4785 respectively, whereas a dramatic decrease of approximately 175-fold is observed for selumetinib. On the other hand, 3D and target engagement assays showed the most similar concentrations with <2-fold differences between the assays for AZ6813, AZD4785 and selumetinib. Whereas ARS1620 displayed a greater difference between these two assays, showing more potent pathway inhibition compared to decreased spheroid viability. Overall, it was decided that the pathway inhibition IC50 and IC90 concentrations would be the most appropriate to use going forward, knowing that at these concentrations, pathway inhibition and good target engagement is achieved, as well as a decrease in cell viability without off-target toxicity.

Table 3.1: Comparison of IC_{50} and IC_{90} concentrations between assays for H358 cells

Inhibitor	Pathway Inhibition		2D Viability		3D Viability	
	IC50 (μM)	IC90 (μM)	IC50 (μM)	IC90 (μM)	IC50 (μM)	IC90 (μM)
AZ6813	0.29	2.63	2.5	22.4	0.48	4.27
ARS1620	0.092	0.83	1.55	13.80	0.34	3.09
AZD4785	0.42	3.72	4.95	44.7	0.79	7.08
Selumetinib	0.0097	0.087	1.1	10.2	0.0062	0.055

To generate resistant H358 cells (H358-R) two independent dosing schedules were carried out for each inhibitor using either a dose escalation starting from the IC50 concentration or a constant IC90 dose. Following challenge with inhibitor dose responses, the IC90 treated H358-R cells showed the better resistance profile from increased cell viability in comparison to naïve cells, and as a result these cells were continued to be treated. A timeline of H358-R generation using IC90 inhibitor concentrations is presented in Figure 3.11 for each inhibitor. All of the H358-R cells maintained resistance to the corresponding inhibitors over time. This was observed by comparing the IC50 concentration between inhibitor treated and naïve cells at each time point, which resulted in a high fold-resistance change of at least ~ 100-fold (Appendix 1). There were some occasions when no change in viability was observed when the cells were assayed, specifically Batch 1 AZ6813 Day 88 (Figure 3.11A), AZD4785 Day 88 (Figure 3.11D) and Selumetinib Day 75 (Figure 3.11E). However successive viability assays continued to show altered drug sensitivity as expected and so these observations were likely to be due to anomalous assays. The time points when cells were thawed was also recorded as some effects from thawing were observed, particularly with AZD4785 treated cells which took much longer to recover from this process. This is demonstrated by the increased time until these cells were ready for the next passage. Importantly all H358-R cell lines did recover following thawing and resistance was retained. A summary of the different cell lines that have been generated and that will be used going forward are presented in Table 3.2.

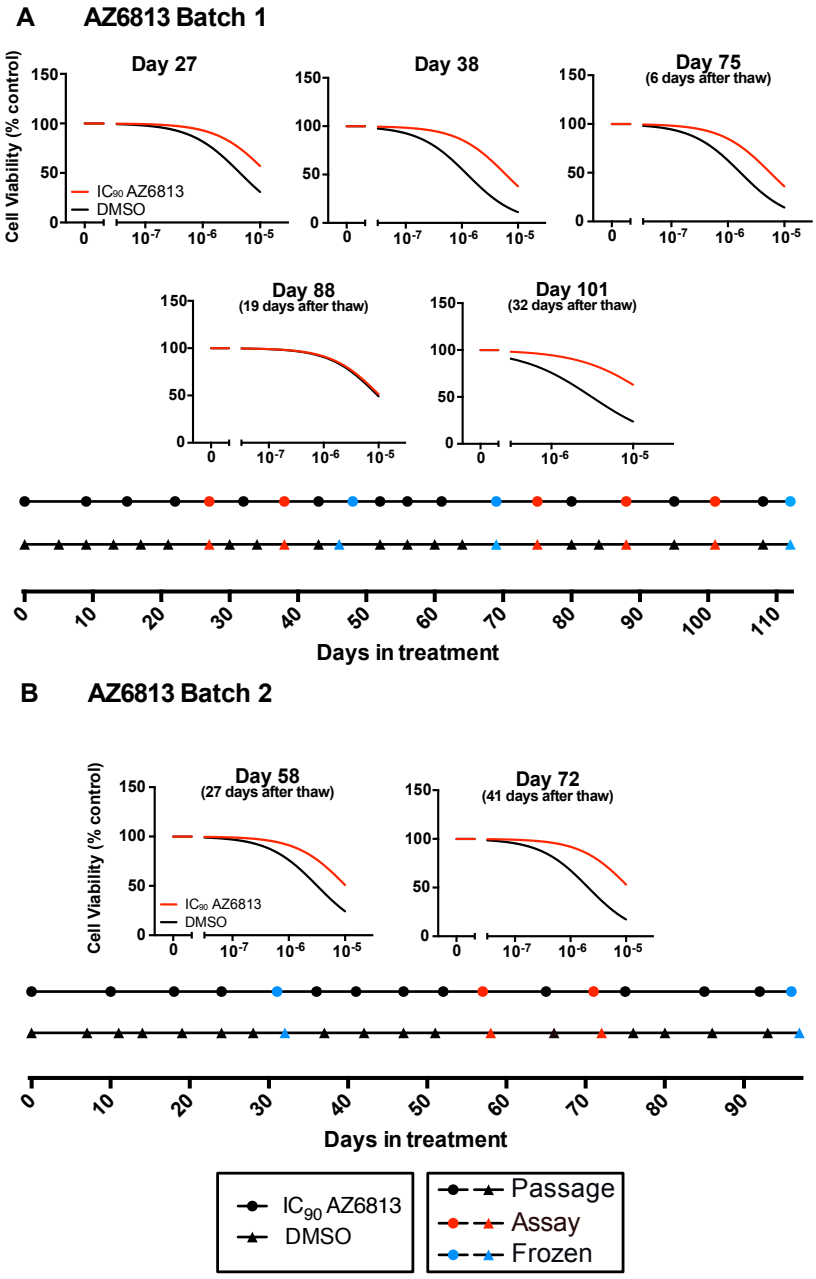

Figure 3.11: Generation of AZ6813, ARS1620, AZD4785 and selumetinib, H358-R cells. Batches of AZ6813 **(A)(B),** ARS1620 **(C)**, AZD4785 **(D)** and selumetinib **(E)(F)** H358 resistant cells were generated by continuously treating cells with an IC90 concentration of each respective inhibitor or vehicle control. Each point on the timelines represents when cells were passaged after reaching confluency. Over time these cells were assayed to determine changes in cell viability when treated with varying concentrations (10nM-10uM) of each respective inhibitor. The time of assay is marked red on the corresponding timeline and the time point where cells were frozen and later thawed is marked blue. Cell viability assays were performed using CellTiter-Glo (Promega) and each inhibitor dose was carried out in duplicates. Cell viability graphs are presented as mean percentage of vehicle control from a single experiment. Figure continued on next two pages.

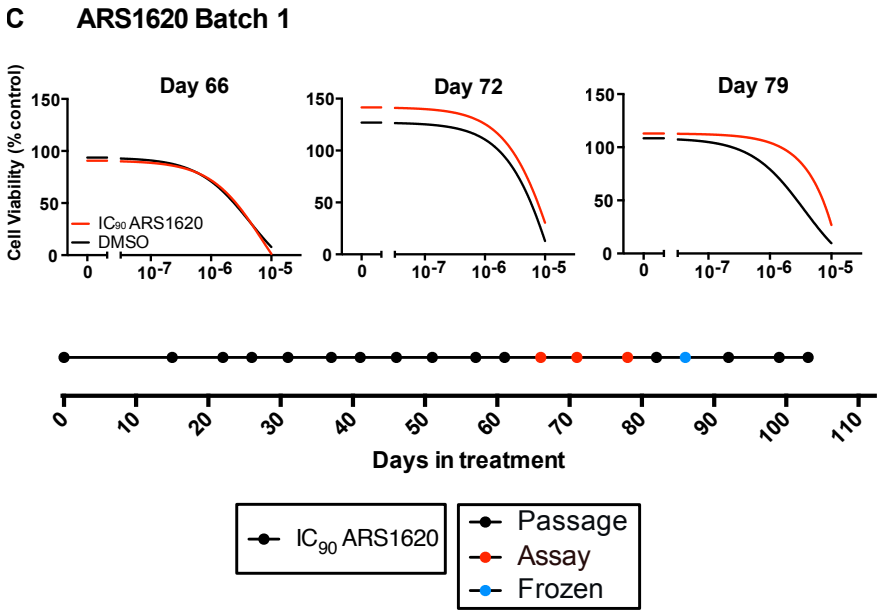
C
ARS1620 Batch 1
Day 66
Day 72
Day 79
Cell Viability (% control)
IC90 ARS1620
DMSO
Days in treatment
IC90 ARS1620
Passage
Assay
Frozen

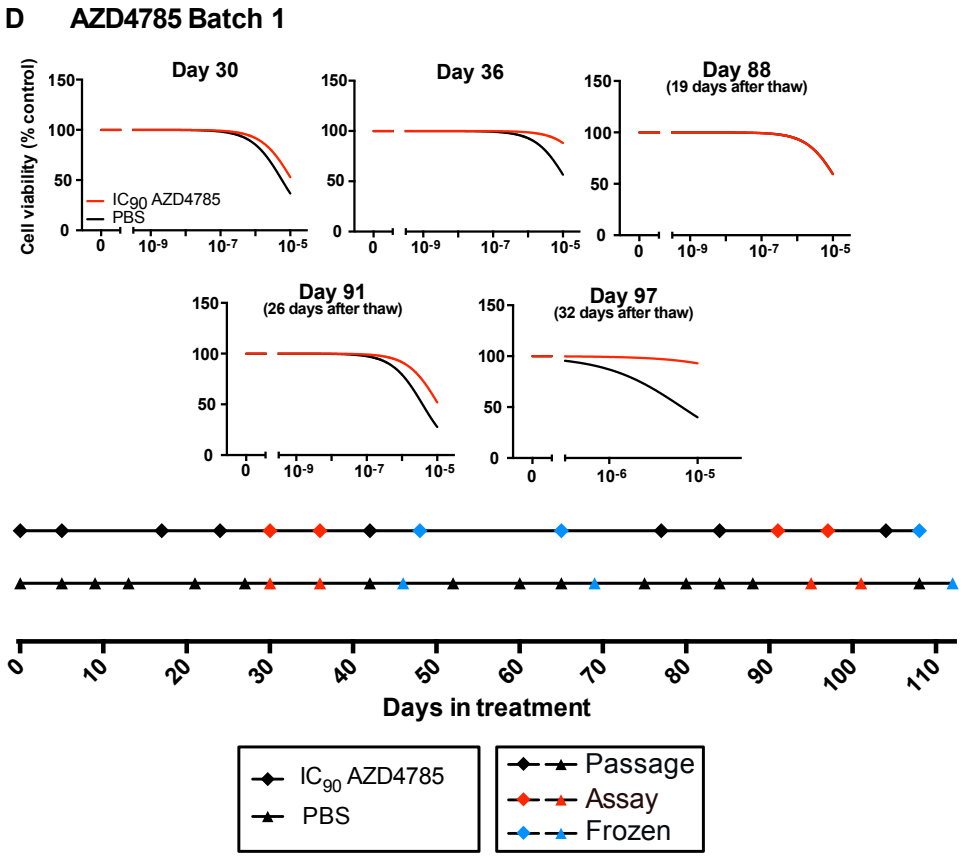
D
AZD4785 Batch 1
Day 30
Day 36
Day 88
(19 days after thaw)
Day 91
(26 days after thaw)
Day 97
(32 days after thaw)
Cell viability (% control)
IC90 AZD4785
PBS
Days in treatment
IC90 AZD4785
PBS
Passage
Assay
Frozen

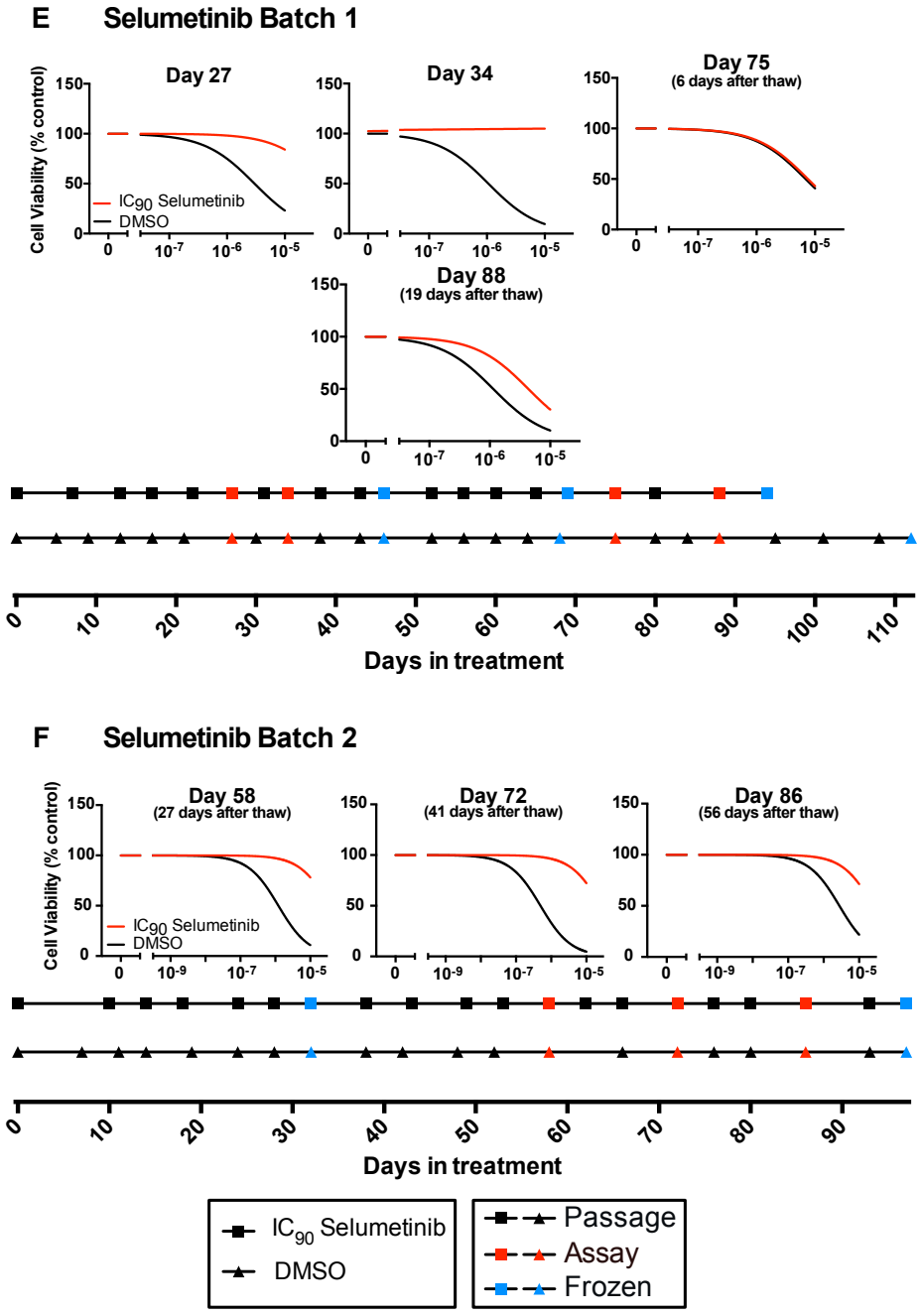
E
Selumetinib Batch 1
Day 27
Day 34
Day 75
(6 days after thaw)
Day 88
(19 days after thaw)
Cell Viability (% control)
IC90 Selumetinib
DMSO
Days in treatment
F
Selumetinib Batch 2
Day 58
(27 days after thaw)
Day 72
(41 days after thaw)
Day 86
(56 days after thaw)
Cell Viability (% control)
IC90 Selumetinib
DMSO
Days in treatment
IC90 Selumetinib
DMSO
Passage
Assay
Frozen

Table 3.2: Summary of different cell lines generated and relevant treatments.

Name of cell line	Number of Batches	Total number of days treated with inhibitor or vehicle
H358-R (long-term resistant)		
H358-R AZ6813	2	112, 96
H358-R ARS1620	1	103
H358-R AZD4785	2	108, 81
H358-R selumetinib	2	94, 97
H358-R selumetinib_DMSO	1	69 days Selumetinib followed by 32 days DMSO
H358-R DMSO	2	112, 97
H358-R PBS	2	112, 97
H358-A (acute)		
H358-A AZ6813	-	7 days AZ6813
H358-A ARS1620	-	7 days ARS1620
H358-A AZD4785	-	7 days AZD4785
H358-A Selumetinib	-	7 days selumetinib
H358-A DMSO	-	7 days DMSO
H358-A PBS	-	7 days PBS

3.2.6 Monitoring RAS pathway changes over time as an indication of resistance development

To monitor the response of resistance over time, changes in protein abundance of major RAS pathway components were analysed by immunoblotting. The different RAS isoforms, along with the RAS downstream effectors DUSP6, ERK, MEK, AKT and their phosphorylated counterparts were analysed. To measure phosphorylated AKT, two phosphorylation sites were detected, Thr-308 (T308) which is phosphorylated by PDK1, and Ser-473 (S473) phosphorylated by the mTORC2 complex [99, 285].

In order to determine how quickly resistance was emerging following inhibitor treatment, an initial time course of inhibitor treatment was carried out for a

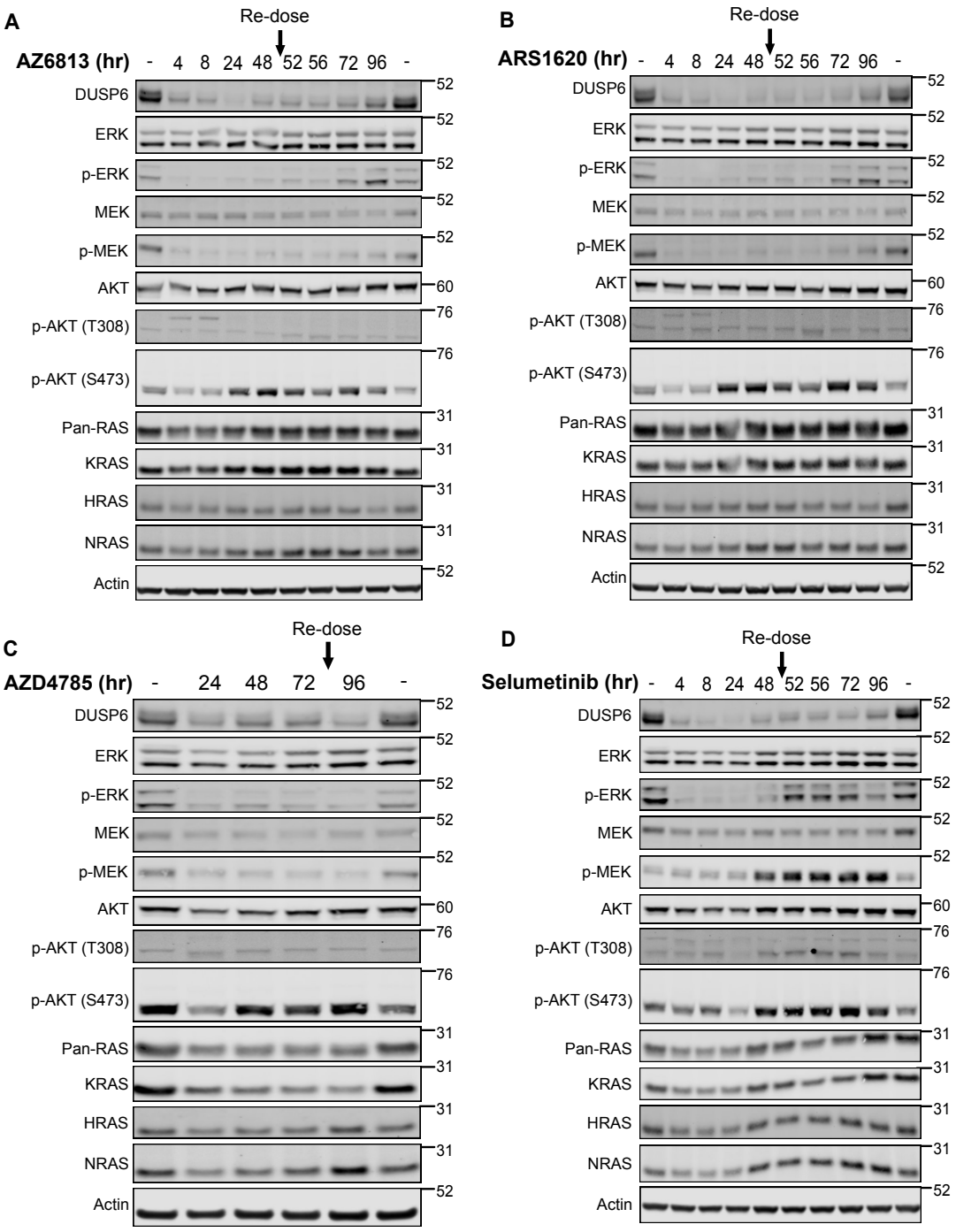

Figure 3.12: Acute inhibitor time course over 96hrs in H358 cells.

H358 cells were treated with vehicle control (-) or IC90 concentrations of each inhibitor **(A)** AZ6813, **(B)** ARS1620 **(C)** AZD4785 and **(D)** Selumetinib for a total period of 96hrs. Cells were re-dosed after 48 hours and lysates prepared at the indicated time points. Ras pathway components were analysed by immunoblotting. Results are from a single experiment.

total of 96 hours, with a drug re-dose at 48 hours (Figure 3.12). Treatment with the KRAS-G12C inhibitor AZ6813 showed an initial decrease in levels of DUSP6, p-ERK, p-MEK and p-AKT(S473) (Figure 3.12A). Reduced p-MEK abundance was maintained throughout the time course, whereas p-AKT(S473) levels began to increase at 24 hours, p-ERK at 72 hours and DUSP6 at 96 hours. On the other hand, no changes in RAS isoform protein expression was observed. Changes in protein levels were similar for cells treated with the other KRAS-G12C inhibitor ARS1620 (Figure 3.12B). Treatment with AZD4785 also showed an initial decrease in DUSP6, p-ERK, p-MEK and p-AKT(S473) abundance, although of these only p-AKT(S473) levels began to increase again at 48 hours (Figure 3.12C). As expected KRAS protein expression decreased with this treatment, although unexpectedly an initial decrease in NRAS was observed which then increased again at 96 hours. In comparison treatment with selumetinib showed an initial decrease in DUSP6, p-ERK and p-MEK abundance although no initial change in pAKT(S473) levels (Figure 3.12D). Protein levels started to increase again following 48 hours for DUSP6, p-MEK and p-AKT(S473) and 52 hours for p-ERK.

In order to determine if these acute changes in RAS pathway protein levels were maintained over time, an extended time course of 10 days with repeated inhibitor dosing every 48 hours was carried out (Figure 3.13). The previously generated long-term cultured H358-R cells were used as a comparison. Treatment with AZ6813 replicated the initial decrease in DUSP6, p-ERK, p-MEK and p-AKT(S473) abundance (Figure 3.13A) previously observed with acute 4-day treatment (Figure 3.12). DUSP6, p-ERK and p-AKT(S473) abundance appeared to fluctuate a little, although generally protein levels increased following 4 days of treatment, and by day 8 matched similar protein levels of the long-term chronically treated cells. Again, a similar pattern of protein abundance changes was observed for cells treated with ARS1620 (Figure 3.13B). With the addition of AZD4785, no initial change in DUSP6, p-MEK or p-AKT(S473) abundance was observed, whereas p-ERK levels decreased more slowly following 24 hours (Figure 3.13C). However, at day 6, both p-ERK and p-AKT(S473) protein levels increased which was again

maintained throughout the remaining time course and matched the protein levels of the long-term treated cells. With selumetinib treatment protein levels of p-ERK, p-MEK and p-AKT(S473) started to increase at day 2 and also matched levels of chronically treated cells (Figure 3.13D).

Overall these two independent time courses of inhibitor treatment highlight that mechanisms of pathway rewiring and potential resistance started occurring within days of the cells being treated, and that the elevated expression levels were generally maintained and matched similar levels of long-term chronically treated H358-R cells. Furthermore, the addition of fresh inhibitor every 48hrs did not prevent p-ERK rebound, indicating that the loss of pathway inhibition was not due to drug metabolism or instability over time.

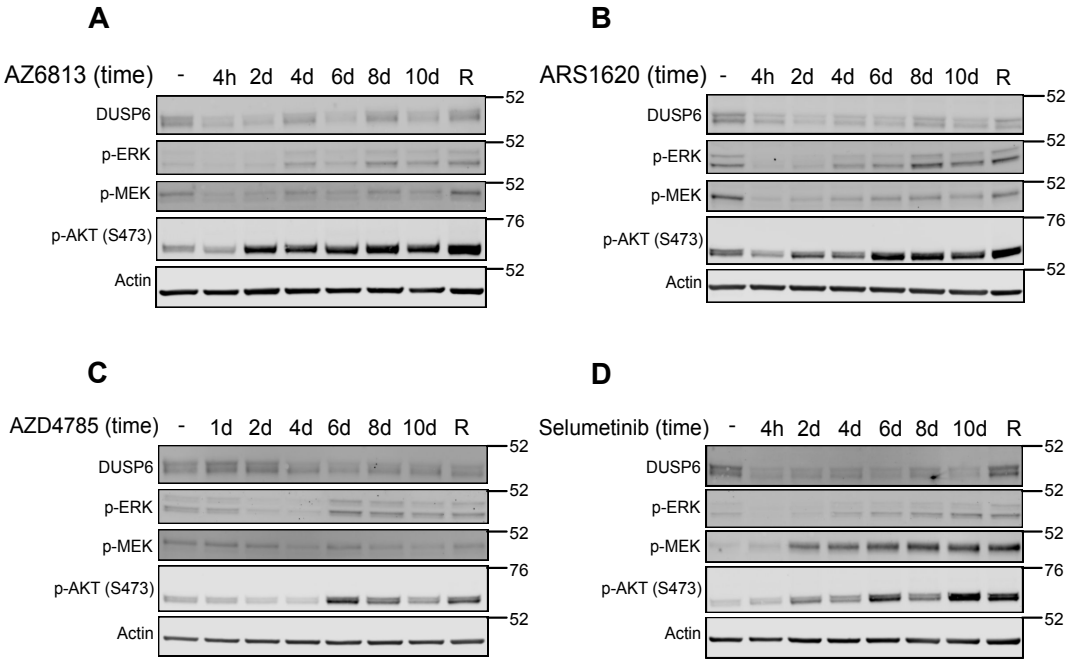

Figure 3.13: Acute inhibitor time course over 10 days in H358 cells.

H358 cells were treated with vehicle control (-) or IC90 concentrations of each inhibitor **(A)** AZ6813, **(B)** ARS1620, **(C)** AZD4785) and **(D)** selumetinib for 10 days with cells re-dosed every 48 hours. Cell lysates were prepared at the indicated time points and Ras pathway components were analysed by immunoblotting. Lysates from H358-R (R) cells were carried out alongside. Results are from a single experiment.

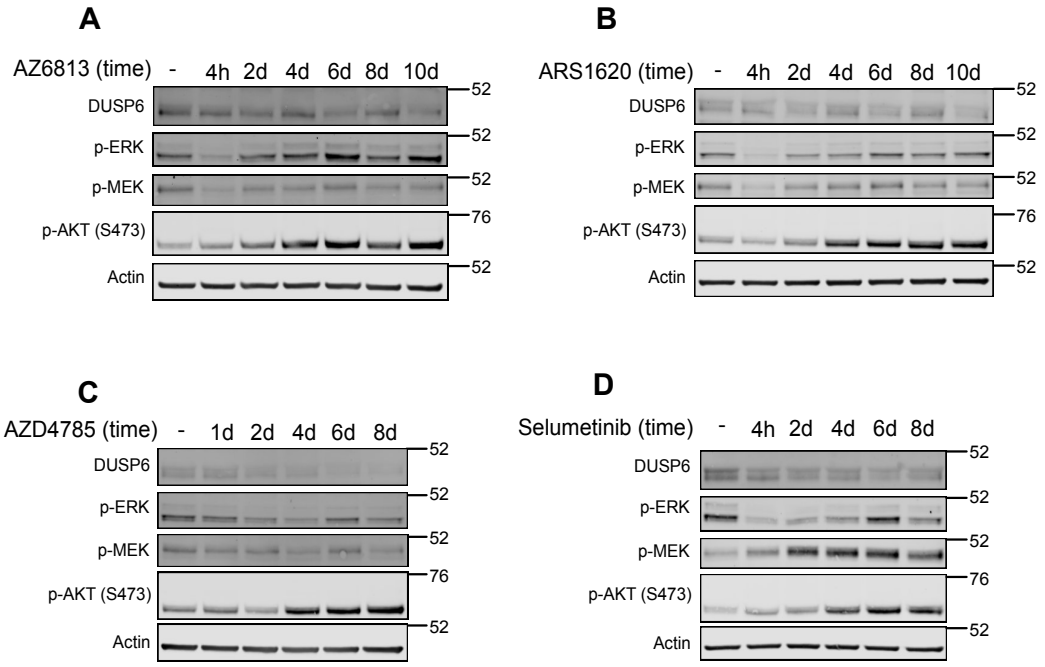

Figure 3.14: Acute inhibitor time course over 10 days in KRAS-G12C mutant H1792 cells.

H1792 cells were treated with vehicle control (-) or IC90 concentrations of each inhibitor **(A)** AZ6813, **(B)** ARS1620, **(C)** AZD4785 and **(D)** selumetinib for 8 or 10 days with cells re-dosed every 48 hours. Cell lysates were prepared at the indicated time points and Ras pathway components were analysed by immunoblotting.

To see if results were consistent in another KRAS-G12C mutant cell line, a time course was repeated in H1792 cells (Figure 3.14). Similar trends with an initial decline in p-ERK and p-AKT(S473) protein levels, followed by a rise in abundance which is maintained over the remaining time course, were observed with AZ6813 and ARS1620 treatment (Figure 3.14A and B). However, in H1792 cells, treatment with AZD4785 showed no change in p-ERK levels, although p-AKT still increased at day 4 (Figure 3.14C). Treatment with selumetinib also showed a similar trend to H358 cells, with a rise in p-MEK levels from day 2, and p-AKT(S473) and p-ERK from day 4 and day 6 respectively (Figure 3.14D). Although no long-term treated cell lines were made using H1792 cells, overall increased protein abundance of these key RAS pathway components was observed and maintained over the time course highlighting similar trends between different lung cancer cells with KRAS-G12C mutation.

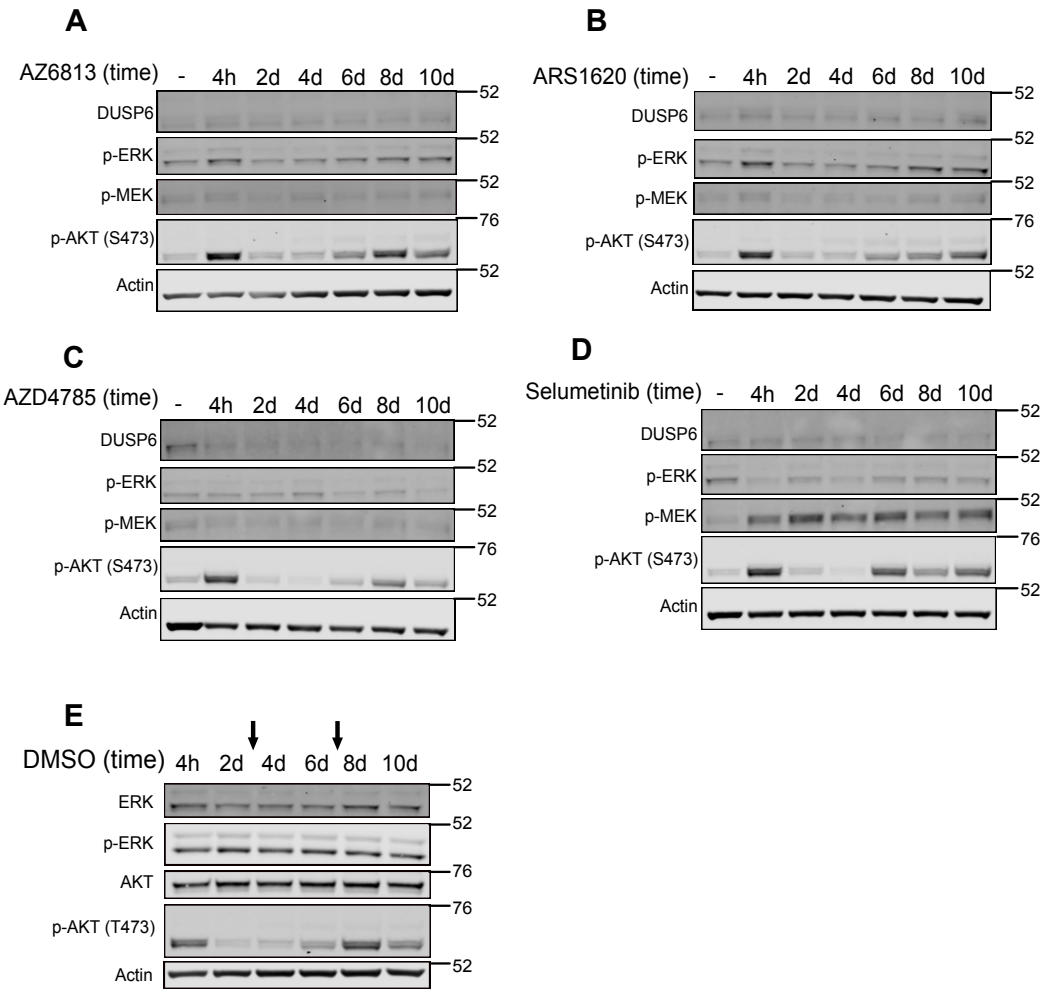

Figure 3.15: Acute inhibitor time course over 10 days with KRAS WT H1793 cells. H1793 cells were treated with vehicle control (-) or IC90 concentrations of each inhibitor **(A)** AZ6813, **(B)** ARS1620, **(C)** AZD4785, **(D)** Selumetinib for 10 days with cells re-dosed every 48 hours. A time match DMSO control was carried out alongside **(E)**, arrows indicate when cells were split. Cell lysates were prepared at the indicated time points and Ras pathway components were analysed by immunoblotting. Results are from a single experiment.

To ensure these trends were KRAS-G12C specific and a consequence of targeted KRAS inhibition, a 10-day time course was repeated in KRAS-WT H1793 cells (Figure 3.15). Reactivation of p-MEK was still observed with selumetinib treatment (Figure 3.15D) however, unlike previous experiments, minimal change in p-ERK levels was observed for any inhibitor treatment (Figure 3.15A-D). On the other hand, p-AKT(S473) levels initially increased upon inhibitor treatment and then continued to fluctuate in all conditions Figure 3.15A-D). Additionally, a matched DMSO time course was carried out

alongside the inhibitor treatments which also showed fluctuations in p-AKT(S473) levels (Figure 3.15E). The time points at which cells were passaged during the time course was also recorded. Evaluating the relationship between these variables, it was hypothesised that p-AKT(S473) levels changed according to cell confluency.

3.2.7 H358-R cells exhibit permanent signalling rewiring

In order to determine whether cells were permanently rewired, continually treated H358-R cells were subject to inhibitor withdrawal, where dosing of inhibitor was replaced with vehicle control over a time course of 10 days (Figure 3.16). Naïve H358 cells that had never been treated with inhibitor were used as a control. In H358-R AZ6813 cells (R-AZ6813) protein levels of p-ERK and p-AKT(S473) remained high throughout the DMSO washout time course compared to untreated cells, although there were some fluctuations at day 2-4 (Figure 3.16A). In comparison to inhibitor treatment, p-MEK increased with DMSO washout, however no change in DUSP6 expression was observed compared to untreated control cells. Overall the changes in p-ERK and p-AKT(S473) levels observed previously in figure 3.13 were sustained following the absence of inhibitor. Despite previous p-AKT(S473) levels fluctuating with cell confluency, the fact that higher protein levels remains in the absence of inhibitor compared to untreated cells provides confidence that this change is due to signalling rewiring in long-term treated H358-R cells. In H358-R ARS1620 cells (R-ARS), DMSO washout provided similar trends in protein levels (Figure 3.16B). In H358-R AZD4785 cells (R-ASO), p-ERK and p-AKT(S473) levels remain elevated during PBS washout, whereas no general trend was observed with p-MEK and in fact DUSP6 levels appeared higher in untreated cells (Figure 3.16C). Similarly, H358-R selumetinib cells (R-Sel) also showed increased p-ERK and p-AKT(S473) abundance compared to untreated cells during DMSO washout, highlighting more permeant rewiring of these RAS pathway components (Figure 3.16D). Whereas the previously observed increase in p-MEK with inhibitor treatment actually decreased during washout, indicating this feedback signalling is transient in these cells.

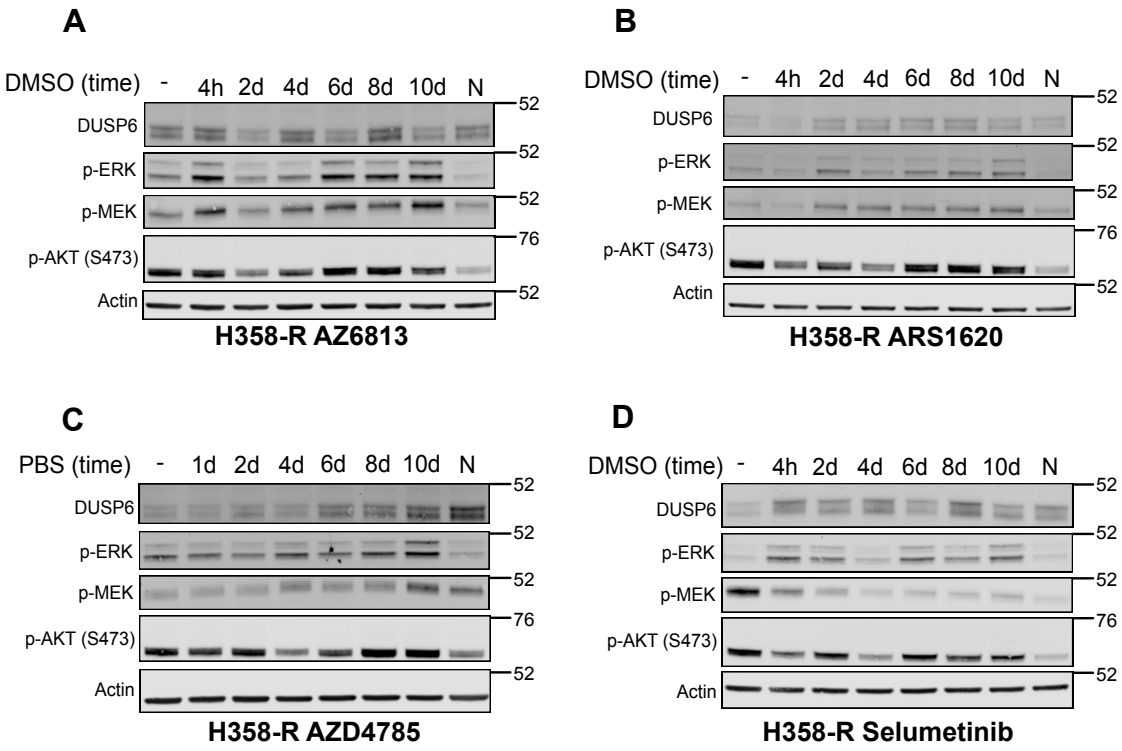

Figure 3.16: Inhibitor washout time course over 10 days in H358-R cells

H358-R cells that had been continually treated with inhibitor (-) were cultured in media containing only appropriate vehicle control (DMSO or PBS) for a total period of 10 days. Cells were re-dosed every 48hrs and lysates prepared at the indicated time points. Ras pathway components were analysed by immunoblotting. Lysates from H358 naive cells (N) were ran alongside. Results are from a single experiment.

3.3 Discussion

In this chapter I have selected three inhibitors (AZ6813, ARS1620 and AZD4785) which directly target KRAS, and carried out validation of the selectivity and sensitivity of these inhibitors in a panel of NSCLC cell lines with different endogenous KRAS mutation status. The MEK inhibitor selumetinib was compared alongside. Target validation was required to determine the appropriate concentrations for drug dosing to generate resistant cells. DUSP6 mRNA expression is a marker of ERK signalling and was measured as a readout to indicate RAS or MEK inhibition. DUSP6 has been shown to be consistently upregulated in mutant KRAS cells and tissues and elevated expression levels are associated with poor prognosis in NSCLC [286, 287]. This dual specificity phosphatase acts as a negative feedback regulator induced by ERK signalling and attenuates MAPK signalling by dephosphorylating and inactivating ERK. It has been shown that in comparison to the phosphorylation status of ERK and MEK, DUSP6 mRNA levels more accurately reflect MAPK pathway activation [288]. Additionally, cell viability and cytotoxicity assays were used for inhibitor validation and provided insight into the biological effect and efficacy of compounds. The inhibitors demonstrated good inhibition of cell growth and specifically induced cell death in mutant KRAS tumour cells, although concentrations $\geq 3\mu M$ induced cytotoxicity (Figures 3.7 and 3.8).

As a result of the KRAS-G12C inhibitor AZ6813 showing evidence of off-target toxicity in KRAS-WT cells (Figure 3.2), a second generation allosteric KRAS-G12C inhibitor ARS1620 was included in the study and demonstrated greater potency and specificity (Table 3.1). Of the effective KRAS inhibitors the ASO AZD4785 was the least potent, presumably due to its mechanism of action targeting KRAS mRNA and the delay of inhibition to KRAS protein production. At the start of this study, AZD4785 was undergoing phase I clinical trials but has since been discontinued by the developers AstraZeneca. Despite this, AZD4785 represents an alternative mechanism of direct KRAS inhibition in this study and is a useful comparator for resistance mechanisms as it targets

both mutant and wildtype KRAS. The MEK inhibitor selumetinib was the most potent inhibitor in the study and represented a clinically approved comparator with known resistance in KRAS mutant cells. On the other hand, the inhibitors fendiline and deltarasin which target RAS membrane localisation showed no evidence of RAS pathway inhibition (Figure 3.1). The non-specific action and lack of specificity of fendiline [274, 289] are likely factors underlying this observation. Additionally, it is unclear how dependent KRAS is on PDE6δ for membrane trafficking, as PDE6δ interacts with a number of other farnesylated proteins [289, 290]. Therefore, this raises concerns of the ability of PDE6δ inhibitors, such as deltarasin, to selectively target RAS. Consequently, fendiline and deltarasin were not included in any further experiments. Despite AZ6813 exhibiting some off-target toxicity, this KRAS inhibitor was still included in the study as good pathway inhibition was still observed in KRAS-mutant cells (Figure 3.1) and it also provides a direct comparison to ARS1620 which has a similar mechanism of action. The inhibitors AZD4785 and selumetinib were also taken forwards.

A direct comparison between 2D adherent monolayer cells and 3D ultra-low adherent spheroids was performed, as it was previously identified by Fujita-Sato and colleagues that differences in culture adherence affect KRAS mutant cells [291]. In the study KRAS mutant cells were found to be more dependent on KRAS in 3D cell culture as a result of enhanced expression of the receptor MET under these growth conditions, which is regulated by RAS-RAF-MEK-ERK pathway signalling [291]. In this study H358 cells grown as spheroids demonstrated greater sensitivity to the panel of KRAS inhibitors compared to 2D monolayer culture (Figure 3.7). This was also represented by the decreased cell viability IC50 and IC90 values of 3D cell culture, which were more comparable to concentrations determined from the pathway inhibition assay (Table 3.1). It is now well accepted that culturing cells in 3D systems is more biologically representative of the *in vivo* environment compared to monolayer cultures, with more clinically relevant gene expression profiles and responses to treatment [284, 292-294]. As observed in tumours, spheroid models exhibit normoxic, hypoxic and necrotic zones with layers of

proliferating, quiescent and apoptotic cells highlighting greater physiological relevance [295]. In this study, ultra-low attachment plates were used to produce spheroids given the flexibility for use in cellular assays, although this simple 3D model lacks the heterogeneity and interaction of cancer cells with the surrounding extracellular matrix (ECM) and stroma observed *in vivo*. Alternative 3D models can incorporate scaffolds, matrices and co-culture to recapitulate these interactions [296]. However, the major challenges of 3D cell culture for drug discovery include lack of reproducibility as well as low cost and time effectiveness. Despite being one of the fastest growing experimental approaches, there is little published information on the long-term culturing of spheroid cells and their use to generate resistant models. With the use of ultra-low attachment flasks to generate bigger cell populations, many questions remained unknown regarding whether spheroids should be passaged and how to obtain reproducible cultures. As a result of the challenges faced with spheroid culturing, it became apparent that it was important to proceed with cells that demonstrated KRAS dependency in 2D cell culture. Of the cell lines in the KRAS-G12C NSCLC panel, H358 cells demonstrated good KRAS dependency as 2D culture and were the easiest cell line to grow and passage. Subsequently resistant cells were generated using this cell line.

In the laboratory drug resistant cell models are developed by repeat exposure of cancer cells to drugs, and after a period of time the surviving daughter cells are then compared to the parental sensitive cells using cell viability assays [282, 297]. In this study resistant cells were developed from H358 (KRAS-G12C) cancer cells using this approach (Figure 3.11). However publications in this research field place little emphasis on the exact methodology of generating resistant cells and some of the key decisions involved, particularly with regard to the dosing strategies, treatment intervals and optimisation of doses [282]. Typically dose escalating schedules starting at the IC50 concentration are more routinely used to generate resistant cells [297-299]. Currently no publications on generating resistant cells to direct KRAS inhibitors have been published, although generation of selumetinib resistant cells have been previously generated by using both dose escalation and a chronic maximum dose [244]. In the CRC cell lines used, a similar or greater

degree of selumetinib resistance occurred following the chronic dosing schedule [244]. As a result, a comparative strategy was adopted and H358 cells were initially treated with either IC50 or IC90 inhibitor concentrations in parallel for each inhibitor to determine the optimum dosing strategy for generating resistance. This selection strategy identified that IC90 treated cells displayed increased viability in comparison to IC50 treated cells upon inhibitor challenge. Furthermore, the chemical stability of the inhibitors was considered for an appropriate dosing schedule. Due to continually growing cells in the presence of inhibitor and the relatively short half-lives of the small molecule inhibitors, a repeat dosing of 48 hours was performed. During the timeline of generating resistant cells, an additional control cell line was generated, H358-R selumetinib_DMSO, which represents cells treated long-term with selumetinib, followed by DMSO only treatment. This comparison originated from the finding that withdrawal of selumetinib in CRC cells can either reverse acquired resistance in BRAF-600E mutant cells or further promote chemoresistance in KRAS-G13D driven cells [300]. It would therefore be of interest to see how H358-R selumetinib_DMSO cells compare to other H358-R cells in this study, particularly as transient p-MEK signalling was observed in R-Sel washout cells (Figure 3.16D).

As is the case with many MEK inhibitors, relief of feedback inhibition and pathway reactivation of ERK1/2 occurs and limits MEKi monotherapy [75, 244]. This was confirmed in H358 and H1792 cells, with the increased abundance of pERK1/2 and pMEK1/2 following acute selumetinib treatment (Figures 3.12 - 3.13). Increases in protein levels of p-ERK1/2 were also observed with direct KRAS inhibitors, indicating the reactivation of ERK1/2 signalling and the development of pathway rewiring underlying resistance. With KRAS-G12C inhibitors, pMEK1/2 appeared to gradually increase, though this was not as strongly as observed with selumetinib treatment and no changes were observed with AZD4785 treatment. Upon inhibitor withdrawal different responses in pMEK1/2 levels occurred. Following selumetinib withdrawal, pMEK1/2 protein abundance gradually declined overtime in spite of increased pERK1/2 levels (Figure 3.16). Whereas with KRAS-G12C inhibitor withdrawal, pMEK1/2 protein levels gradually increased alongside

pERK1/2. It has previously been identified that gene amplification of the addicted oncogene in KRAS-mutant CRC cells is a common mechanism to maintain ERK1/2 signalling under selumetinib resistance [244], and following inhibitor withdrawal cells are able to maintain resistance to selumetinib [300]. The increased abundance of pERK1/2 signalling under both KRAS and MEK inhibition, as well as during inhibitor withdrawal confirms reactivation of pERK1/2 as a common resistance mechanism, albeit differences in pMEK1/2 levels might suggest this can occur via different signalling pathways in chronically treated cells. These protein changes were also coupled with changes in pATK(S473) levels which generally increased with the inhibitor treatments and was maintained over time and during inhibitor withdrawal. However, surprisingly fluctuations in pAKT(S473) was also observed in KRAS-WT cells with the targeted KRAS-G12C inhibitors, and a matched DMSO time course indicated p-AKT(S473) abundance was also influenced by changes in cell confluency (Figure 3.15). This observation has been identified in several other studies, suggesting that cells with higher cell confluency exhibit lower pAKT protein levels as a result of increased contact inhibition, whereas the opposite is observed in cells that have high proliferative ability [301, 302]. In spite of this, the sustained increased abundance of pAKT(S473) following acute and chronic inhibitor treatment, as well as during inhibitor withdrawal (Figure 3.16), gives confidence that this increase is a result of resistance-mediated signalling rewiring. Overall since pERK and pAKT rewiring occurred within just a few days of KRAS inhibitor treatment, a comparison of acutely treated cells for 7 days (H358-A) would be compared to the long-term chronically treated H358-R cells generated, enabling any changes in resistance mechanisms over time to also be compared.

Previously there were no models for monitoring resistance to direct KRAS inhibitors, and from this study I now have different batches of H358 cells that are resistant to each of the inhibitors (AZ6813, ARS1620, AZD4785 and selumetinib) (Table 3.2). As well as comparisons between different inhibitors, comparisons between different cell batches could also be carried out to identify if different sub-populations arise and whether similar or different resistance mechanisms develop in independently treated cells [303].

Furthermore, comparisons between the length of drug treatments will provide the ability to compare short-term drug tolerances with long-term permanent resistance mechanisms and help to identify any changes that are selected for over time. Previous modelling of acute responses highlights intrinsically drug tolerant subpopulations play a crucial role in promoting long-term acquired drug resistance [304]. In the future it would also be insightful to generate resistant cells from the other NSCLC cell lines in this panel, as well as potentially from 3D spheroid models.

In summary, the aims of validating a set of direct KRAS inhibitors in a panel of NSCLC cells, as well as generating resistant cell lines, have been successfully met. As a result, I can now apply the resistant cells I have generated to investigate mechanisms of resistance.

Chapter 4

Omic profiling of H358-A and H358-R cells

4.1 Introduction

As detailed in the previous chapter, H358-R cells showed an increased cell viability compared to naïve cells and immunoblotting demonstrated they maintained altered p-ERK1/2 protein abundance levels, suggesting more permanent signalling rewiring mechanisms (Figures 3.11, 3.13 and 3.16). Previous clinical efforts to target the RAS-RAF-MEK pathway have been hindered by adaptive feedback reactivation of pathway signalling, resulting in incomplete suppression of the pathway targeted and many of the crosstalk mechanisms involved have been well documented (See Table 1.1). For example, MEK inhibitors have shown limited clinical activity as mono-therapies in KRAS-mutant tumours due to mechanisms of feedback activation via the PI3K pathway [305], as well as upregulation of multiple RTKs and their ligands [278]. Furthermore wild-type RAS isoforms present in cells harbouring mutant RAS can still promote and sustain oncogenic signalling of downstream effector pathways when oncogenic RAS is depleted [306]. Such studies highlight that direct RAS inhibitors will not be broadly effective across all RAS-mutant tumours, and suggests alternative signals can support cell growth and survival when mutant KRAS is absent [225, 307]. As a result, vertical inhibition of the RAS pathway and targets of other RAS effector pathways that can be used alongside RAS inhibitors should be explored to increase therapeutic efficacy. In mutant KRAS mouse models combined inhibition of MEK and PI3K caused more dramatic tumour regression than either inhibitor alone [193, 308]. Similarly, MEK and PI3K-mTOR inhibition in mouse xenograft NSCLC models

demonstrated greater antitumor efficacy than the respective monotherapies [309]. Despite promising preclinical studies and manageable toxicity, the combination of MEK and PI3K inhibitors in clinical trials has demonstrated mixed response rates for KRAS-mutant tumours [196, 200, 310]. Alternatively, other pathways such as the cell cycle, apoptosis and upstream RTKs have presented alternative targets for therapeutic combination with RAF-MEK-ERK inhibitors in KRAS mutant cancers [311-313]. Following good efficacy in preclinical studies [314, 315], the combined inhibition of CDK4/6 and MEK is currently undergoing clinical trial in KRAS-mutant NSCLC (NCT03170206). Furthermore there is increasing evidence to support the combination of MEK and PI3K inhibitors with pharmacological inhibition of antiapoptotic proteins BCL-XL and BCL-2 in several KRAS-mutant cancers [313, 316, 317]. Additionally, RTKs of the HER family and FGFR1 have been identified as additional targets for combination with MEK inhibitors [278, 311]. Therefore, it is important to investigate the potential resistance mechanisms associated with direct KRAS inhibition in order to identify new opportunities to improve these therapies from understanding how and when certain combination therapeutics should be given.

Advances in molecular profiling approaches and the integration of multi-omics data offer a more compressive insight into the cellular changes associated with resistance mechanisms. RNA-sequencing (RNA-Seq) presents a powerful tool for genome-wide transcriptome profiling, using high throughput sequencing technologies to detect differentially expressed genes, of both known and novel transcripts, to better understand the biological context of a drug treatment or disease phenotype [318]. RNA-seq is widely used during drug discovery and development, and has previously been used to identify genes associated with drug resistance [319]. In comparison to microarrays, RNA-Seq has several advantages including very low background signal and high resolution, as well as covering a large dynamic range with both high sensitivity and reproducibility [320]. However challenges include the bioinformatic analysis of large amounts of sequence data, requiring complex informatics for mapping reads, reducing errors in base-calling and removing low-quality reads [320]. Additionally, sequence coverage is an important issue

and in order to detect rarer transcripts considerable depth is required [320]. It also remains a challenge to interpret genome-wide transcriptomic data to extract biologically meaningful insights. As a result, functional annotation tools, such as gene ontology (GO) enrichment analysis, are widely used to reduce complexity and to identify functionally related gene groups that differentially expressed genes are enriched for [321, 322]. GO analysis is structured to characterise genes according to biological processes, molecular function and cellular component. Rather than analysing gene expression changes on an individual gene-orientated view, this instead makes analysis of large gene lists relevant to specific gene groups and increases the identification of important insights and relevant biological processes involved in the area under study [321].

On the other hand, proteomic approaches help to characterise the transcriptomic information flow within cells with the associated protein pathways and networks activated under certain conditions [323]. The abundance of proteins present is modulated by additional post-transcriptional modifications and protein degradation mechanisms altering the level of protein expression which cannot be detected by transcriptomic analysis alone [324]. As a result, gene-expression data may not accurately reflect active cellular functions. Profiling phosphorylation in particular is a key strategy for identifying responses to therapeutics, resistance and therapeutic targets, which widely involve deregulated kinases [325]. There are several technologies available for broad proteomic analysis. Mass-spectrometry-based technologies enable the analysis of thousands of proteins although complex sample preparation and lower-sensitivity for low-abundant proteins makes it difficult for analysing cancer signalling proteins [326] . Alternatively, reverse-phase protein array (RPPA) is a highly sensitive medium-throughput technique which allows screening of samples for a large panel of proteins of interest, including phosphoproteins. The method is based on protein microarray where simultaneously single arrays or spots containing protein lysate are incubated with a specific antibody. Its reliability however largely depends upon the quality of the antibodies [327].

The combined contribution of quantitative transcriptomic and proteomic approaches has been widely applied for profiling resistance mechanisms and have successfully yielded biomarkers and therapeutic targets in many different cancers [325, 328-330].

Aims

In order to determine potential mechanisms and alternative pathways of resistance under KRAS inhibition, I took a genome-wide approach to investigate the transcriptional and proteomic programming of H358-R and H358-A cells treated with various KRAS inhibitors (Table 3.2).

Using these approaches, I aimed to:

- Identify gene signatures associated with emerging resistance in acutely treated (H358-A) and long-term (H358-R) treated cells
- Determine any differences between different mechanisms of RAS pathway inhibition
- Determine if similar trends occur across transcriptomic and proteomic data
- Identify potential pathways associated with resistance mechanisms

4.2 Results

4.2.1 Comparison of gene expression between RNA-seq data sets

RNA-seq was performed by BGI Genomics Co. Ltd. (Hong Kong) using BGISeq-500 and DNBSeq platforms to compare H358-R and H358-A cells cultured in the presence of KRAS inhibitors and vehicle controls (Table 4.1). Two sets of H358-R samples were processed independently (H358-R1 and H358-R2), enabling repeat conditions to be compared. The second set included the more potent KRAS-G12C inhibitor ARS1620 and was processed alongside H358-A samples, enabling differences between early and late resistance mechanisms to be compared.

	Run 1	**Run 2**	
Sequencing Platform	BGISEQ-500	DNBSeq	
Sample Treatment	Chronic (H358-R1)	Chronic (H358-R2)	Acute (H358-A)
DMSO	✓	✓	✓
PBS	✓	✓	✓
AZ6813	✓	✓	✓
Selumetinib	✓	✓	✓
AZD4785	✓	✓	✓
Selumetinib_DMSO	✓	×	×
ARS1620	×	✓	✓
ASO CTRL	×	×	✓

Table 4.1: Summary of RNA-seq data sets processed by BGI Genomics. Two RNA-seq runs were processed separately at different times. Run 1 was performed using the BGISEQ-500 platform for the indicated chronically treated samples. Run 2 was performed using the comparable DNBSeq platform for both acute and chronically treated samples.

The RNA samples were prepared using Trizol extraction and a total RNA sample QC was carried out using the Agilent 2100 Bioanalyzer and Agilent RNA 6000 Nano Kit to determine RNA concentration, RIN value, 28S/18S and

fragment length distribution. The library construction, sequencing and subsequent bioinformatic workflow was carried out by BGI Genomics Co. Ltd. (Hong Kong). The analysis pipeline is shown in Figure 4.1.

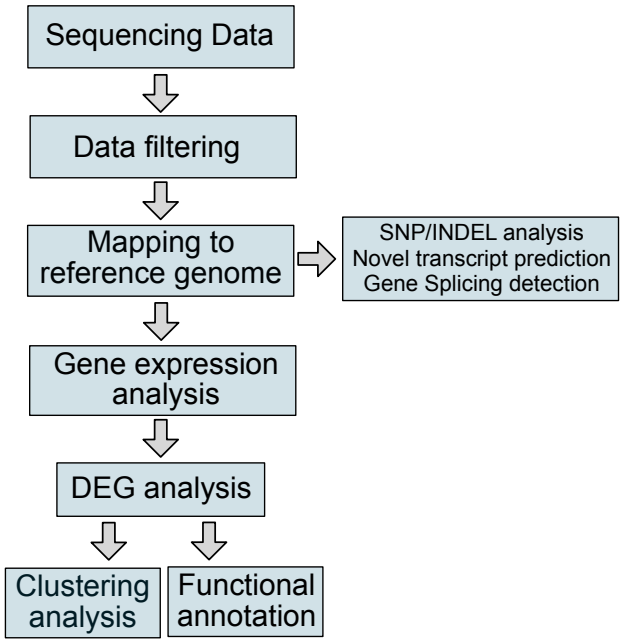

Figure 4.1: RNA-Sequencing bioinformatics workflow.
Raw sequencing data was first filtered to remove low quality reads, reads with adaptors and reads with unknown bases. Clean reads were then mapped to the reference genome along with SNP/INDEL calling, novel gene prediction and gene-splicing detection. Gene expression levels were determined using RSEM [268], followed by detection of differentially expressed genes (DEGs) between samples. Finally, hierarchical clustering analysis and functional annotation using GO analysis and pathway analysis were carried out.

An overview for each data set was produced, highlighting the total number of genes expressed for each condition as well as how many transcripts were high, low and medium expressed using different Fragments Per Kilobase Million (FPKM) ranges (Figure 4.2A). In all data sets, >15000 genes were identified, and a similar distribution of high, medium and low expressed genes were detected within and across data sets. In addition, the total number of shared genes within a data set were calculated, as well as the number shared by at least two conditions and the number of unique genes for each condition (Figure 4.2B). In all data sets the vast majority of genes >14000 were shared across all samples, and approximately 2000 genes were shared between at

least two conditions. In H358-R1 and H358-R2 data dets, AZD4785-treated cells harboured the greatest number of uniquely expressed genes in comparison to other conditions.

Furthermore, the number of shared genes expressed between control and treated samples within each data set were compared, alongside the number of unique genes and the number of those differentially expressed (DEGs) (Figure 4.3). In all data sets the majority of expressed genes are shared, with small fluctuations in the number of unique genes. Overall more DEGs are up-regulated across the different conditions than are down-regulated and AZD4785-treated cells displayed the greatest number of DEGs in relation to their corresponding control.

Next the number of DEGs shared between inhibitor treated samples was compared for each data set (Figure 4.4 A, C, E). The number of DEGs shared across H358-R1, H358-R2 and H358-A inhibitor treated samples were 267, 728 and 312 respectively. However, when the same three inhibitors used in H358-R1 were compared, 189 DEGs were shared in H358-R2 (Figure 4.4C). Again, AZD4785-treated resistant cells exhibited the greatest number of uniquely expressed DEGs, which was not observed with acutely treated cells (H358-A). Hierarchical gene clustering was performed for each data set of shared DEGs which clearly highlighted the differential gene expression between control and treated cells (Figure 4.4 B, D, F). The majority of DEGS were up-regulated in treated cells compared to controls and few DEGs showed mixed responses in H358-R data sets. Additional comparison of DEGs shared across H358-R1 selumetinib and selumetinib_DMSO (SEL_DMSO) treated cells showed similar gene expression responses between the two conditions compared to DMSO treated cells (Figure 4.4B). Overall there were few mixed DEGs, highlighting that despite drug withdrawal, SEL_DMSO cells retained a resistant gene expression signature. Hierarchical gene clustering was also performed combining all the DEGs across the three data sets and the resulting dendrogram presented to show the clustering of each sample (Figure 4.4G). Firstly, AZD4785-treated resistant cells from both data sets distinctively cluster together and show the greatest divergence from the other samples.

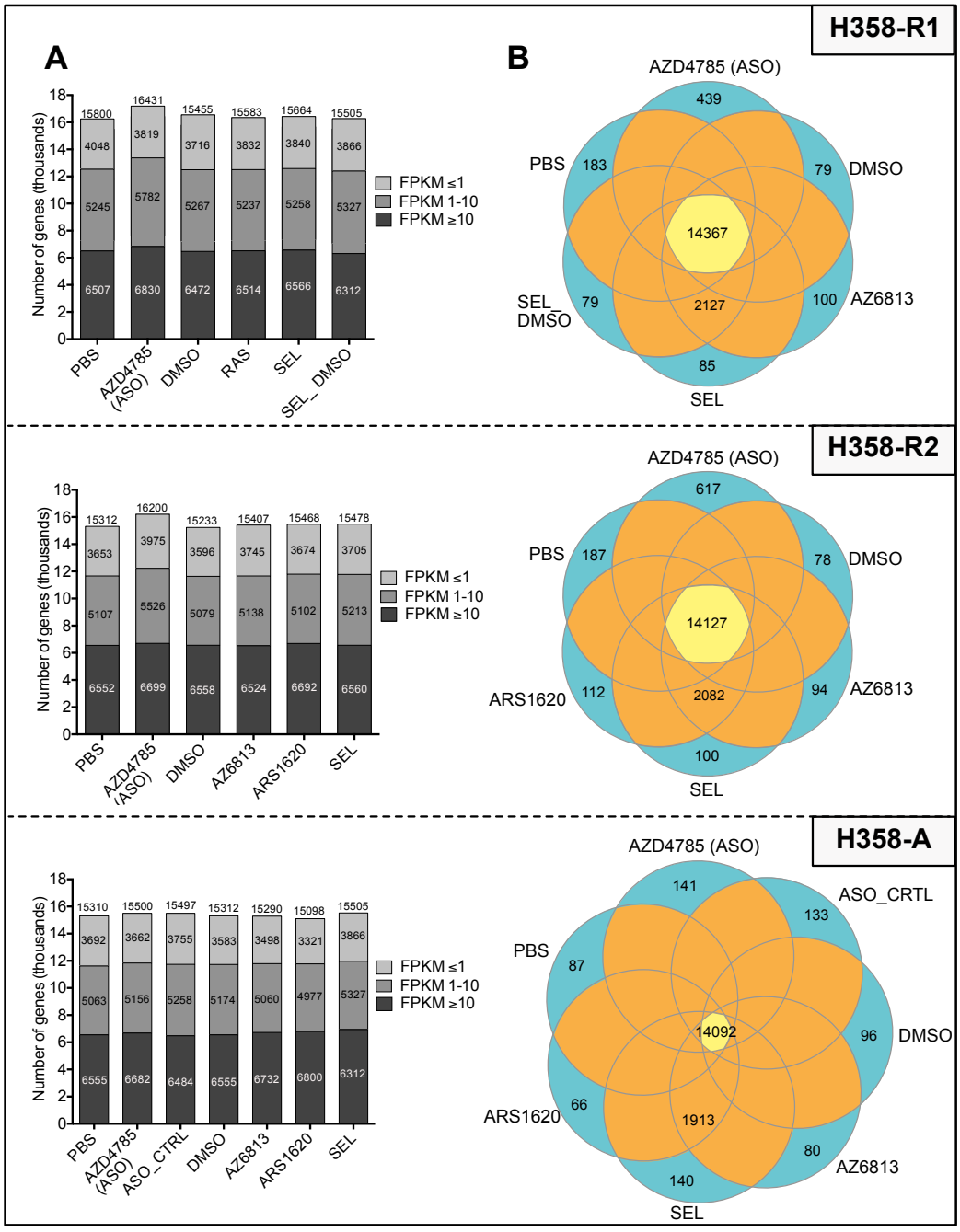

Figure 4.2: Comparison of the total number of expressed genes in each data set.

(A) Shows the gene expression distribution of transcripts from each data set represented by Fragments Per Kilobase Million (FPKM). The dark grey indicates the number of highly expressed genes and the light grey the number of genes with low expression. The total number of genes sequenced for each condition are show at the top of each bar. **(B)** Venn diagrams for each data set to show the number of unique genes for each condition (turquoise), the total number of genes shared between at least two conditions (orange) and the number of genes shared between all conditions (yellow).

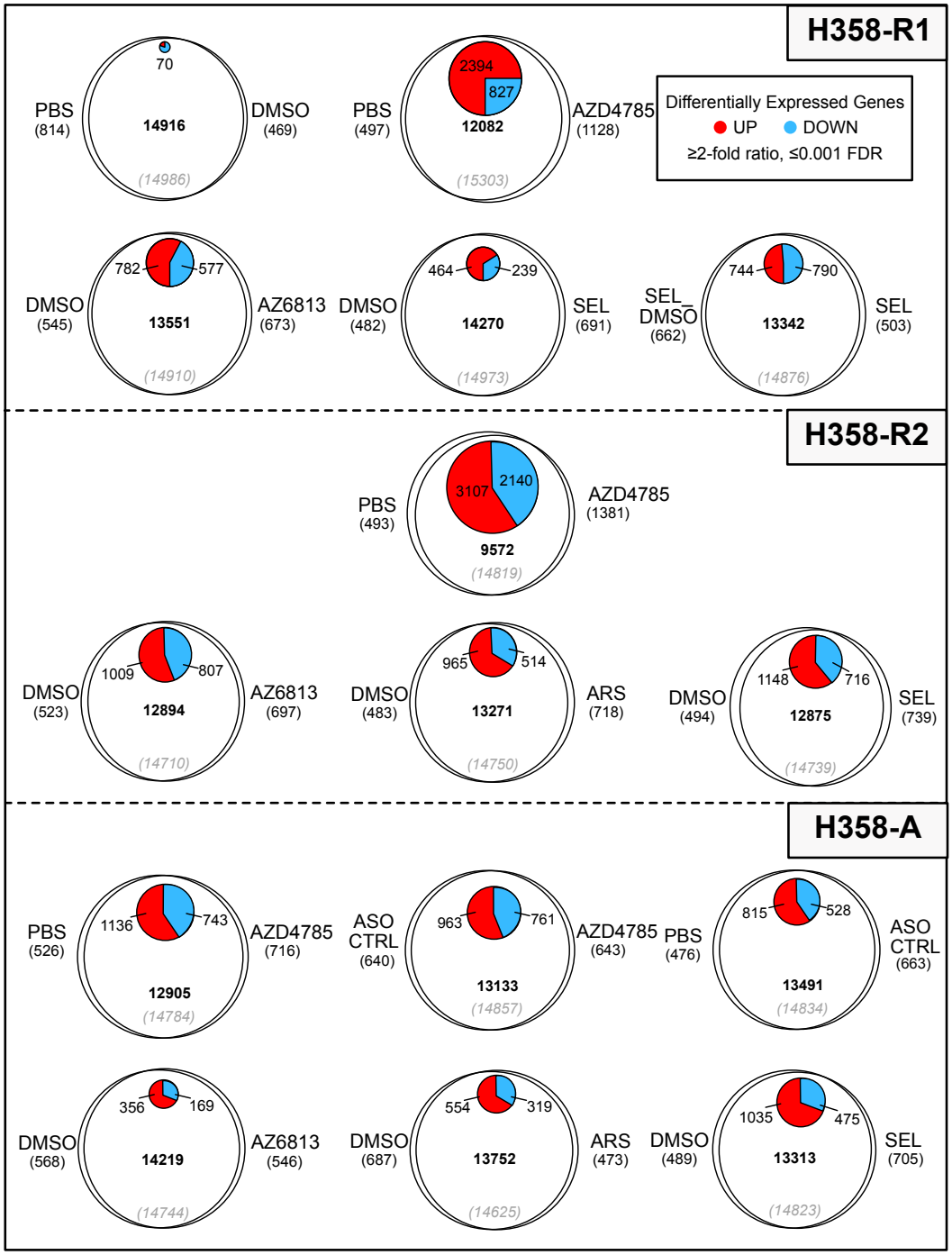

Figure 4.3: Comparison of differentially expressed genes in each data set.

Shows proportional comparisons of the number of differentially expressed genes (DEGs) between control and treated samples in each data set (H358-R1, H368-R2, H358-A). Venn diagrams highlight the number of unique genes between each treatment (in brackets), the total number of common genes (grey) and the number of these that were differentially expressed, represented by up regulated (red) and down regulated (blue) DEGs.

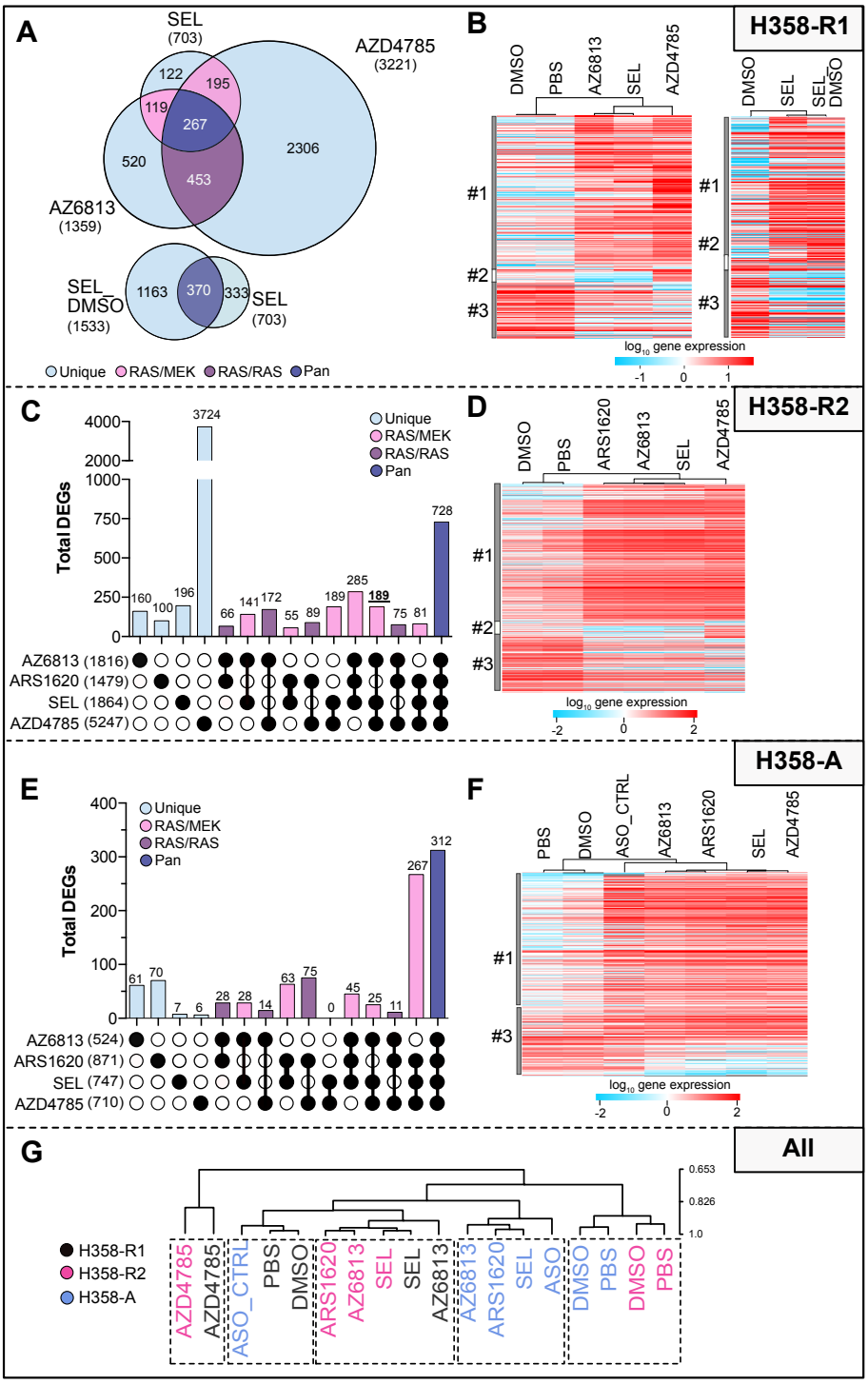

Figure 4.4: Comparison of differentially expressed genes.

(A, C, E) Shows comparisons of DEGs between the inhibitor treated samples from each data set. The total number of DEGs is shown in brackets for each treatment. Black circles represent the treatments included in the analysis, indicating the total number of unique DEGs and those in common between samples (joined circles). **(B, D, F)** Hierarchical clustering of pan gene expression values from each data set which have been logarithmically converted. #1 represents genes that are up-regulated compared to the control, #2 are mixed responses and #3 are down-regulated genes compared to controls. **(G)** Hierarchical clustering of all pan DEGs from each data set combined.

The controls from H358-R1 cluster together alongside the ASO-CTRL of H358-A treated cells, whereas the remaining controls from H358-A and H358-R2 also group separately. This potentially highlights some influence of experiment timing and processing. All small molecule inhibitors from both H358-R data sets also group together, highlighting similar DEG responses, and the H358-A inhibitor treated samples also cluster. As H358-A and H358-R2 samples were prepared and processed at the same time, the differential clustering indicates there are clear differences between acute and long-term resistance gene expression responses.

To compare DEGs for each inhibitor between different data sets, scatter plots were used to show correlation and to highlight if individual genes are regulated in the same way (Figure 4.5). Comparison of H358-R1 and H358-R2 indicated no overall correlation of AZ6813 DEGs although a general trend was observed for selumetinib DEGs and a good pattern of correlation for AZD4785 DEGs. On the other hand, comparison of H358-R2 and H358-A showed a majority of DEGs correlating for all inhibitors, highlighting greater consistency between these two data sets which were processed at the same time.

4.2.2 GO analysis for differentially expressed genes

DAVID (the database for annotation, visualisation and integrated discovery) was used for GO analysis, and GO terms associated with DEGs for each inhibitor were identified for links with relevant biological processes [331, 332]. GO terms were ranked according to significant p-values (<0.05) using EASE score, a modified Fisher Exact P-value. Distinctive enriched terms with higher numbers of genes involved were selected and presented in a heat map (Figure 4.6). For H358-R GO terms, DEGs expressed in both H358-R1 and H358-R2 data sets were selected for and GO analysis performed. Data labelled as ‘combined’ represents the DEGs shared by all inhibitors presented in Figure 4.4. In H358-A treated cells, microtubule and cell cycle processes stand out as highly significant across all individual inhibitors and combined data. Processes relating to cell stress, cell cycle and proliferation, as well as

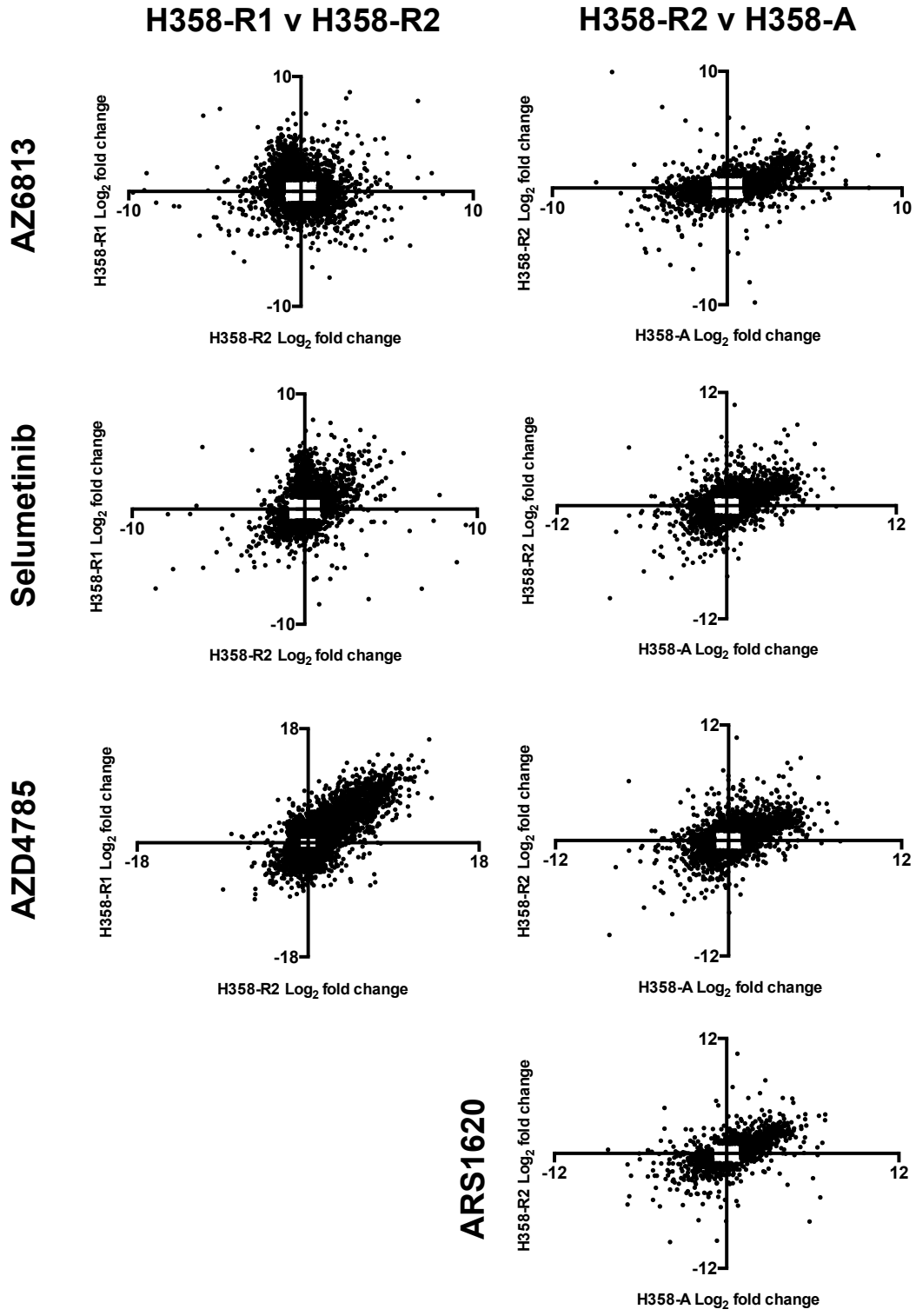

Figure 4.5: Comparison of differentially expressed genes between data sets

Scatter plots comparing genes that are differentially expressed in two long-term treatment conditions (H358-R1 v H358-R2) aswell as between acute and long-term conditions (H358-R2 v H358-A).

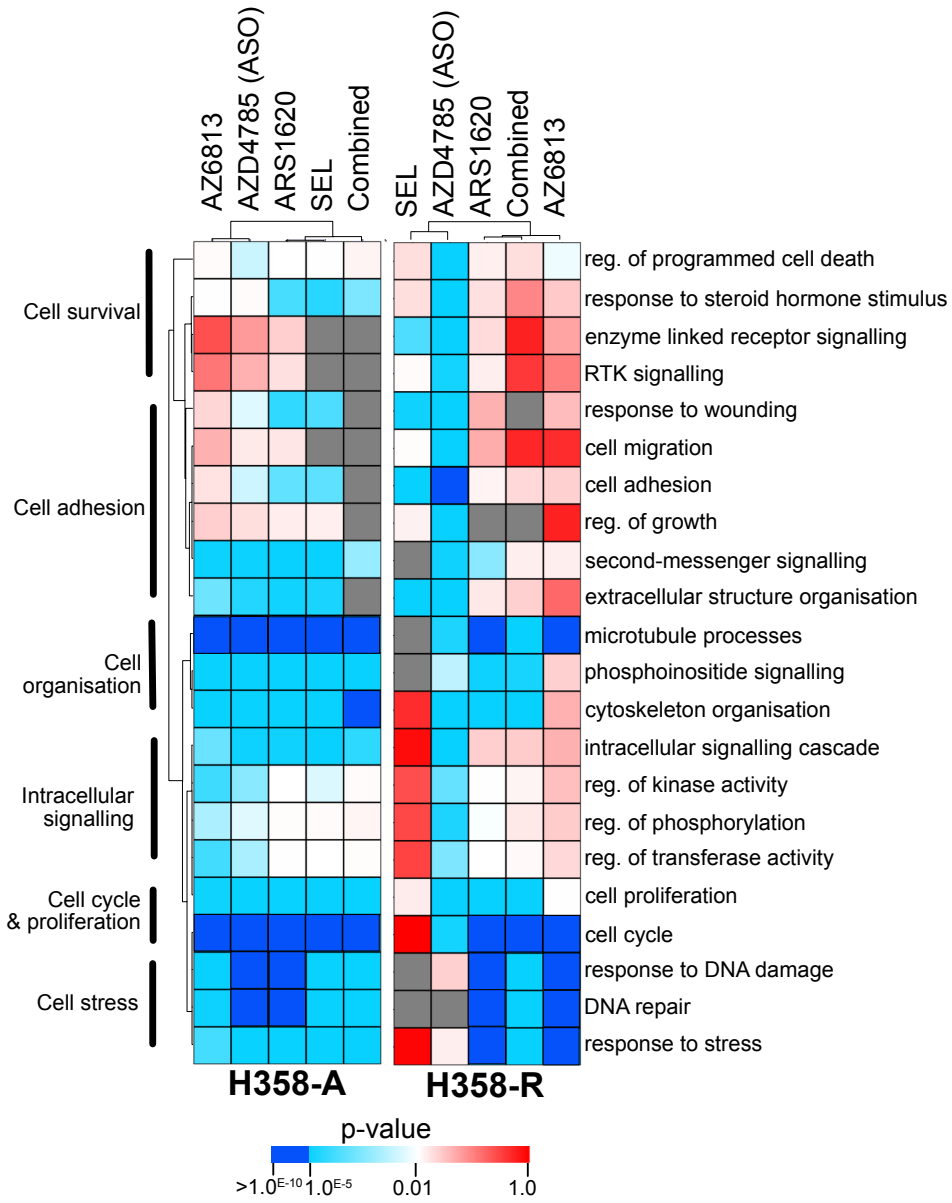

Figure 4.6: GO analysis for differentially expressed genes.
Hierarchical clustering of significant GO terms based on p-values for H358-A and H358-R treated cells. H358-R represents the most significant terms from two independent RNA sequencing data sets. Terms highlighted in dark blue represent those with very high significance (p-value >1.0E-10).

intracellular signalling were also very significant and enriched for, and overall a similar trend was observed for all inhibitors. On the other hand, resistant cells (H358-R) show different trends between inhibitors. Firstly, in AZD4785-treated resistant cells a greater number of processes were significant including intracellular signalling cascade which is not significant with other inhibitors.

Moreover, cell adhesion, response to wounding, ECM structure and cell migration were significantly enriched in AZD4785- and selumetinib-treated resistant cells but not with cells chronically treated with KRAS-G12C inhibitors. Processes such as the cell cycle and response to stress were significant across all chronically treated samples with the exception of selumetinib-treated resistant cells. In addition, processes associated with cell stress appeared specifically highly significant for cells treated with KRAS-G12C inhibitors. Comparison between acute (H358-A) and chronic (H358-R) treatments show cell cycle and microtubule processes as the most significant terms shared across both treatment conditions. Whereas intracellular signalling switched from being significant across all inhibitors with acute treatments, to being not significant in several chronic treatments. Alternatively, RTK signalling wasn't significant under acutely treated conditions, but was significantly enriched for in AZD4785-, selumetinib- and ARS1620-treated resistant cells.

4.2.3 KRAS-G12C inhibitors demonstrate similar responses

A comparison between the KRAS-G12C inhibitors AZ6813 and ARS1620 was also carried out to investigate any differences in gene expression and associated biological processes (Figure 4.7). Scatter plots highlight that within H358-R2 and H358-A data sets the two KRAS-G12C inhibitors correlate well and share the vast majority of DEGs which are similarly up-regulated or down-regulated (Figure 4.7A). Comparison of inhibitors between acute and long-term treatment indicated a similar number of shared genes expressed although with both inhibitors more genes become down-regulated following longer treatment (Figure 4.7B). Hierarchical clustering of DEGs shows that the acute treated samples group together as well as the long-term treated samples, highlighting greater effect between treatment conditions rather than the inhibitors themselves (Figure 4.7C). Of the DEGs that correlate with both inhibitors, GO analysis showed the cell cycle and microtubule processes were again the most significant processes associated with KRAS-G12C inhibitors (Figure 4.7D). Whereas RTK signalling, cell growth and cell migration were

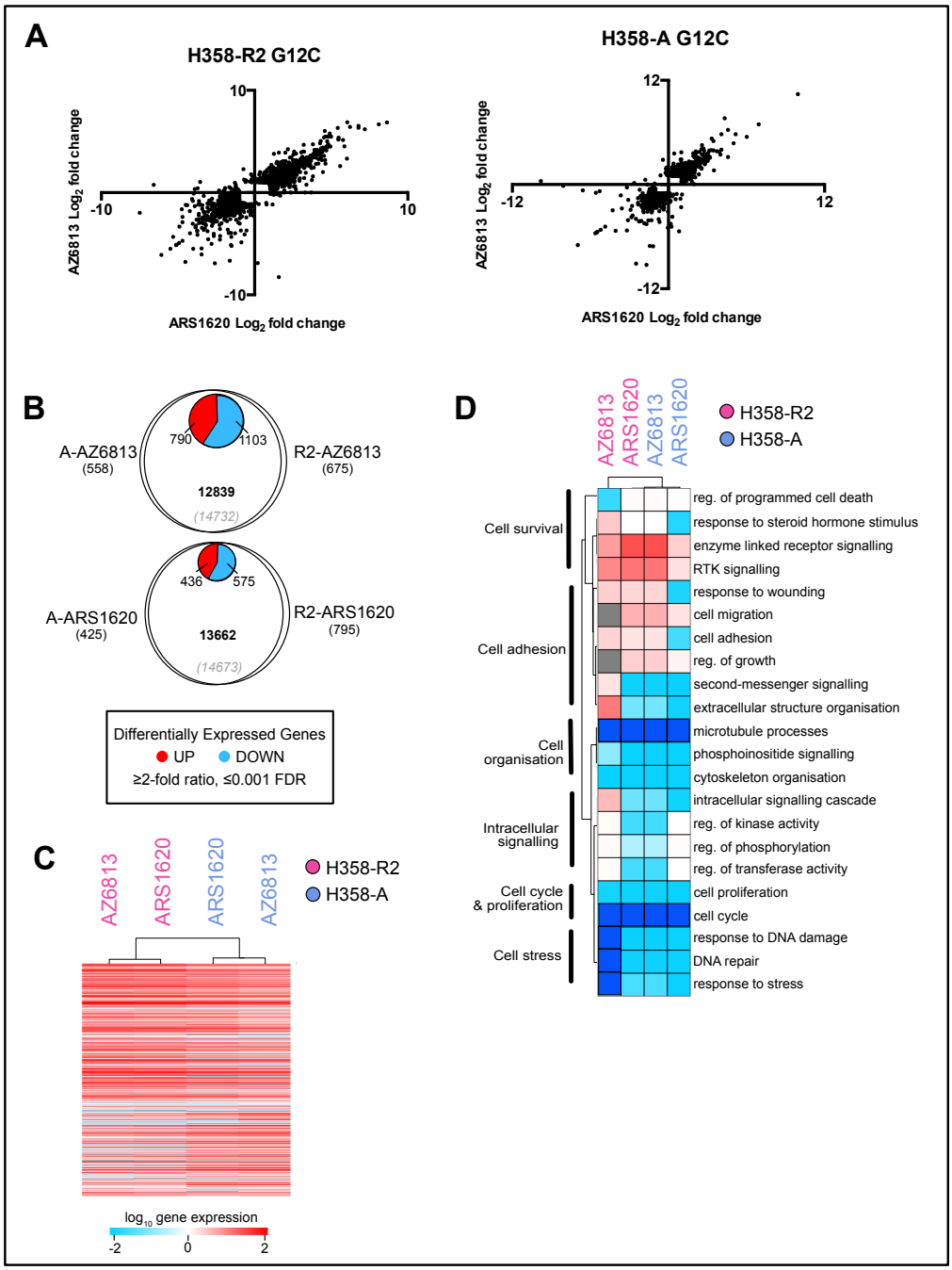

Figure 4.7: Comparison of G12C inhibitors between and across data sets.

(A) Scatter plots showing correlation of DEGs between G12C inhibitors from each data set. **(B)** Comparisons of the number of differentially expressed genes (DEGs) between acute (H358-A) and long-term treated (H358-R2) samples. Venn diagrams highlight the number of unique genes between each condition (in brackets), the total number of common genes (grey) and the number of these that were differentially expressed, represented by up regulated (red) and down regulated (blue) DEGs. **(C)** Hierarchical clustering of DEG gene expression values from H358-R2 and H358-A data sets which have been logarithmically converted. **(D)** Hierarchical clustering of significant GO terms based on p-values for H358 cells treated with G12C inhibitors. Terms highlighted in dark blue represent those with very high significance (p-value >1.0E-10).

not significant with KRAS-G12Ci. Comparison of treatment conditions shows that with ARS1620 both cell adhesion and response to wounding switch between acute and long-term treatment, becoming insignificant following longer treatment. On the other hand, with AZ6813 intracellular signalling, second messenger signalling, and extracellular organisation are more significantly enriched for under acute treatment, whereas terms associated with cell stress become more significant with long-term AZ6813 treatment. Overall, despite having the same mechanism of action, this indicates some differences between cell resistance mechanisms between the two inhibitors, possibly influenced by the difference in potency and selectively of the two inhibitors.

4.2.4 Comparison of protein expression between RPPA data sets

RPPA analysis was carried out at the MD Anderson Cancer Center (USA) to analyse changes in protein levels and protein modifications in resistant (H358-R) and acutely treated (H358-A) cells cultured in the presence of KRAS inhibitors and vehicle controls. Hierarchical clustering of all 466 antibodies was performed for both data sets (Figure 4.8A and B). In both H358-A and H358-R data sets, the vehicle controls cluster together separately from the inhibitor treated cells. Acutely treated cells demonstrated greater up- and down-regulation of proteins compared to the controls. Whereas in resistant cells, this trend is only present in AZD4785-treated cells. Combined hierarchical clustering of H358-R and H358-A data sets was also carried out (Figure 4.8C). As before all the controls from each data set cluster together as do the majority of inhibitor treated cells with only AZD4785-treated resistant cells clustering separately. AZ6813- and ARS1620-treated resistant cells clearly demonstrate fewer changes in protein expression compared to other inhibitor treated cells.

To compare differentially expressed proteins and modifications for each inhibitor across H358-R and H358-A data sets, scatter plots were used to highlight correlations between individual RPPA proteins (Figure 4.9). Comparison of AZ6813-treated cells indicated a mixed correlation of total

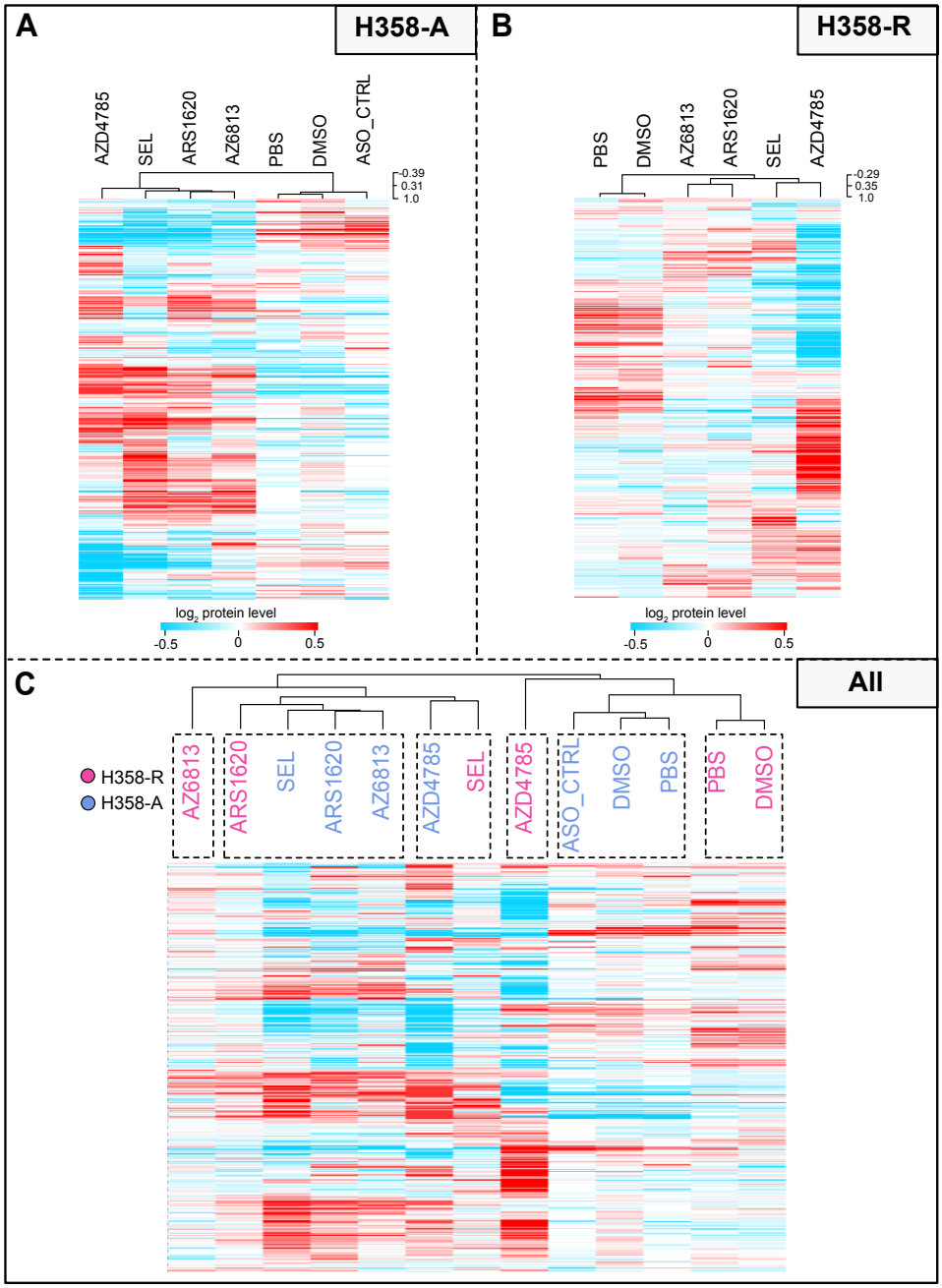

Figure 4.8: Comparison of protein expression levels in H358-A and H358-R treated cells. Hierarchical clustering of RPPA protein expression levels from (**A**) H358-A and (**B**) H358-R treated cells. (**C**) Hierarchical clustering of all RPPA samples from both data sets combined.

protein and modified protein expression, whereas ARS1620- and selumetinib-treated cells showed a majority of proteins correlating across the two data sets. On the other hand, AZD4785-treated cells showed no overall correlation, indicating mixed expression changes across the majority of proteins. Proteins which show the greatest changes between acute and chronic treatments are highlighted in Appendix 2.

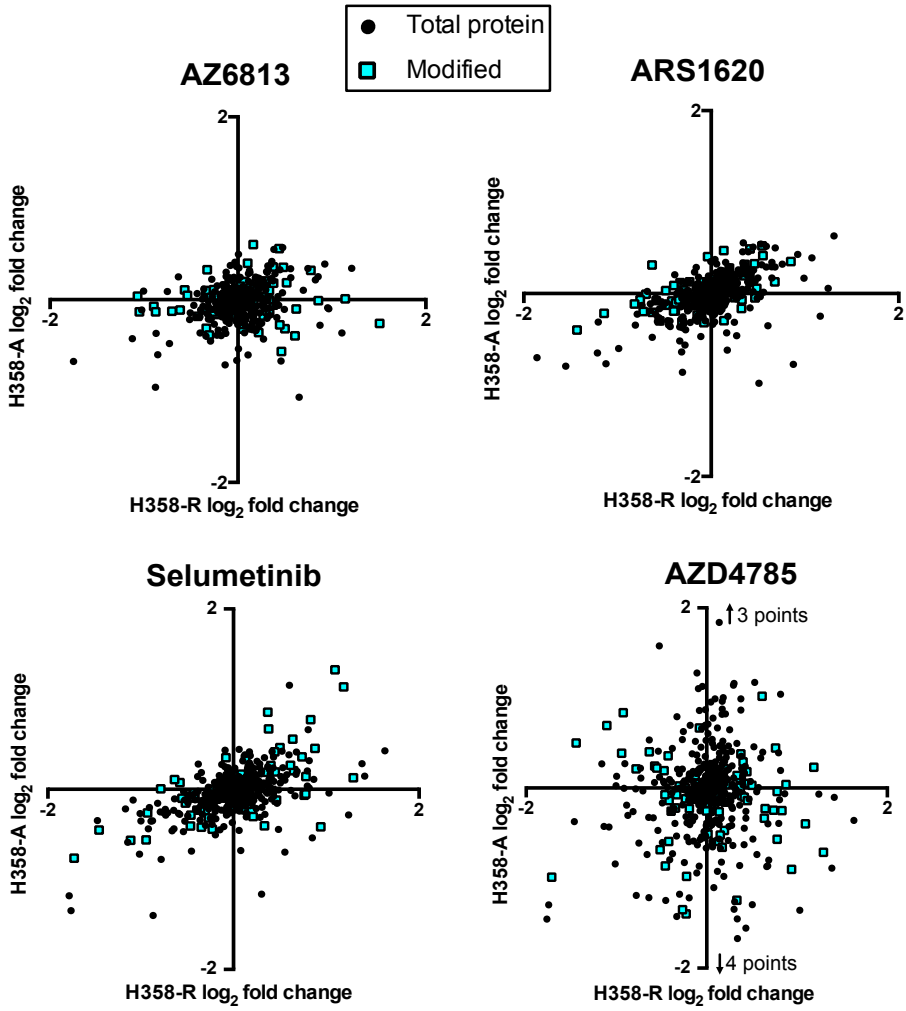

Figure 4.9: Correlation of total protein and modified protein expression levels between treatments.

Scatter plots comparing total protein and modified (phosphorylated or cleaved) protein levels that are differentially expressed between acute and long-term treated cells (H358-A v H358-R).

4.2.5 RAS pathway and cancer network analysis

Having analysed the main comparisons between different conditions within the RNAseq and RPPA data, and demonstrating they show good coverage of gene and protein expression, the data was applied to identify potential mechanisms of resistance. As previously mentioned, resistance mechanisms to KRAS inhibitors are also likely to be directly linked to the key signalling

pathways associated with the RAS-MAPK pathway [307]. Using the RAS network genes published by the RAS Initiative (National Cancer Institute), a RAS pathway was generated to map the signalling interactions of upstream and downstream effectors (Figure 4.10). Differential gene expression in Ras pathway genes was mapped for AZD4785-treated resistant cells in relation to control cells (Figure 4.11), which demonstrated the greatest pathway expression changes in comparison to the other inhibitors (Appendix 3).

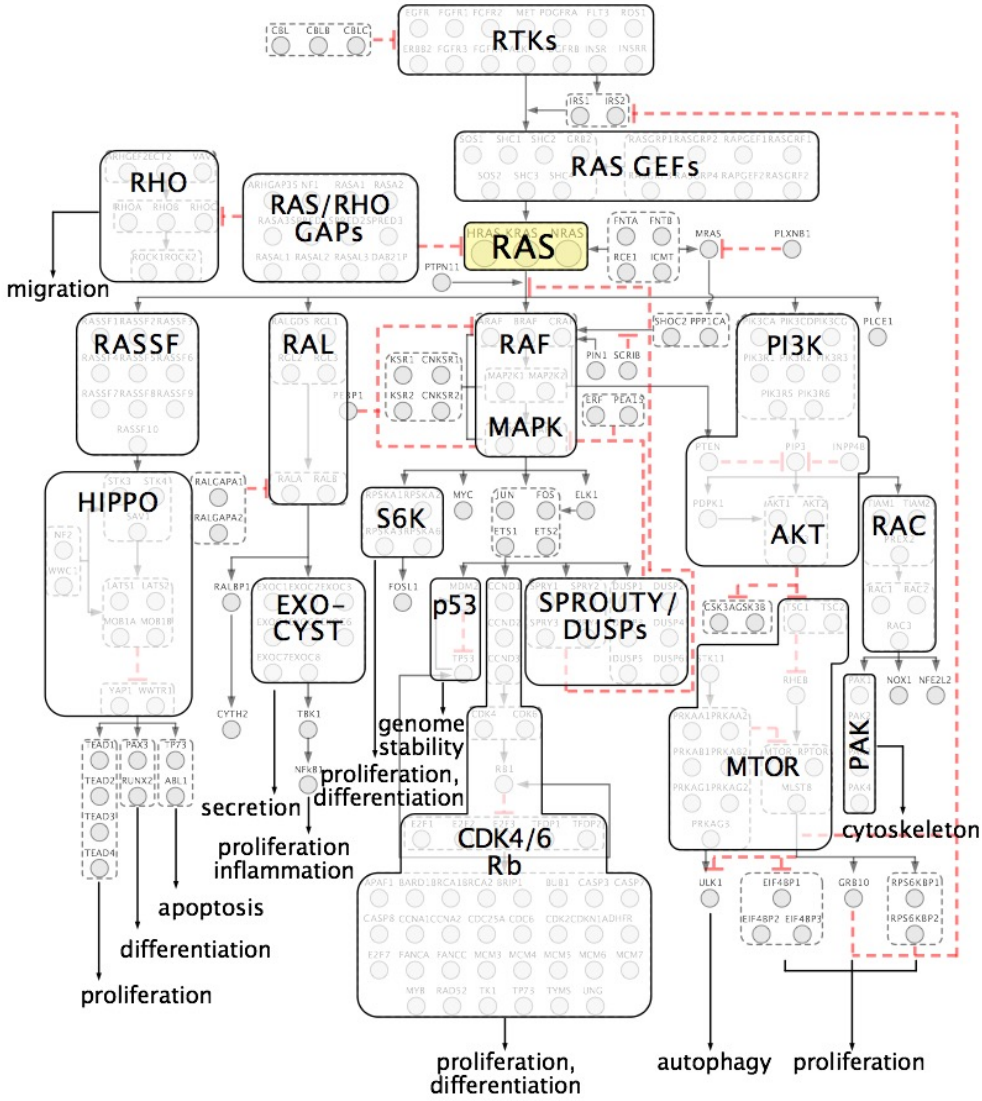

Figure 4.10: Network of the Ras Pathway.

Diagram highlighting the upstream and downstream signalling pathways associated with the Ras pathway.

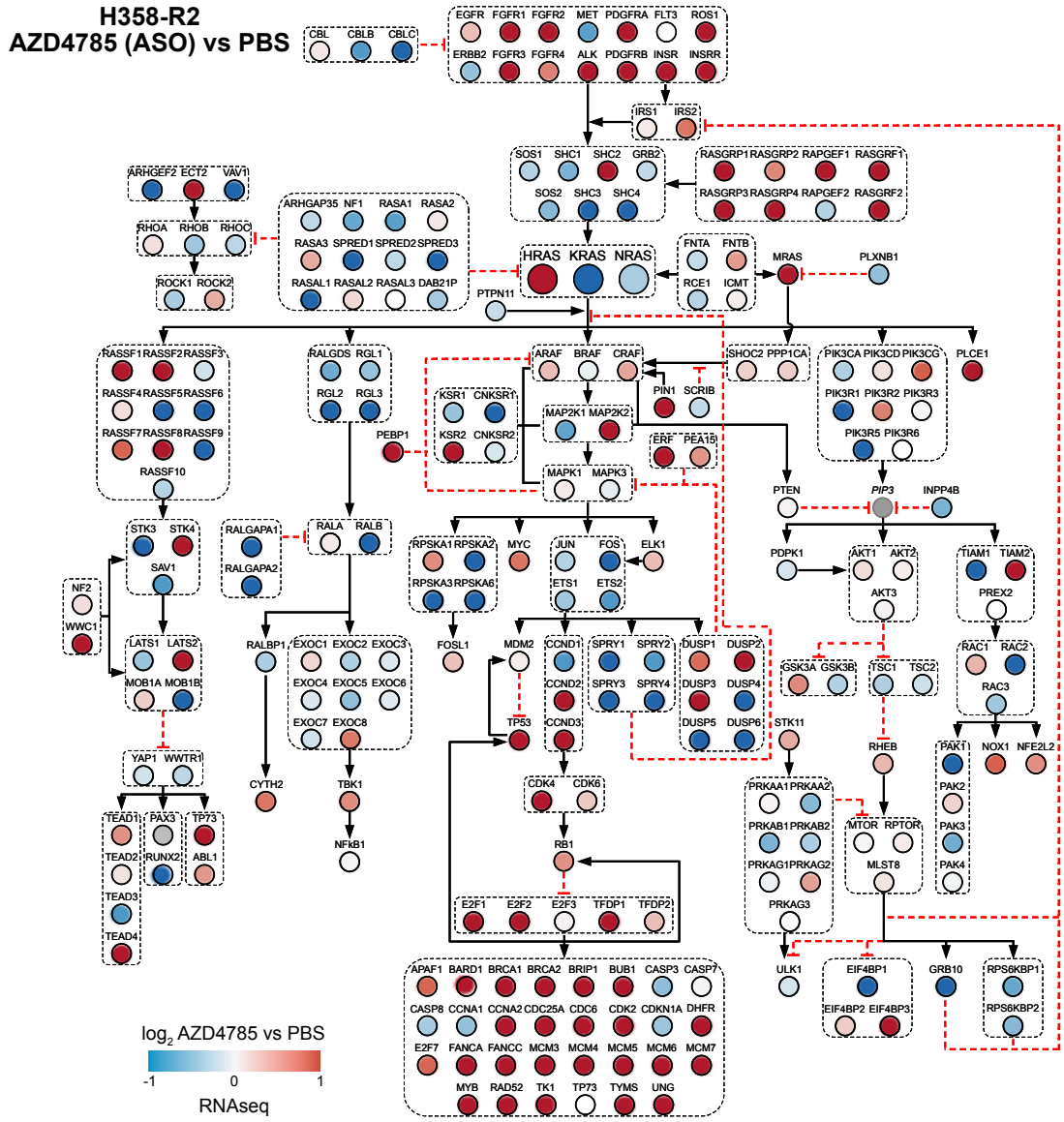

Figure 4.11: Ras Network Expression for H358-R AZD4785.

Heat map illustrating RNA-Seq differential gene expression in Ras pathway genes. Red indicates positive log fold change and represents increased expression in inhibitor treated cells compared to the corresponding vehicle control, whilst blue indicates negative log fold change and a decrease in expression.

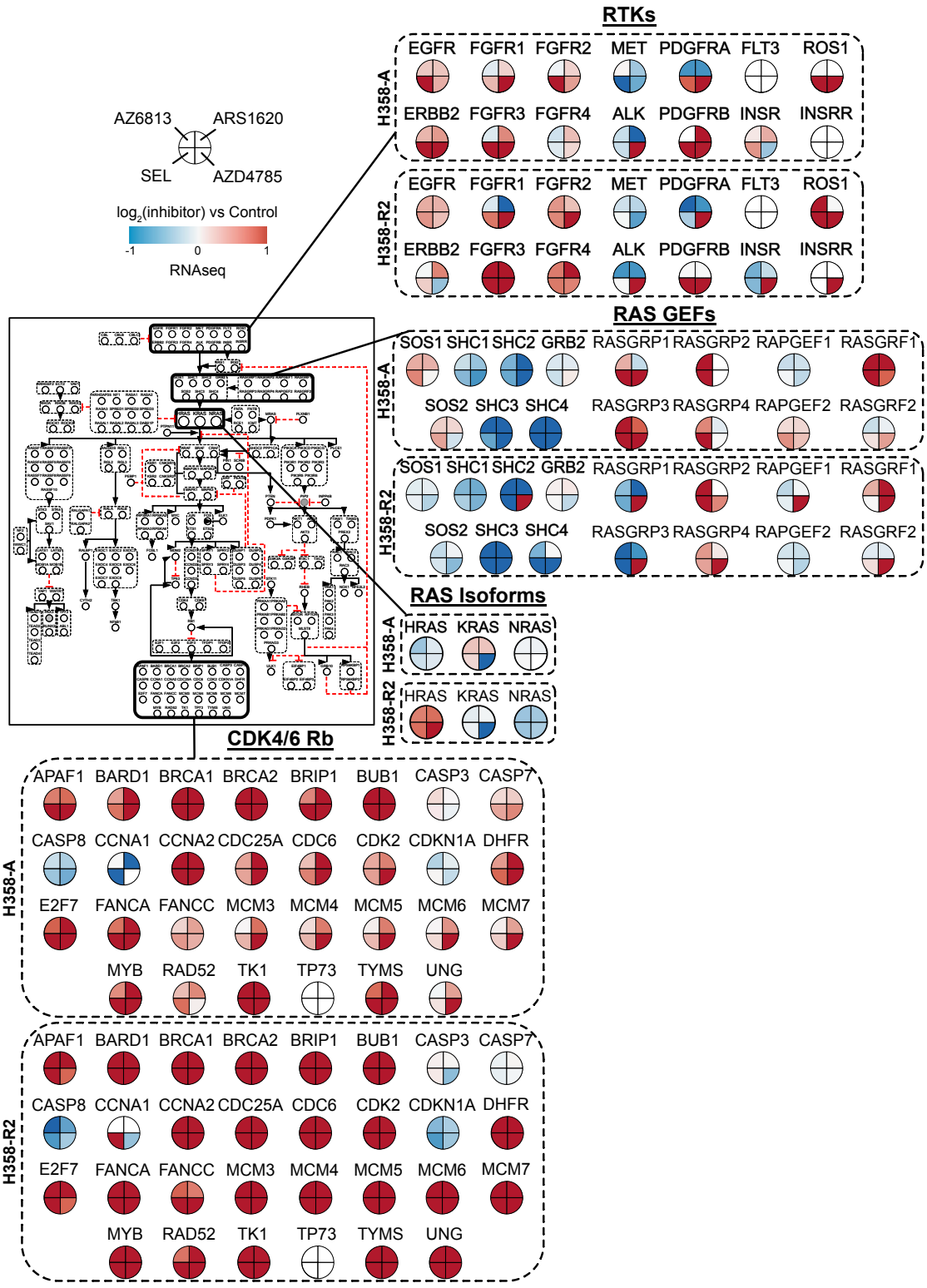

Figure 4.12: Expression changes of key nodes of the Ras Network.

Heat map illustrating RNAseq differential gene expression in key nodes of the Ras pathway between H358-A and H358-R2 data sets. Red indicates a positive log fold change and represents increased expression in inhibitor treated cells compared to the corresponding vehicle control, whilst blue indicates a negative log fold change and a decrease in expression.

In summary the RTK, RAS-GEFs and downstream CDK4/6 Rb effectors showed the greatest collective up-regulation in the RAS pathway. As a result, expression changes in these gene groups, alongside the RAS isoforms, were investigated further across all inhibitors (Figure 4.12). Interestingly in comparison to acutely treated cells (H358-A), HRAS became upregulated in all chronically treated resistant cells (H358-R), whereas KRAS and NRAS were downregulated, potentially indicating RAS isoform switching. Acute inhibitor treatments generally demonstrated upregulation of several RTKs including EGFR, FGFR1-4, ERBB2, PDGFRB and INSR, although some demonstrated mixed responses between inhibitors. On the other hand, MET, ALK and PDGFRA (G12C inhibitors) were generally down regulated. In resistant cells EGFR and FGFR expression remains high, whereas ERBB2, PDGFRB and INSR demonstrate down-regulation with some inhibitors. The majority of RTKs however remain up-regulated for AZD4785-treated resistant cells. Similarly, RAS GEFs also show general up-regulation of SOS1/2, RASGRP1-4, RAPGEF2 and RASGRF1 in H358-A cells. In contrast SOS1/2 along with RASGRP1/3 become down regulated in H358-R cells, although most RAS GEFs remain up-regulated for AZD4785-treated resistant cells. This highlights that RAS GEF mediated resistance mechanisms might not be a long-term mechanism. In contrast downstream CDK4/6 Rb effectors demonstrate similar up-regulation across acute and chronic treatments.

Next a wider cancer gene network was generated from 10 key signalling pathways associated with tumorigenesis from the Cancer Genome Atlas and highlights further pathway members and interactions [333]. A heat map for the genes associated with these pathways was mapped for RNAseq H358-A and H358-R2 data sets (Figure 4.13). Hierarchical clustering showed that samples within each data set group together. The greatest number of up-regulated genes were associated with RTKs, cell cycle and Wnt signalling across both H358-A and H358-R2 treatments, whereas PI3K signalling was generally down-regulated. A heat map was also generated for RPPA H358-A and H358-R data sets (Figure 4.14). Generally, components of the MAPK and PI3K pathways were up-regulated in acutely treated cells compared to chronically

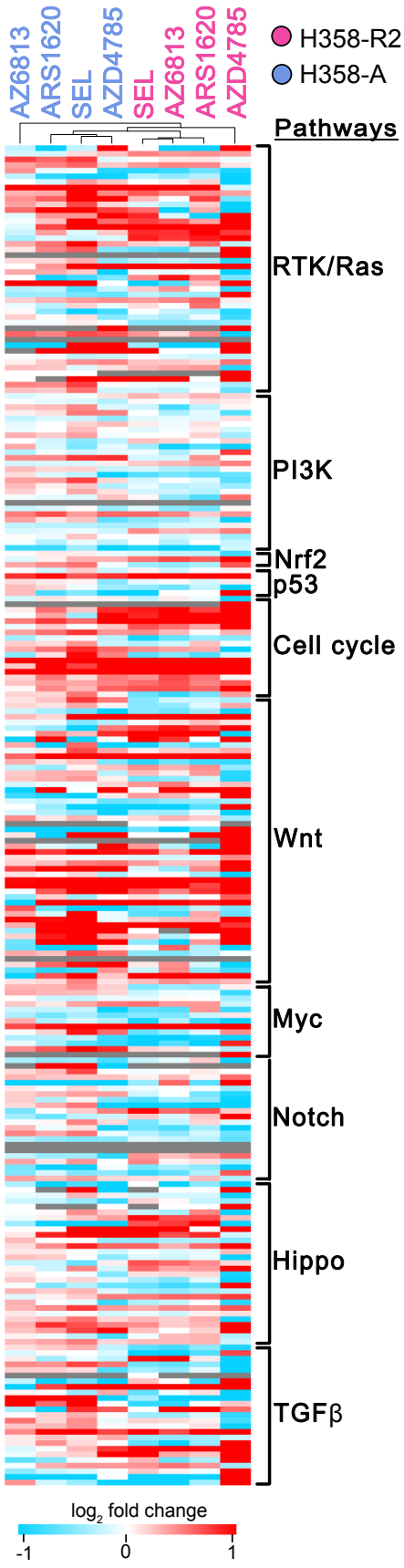

Figure 4.13: Heat map of the Cancer Gene Network.

H358-A and H358-R2 RNAseq data sets were compared and a heat map was generated for signalling pathways in the cancer gene network. Data is presented as log_2 fold change of each inhibitor compared to its corresponding control (DMSO/PBS). Red indicates a positive log fold change and represents increased expression in inhibitor treated cells compared to the corresponding vehicle control, whilst blue indicates a negative log fold change and a decrease in expression.

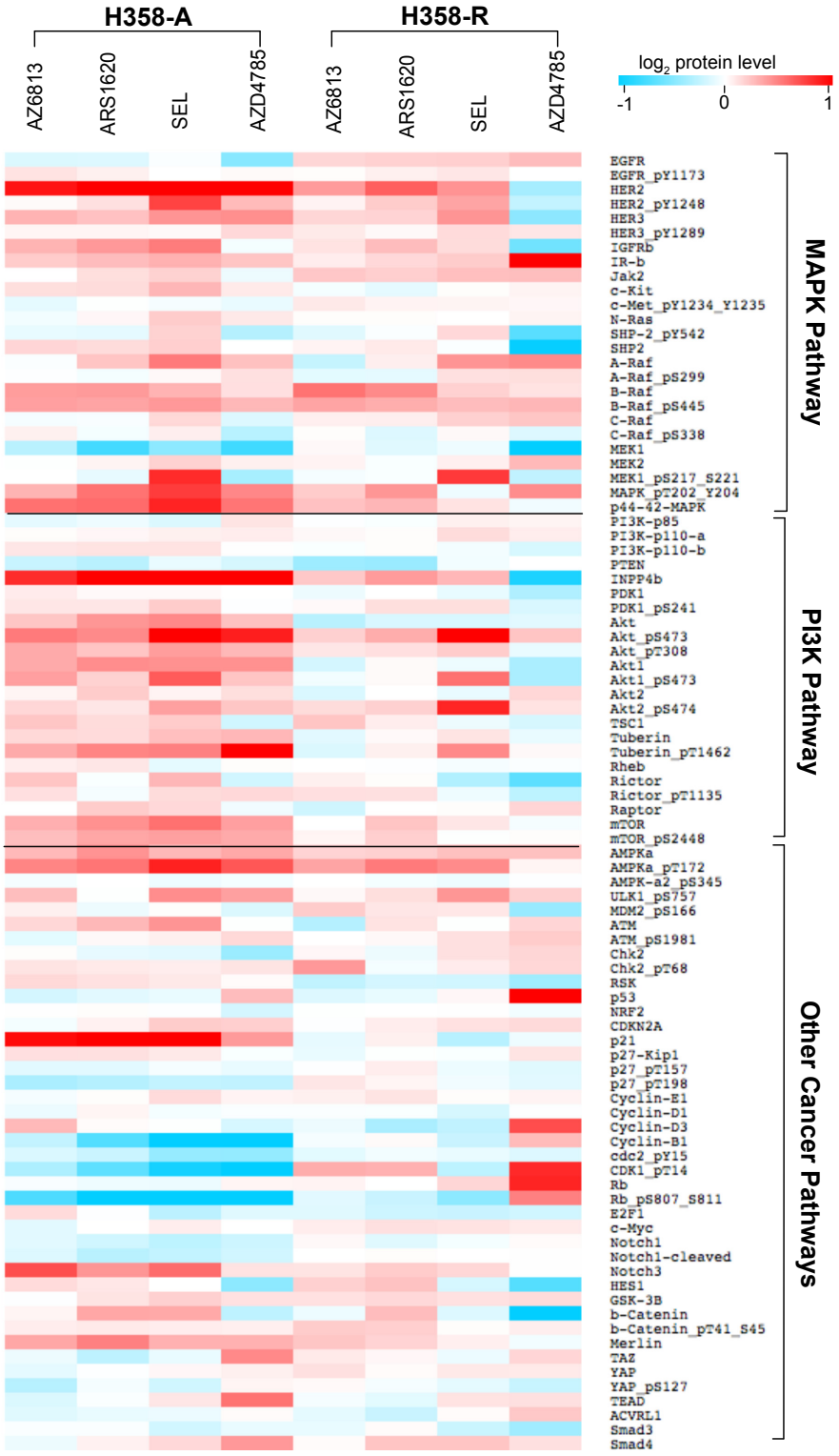

Figure 4.14: Heat map of RPPA cancer network protein expression.

A heat map was generated for RPPA proteins involved in various signalling pathways in the cancer gene network. Data is presented as $\log_2$ fold change of each inhibitor compared to its corresponding control (DMSO/PBS). Red indicates a positive log fold change and represents increased expression in inhibitor treated cells compared to the corresponding vehicle control, whilst blue indicates a negative log fold change and a decrease in expression.

treated resistant cells. In the MAPK pathway HER2/3, MAPK_pT202_Y204 and p44-42-MAPK were all highly up-regulated in acutely treated cells. In resistant cells, RTKs remained largely upregulated, particularly IR-b in AZD4785-treated cells. Although in contrast, the majority of MAPK components were instead down-regulated in these cells including HER2/3, IGFRb, SHP2 and SHP-2_pY542. In the PI3K pathway INPP4b, AKT_pS473, Tuberin_pT1462, mTOR and mTOR_pS2448 were also highly upregulated in H358-A cells. Whereas the majority of PI3K pathway components had lower expression levels in H358-R cells, particularly AZ6813- and AZD4785-treated cells. AKT phosphorylation however remained upregulated in selumetinib-treated resistant cells. In other cancer pathways, AMPKA, AMPKA_pT172, ULK1_pS757, ATM, p21, Notch 3 and Merlin were all up-regulated in acutely treated cells, whereas cell cycle related proteins cyclin-B1, cdc2_pY15, CDK1_pT14 and Rb_pS807_S811 were highly down-regulated. On the other hand, in AZD4785-treated resistant cells p53, cyclin D, CDK1_pT14, Rb and Rb_pS807_S811 were highly up-regulated and HES1 and b-catenin down-regulated. In summary, whilst both the RNAseq and RPPA datasets showed distinct responses in acute vs chronically treated cell lines across a wide range of cancer-relevant pathways, there was a general concordance of responses between the RAS inhibitors albeit with some divergence by the AZD4785.

To confirm the consistently altered expression of key RTKs seen throughout the RNA-seq and RPPA data, I further analysed changes in protein expression by western blotting (Figure 4.15). H358 cells treated with ARS1620 show an initial decrease in EGFR expression upon acute inhibitor treatment which increases back to control levels in chronically treated resistant (H358-R) cells, although this was accompanied by no change in pEGFR levels over time (Figure 4.15A). On the other hand, ERBB2 and pERBB2 abundance increases following 2 days of acute ARS1620 treatment and increased levels are maintained in resistant cells, whereas no changes in PDGFR-β and FGFR1 levels were observed. Similar trends were observed in H358 cells treated with selumetinib (Figure 4.15B). However differential responses are observed with H358 cells treated with AZD4785 (Figure 4.15C). In these cells EGFR

expression appears to decrease over time with acute treatment, and in H358-R cells pEGFR is absent. As with the other inhibitor treatments a similar increase in ERBB2 and pERBB2 expression is observed with acute treatment, however this response is absent in the chronically treated H358-R cells, and instead there are increases in PDGFR-β and FGFR1 protein levels. Overall these results are consistent to those observed for the RPPA proteomic data and further highlight the differential RTK signalling between acute and chronically treated resistant cells, as well as the differential reliance upon RTKs of AZD4785-treated resistant cells.

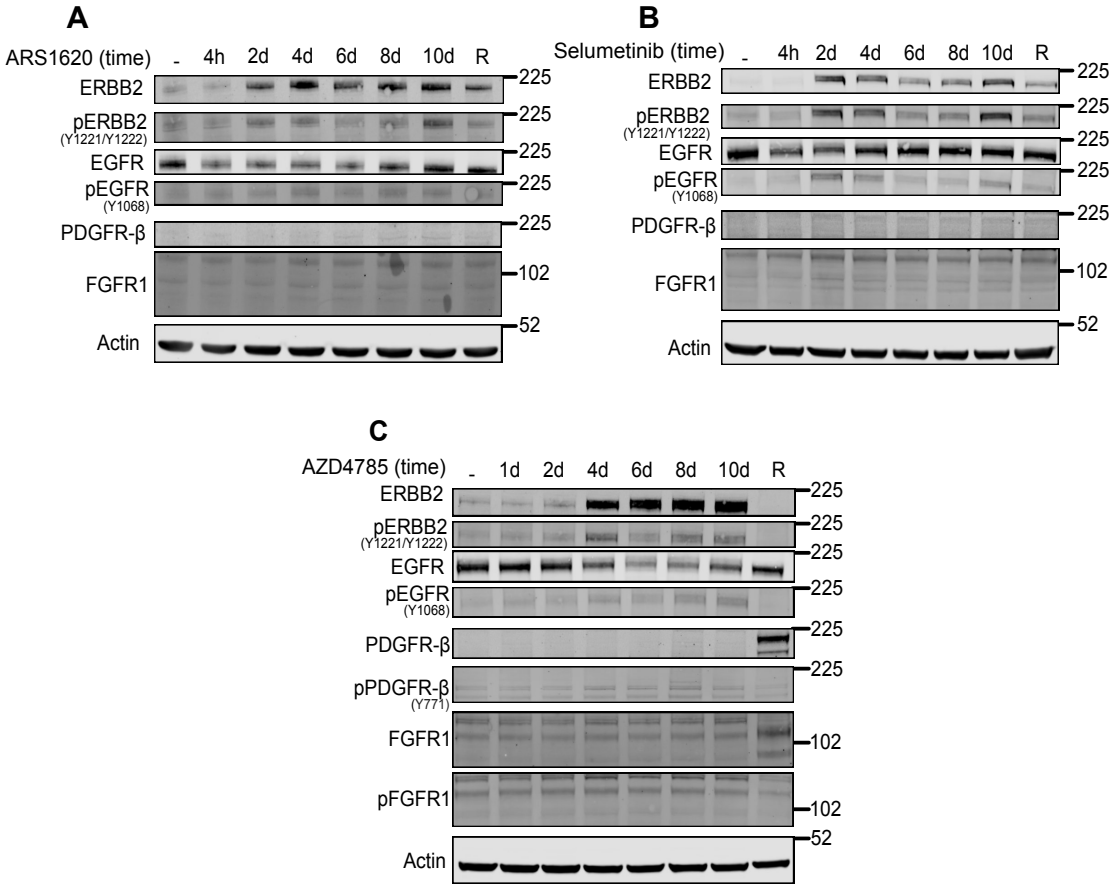

Figure 4.15: RTK expression over an acute inhibitor time course and in resistant cells. H358 cells were treated with vehicle control (-) or IC90 concentrations of each inhibitor **(A)** ARS1620, **(B)** Selumetinib and **(C)** AZD4785 for 10 days with cells re-dosed every 48 hours. Cell lysates were prepared at the indicated time points and RTK protein expression levels were analysed by immunoblotting. Lysates from chronically treated resistant H358-R (R) cells were carried out alongside. Blots are representative from two separate repeats.

To further investigate potential isoform switching observed in the RNA-seq data and to identify any changes in RAS activity levels associated with resistance, a RAS activity pull-down assay was performed (Figure 4.16). An initial decrease in active Pan-RAS and KRAS expression was observed with acute ARS1620 treatment (Figure 4.16A). However consistent with the onset of resistance development previously identified (Chapter 3, section 3.2.6), KRAS activity levels increased again at day 7 as well as in long-term resistant cells. No changes in active HRAS or NRAS were observed. In H358 cells treated with AZD4785 a decrease in active Pan-RAS and KRAS expression was also observed (Figure 4.16B), indicating consistency with KRAS mRNA knockdown from the mechanism of ASO inhibition. These also remained downregulated in AZD4785-treated resistant (H358-R) cells. Instead a slight increase in active HRAS expression was observed which is consistent with the RNA-seq data for these cells (Figure 4.12).

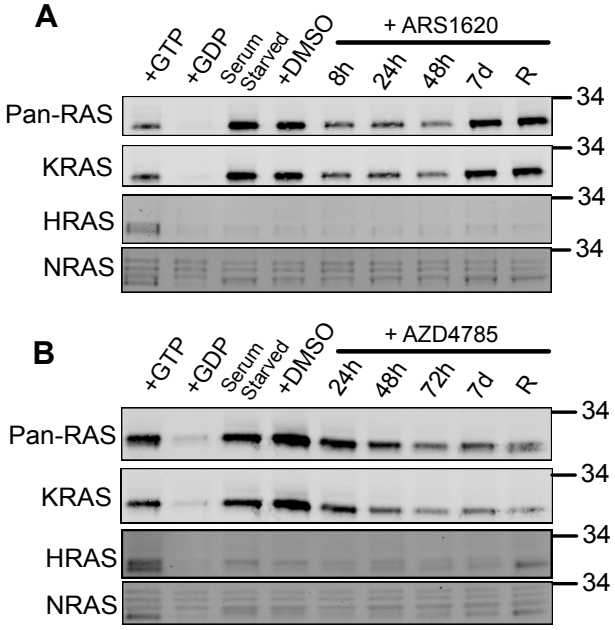

Figure 4.16: Changes in RAS activity over time

H358 cells were treated with GTP (positive control), GDP (negative control), DMSO (vehicle control) or IC90 concentrations of **(A)** ARS1620 and **(B)** AZD4785 for 7 days with cells re-dosed every 48 hours. Cell lysates were prepared at the indicated time points and lysates from H358-R (R) cells were also collected. A RAS activity pull-down assay was performed, and levels of active RAS expression were analysed by immunoblotting. Results are from a single experiment.

Following upregulation of cell cycle gene expression, changes in cell cycle protein expression and the importance of cell cycle regulation in tumorigenesis, the interactions of cell cycle signalling was focused on in more detail (Figure 4.17). The major regulatory cell cycle checkpoints occur at the G1/S and G2/M boundaries, ensuring that cells can only continue to progress through these stages in the presence of the correct stimuli and absence of DNA damage. During the cell cycle, cyclins interact with cyclin-dependent kinases (CDKs) to promote cell cycle progression, whereas CDK inhibitors prevent it (Figure 4.17A). Both RNAseq and RPPA expression data, including phosphorylation sites were mapped to a network of the cell cycle (Figure 4.17B). In acutely treated cells, CDKN1A (p21) protein expression and CDKN2C (p18) gene expression are highly upregulated across all inhibitor treatments, indicating inhibitory signalling for cell cycle progression. This response can be stimulated by DNA damage [334]. However downstream cyclin-D (CCND1-3), cyclin-E (CCNE1) and CDK expression showed mixed responses that suggested cell cycle progression. For example, CCND3, CDK2 and CDK6 generally showed increased expression levels with the majority of inhibitors. Despite high RB1 gene expression, RB1 protein expression and phosphorylation was down-regulated, whilst E2F1-3 and TFDP1/2 gene expression was generally upregulated, also indicating cell cycle progression. The gene expression of cyclin-A (CCNA2) and cyclin-B (CCNB1-3), involved in the later cell cycle S phase and mitosis, were also upregulated, although again protein expression of CCNB1 was conflicting. However inactivating phosphorylation sites at the corresponding CDK1 showed down regulation, also indicating progression through the cell cycle. In contrast chronically treated resistant cells showed a notable loss of p21 protein expression, although p18 gene expression remained high. Consequently, downstream cyclin-E (CCNE1), cyclin-D (CCND3 and CCND2 for AZD4785-treated cells) and their corresponding CDKs (CDK2/4/6) had increased expression compared to acutely treated cells. This data therefore also suggests promotion of the cell cycle in H358-R cells. In addition, cyclin-B (CCNB1-3) and cyclin-A (CCNA1/2) expression remained generally high in H358-R cells, although notably inactivating phosphorylation of the corresponding CDK1-3 at site T14 was upregulated in the majority of inhibitors.

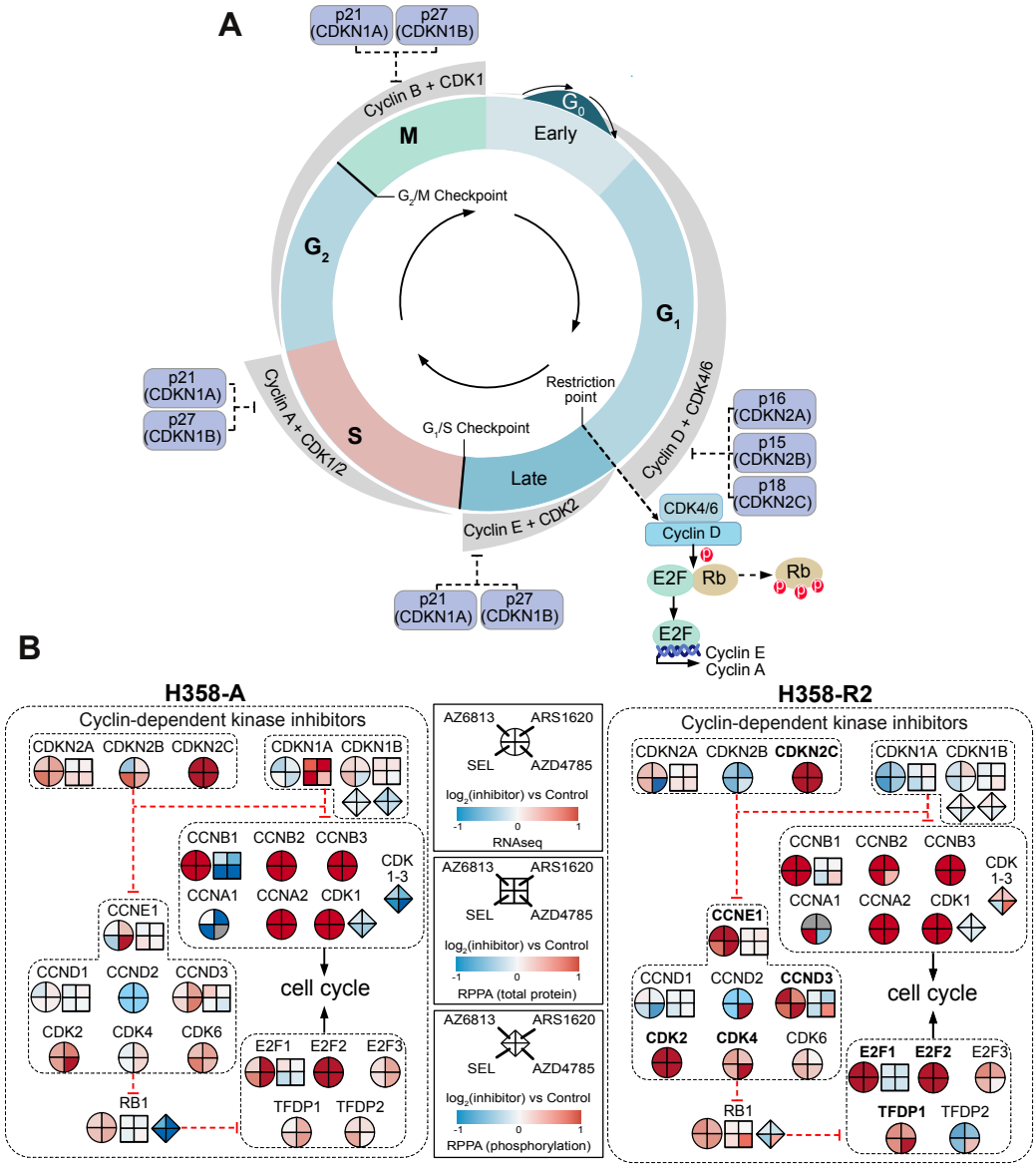

Figure 4.17: Changes in gene expression of the cell cycle genes.

(A) Illustration of the cell cycle which includes four distinct phases G1 (Gap 1), S (DNA synthesis), G2 (Gap 2) and M (Mitosis). At G0 cells can enter and exit a quiescent state. Regulation of the cell cycle is controlled by the formation of heterodimers of cyclins (cyclin -A, -B, -D, -E) and cyclin dependent kinases (CDKs) (CDK -1, -2, -4, -6). Several checkpoints (G1/S and G2/M checkpoints) ensure cells containing damaged DNA do not enter mitosis and are regulated by cyclin-dependent kinase inhibitors p21 and p27. Cell cycle progression past the restriction point occurs from phosphorylation of Rb by Cyclin D + CDK4/6, enabling E2F-mediated transcription of S-phase genes. **(B)** Network illustrating RNAseq differential gene expression and RPPA differential protein expression, including phosphorylation in cell cycle genes between H358-A and H358-R2 data sets. Red indicates a positive log fold change and represents increased expression in inhibitor treated cells compared to the corresponding vehicle control, whilst blue indicates a negative log fold change and a decrease in expression. Genes highlighted in bold represent those that are transcriptionally up-regulated in H358-R2 cells.

Another cancer pathway associated with resistance is the epithelial-mesenchymal transition (EMT) pathway [335-337]. It was previously shown that in KRAS-G13D mutant CRC cells, MEK inhibitor resistance promoted ERK1/2 hyperactivation and induced ZEB1-dependent EMT and chemoresistance [300]. As a result, epithelial and mesenchymal markers were identified from both the RNAseq and RPPA data (Figure 4.18). A heat map for differential gene expression of EMT markers highlights the distinctive clustering of H358-A and H358-R2 data sets indicating differences in cell morphology and adhesion between acute and chronic treatment conditions (Figure 4.18A). The differential expression of these genes was also presented as a network along with protein expression data from the RPPA (Figure 4.18B). In H358-A cells, expression of EMT transcription factors was mixed with SNAI1, TWIST1 and ZEB1 protein expression levels stable, despite changes in gene expression levels. Epithelial markers CDH1 (E-cadherin), TJP1, MUC1 (protein) were upregulated with all inhibitors, whereas DSG3 and LAMA2 were downregulated. In contrast the mesenchymal marker CDH2 (N-cadherin) remained downregulated except for AZD4785-treated cells. However other mesenchymal markers VCAN, CTGF, FN1 and VIM were generally upregulated. In H358-R cells SNAI1 and ZEB1 transcription factors were more upregulated in comparison to acute treated cells, which was expected to have a more inhibitory effect on epithelial marker expression and a stimulatory effect for mesenchymal markers. As anticipated, this was accompanied by a decrease in CDH1 gene and protein expression, along with loss of TJP1 and MUC1 expression. Conversely epithelial markers DSG3 and COL1A1 surprisingly increased in expression. On the other hand, CDH2, FN1, VCAN, VIM and ACTA2 gene expression was highly upregulated, although CTGF became downregulated. To explore changes in EMT markers further, immunoblotting was carried out on H358-A and H358-R cell lysates (Figure 4.18C) as well as immunofluorescence of several EMT markers (Appendix 4 and 5). Immunoblotting showed the epithelial marker CDH1 was highly expressed in all cells with the exception of AZD4785-treated resistant cells, which showed a clear decrease in protein levels. Correlating to gene expression data, this was also coupled with an increase in vimentin expression

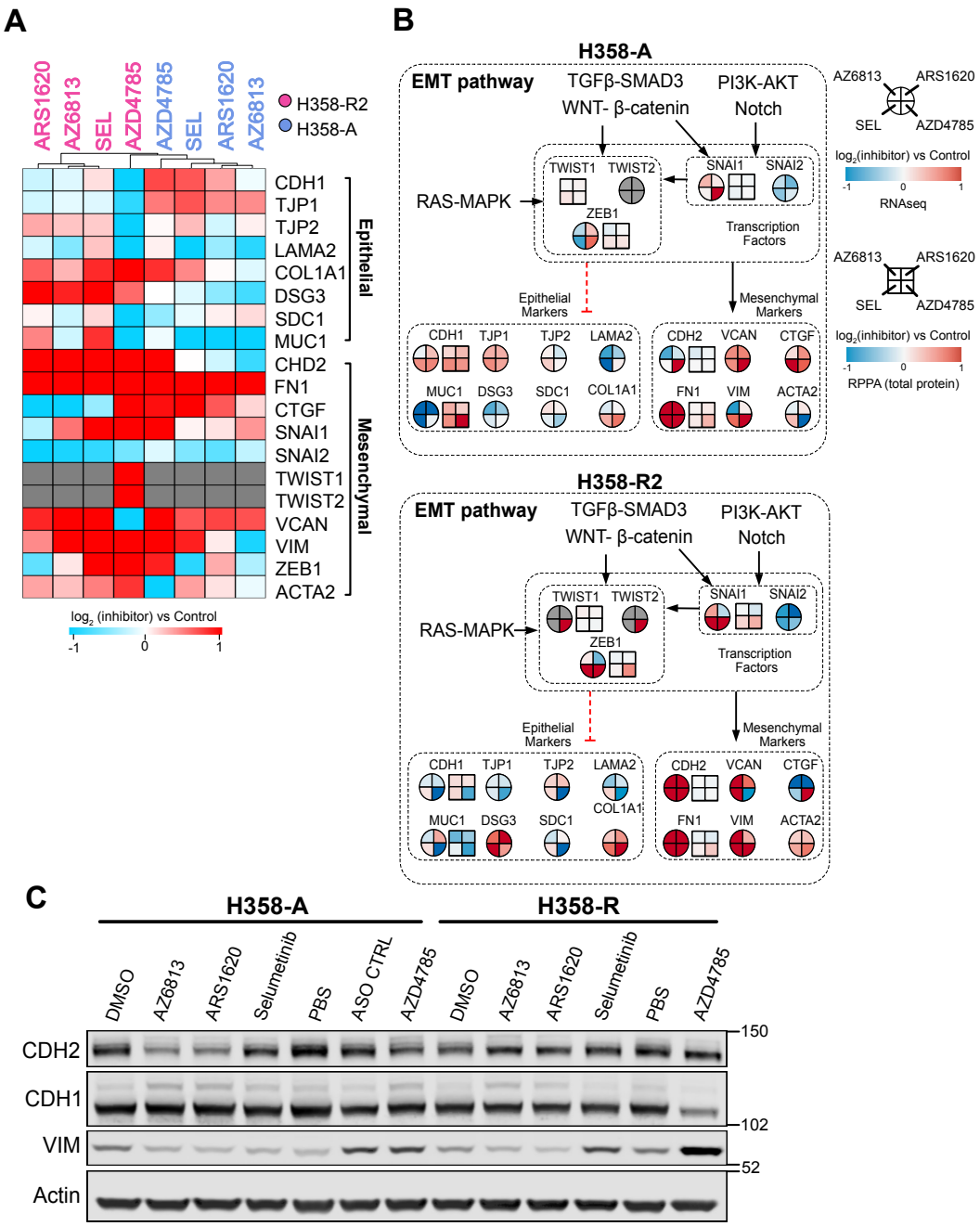

Figure 4.18: Gene and protein expression changes of the EMT Pathway.

(A) Heat map of differential gene expression in EMT genes between H358-A and H358-R2 data sets and **(B)** presented as a gene network adapted from [338], including RPPA protein expression data. Data is presented as log_2 fold change of each inhibitor compared to its corresponding control (DMSO/PBS). Red indicates a positive log fold change and represents increased expression in inhibitor treated cells compared to the corresponding vehicle control, whilst blue indicates a negative log fold change and a decrease in expression. **(C)** H358-A and H358-R cells seeded and treated with IC90 inhibitor concentrations or DMSO/PBS control and re-dosed every 48hrs. Cell lysates were prepared and EMT markers were analysed by immunoblotting with the antibodies shown (CDH1, E-cadherin; CDH2, N-cadherin; VIM, vimentin). Blots are representative from two separate repeats.

in these cells, indicating a more mesenchymal phenotype. A slight decrease in mesenchymal marker CHD2 expression was observed following KRAS-G12C inhibition in H358-A cells relative to controls, although no other differences could be determined across H358-R cells. Vimentin protein expression following KRAS-G12C inhibition also remained low in both H358-A and H358-R cells, suggesting these cells maintain an epithelial phenotype. Whereas selumetinib-treated resistant cells show some increase in vimentin expression. On the other hand, no clear phenotype distinctions could be determined by immunofluorescence with H358-A and H358-R cells expressing both E-cadherin and N-cadherin unanimously.

To integrate both RNAseq and RPPA data for combined multi-omic analysis, the webtool PaintOmics (v0.45) was used enabling additional significant pathways and potential mechanisms to be identified [339, 340]. Top significant KEGG pathways associated with H358-A and H358-R2 data sets are detailed in Table 4.2. Several KEGG pathways, particularly with chronically treated resistant cells are associated with the DNA damage response. A network heat map was also generated encompassing genes involved in the Fanconi anemia pathway for DNA interstrand crosslink (ICL) repair (Figure 4.19). In both acutely- and chronically-treated resistant cells there is up-regulation of DNA damage senor genes (ATR and ATRIP) as well as Fanconi anemia core complex genes which act as a scaffold for recruiting DNA damage repair proteins. In both treatment conditions BRCA1/2 genes were also transcriptionally upregulated, although discrepancies between gene and protein expression were again observed.

Table 4.2: Top KEGG pathways and p-values associated with RNAseq and RPPA data.

H358-A		H358-R2	
Pathway	**Combined p-value**	**Pathway**	**Combined p-value**
DNA replication	1.5350e-8	DNA replication	5.3009e-8
Biosynthesis of amino acids	1.6313e-4	Cell cycle	6.0473e-5
Transcriptional mis-regulation in cancer	0.00170	**Fanconi anemia pathway**	2.3817e-4
Mismatch repair	0.00391	P53 signalling	6.6208e-4
Apoptosis	0.00758	MAPK signalling pathway	8.8032e-4
Wnt signalling	0.00918	ECM-receptor interaction	0.00112
Necroptosis	0.00995	**Homologous recombination**	0.00271
MAPK signalling	0.01424	**Mismatch repair**	0.00541
Central carbon metabolism in cancer	0.01529	Regulation of actin cytoskeleton	0.01702
Cell cycle	0.02387	Rap1 signalling	0.03706

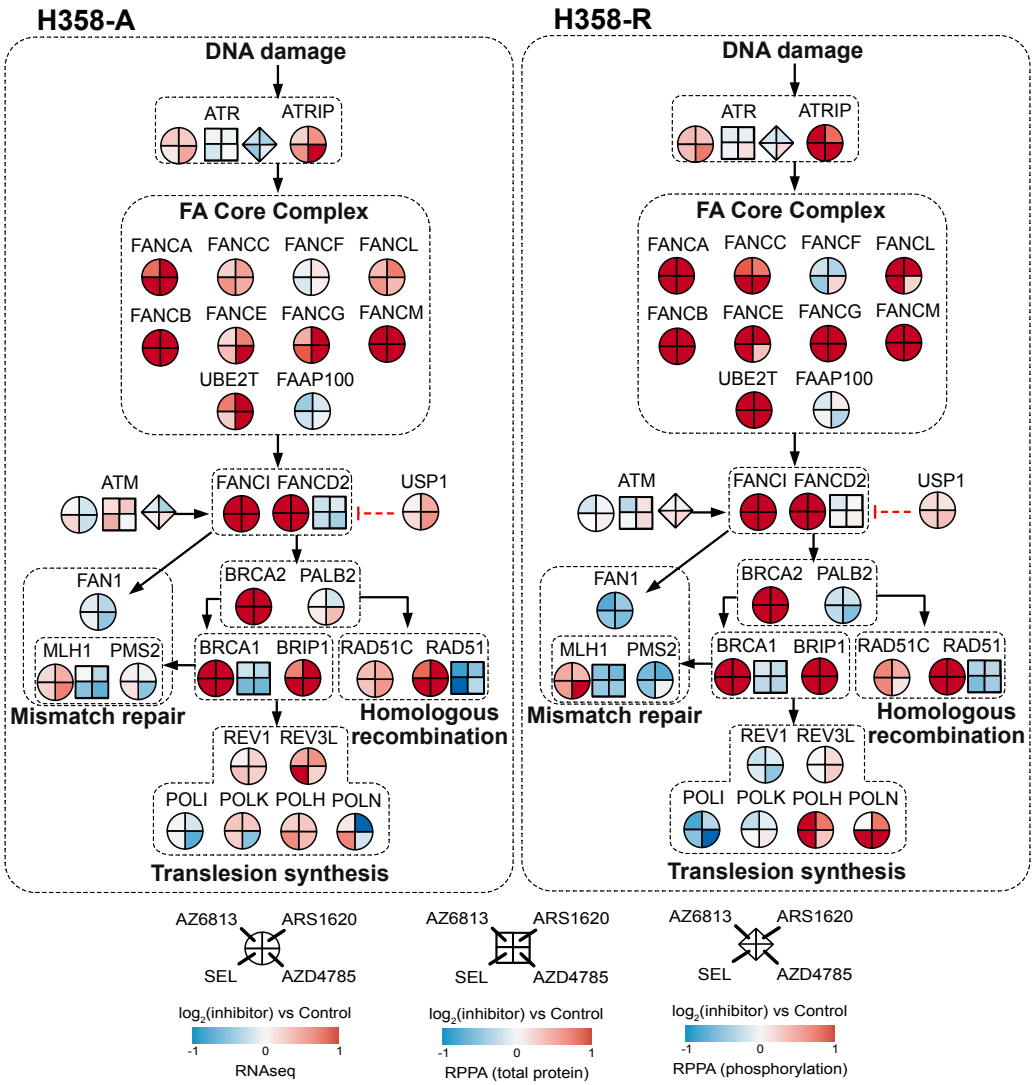

Figure 4.19: Changes in gene and protein expression involved in DNA damage recognition

Network illustrating RNAseq differential gene expression and RPPA differential protein expression between H358-A and H358-R2 data sets. Red indicates a positive log fold change and represents increased expression in inhibitor treated cells compared to the corresponding vehicle control, whilst blue indicates a negative log fold change and a decrease in expression.

4.3 Discussion

In this chapter I have identified several cancer pathways, that are upregulated in cells treated with various KRAS inhibitors and which are associated with known mechanisms of resistance. RNAseq and RPPA analysis were performed to profile and determine changes in gene and protein expression. RNAseq analysis of acute (H358-A) and chronic (H358-R) treated cells demonstrated good coverage of the number of genes across data sets, highlighting consistent processing and quality of samples (Figure 4.2 and 4.3). However, some differences in the correlation of genes expressed between repeat H358-R data sets was also observed (Figure 4.5), indicating that the timing of sample preparation may have had some influence. Furthermore, variability between some RNA and protein levels were observed, which may be associated with the different measurements and sensitivities of RNAseq and RPPA, as well as mechanisms of translational control such as mRNA stability, transcription rates and protein degradation [324]. Overall clear differences in gene and protein expression between control and treated cells was observed from hierarchical clustering analysis (Figure 4.4 and 4.8). Additionally, similarities and differences between inhibitor treatments were observed. As anticipated, the two KRAS-G12C inhibitors elicited similar responses, and this was seen for both acute and chronic treatments (Figure 4.7). On the other hand, AZD4785 (KRAS ASO) exhibited the greatest dissimilarity from the other inhibitors. For example a greater number of DEGs was observed in both H358-A and H358-R RNAseq samples (Figure 4.4A,C,E), as well as displaying distinct hierarchical clustering (Figure 4.4G). Analysis of protein abundance highlighted that cells treated chronically with AZD4785 displayed more up- and down-regulated proteins (Figure 4.8). The fact that this inhibitor reduces both KRAS-WT and KRAS-mutant mRNA is the most likely explanation for this. However, GO analysis of differentially expressed genes demonstrated that several similar biological processes were enriched for across all inhibitors, including the cell cycle, response to DNA damage and cellular stress (Figure 4.6).

In order to investigate relevant network rewiring and potential resistance mechanisms in more detail, components of the RAS pathway were focused on (Figure 4.10-4.12). Up-regulation of RTKs, RAS-GEFs and downstream CDK4/6 Rb effectors was observed (Figure 4.12) which indicates evidence of RAS stimulatory inputs and RAS activation. The upregulation of various RTKs following relief of negative feedback upon RAS pathway inhibition via RAF and MEK inhibition has been previously identified in several studies [278, 341, 342], and as I have shown also corresponds to direct KRAS inhibitors. Furthermore a recent study using the KRAS-G12C inhibitor ARS1620 also demonstrated upregulation of RTKs, in particular ERBB2/3, FGFR2/3 and PDGFRα/β following acute inhibitor treatment [343], which is consistent with results I have obtained. The high rate of GTP hydrolysis of the KRAS-G12C mutant compared to other RAS mutations [123], indicates a greater reliance on GEF-mediated activation. As KRAS-G12C inhibitors bind to the GDP-bound form of KRAS-G12C [207, 223], differential activation of RTKs and RAS-GEFs to promote GTP-bound KRAS-G12C may impair inhibitor binding to target, thereby mediating resistance. Studies also suggest that SHP2 and SOS1/2, which regulate RAS activity downstream of RTKs, are required for reactivation of RAS under both MEK inhibition [164, 343], and KRAS-G12C inhibition [344, 345]. Subsequent co-inhibition of SHP2 or SOS1/2 supressed this reactivation and development of adaptive resistance [343-345]. SOS1/2 are upregulated with acute treatment of AZ6813, ARS1620 and selumetinib, whereas with chronic AZ6813-, ARS1620-, selumetinib- and AZD4785-treatment in resistant cells SOS1/2 were downregulated (Figure 4.12). This might suggest that SOS1/2 activation might not be a permanent or long-term resistance mechanism. Furthermore, additional RAS-GEFs including RASGRP1-4, RAPGEF1/2 and RASGRF1/2 also showed upregulation in both acute and chronic treatments (Figure 4.12), and therefore inhibiting a single RAS-GEF in combination may not be enough to prevent adaptive resistance. Interestingly, H358 cells treated with AZD4785 demonstrated increased upregulation of RTKs and RAS-GEFs not upregulated by other inhibitors, suggesting some reliance on different RTKs and RAS-GEFs and highlighting that loss of KRAS mRNA altogether still promoted RAS pathway activation via

alternative mechanisms. The reliance on different RTKs was also highlighted by western blotting (Figure 4.15) which showed increased ERBB2 expression in acutely treated cells, as well as differential upregulation of FGFR1 and PDGFR-β in AZD4785-treated resistant cells which were not observed with either KRAS-G12C or MEK inhibition. Consistent with increased RTK and RAS-GEF activity, KRAS activity itself was also reactivated in ARS1620-treated resistant cells (Figure 4.16). This observation is consistent with those from other studies [220, 346], although these studies suggest differences in the mechanisms of KRAS activation, either by wildtype RAS or newly synthesised KRAS-G12C. However, in AZD4785-treated resistant cells, lower levels of KRAS activity from targeting KRAS mRNA were coupled with a small increase in HRAS expression, indicating potential reliance upon alternative RAS isoforms for pathway reactivation. Upregulation of *HRAS* gene expression was also observed from RNA-sequencing (Figure 4.12).

Throughout the cancer network analysis differences between acute (H358-A) and chronic (H358-R) treatments was also apparent. Differentially expressed proteins were identified from outliers in scatter plots showing how RPPA proteins correlated between conditions (Figure 4.9 and Appendix 2). Again, cells treated with AZD4785 highlighted greater differences in expression between conditions, further highlighting the divergence of these cells. When proteins were characterised according to pathways (Figure 4.14), MAPK and PI3K pathways showed greater protein upregulation in all acutely treated cells compared to chronic treatments. This suggests cells continually adapt over time and mechanisms of adaptive resistance are flexible and changing [347-349].

Gene and protein changes in the cell cycle signalling network highlighted mixed responses between inhibitors and treatments (Figure 4.17). Notably the loss of tumour suppressor CDKN1A (p21) protein expression as seen in H358-R cells (Figure 4.17B), has been proposed to mediate a drug-resistance phenotype [350]. Along with reduced expression of CDKN2A (p16) and subsequent upregulation of CDK2/4, this suggests these cells have rewired

signalling to promote the cell cycle in the presence of KRAS inhibitors [351]. Therefore, they may be susceptible to cell cycle and CDK inhibitors as part of a therapeutic combination strategy [352].

Expression analysis of the EMT pathway gave mixed results, though overall from transcriptomic data H358-A cells suggested a more epithelial phenotype, whilst H358-R cells suggested a more mesenchymal phenotype from the loss of CDH1 coupled with the increase of CDH2 and EMT transcription factors (Figure 4.18). In particular, AZD4785-treated resistant cells indicated the most mesenchymal phenotype from immunoblotting. Phenotype analysis by immunofluorescence was inconclusive and provide no clear distinction of EMT alterations (Appendix 4 and 5). Studies have also shown that NSCLC cells and patient-derived xenografts (PDXs) which express epithelial markers are more sensitive to EGFR inhibition, whereas those expressing mesenchymal markers are insensitive [255]. Interestingly it has been observed that following MEK inhibition in KRAS-mutant lung cells, EMT rewired RTK expression which resulted in differential activation of the MAPK pathway [258]. For example, epithelial cells activated MEK and AKT via ERBB3, whereas in mesenchymal cells this was via FGFR1. The combination of MEK inhibition and FGFR1 inhibition promoted tumour shrinkage *in vivo*. Although some H358-A and H358-R cells demonstrated mixed EMT responses, the upregulation of certain RTKs observed in these cells may subsequently be linked to the EMT process which further supports therapeutically targeting these pathways. For example, the differential expression of FGFR1 in AZD4785-treated resistant cells is therefore likely to be linked to their more mesenchymal phenotype.

Genomic instability from dysregulated DNA damage sensing and repair mechanisms is also a well-known hallmark of many cancers. Both H358-A and H358-R cells demonstrated upregulation of DNA repair genes, a common reprogramming mechanism associated with resistance (Figure 4.19) [353, 354]. As a result, cells resistant to KRAS inhibitors may be vulnerable to inhibitors which target DNA repair and DNA stress pathways.

Other pathways which could be related to KRASi resistance mechanisms include altered cellular metabolism. In H358-R cells, a general decrease in mTOR and PI3K pathway protein expression from RPPA data, coupled with raised AMPKA protein expression could indicate a switch from protein synthesis to autophagy (Figure 4.14). This observation is in agreement with other studies which have shown increased autophagy following KRAS suppression and inhibition in KRAS-mutant PDAC cells [355, 356].

Overall it is uncertain whether these changes in RTKs, RASGEFs, cell cycle and DNA damage pathways are a cause or a consequence of developing resistance to KRAS inhibitors. Throughout RNAseq and RPPA analysis they demonstrated consistently altered expression. These processes are directly linked to the RAS pathway and are also previously associated with known resistance mechanisms. As a result, I can now test different compounds targeting these pathways as potential strategies for combination therapies alongside KRAS inhibitors.

Chapter 5

Combination Therapeutics for KRAS inhibitors

5.1 Introduction

To overcome the identified resistance mechanisms associated with targeted KRAS therapeutics, the identification of effective drug combinations will be key to determining their full therapeutic potential. Combinatorial inhibitor strategies circumvent resistance mechanisms by co-inhibition of horizontal or vertical pathways in a synergistic or additive manner with the aim of increasing tumour cell killing and reducing adaptive signalling re-wiring within cancer cells, whilst minimising overlapping toxicity [166]. However, this strategy is hugely challenging, with relatively few drug combinations successfully making it through to the clinic. Several examples targeting the RAS pathway that have been FDA approved and are used clinically include the combination of dabrafenib (BRAFi) with trametinib (MEKi) for advanced BRAF-V600E mutated melanoma [357], and also encorafenib (BRAFi) plus cetuximab (EGFRi) for BRAF-V600E mutated CRC [358]. Furthermore a phase III trial investigating encorafenib, binimetinib and cetuximab in BRAF-mutated CRC shows promising results and improved overall survival (NCT02928224) [359].

The results presented in chapter 4 from omics analysis, showed consistently upregulated expression of RTKs, RAS-GEFs, cell cycle and DNA damage pathways in cells resistant to KRAS inhibitors, and therefore it is anticipated that they will be sensitive to inhibitors targeting these pathways and signalling nodes (summarised in Table 5.1). Indeed, other studies investigating KRAS-G12C inhibitor resistance have also identified this can be driven by feedback

activation from multiple RTKs and highlight that vertical pathway inhibition can enhance the efficacy of KRAS-G12C inhibitors [220]. In particular inhibition of SHP2 (SHP2i), an RTK-associated phosphatase, has shown promising potential as a combination strategy [220]. SHP2i prevented RAS pathway feedback reactivation from multiple RTKs following KRAS-G12C inhibition and enhanced KRAS-G12C inhibitor efficacy via increased KRAS-GDP occupancy [344]. Similarly, inhibition of SOS1 was found to synergise with KRAS-G12C inhibitors by disrupting RAS activation [345]. Other studies have highlighted that targeting parallel and downstream survival pathways such as CDK4/6 or PI3K pathways represents another effective combination strategy to enhance KRAS-G12C inhibitor efficacy [360, 361]. These combinatorial approaches increased the suppression of phospho-S6, a ribosomal protein downstream of mTORC1 which represents a good predictor of inhibition of cell viability [360-362]. In preclinical KRAS-mutant colorectal cancer models the combination of CDK4/6 and MEK inhibition showed good efficacy [314], and several clinical trials are currently being undertaken with CDK4/6 inhibitors for KRAS-mutant NSCLC (NCT03170206, NCT02022982, NCT02152631). In another preclinical study, the addition of both mTOR and upstream IGF1R inhibitors alongside KRAS-G12C inhibition further enhanced the suppression of cell proliferation through strong inhibition of AKT, S6 and ERK signalling [363]. Clinical trials of KRAS-G12C inhibitors are currently ongoing, and additional clinical trials combining KRAS-G12C inhibitors with other targeted inhibitors and chemotherapeutic agents have already started (Table 5.2). Identifying the best combination partners to maximise the benefit of targeted KRAS inhibitors will be crucial for effectively treating KRAS-mutant tumours.

Table 5.1: Potential inhibitors for combination with KRAS inhibitors.

Inhibitor	Target	Type of inhibition	Mechanism	Ref.
SHP099	SHP2	Allosteric inhibitor	SHP099 binds to the N-terminus and C-terminus of SHP2, and its tyrosine phosphatase domains.	[364]
RMC-4550	SHP2	Allosteric inhibitor	RMC-4550 inhibits the activity of full-length wild-type SHP2 enzyme activated by a di-phosphotyrosine peptide but lacks activity against the free catalytic domain of SHP2.	[365]
BAY-293	KRAS-SOS1	Competitive inhibitor	Selectively inhibits the KRAS–SOS1 interaction.	[345]
BI-3406	KRAS-SOS1	Competitive inhibitor	Binds to the catalytic domain of SOS1 and prevents the interaction with KRAS-GDP.	[366]

Infigratinib	FGFR1-4	ATP competitive inhibitor	Inhibits kinase activity and autophosphorylation of receptors.	[367]
AZD4547	FGFR1-4	ATP competitive inhibitor	Inhibits autophosphorylation of FGFR1, 2, and 3 tyrosine kinases and weaker inhibition of FGFR4 kinase activity.	[368]
Gefitinib	EGFR	ATP competitive inhibitor	Inhibits kinase domain and autophosphorylation of seven major tyrosine phosphorylation sites on EGFR (Tyr1173/1148/1086/ 1068/1045/992/845).	[369]
Erlotinib	EGFR	ATP competitive inhibitor	Binds to EGFR kinase domain and prevents EGFR autophosphorylation.	[370]
Lapatinib	EGFR + ERBB2	ATP competitive inhibitor	Binds to EGFR/ERBB2 kinase domains and prevents autophosphorylation of receptors.	[371]
CP-673451	PDGFRα/β	ATP competitive inhibitor	Selective for PDGFR kinase domain and inhibits autophosphorylation of receptors.	[372]
Crenolanib	PDGFRα/β, FLT3	ATP competitive inhibitor	Binds to kinase domain and prevents receptor autophosphorylation.	[373]
NVP-ADW742	IGF-1R, INSR	ATP competitive inhibitor	Binds to kinase domain and prevents receptor autophosphorylation.	[374]
Flavopiridol	Broad CDK inhibitor	Competitive kinase inhibitor	Inhibits multiple CDKs including CDK1, CDK2, CDK4, CDK6, CDK7 and CDK9. Binds to the ATP-binding site of CDKs and directly inhibits kinase activity. Causes cell cycle arrest at G2 and prevents mitosis.	[375]
AZD5438	CDK1, CDK2 and CDK9	ATP competitive inhibitor	Potent inhibitor of CDK1/2/9 kinase activity.	[376]
Roscovitine	Broad CDK inhibitor	ATP competitive inhibitor	Potent and selective inhibitor for CDK1, CDK2, CDK5, CDK7 and CDK9. Competes at ATP binding site and inhibits kinase activity.	[377]
Palbociclib	CDK4 and C DK6	ATP competitive inhibitor	Selective inhibitor of CDK4/6 with little or no activity against other CDKs. Competes at ATP binding site and inhibits kinase activity.	[378]
Ribociclib	CDK4 and C DK6	ATP competitive inhibitor	Selective inhibitor of CDK4/6 with little or no activity against other CDKs. Competes at ATP binding site and inhibits kinase activity.	[379]
Olaparib (AZD2281)	PARP1/2	Competitive inhibitor	Inhibition of PARP enzyme activity by competitive inhibition of the catalytic domain. PARP inhibitors prevent the release of PARP enzymes from damaged DNA leading to persistent single/double strand breaks and interference of DNA damage repair, thus ultimately leading to cell death.	[380]
Talazoparib	PARP1/2	Competitive inhibitor	Inhibition of PARP enzyme activity by competitive inhibition of the catalytic domain, resulting in inhibition of DNA damage repair	[381]
Niraparib	PARP1/2	Competitive inhibitor	Inhibition of PARP enzyme activity by competitive inhibition of the catalytic domain, resulting in inhibition of DNA damage repair	[382]
AZD0156	ATM	ATP competitive inhibitor	Inhibition of ATM kinase activity and subsequent prevention of DNA damage checkpoint activation. Causes disruption to DNA damage repair and prevents progression through the G1 cell cycle checkpoint.	[383, 384]
Berzosertib	ATR	ATP competitive inhibitor	Inhibits ATR kinase activity and prevents DNA repair and progression through the G2 cell cycle checkpoint.	[384, 385]
Adavosertib (AZD1775)	WEE1	ATP competitive inhibitor	Inhibitor of Wee1 kinase. Prevents the phosphorylation of CDK1 and CDC2 and impairs the G2 DNA damage checkpoint.	[386]
Everolimus	mTORC1	Allosteric inhibitor	Binds to the FKBP12 receptor which directly interacts with mTORC1, and thus inhibits its downstream signalling. This results in dephosphorylation of S6K1 and prevents cell cycle progression.	[387, 388]
Sapanisertib	mTOR	ATP competitive inhibitor	Binds to and occupies the ATP binding site on both mTORC1 and mTORC2 complexes of mTOR.	[389, 390]
AZD8055	mTOR	ATP competitive inhibitor	Inhibits both mTORC1 and mTORC2. Occupies the ATP binding site to prevent mTOR phosphorylation.	[391]

Table 5.2: Current KRAS-G12C inhibitor clinical trials.

Drug	Company	Phase	Clinical Trial	Cancer	Combinations
MRTX849 (Adagrasib)	Mirati	Phase 2	NCT04613596	KRAS-G12C NSCLC	Pembrolizumab (PD1)
		Phase 1/2	NCT03785249	KRAS-G12C mutant solid tumours	Pembrolizumab (PD1) Cetuximab (EGFR) Afatinib (ERBB2)
		Phase 1/2	NCT04330664	KRAS-G12C mutant solid tumours	TNO155 (SHP2)
AMG510 (Sotorasib)	Amgen	Phase 1/2	NCT03600883 (CodeBreak 100)	KRAS-G12C mutant solid tumours	Anti PD-1/L1 Midazolam
		Phase 1/2	NCT04185883 (CodeBreak 101)	KRAS-G12C mutant solid tumours	PD-1i MEKi SHP2i Pan-ERBBi PD-L1i EGFRi mTORi CDKi Chemotherapy MEKi + EGFRi EGFRi + Chemotherapy
		Phase 3	NCT04303780 (CodeBreak 200)	KRAS-G12C advanced NSCLC	Docetaxel

Aims

In order to identify translational opportunities to overcome drug resistance mechanisms associated with direct KRAS inhibitors, I aimed to identify inhibitor combinations that are effective alongside KRAS inhibitors. This will be the first study to compare inhibitor combinations alongside multiple types of KRAS inhibitor, as well as comparison across multiple resistant cells lines. Insights into potential resistance mechanisms highlighted from the omics data (see Chapter 4) revealed upregulation of several components of the RAS pathway and some wider cancer pathways. Following this, I have tested various compounds targeting these pathways and have utilised these in different inhibitor combinations. Comparison between different resistant phenotypes will elucidate altered sensitivity or resistance across different inhibitor combinations. Using this approach, I aimed to:

- Identify combinations of inhibitors that re-sensitise KRASi-resistant cells
- Compare the sensitivities of different resistant cells to combined inhibitors

- Determine whether these combinations delay or overcome resistance in naïve cancer cells

5.2 Results

5.2.1 Cells resistant to KRAS inhibitors showed differential sensitivity to other targeted inhibitors

To evaluate combination strategies, resistant cells were treated with inhibitors targeting pathways of previously identified resistance mechanisms (Chapter 4). Alongside changes in cell confluency (Figure 5.1), proliferation and cytotoxicity were also monitored (Appendix 6 and 7). Treatment with different RTK inhibitors showed differential sensitivity across the different resistant cells. For example, ARS1620-treated resistant cells (R-ARS) retained sensitivity to EGFR and ERBB2 inhibitors (erlotinib, gefitinib, lapatinib and tucatinib) as well as IGFR/INSR inhibition (NVP-ADW742) (Figure 5.1A). This is consistent with my previous transcriptomic and proteomic results where upregulation of these receptors was observed (Chapter 4). In comparison both selumetinib-treated resistant cells (R-Sel) and AZD4785-treated resistant cells (R-ASO) showed increased resistance to these inhibitors. In contrast, R-ASO cells were more sensitive to FGFR inhibition using AZD4547. On the other hand, PDGFR inhibition (CP-673451 and crenolanib) had no effect on any resistant cells. This highlights different dependencies of RTK signalling across resistant cells treated with different KRAS inhibitors.

To assess whether feedback from multiple RTKs could be inhibited, I evaluated the effect of SHP2 and KRAS-SOS1 inhibition across the resistant cells. SHP2 inhibition (SHP099 and RMC-4550) was most effective in R-ARS cells, demonstrating comparable sensitivity to control DMSO-treated cells (R-DMSO) (Figure 5.1B). R-ARS cells also showed sensitivity to KRAS-SOS1 inhibition using BAY-293. However, R-Sel and R-ASO resistant cells still exhibited increased resistance to these modes of inhibition.

Cross-inhibition of resistant cells with the original KRAS and MEK inhibitors used in this study (ARS1620, AZD4785 and selumetinib) highlighted increased

resistance to alternative KRAS inhibition in all cells (Figure 5.1C). Despite this, R-ASO cells were particularly sensitive to MEK inhibition with selumetinib which was comparable to control cells.

Comparison of different inhibitors targeting the cell cycle demonstrated that all resistant cells were sensitive to the broad CDK inhibitor flavopiridol, as well as some sensitivity to AZD5438 at higher concentrations targeting CDK1/2/9 (Figure 5.1D). R-ARS cells also showed selective sensitivity to roscovitine, another broad CDK inhibitor targeting CDK1 and CDK2/5, whereas selective CDK4/6 inhibitors (palbociclib and ribociclib) had no effect on all resistant cells.

Furthermore, PARP inhibition (olaparib, talazoparib and niraparib) which prevents the ability of cells to repair damaged DNA, also showed no effect in resistant cells (Figure 5.1E). Little effect on cell proliferation was also observed in R-DMSO cells suggesting a higher inhibitor concentration might be required. Resistance to the ATR inhibitor berzosertib was also observed, although interestingly R-ASO cells demonstrated increased sensitivity to the ATM inhibitor AZD0156, highlighting increased dependency on this DNA repair pathway. Furthermore, all resistant cells showed some sensitivity to the Wee1 inhibitor adavorsertib, although at higher concentrations.

All resistant cells were sensitive to the mTOR inhibitors sapanisertib and AZD8055, particularly R-ASO cells which also demonstrated sensitivity to the mTORC1 inhibitor everolimus even at low concentrations (Figure 5.1F). The differential responsiveness of R-ARS and R-Sel cells to mTOR and mTORC1 inhibitors might suggest that these cells can still signal via mTORC2 when mTORC1 is inhibited.

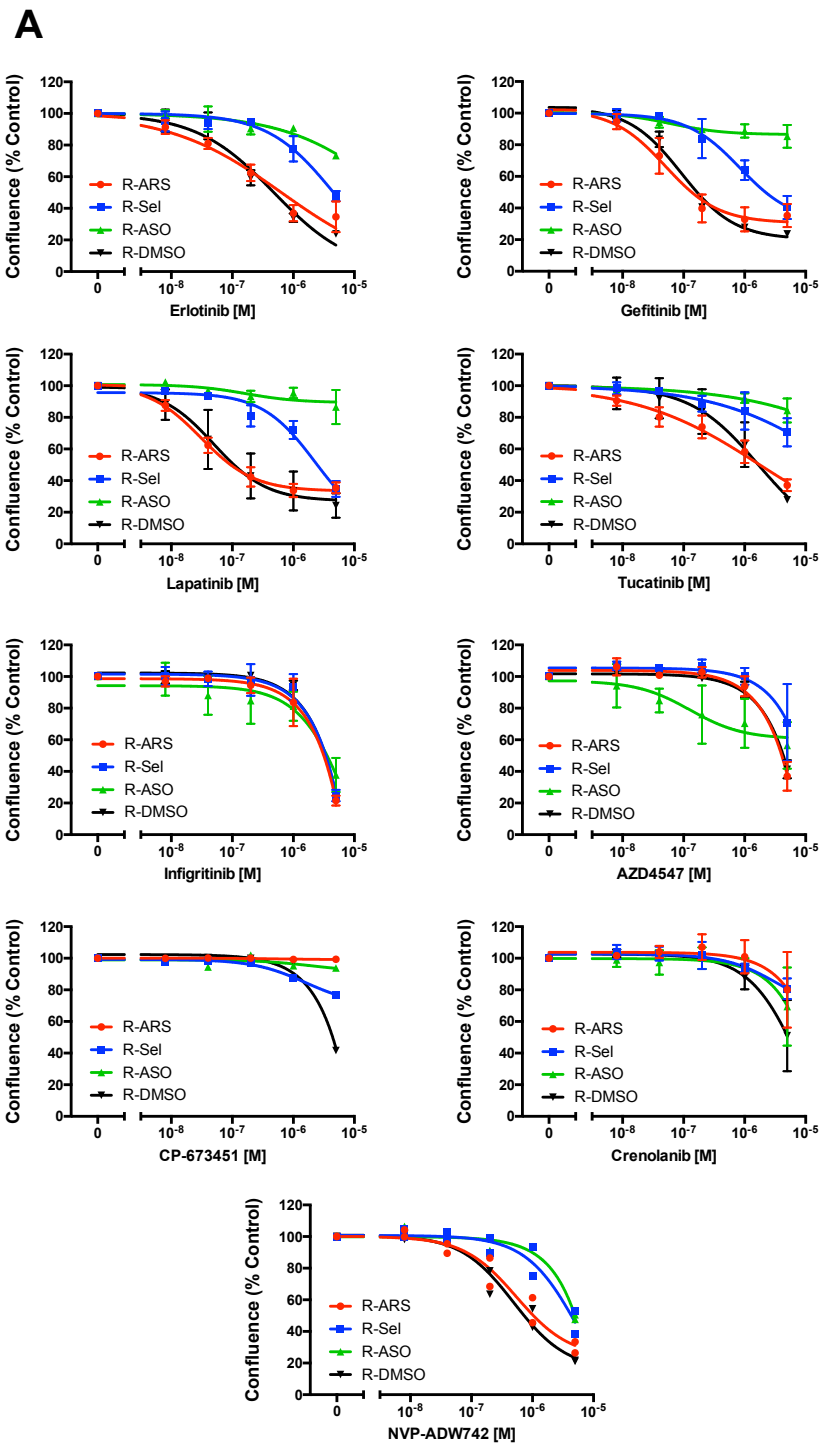

Figure 5.1: Dose responses of combination therapeutics in resistant cells.

Resistant H358 cell lines treated with ARS1620 (R-ARS), selumetinib (R-Sel) and AZD4785 (R-ASO), alongside naïve parental H358 cells treated with DMSO (R-DMSO) were treated with their previous IC90 inhibitor treatments (ARS1620, Selumetinib, AZD4785 and DMSO respectively) in combination with dose responses of additional targeted inhibitors (see table 5.1); **(A)** RTKi, **(B)** alternative RASi, **(C)** cross treatment with KRASi and MEKi, **(D)** CDKi, **(E)** DNA damage pathway inhibitors, **(F)** mTORi. The change in confluency was recorded following 4 days of inhibitor treatment. Graphs are presented as mean percentages of vehicle controls ±SEM from technical triplicates of one-three independent experiments. Figure continued on next three pages.

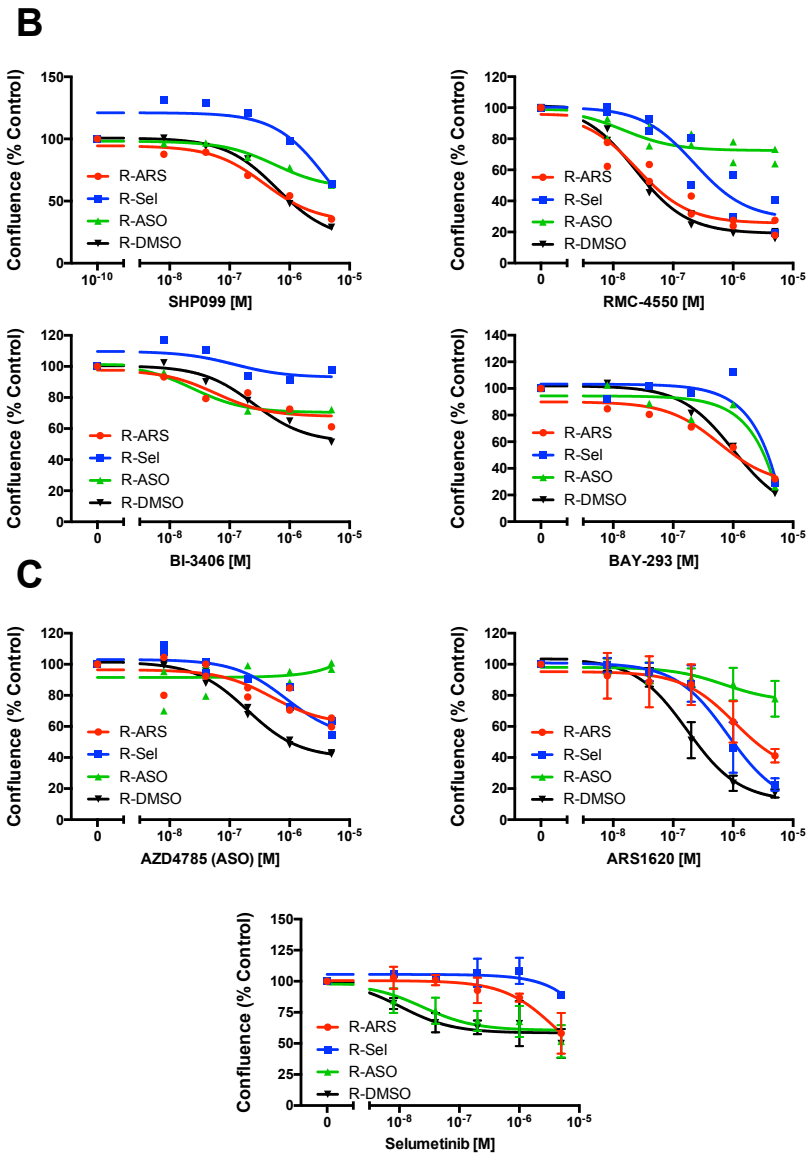
B
Confluence (% Control)
R-ARS
R-Sel
R-ASO
R-DMSO
SHP099 [M]
RMC-4550 [M]
BI-3406 [M]
BAY-293 [M]
C
AZD4785 (ASO) [M]
ARS1620 [M]
Selumetinib [M]

D

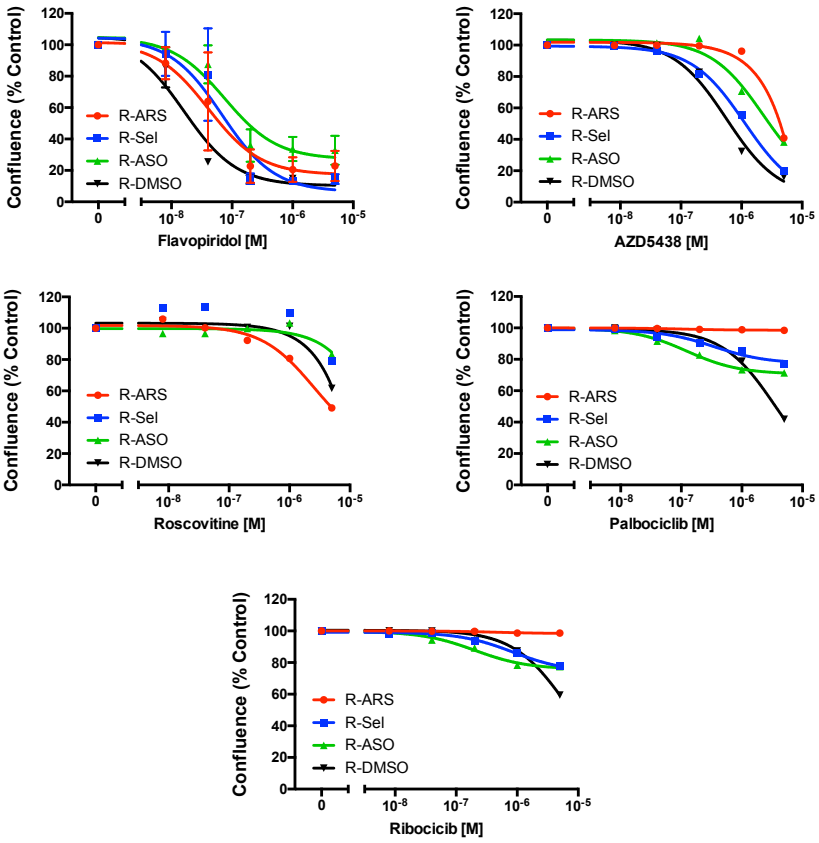
Confluence (% Control)
R-ARS
R-Sel
R-ASO
R-DMSO
Flavopiridol [M]
AZD5438 [M]
Roscovitine [M]
Palbociclib [M]
Ribocicib [M]

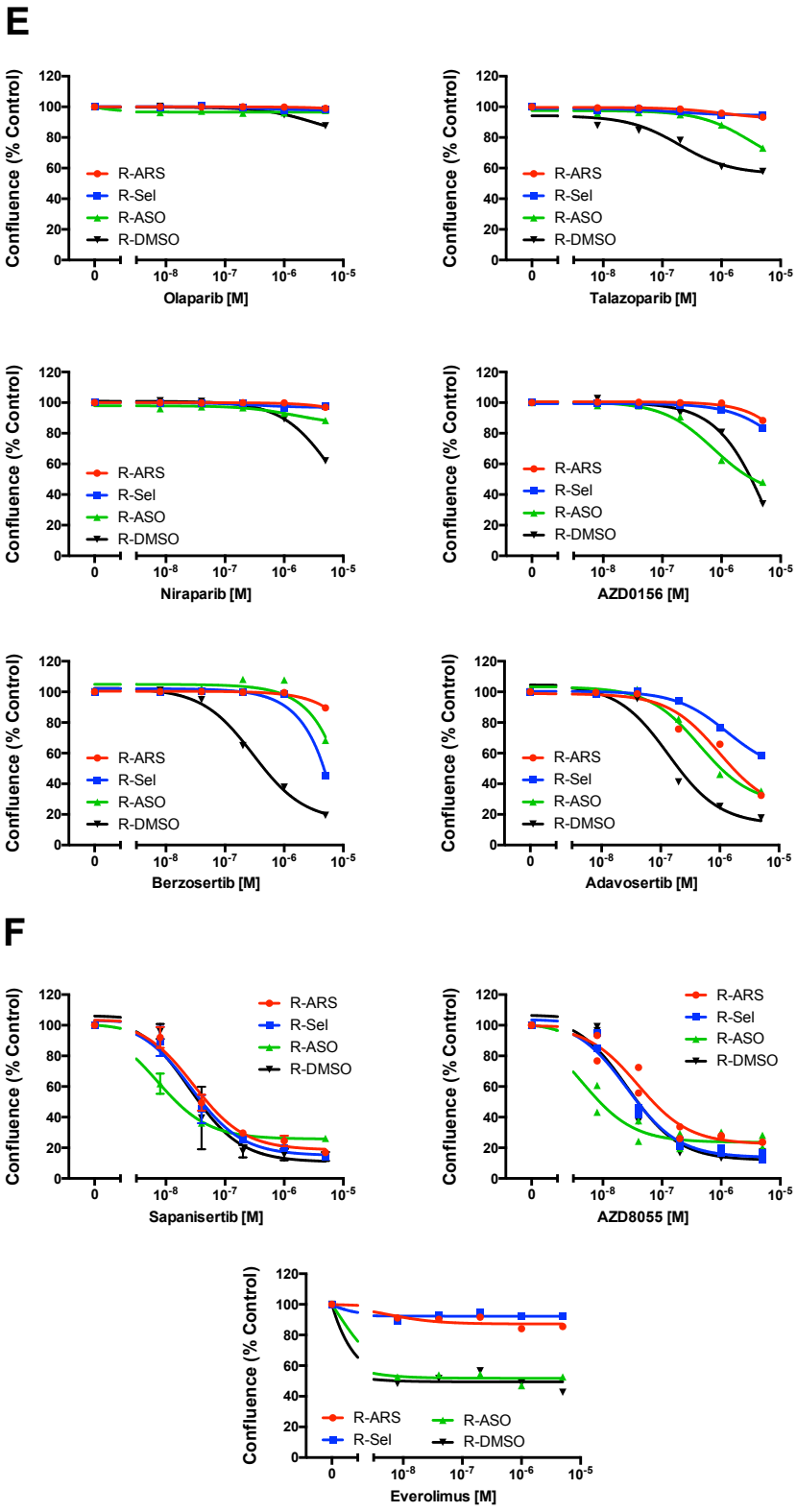
E
Confluence (% Control)
R-ARS
R-Sel
R-ASO
R-DMSO
Olaparib [M]
Talazoparib [M]
Niraparib [M]
AZD0156 [M]
Berzosertib [M]
Adavosertib [M]
F
Sapanisertib [M]
AZD8055 [M]
Everolimus [M]

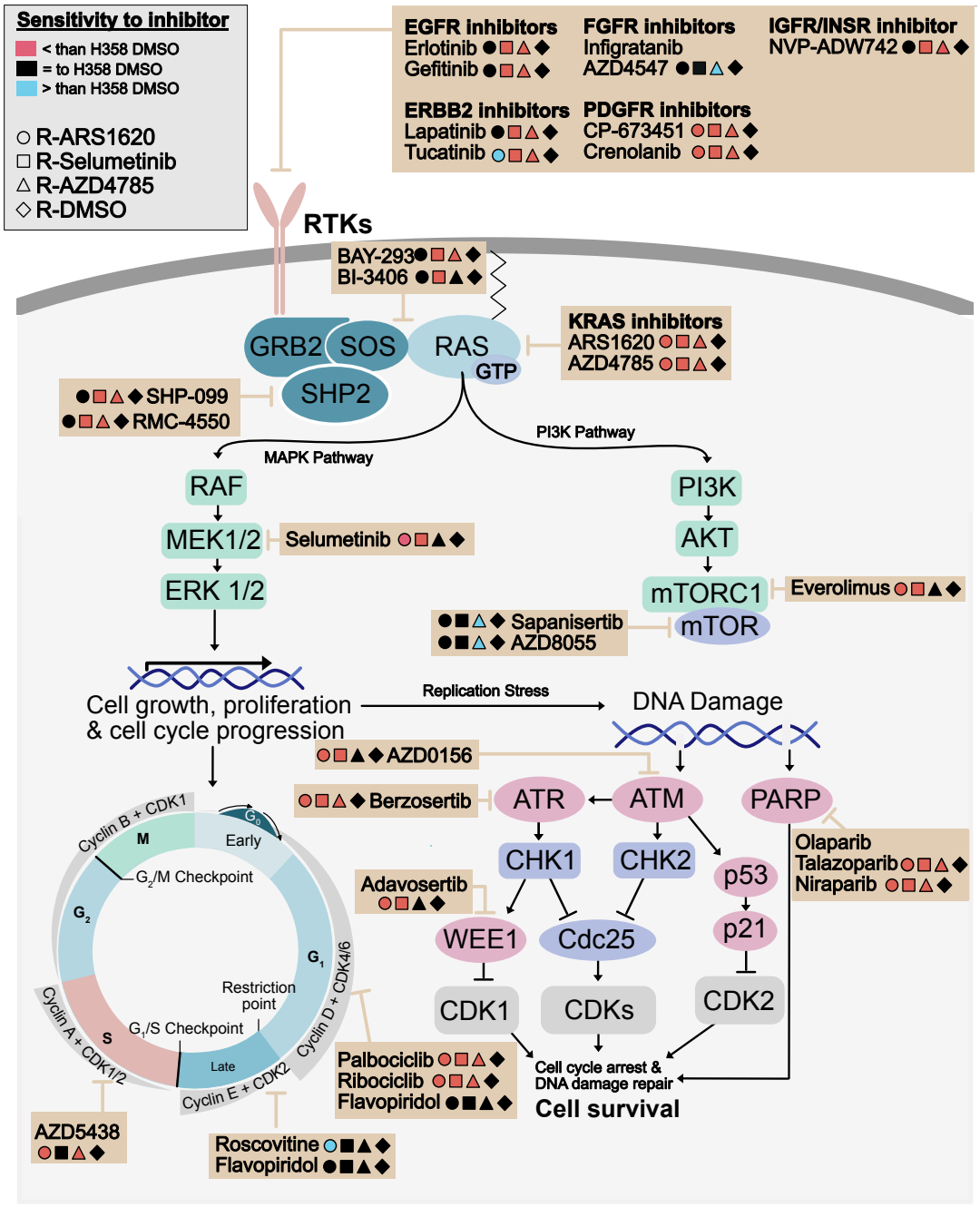

Figure 5.2: Sensitivity profile of resistant cells to combined targeted therapeutics. Resistant H358 cell lines treated with ARS1620 (R-ARS1620), selumetinib (R-Selumetinib) and AZD4785 (R-AZD4785), alongside naïve parental H358 cells treated with DMSO (R-DMSO) were treated with their previous IC90 inhibitor treatments (ARS1620, Selumetinib, AZD4785 and DMSO respectively) in combination with dose responses of additional targeted inhibitors The change in cell confluency of resistant cells compared to naïve cells is presented by a symbol for each cell type. Blue represents increased inhibitor sensitivity, red represents decreased inhibitor sensitivity and black represents a similar inhibitor sensitivity observed for H358 DMSO cells.

These differential responses are also summarised in Figure 5.2 which highlights the various signalling pathways targeted in this combinatorial screen. Overall this figure highlights that in general cells resistant to direct KRAS inhibitors also exhibit resistance to a variety of other inhibitors targeting different nodes of these signalling pathways. Cells resistant to KRAS-G12C inhibition (R-ARS1620) are most sensitive to EGFR/ERBB2, SHP2 and KRAS-SOS1 inhibition, indicating some reliance on the MAPK pathway for cell survival. Whereas cells resistant to KRAS mRNA depletion (R-AZD4785) demonstrate greater reliance on alternative pathways and were most susceptible to mTOR inhibition.

5.2.2 Identifying effective triple inhibitor combinations

After identifying differential sensitivities of my resistant cells to inhibitors targeting recognised resistance mechanisms, appropriate triple inhibitor combinations (RAS/MEK inhibitor plus two additional inhibitors) were identified in order to improve the efficacy of vertical or horizontal pathway inhibition. Using this combinatorial approach may not only help to delay the onset of resistance, but also enable lower doses of individual drugs to be used as a result of increased synergy between them. Combenefit software was used to visualise dose responses (Figure 5.3) and identify synergistic effects between inhibitor combinations [392] (Figure 5.4, Appendix 8).

The dose response matrices of the triple inhibitor combinations highlight that in most cases better responses and reduced cell viability are observed in R-DMSO cells that had not been previously treated with a RAS or MEK inhibitor (Figure 5.3). Moreover, some combinations show differential responses across the panel of resistant cells. For example, upstream EGFRi and SHP2i was most effective in R-ARS cells, whereas R-Sel cells were less responsive and R-ASO cells exhibited no change in cell viability (Figure 5.3A). A similar response was observed using lapatinib, a dual EGFR and ERBB2 inhibitor, with SHP2i (Figure 5.3C), as well as with NVP-ADW742, a dual IGFR1/INSR inhibitor, with SHP2i (Figure 5.3F). Interestingly the combination of RTK inhibition and SHP2i showed the most synergy in R-DMSO and R-Sel cells,

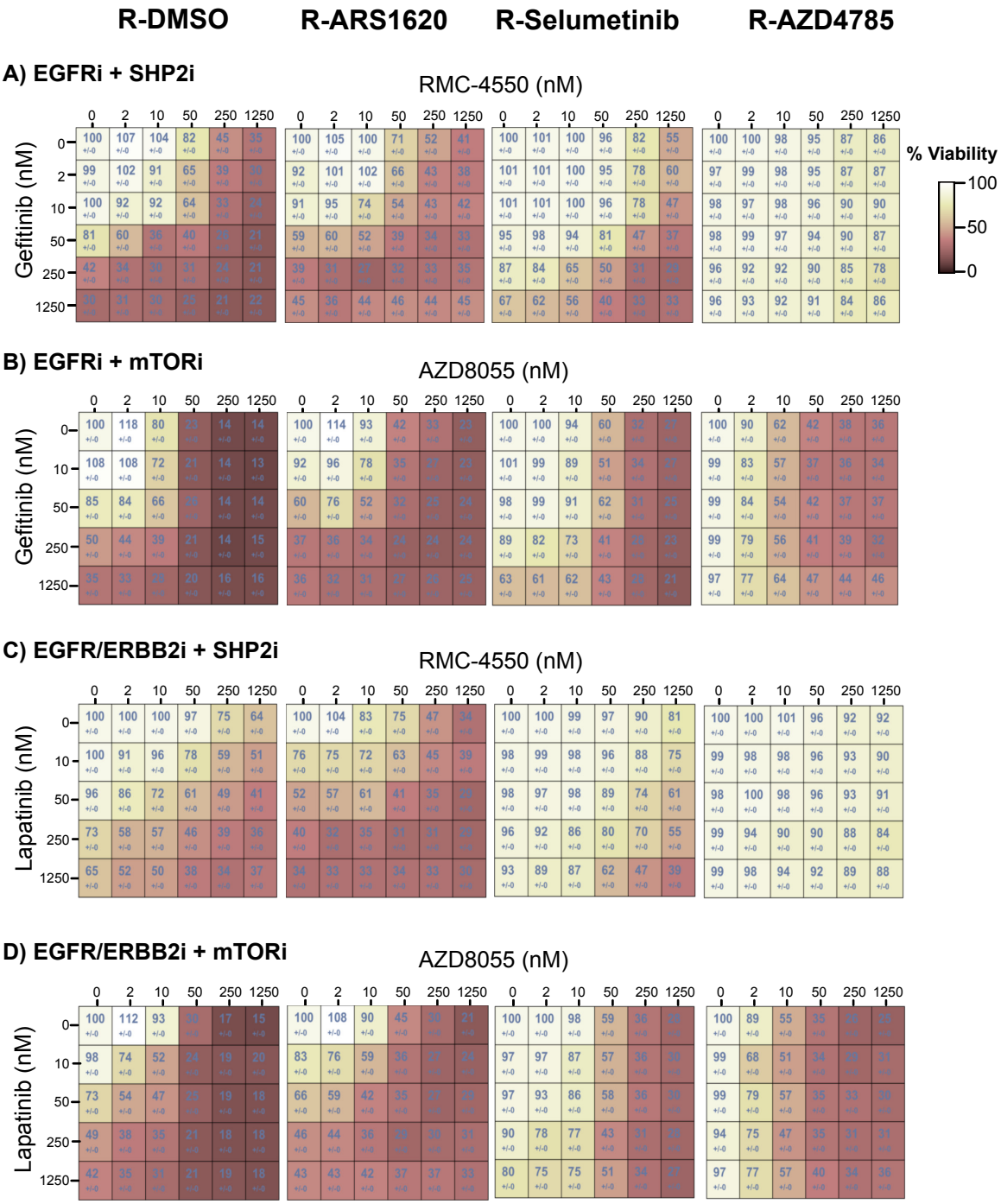

Figure 5.3: Dose response matrixes of triple combination therapeutics in resistant cells. Resistant cell lines treated with ARS1620 (R-ARS1620), selumetinib (R-Selumetinib) and AZD4785 (R-AZD4785) and naïve H358 cells (R-DMSO) were treated with their previous IC90 inhibitor treatments (ARS1620, Selumetinib, AZD4785 and DMSO respectively) in combination with dose responses of two targeted inhibitors **(A-G)**. The change in confluency was recorded following 4 days of inhibitor treatment and data are presented as mean percentages of vehicle controls from triplicate repeats of a single experiment. Figure continued on next page.

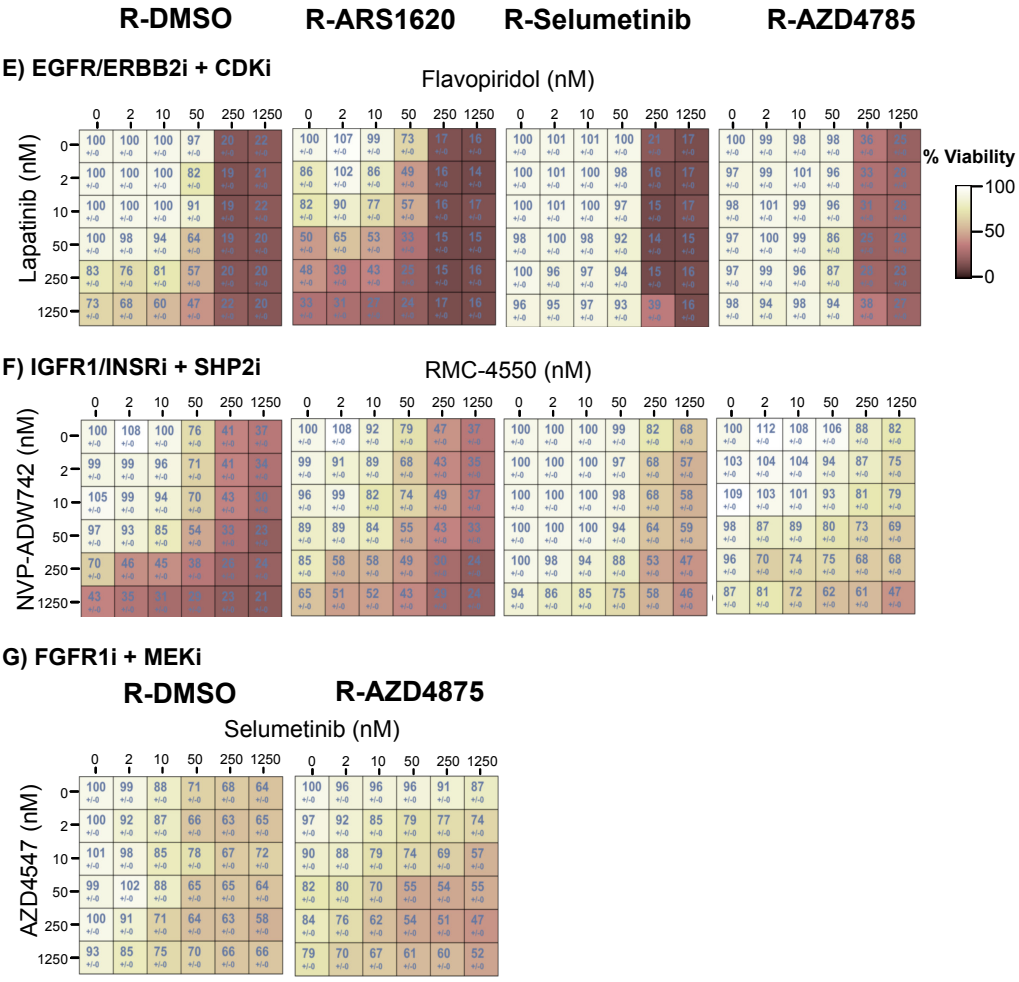

albeit at higher concentrations (Figure 5.4A,C and F).

On the other hand, substitution of SHP2i with mTORi in combination with upstream RTK inhibitors was more effective at reducing cell viability across all resistant cells (Figure 5.3B and D), although these combinations showed less synergy overall (Figure 5.4). Furthermore, substitution with the CDK inhibitor flavopiridol was also most effective in R-ARS cells, whereas the addition of lapatinib in this combination had no additional benefit in both R-Sel and R-ASO cells (Figure 5.3E). Finally, the combination of FGFRi and MEKi, using AZD4547 and selumetinib, both of which previously showed selective effectiveness in R-ASO cells (Figure 5.1A and C), further reduced cell viability with highly synergistic effect (Figure 5.3G and 5.4G). Though interestingly the effect on cell viability of this combination was still less than other inhibitors such as mTORi.

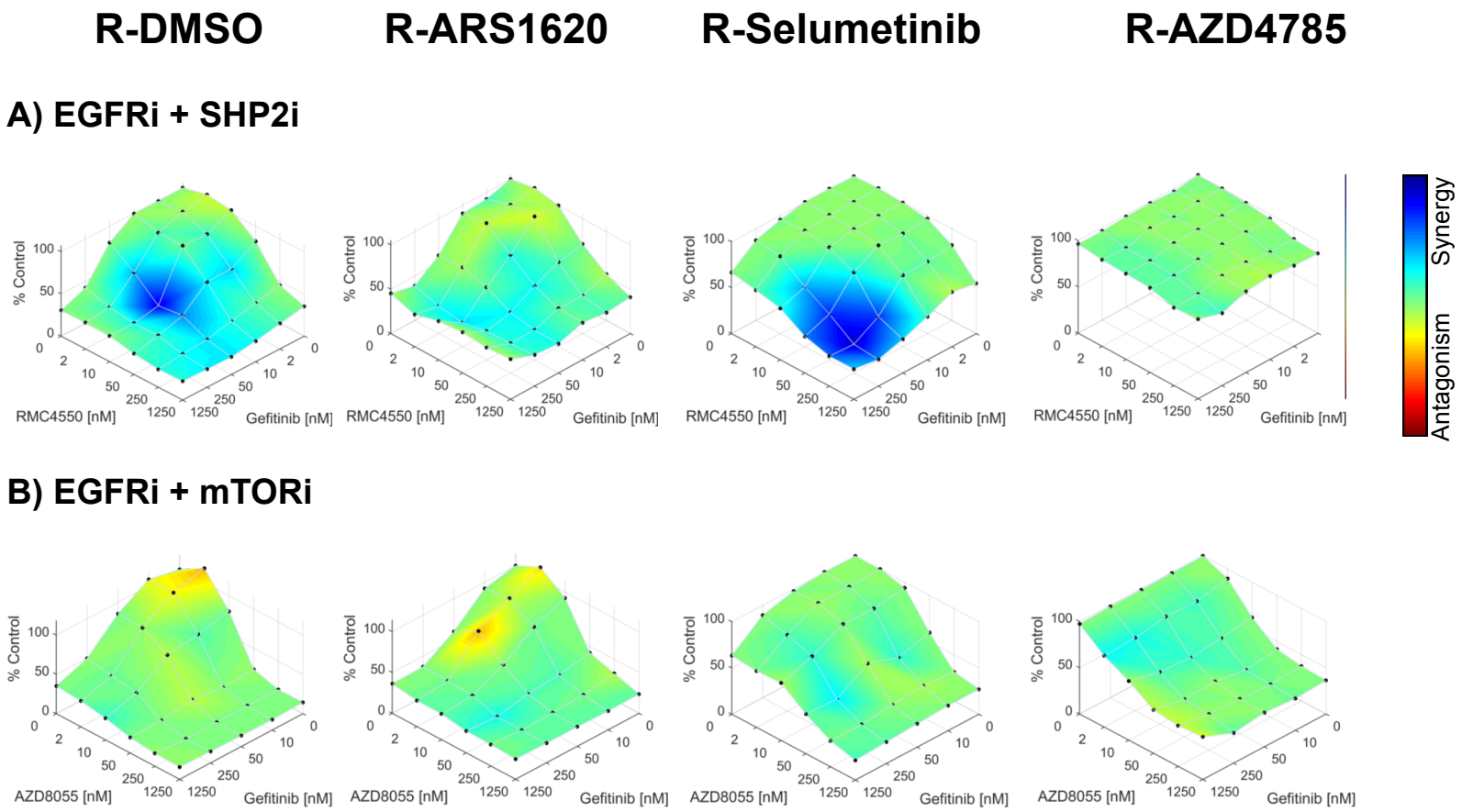

Figure 5.4: Synergy vs dose response matrixes of triple combination therapeutics in resistant cells.

Synergy scores from double inhibitor combination assays were calculated using the Loewe model and plotted against dose responses (% viability) using Combenefit software [392]. Areas coloured blue indicate drug combinations that are synergistic. Figure continued on the next two pages.

R-DMSO **R-ARS1620** **R-Selumetinib** **R-AZD4785**

C) EGFR/ERBB2i + SHP2i

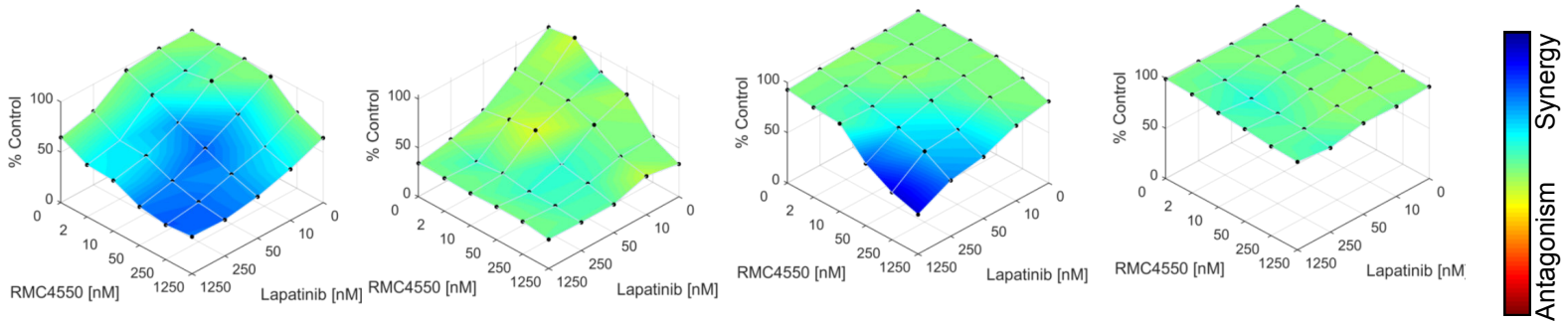

D) EGFR/ERBB2i + mTORi

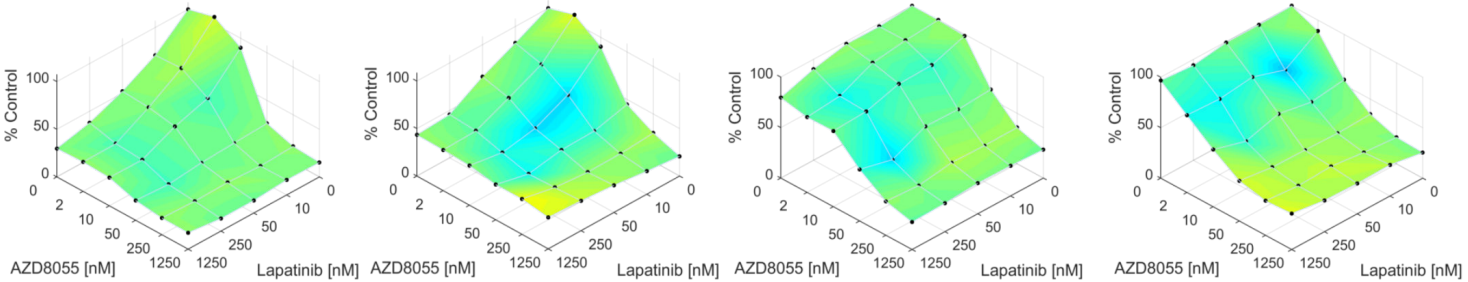

R-DMSO **R-ARS1620** **R-Selumetinib** **R-AZD4785**

E) EGFR/ERBB2i + CDKi

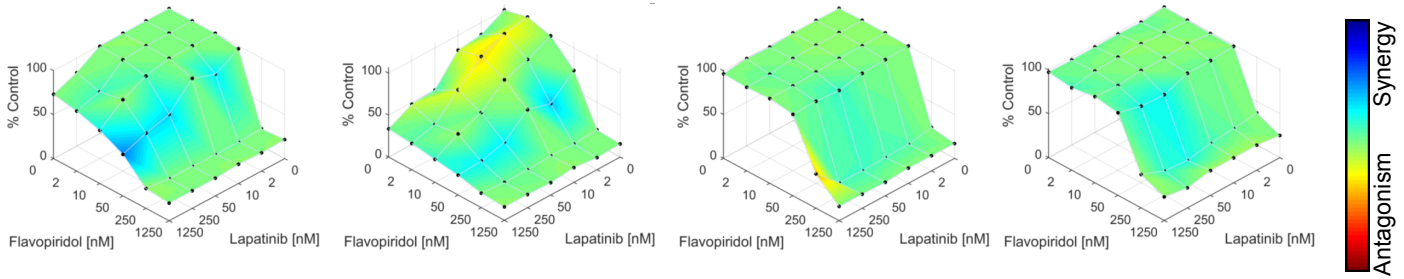

F) IGFR1/INSRi + SHP2i

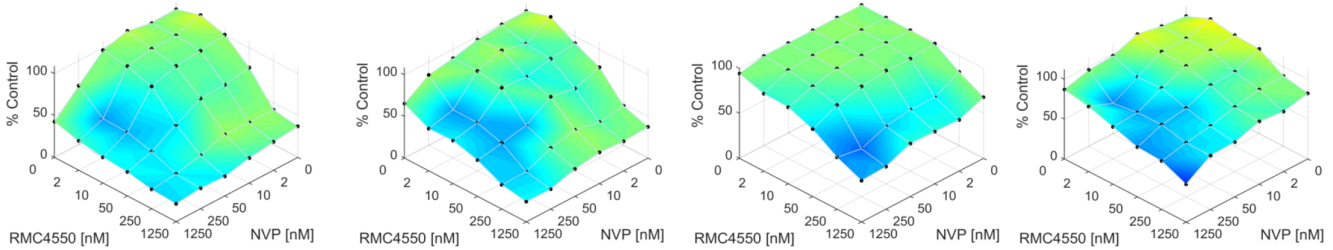

G) FGFR1i + MEKi

R-DMSO **R-AZD4785**

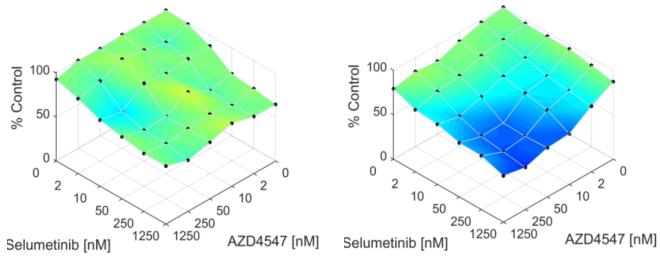

Table 5.3: Triple combination inhibitor combinations.

Set	Inhibitors	Cells			
		R-DMSO	**R-ARS1620**	**R-Selumetinib**	**R-AZD4785**
1	RAS/MEKi	IC90 DMSO	IC90 ARS1620	IC90 Selumetinib	IC90 AZD4587
	Gefitinib (nM)	50	250	250	250
	RMC-4550 (nM)	10	10	250	250
2	RAS/MEKi	IC90 DMSO	IC90 ARS1620	IC90 Selumetinib	IC90 AZD4587
	Gefitinib (nM)	50	50	50	50
	AZD8055 (nM)	50	50	50	50
3	RAS/MEKi	IC90 DMSO	IC90 ARS1620	IC90 Selumetinib	IC90 AZD4587
	Lapatinib (nM)	50	50	250	50
	RMC-4550 (nM)	50	50	250	50
4	RAS/MEKi	IC90 DMSO	IC90 ARS1620	IC90 Selumetinib	IC90 AZD4587
	Lapatinib (nM)	10	10	10	10
	AZD8055 (nM)	10	10	10	10
5	RAS/MEKi	IC90 DMSO	IC90 ARS1620	IC90 Selumetinib	IC90 AZD4587
	Lapatinib (nM)	50	50	50	50
	Flavopiridol (nM)	50	50	50	50
6	RAS/MEKi	IC90 DMSO	IC90 ARS1620	IC90 Selumetinib	IC90 AZD4587
	NVP-ADW742 (nM)	250	50	250	50
	RMC-4550 (nM)	50	50	250	50
7	RAS/MEKi	IC90 DMSO	-	-	IC90 AZD4587
	AZD4547 (nM)	250	-	-	50
	Selumetinib (nM)	10	-	-	50

Following inhibitor combination screening in H358-R cells, the most synergistic drug concentrations were determined for each set of inhibitor combinations (see Table 5.3). Where inhibitor concentrations resulted in a similar reduction of cell viability, the lower inhibitor concentration was chosen in order to minimise potential off-target toxicity issues.

Using these synergistic inhibitor concentrations, the expression of downstream RAS signalling components was monitored over time in order to determine whether inhibitor combinations improved the inhibition of signalling pathways compared to monotherapy treatments (Figure 5.5). A comparison of vertical and horizontal combination strategies was performed using EGFRi with either SHP2i or mTORi across the panel of resistant cells.

In DMSO-treated cells, no changes in pEGFR levels occurred with any of the monotherapy or combination treatments (Figure 5.5A). Inhibition of mTOR with

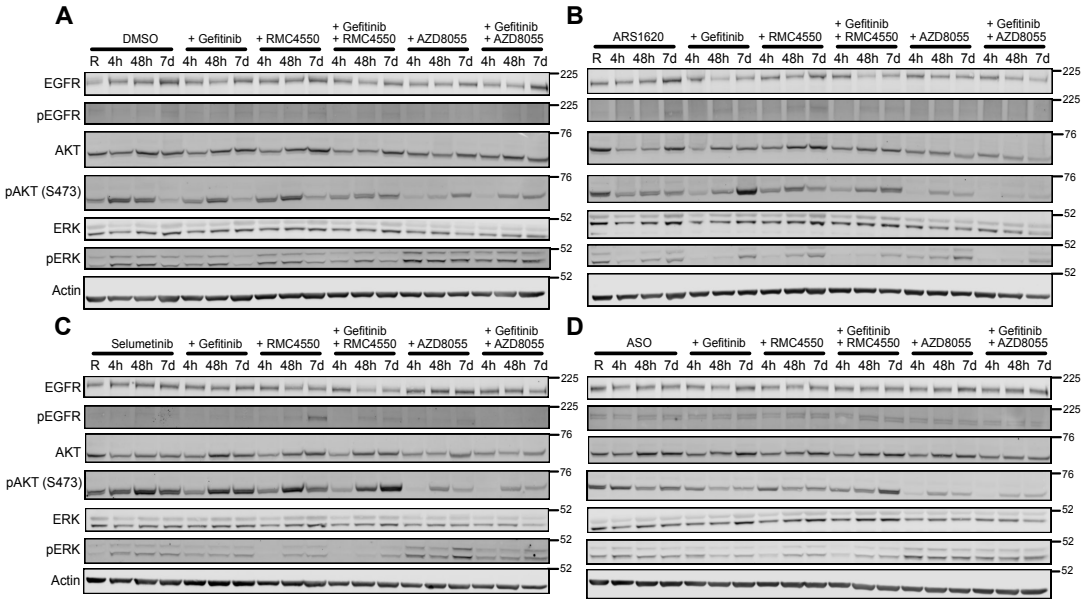

Figure 5.5: Changes in signalling pathways following vertical or horizontal inhibitor combination treatment in H358-R cells.

H358-R cells were treated with IC90 concentrations of each inhibitor or control **(A)** DMSO, **(B)** ARS1620, **(C)** selumetinib and **(D)** AZD4785. Cells were also treated with the indicated inhibitor combinations for up to 7 days with cells re-dosed every 48 hours. Cell lysates were prepared at the indicated time points and RAS pathway components were analysed by immunoblotting. Lysates from H358-R (R) cells were carried out alongside. Results are from a single experiment.

AZD8055 as both a monotherapy and combination with EGFRi initially decreased pAKT levels, although this was shown to rebound within 48 hours to 7 days. This was accompanied with a compensatory increase in pERK. On the other hand, following longer 7-day EGFRi and SHP2i monotherapy and combination treatments, a slight decrease in pERK was observed. Overall it was surprising that there was no complete loss of these downstream signalling pathways correlating to the decreased cell viability previously seen with these inhibitor treatments (Figure 5.1 and 5.3).

In ARS1620-treated resistant cells, the combination of EGFRi and mTORi reduced pAKT compared to either monotherapy (Figure 5.5B). In addition, pERK was initially reduced following EGFRi and SHP2i, however with both inhibitor combination approaches the loss of pERK was improved. Overall

horizontal inhibition with EGFRi and mTORi demonstrated reduction of both pAKT and pERK signalling pathways, corresponding to the greater loss of cell viability previously observed with this treatment (Figure 5.3B).

In comparison, in selumetinib-treated resistant cells, mTOR inhibitor treatment only initially decreased pAKT, which rebounded within 48 hours (Figure 5.5C). EGFRi and SHP2i also appeared to increase pAKT(S473) levels over time, highlighting greater reliance on this pathway under these conditions. On the other hand, pERK was reduced the most under the highly synergistic EGFRi and SHP2i combination.

Finally, with AZD4785-treated resistant cells, no clear changes in pERK and pAKT protein levels were observed following EGFRi and SHP2i monotherapy or combination therapy (Figure 5.5D), which reflects the high cell viability previously observed with these treatments and resistance to vertical inhibition (Figure 5.3A). mTORi only initially reduced pAKT protein levels which also rebounded within 48 hours and was accompanied by slightly increased pERK.

Overall these results highlight the reactivation of compensatory signalling mechanisms that arise with both horizontal and vertical inhibition mechanisms. Despite using the lowest inhibitor concentrations that exhibited good synergy and loss of cell viability, increasing inhibitor concentrations may help to improve inhibition of some downstream signalling pathways and further delay or reverse resistance developing.

5.2.3 Combinations with RAS/MEK inhibitors prevent or delay resistance in H358 cells

The synergistic inhibitor combinations were also used to treat naïve H358 cells in order to determine whether the onset of resistance to RAS or MEK inhibitors could be delayed or prevented (Figure 5.6). The majority of inhibitor combinations only marginally delayed the growth of H358 cells compared to the DMSO only control (Figure 5.6A). On the other hand, with the addition of ARS1620 (Figure 5.6B), cell confluency remained low with most of the inhibitor

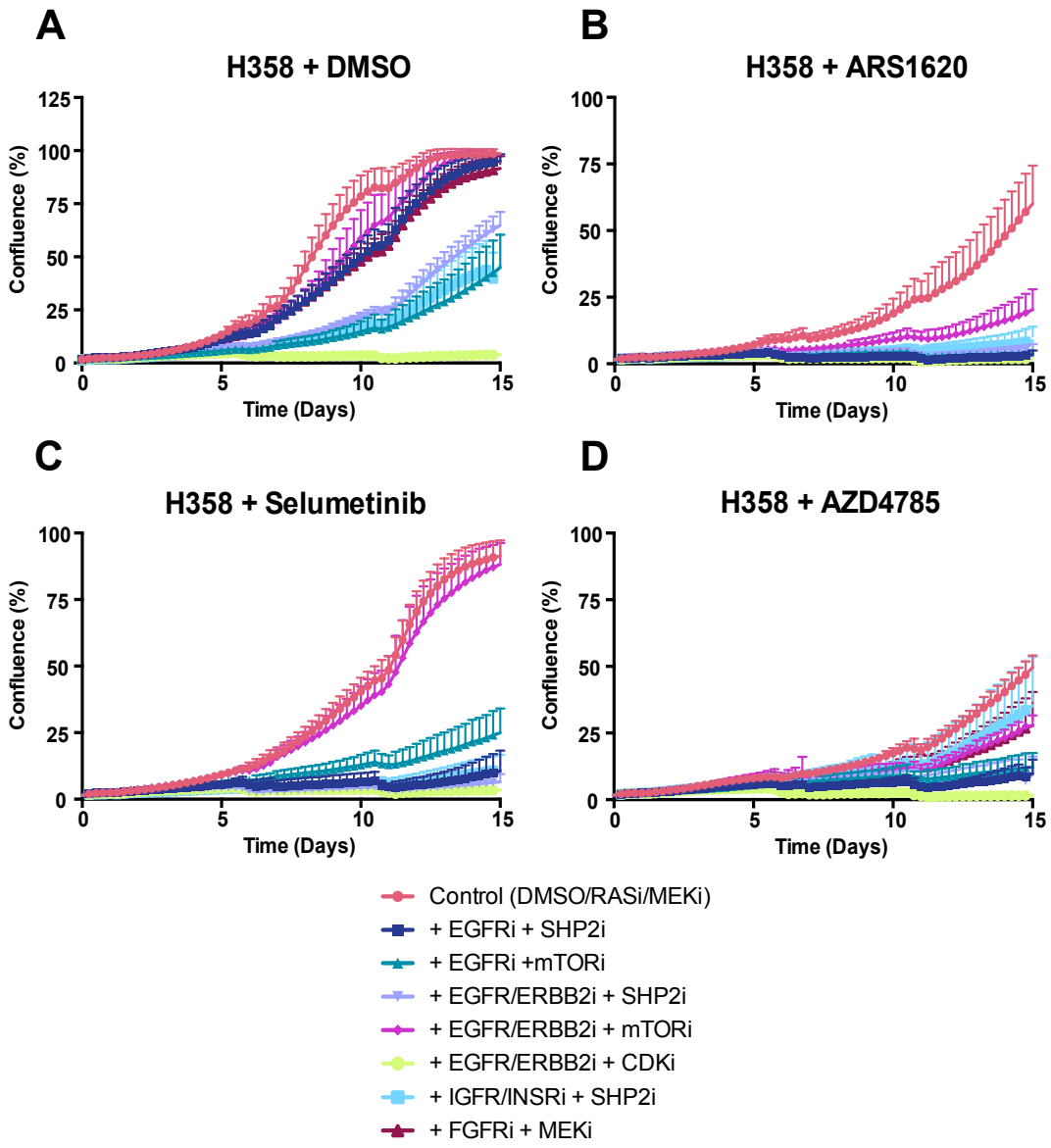

Figure 5.6: Triple inhibitor combinations in naïve H358 cells.

H358 cells were seeded at 1000 cells per well in a 96-well TC treated plate and treated with IC90 concentrations of **(A)** DMSO, **(B)** ARS1620, **(C)** selumetinib, **(D)** AZD4785, plus synergistic concentrations (see table 5.2) of additional inhibitor combinations. Cells were re-treated every 5 days and the change in confluency was recorded every 6 hours for 15 days. Inhibitors used; gefitinib (EGFRi), RMC-4550 (SHP2i), AZD8055 (mTORi), lapatinib (EGFR/ERBB2i), flavopiridol (CDKi), NVP-ADW742 (IGFR/INSRi), AZD4547 (FGFRi) and selumetinib (MEKi). Data are from triplicate repeats of four independent experiments.

combinations. This highlights that despite the fact that resistance does develop to KRAS-G12C inhibitor monotherapy, the addition of a KRAS-G12C inhibitor in a combinatorial approach can dramatically reduce cell growth and therefore help delay or prevent the onset of resistance in KRAS-G12C mutant

cells. This trend was also observed with cells treated with selumetinib (Figure 5.6C).

Surprisingly in all of these conditions, the horizontal combination strategy of lapatinib and AZD8055 (EGFR/ERBB2i + mTORi) was the least effective combination overall, whereas previously in resistant cells this combination was effective in all resistant cells (Figure 5.3D). This could be due to the lower synergistic inhibitor concentrations used in this combination, or because the inhibitory interplay only becomes important once resistance rewiring has already occurred. In cells treated with selumetinib, gefitinib and AZD8055 (EGFRi + mTORi) treatment also demonstrated reduced efficacy over time, whereas corresponding RTK inhibitors with SHP2i were more effective at delaying cell growth, indicating that these cells are more sensitive to vertical RAS pathway inhibitor combinations. In contrast, cells treated with AZD4785 inhibitor combinations demonstrated mixed responses and reduced sensitivity to certain combinations according to the RTK inhibitor used (Figure 5.6D). Furthermore, it is apparent that it also takes longer for resistance to develop in these cells. In naïve H358 cells, targeting IGFR/INSR, FGFR1 and ERBB2 receptors appeared to be less effective than combinations with EGFR inhibition. This further highlights how these cells are differentially wired compared to chronic resistant cells which have become KRAS independent, and therefore the combinations based on overcoming this resistance are not as effective in naïve cells compared to those which have acquired sensitivity to these additional inhibitors. Overall, across all combinations, the use of a broad CDK inhibitor appeared to be the most effective at preventing any further cell growth regardless of the other inhibitors used in the combination. It appears the cells are killed before any resistance to other inhibitors can be acquired and therefore represents a potential universal therapeutic avenue.

5.3 Discussion

In this chapter I have identified various KRAS inhibitor combinations which show increased efficacy in both naïve and resistant KRAS-mutant lung cancer cells. From initial compound screening, several inhibitors were identified that

re-sensitised different KRASi-resistant cells resulting in decreased cell viability (Figure 5.1). Interestingly RTK inhibitors demonstrated the most variable responses across the panel of resistant cells. For example, cells resistant to ARS1620 were most sensitive to gefitinib, lapatinib and NVP-ADW742, targeting the EGFR, ERBB2 and IGFR/INSR receptors which is consistent to my transcriptomic and proteomic data where I observed upregulation of these receptors in these cells (Figure 5.1A, 4.12, 4.14 and 4.15). Alternatively the increased resistance of long-term selumetinib-treated cells to RTK inhibitors could be due to increased dependence upon RAF or amplification of RAS signalling as a potential mechanism of resistance [242]. AZD4785-treated resistant cells showed the most resistance to these inhibitors, further confirming reliance upon alternative RTKs and pathway signalling for cell survival. Unlike ARS1620- or selumetinib-treated resistant cells, these cells were instead uniquely sensitive to FGFRi. Furthermore, cross inhibition of resistant cells with ARS1620, selumetinib and AZD4785 highlights the KRAS-independent state of ARS1620- and AZD4785-treated resistant cells (Figure 5.1C). The fact that AZD4785-treated resistant cells also uniquely exhibited some sensitivity to selumetinib could be attributed to the loss of KRAS-WT with this inhibitor, which has been shown to increase sensitivity to MEKi through disruption of KRAS-mutant and KRAS-WT dimerisation [393, 394]. Other interesting combination strategies identified from the initial compound screen include SHP2 and mTOR inhibitors (Figure 5.1B and F), which have shown previous efficacy as potential combination strategies to overcome KRAS-G12C inhibitor resistance [219, 220, 344, 363] and are currently undergoing clinical evaluation (Table 5.2). mTORi was effective across all resistant cells, indicating greater reliance upon the PI3K pathway for cell survival as a common resistance mechanism.

Unexpectedly KRAS-SOS1 inhibitors (BAY-293 and BI-3406) were not as effective as expected from previous studies in KRAS-mutant NSCLC cells [345]. SOS1 is not the only RAS-GEF known to activate RAS and a loss of SOS1 gene expression was observed in all chronically treated H358-R cells, coupled with up-regulation of some alternative RAS-GEFs such as RAS-GRP2/4 and RAS-GRF1/2 (Figure 4.12). This suggests potential involvement

of these alternative RAS-GEFs in chronically treated resistant cells. In addition, surprisingly there was a lack of sensitivity to several DNA damage pathway inhibitors, particularly PARP inhibitors in H358-R cells (Figure 5.1E). A previous study using similar drug concentration ranges also observed KRAS-mutant cell lines exhibited resistance to PARPi, yet were sensitive to combined PARPi and MEKi which induced greater DNA damage and apoptosis [395]. The lack of efficacy of PARPi monotherapy could be a result of restored homologous recombination and reliance upon alternative DNA repair pathways and cell cycle regulators in resistant cells treated with KRAS inhibitors [396]. Interestingly AZD4785-treated resistant cells demonstrated sensitivity to ATM inhibition, indicating reliance upon homologous recombination. Reduced cell viability was also observed with Wee1 inhibition (adavosertib) across all resistant cells. Inhibition of Wee1 blocks DNA damage-induced inhibitory phosphorylation of CDK1 and CDK2, and therefore compromises cell-cycle checkpoint function which can promote cell death during mitosis [397]. Cells with loss of p53 function, such as H358 cells, are particularly sensitive to this mechanism of synthetic lethality [398].

Furthermore all H358-R cells showed resistance to CDK4/6 inhibitors (Figure 5.1D), previously identified as potentially effective combination strategies in KRAS-mutant NSCLC from synthetic lethal screens [360, 399]. Despite this, results from the JUNIPER clinical trial of CDK4/6 inhibition as a monotherapy in KRAS-mutant NSCLC were not encouraging [400]. The resistance to CDK4/6 inhibitors observed in H358-R cells could be a result of cyclin E or E2F transcription factor upregulation (Figure 4.17), which could represent a mechanism to overcome CDK4/6 inhibition [401]. Alternatively, the broad CDK inhibitor flavopiridol demonstrated much greater efficacy and loss of cell viability. Flavopiridol is a first generation pan-CDK inhibitor, yet despite demonstrating significant anti-tumour activity in other preclinical studies [402, 403], clinical studies reported insufficient efficacy for solid cancers at well tolerated concentrations with monotherapy treatment [404, 405]. Flavopiridol has since been evaluated as a combinatorial approach alongside other chemotherapies which has showed more promising results [406, 407]. Overall as well as identifying inhibitors which show efficacy in resistant cells, this

combinatorial screening has also identified ways in which initial KRAS or MEK inhibitor treatments can make the cells become more resistant to other types of inhibitors to which they would otherwise be sensitive.

From this initial combinational screening in resistant cells, certain combination strategies were investigated further to determine whether combining two of these inhibitors, alongside the initial RAS or MEK inhibitor, could improve efficacy and delay or overcome resistance. Combinations using several RTKi that demonstrated initial effectiveness were combined with either SHP2 or mTOR inhibitors to compare vertical or horizontal signalling pathway inhibition strategies (Figure 5.3). Given the differential sensitivities to some RTK inhibitors, targeting SHP2 in combination could further prevent upstream signalling from multiple RTKs and supress feedback activation of the RAS pathway, whereas targeting mTOR would help to block alternative signalling from the PI3K pathway. In preclinical mouse studies targeting both MAPK and PI3K pathways showed efficacy in KRAS-mutant tumours [193]. For AZD4785-treated resistant cells, an additional combination using FGFRi with MEKi was also carried out, as these cells demonstrated unique sensitivity to both of these inhibitors.

Overall the panel of resistant cells showed mixed responses to vertical and horizontal inhibition. For ARS1620-treated resistant cells, both strategies worked well to effectively reduce cell viability, regardless of targeting different RTKs (Figure 5.3). Downstream pERK and pAKT expression was also reduced following EGFRi with SHP2i or mTORi (Figure 5.5B). Previous studies have also independently identified that both vertical and horizontal inhibition strategies in combination with KRAS-G12C inhibitors are effective and help prevent resistance [220, 361, 363]. It will be interesting to see how well these combinations succeed in the ongoing clinical trial (NCT04185883). For selumetinib-treated resistant cells, increased sensitivity and synergy was observed with EGFR and SHP2 inhibitor combinations compared to targeting other RTKs with SHP2i (Figure 5.3 and 5.4). With this combination pERK expression was also reduced (Figure 5.5C), highlighting increased reliance upon MAPK vertical pathway signalling, which could be driven by pathway

feedback activation. On the other hand, AZD4785-treated resistant cells demonstrated resistance to EGFRi and SHP2i vertical combinations. Interestingly it has been identified that FGFR-dependent cells are often insensitive to SHP2i compared to EGFR-dependent cells [408]. Furthermore signalling from FGFR has been found to drive feedback-induced activation of RAS independently of SHP2 in a subset of BRAF-mutant tumours resistant to ERK and SHP2 inhibition [164]. Interestingly resistant cells treated with AZD4785 demonstrated increased sensitivity to the combination of FGFR1 and MEK inhibition (Figure 5.3G). The high synergy observed with FGFR and MEK inhibitor combinations in these cells (Figure 5.4) could also be attributed to their more mesenchymal phenotype which has been previously attributed with high FGFR1 expression and reduced ERBB family expression following EMT induction [258]. This is also consistent with my earlier observations (Figure 4.15 and 4.18).

Treatment with the same inhibitor combinations in naïve H358 cells revealed that some combinations were more effective at reducing cell proliferation over a longer time course than others, particularly vertical inhibitor combinations containing SHP2i alongside KRAS-G12C and MEK inhibitors (Figure 5.6). On the other hand, some combinations that were previously effective in resistant cells were not as effective in naïve H358 cells, such as EGFR/ERBB2i plus mTORi for combinations with KRAS-G12C and MEK inhibitors, and alternative RTKi for AZD4785 combinations, indicating that adaptive signal rewiring may not yet have occurred. This therefore implies that targeting multiple nodes of the MAPK pathway could be more effective for cells still dependent upon KRAS signalling [409, 410].

As identified earlier, use of a broad CDK inhibitor flavopiridol proved to completely prevent cell proliferation and resistance developing in naïve H358 cells, irrelevant of the inhibitor combination. This represents a highly promising therapeutic strategy for the treatment of KRAS-mutant cancers and further investigation into the clinical validity of flavopiridol to improve patient outcomes and reduce tumour growth is required. Despite other studies demonstrating flavopiridol-mediated cytotoxicity in KRAS-mutant NSCLC cell lines [402, 403],

the results presented here demonstrate sustained prevention of cell proliferation over a greater period of time and at much lower drug concentrations. Flavopiridol is still undergoing clinical evaluation for various cancer types, including NSCLC, though there remain some concerns over drug-related toxicity [405, 411]. Results from this study suggest further investigation into the effectiveness of alternative targeted CDK inhibitors, particularly the additional targets of flavopiridol besides CDK4/6. Research into the pharmacology of flavopiridol identified that it appeared to exert its pharmacological effect through its ability to potently inhibit CDK9 [412]. CDK9 plays a key role in the regulation of basal gene transcription and its ability to maintain levels of the anti-apoptotic protein MCL1 is considered to promote cancer cell survival [413, 414]. This important function coupled with the dysregulated transcriptional programs associated with tumours, have made CDK9 an attractive therapeutic target [415]. Subsequently there has been particular interest to develop more specific targeted CDK9 inhibitors for improving targeted therapeutic strategies with reduced overall toxicity [414, 416]. With this in mind, combinations used in this study which include multiple specifically targeted inhibitors are currently favoured as more clinically relevant approaches, due to their synergistic potential to reduce potential toxicity issues and ability to target multiple signalling nodes.

Based on this current data, a combination of EGFR and mTOR inhibition would be most recommended to re-sensitise acquired resistance to KRAS-G12Ci. This combination is associated with strongly decreased cell viability coupled with loss of both pERK and pAKT signalling pathways in ARS1620-treated resistant cells (Figures 5.3, 5.5). This approach also appears effective in combination with KRAS-G12C inhibitors to delay the onset of resistance initially developing in naïve cells (Figure 5.6). Moreover KRAS-G12C combinations with EGFRi and SHP2i are equally effective at slowing the emergence of resistance. Evaluating the combination strategies for AZD4785-treated resistant cells also provides potential insight into effective strategies relevant for future pan-KRAS inhibitors [417]. To re-sensitise acquired resistance to this mechanism of KRAS inhibition, where both WT and mutant RAS signalling is targeted and the cells have become KRAS independent,

combinations with mTORi are most effective and reduced pAKT signalling (Figures 5.3 and 5.5). Additionally, FGFR and MEK inhibition are also recommended as alternative strategies that reduce cell viability and exhibit high synergy (Figure 5.3 and 5.4), though how this combination affects downstream signalling remains to be determined. However, to slow resistance from developing to pan-KRAS approaches in naïve cells, alternative combination approaches utilising EGFRi with either mTORi or SHP2i are still most effective.

One of the biggest challenges in developing combination therapies of targeted inhibitors is minimising overlapping toxicities. There are limitations of 2D-based *in-vitro* studies when it comes to extrapolating to potential clinical studies. The potential toxicities of drug combinations can be uncertain and misrepresented in preclinical cell-based work. Additional complexities from interactions with the tumour microenvironment, underlying tumour heterogeneity and differences in cell morphology are not accounted for. Future studies will need to confirm the tolerability and toxicity profiles of these combination strategies to determine their clinical potential. To more accurately reflect *in-vivo* therapeutic responses, these combinations should be assessed in more complex 3D cell models, including patient-derived organoids and xenografts (PDXs) [294, 418-422]. Furthermore, pre-existing tumour heterogeneity within *in-vivo* studies can help to identify intrinsic mechanisms of resistance giving rise to subpopulations of cells which are resistant to selected targeted inhibition. Currently there is little evidence on what *de novo* mutations may arise with KRAS inhibitor treatment, and therefore it would also be useful to identify any potential genetic alterations or secondary mutations that may occur following treatment.

To summarise, drug resistance remains one of the greatest challenges in cancer therapy. As observed in this study, generally cells become increasingly resistant to multiple therapies and over time fewer treatments are effective. In order to pre-empt or overcome resistance, a greater understanding of these biological processes are required to anticipate how cancer cells will evolve so that weakness in the cells can be subsequently targeted. If it was possible to

completely prevent resistance, then all cancerous cells would need to be killed to prevent the outgrowth of new resistant clones, despite underlying tumour heterogeneity and cancer stem cell populations. Consequently, in patients, almost inevitably a subset of cells will develop alternative survival mechanisms and resist current therapy. Instead, strategies utilising cocktails of inhibitor combinations, with different mechanisms of action and targeting multiple signalling nodes, can make multi-drug resistance more difficult to be selected for. Exhausting potential evasion mechanisms, giving the cells no time to evolve can therefore help to improve patient outcomes and progression free survival [423]. The overall goal of this approach is to maximise synergistic effects in order to minimise overlapping toxicity. However due to underlying heterogeneity and complexity of tumour evolution, identifying how cancers will evolve and the best combination strategy to overcome drug resistance is challenging. Treatment outcomes also depend upon the maximum toxicity tolerance of patients and their unique resistance profile of tumours. Due to individual differences in mutations of cancer genes, some treatments might not be effective as a general strategy, warranting more personalised approaches.

The multiple comparisons of inhibitor combinations, encompassing different KRAS inhibitors and resistant cells, performed in this study provides novel insights into effective strategies that may help to overcome acquired resistance to direct KRAS and MEK inhibitors in KRAS-mutant NSCLC. Combinations of EGFR and mTOR inhibition appear most effective at re-sensitising acquired resistance to KRAS-G12C inhibitors, whilst both EGFR and mTOR/SHP2 inhibition are effective alongside KRAS inhibitors to delay initial resistance developing. These combinations are currently being clinically investigated in phase II clinical trials. Overall their potential clinical success will ultimately depend upon their ability to block RAS pathway and adaptive pathway signalling, whilst limiting the additive toxicity of combining multiple inhibitors.

Chapter 6

Discussion and Future Directions

KRAS is one of the most frequently mutated oncogenes in cancer and its mutational activation plays a crucial role in cancer cell survival and proliferation. The recent breakthrough development of selective KRAS-G12C inhibitors provides significant promise to transform the treatment landscape of KRAS-mutant tumours and two inhibitors, sotorasib (previously known as AMG-510) and adagrasib (previously known as MRTX849) have already advanced to FDA approval following positive phase 2 clinical trial results (NCT03600883, NCT03785249). Sotorasib is the first KRAS-G12C inhibitor to be clinically approved for locally advanced or metastatic NSCLC where patients have previously received at least one other cancer treatment. Accelerated approval was based on the encouraging results from the CodeBreak 100 multicentre clinical trial (NCT03600883), in which treatment with sotorasib shrank the tumours of 36% of NSCLC patients and showed a median overall response of 11 months [424]. The CodeBreak clinical development program was designed to address the longstanding unmet medical need to treat advanced KRAS-G12C mutant solid tumours, and since starting, trials so far have enrolled more than 500 patients across 13 tumour types. Continued approval of sotorasib is contingent upon verification of clinical benefit from further trials, including a phase 3 CodeBreak 200 trial for NSCLC (NCT04303780), and several phase 1b combination trials in KRAS-mutant solid tumours (NCT04185883). Despite these encouraging results, there are also indications of varying responses among patients, with 50% of NSCLC and only 10% of CRC patients responsive to AMG-510 during the initial phase 1 trial (NCT03600883) [425]. The development of acquired drug

resistance is a major obstacle that frequently occurs with other targeted cancer therapies and the findings from early phase clinical trials suggests that acquired resistance will also limit the efficacy of these KRAS inhibitors [208, 219]. Therefore, the focus of this research project has been to increase our understanding of acquired resistance mechanisms associated with KRAS inhibitors, which is crucial for improving treatment options, patient stratification and identifying suitable combination strategies that can achieve a more durable treatment response. In this chapter, the findings of this research are summarised, along with discussion of their wider implications and potential future directions.

6.1 Mechanisms of resistance to KRAS inhibitors in KRAS-mutant cells

In this study, initial validation of several KRAS inhibitors in a panel of NSCLC cell lines was performed to determine their sensitivity and specificity (see chapter 3). Three direct KRAS inhibitors, AZ6813, ARS1620 and AZD4785, alongside the MEK inhibitor selumetinib were selected to generate resistant cells. At the time of this study starting, AZ6813 and ARS1620 were the only KRAS-G12C inhibitors readily available. This is the first study to date, to create a panel of resistant cell lines from different KRAS inhibitors, across both acute and chronic treatment regimes, enabling multiple comparisons of acquired resistance mechanisms to be performed. Monitoring of RAS pathway signalling showed that pathway reactivation of downstream signalling components occurred within days of treatment with high doses of targeted KRAS and MEK inhibitors, and resistant H358 cells exhibited permanent pathway rewiring. The reactivation of p-ERK1/2 and p-AKT under KRAS inhibition highlights the continual dependence of resistant cells on these pathways to maintain cell survival. Similar p-ERK1/2 pathway reactivation has since been observed following 48hr treatment with MRTX849 and ARS1620 in other KRAS-G12C cell lines, including colon and pancreatic cells [219, 220]. This highlighted that direct KRAS inhibitors may not be clinically effective long-term as single agent therapeutics and ultimately resistance to these inhibitors enables tumour growth.

Previous studies with other MAPK pathway inhibitors provided some understanding of the potential mechanisms of resistance that might also be observed with KRAS inhibitors (discussed in section 1.4). However, it remained unclear whether these mechanisms would be similar across different approaches of KRAS inhibition or change over the duration of treatment. In-depth analysis was performed using RNA-seq and RPPA, which revealed genome-wide changes in gene and protein expression with different KRAS inhibitors across acute and chronic treatment regimens (see chapter 4). Comparisons across these different resistant models gave additional insights into generic and unique resistance mechanisms. Overall consistent up-regulation of RTKs, RAS-GEFs and downstream cell cycle and DNA damage repair pathways were observed across both KRAS and MEK inhibition, indicating reliance on similar cell signalling pathways and processes for cell survival. The observation that multiple RTKs can drive pathway reactivation indicated that co-targeting with a single RTK inhibitor may be ineffective at preventing adaptive resistance (Figures 4.12 and 4.15). These findings were consistent with observations made by other groups working with KRAS-G12C inhibitors across NSCLC, pancreatic and colon KRAS-G12C cell lines [219, 220]. Furthermore, distinct differences were also observed across acute and chronic treatments, indicating reliance on RTKs can alter over time. For example, acute treatment with KRAS or MEK inhibitors showed up-regulation of ERBB2, which was maintained in chronic resistant cells, with the exception of AZD4785-treated resistant cells (Figure 4.15). In these cells, loss of ERBB2 expression was coupled with increased expression of alternative FGFR1 and PDGFRβ receptors, which were not observed with other KRAS inhibitors. This highlighted that chronically targeting KRAS by different approaches can result in dependence of alternative RTKs.

Another interesting observation was the increase in HRAS gene and protein expression coupled with the loss of KRAS expression and activity in AZD4785-treated resistant cells, suggesting a loss of KRAS dependency for cell survival and proliferation (Figures 4.12 and 4.16). These results suggest that these cells activate other wildtype RAS isoforms to restore MAPK signalling as a

result of increased upstream RTK signalling. Alternatively, cells resistant to KRAS-G12C inhibition regained KRAS activity. This finding was also consistent with observations by other groups, whereby RAS pathway reactivation following KRAS-G12C inhibition was mediated via wildtype RAS [220]. Other groups have also found that acquired resistance to KRAS-G12Ci was dependent upon newly synthesised KRAS-G12C to regain KRAS activity [346]. It remains unclear which process acquired resistance is mediated through across the different KRAS inhibitory mechanisms. To follow this up, additional studies should be performed using protein standard absolute quantification and digital-droplet PCR to more accurate quantify changes in RAS isoform abundance or RAS mutant allele frequency [426, 427]. Clarifying this mechanism would help to provide additional understanding of resistance between generic and allele specific KRAS inhibitors. This could also provide clarification for utilisation of suitable pan-RAS combination approaches, such as targeting SOS1-GRB2 which is currently under clinical evaluation (NCT04111458). An additional consideration observed from this study is that despite being initially upregulated, following chronic KRASi SOS1/2 gene expression became downregulated and coupled with upregulation of alternative RAS-GEFs. As a result, targeting this single interaction may not be enough to prevent RAS activation long-term and overcome acquired resistance. In addition, it remains to be investigated whether alternative KRAS mutations could be selected for and promote resistance to KRAS-G12C inhibitors. Further genomic sequencing with sufficient depth to identify emergent mutations should also be performed. Overall increasing our understanding of the development of drug resistance mechanisms can enable innovative treatment options with improved longer-lasting benefits to patients.

6.2 Therapeutic combination strategies to delay or overcome acquired resistance to KRAS inhibitors

Analysis of 25 targeted inhibitors against pathways of the recognised resistance mechanisms, identified 15 inhibitors which mitigated resistance to KRASi (see chapter 5). Of these, only 3 inhibitors, the broad CDK inhibitor flavopiridol and two mTOR inhibitors AZD8055 and sapanisertib, were

effective across all resistant cell lines. As such prior resistance to KRASi or MEKi can cause cells to become resistant to a range of other targeted inhibitors, both uniquely or collectively, including several RTK, DNA damage pathway and CDK inhibitors. Vertical and horizontal inhibitor combinations demonstrated mixed responses across resistant cells. EGFRi with mTORi were particularly effective at re-sensitising acquired resistance to KRAS-G12Ci, which strongly decreased cell viability and downstream pERK and pAKT signalling pathways. On the other hand, mTORi, or alternatively FGFRi and MEKi were effective strategies to re-sensitise resistance that developed to pan-KRASi using AZD4785.

Further investigation into multiple inhibitor combinations in naïve parental cells confirmed that to maximise the therapeutic potential of various KRAS inhibitors, co-inhibition with other targeted agents is required to overcome acquired resistance. Despite emerging resistance, the addition of a KRAS inhibitor was beneficial in a multi-combinational approach and dramatically delayed and prevented KRAS-mutant cancer cell growth. All 7 inhibitor combinations slowed the emergence of resistance, with EGFRi and mTORi or SHP2i being particularly effective in combination with all KRAS inhibitors. Due to this multi-targeted approach, in particular the specificity that allele specific KRAS inhibitors provide for targeting mutant KRAS, it is hoped that such combinations used at lower doses may be better tolerated in patients. Flavopiridol, a broad CDK inhibitor was also effective at preventing cell growth and resistance, however due to its ability to inhibit multiple CDKs, there are concerns over its potential clinical applications which instead warrants further investigation into additional targeted CDK inhibitors.

Due to the limitations of 2D cell lines to accurately represent clinical responses, future work should build on these findings to validate these therapeutic combinations in advanced preclinical models. For example 3D cell-cultures and tumour-derived organoids enable differences in KRAS dependency, tumour microenvironment and heterogeneity to be accounted for, which can influence the extent of drug responses [428]. KRAS-mutant tumours are also complicated by a diversity of differential effector engagement

across cell lines and tissues [429]. A recent phosphoproteomics study also identified cell-type adaptive responses to KRAS-G12Ci according to the cell-type EMT status, which were associated with different protein signalling responses [430]. This could have implications for driving tumour invasiveness and metastasis. Similar findings were observed in this study, where chronic treatment with AZD4785 promoted a more mesenchymal phenotype associated with differential RTK signalling (see chapter 4). This highlights a potential therapeutic rationale for stratification of treatment according to EMT characteristics and KRAS dependency. Due to the complexity of KRAS signalling and the high heterogeneity across different cancer types, a variety of combinational approaches may therefore be required, particularly for the treatment of advanced cancers. This warrants further validation of combinational approaches across additional KRAS-G12C mutant cancer types.

Additional promising strategies for combination with KRAS inhibitors could also be investigated and compared across the panel of resistant cells. In particular immune checkpoint inhibitors, which target the programmed death protein 1 (PD-1) receptor and its ligand PD-L1, show promising therapeutic potential alongside KRAS inhibitors. From clinical trials it was identified that patients with KRAS mutations had increased PD-L1 levels and in terms of overall survival had greater benefit from anti-PD-1 immunotherapies [431, 432]. Cell-based studies confirmed that mutant RAS signalling directly upregulates PD-L1 expression contributing to immunoresistance, and that treatment with a KRAS-G12C inhibitor significantly reduced its expression [433]. Furthermore in mouse-models, combined treatment of AMG-510 and anti-PD-1 inhibitors synergised well to promote complete tumour regression and also promoted a long-term tumour-specific T-cell response that protected against tumour re-challenge [208]. These responses were not observed with either agent alone, indicating specific KRAS inhibition can improve responses to PD-1 therapies. This combination strategy is therefore particularly interesting for the potential treatment of heterogeneous KRAS-mutant tumours and metastases in which KRAS mutational status can vary. Ultimately using immune-targeted drugs to modulate the patient's immune response

represents a critical strategy for treating advanced tumours which may eventually relapse with standard targeted combination therapies. Currently both AMG-510 and MRTX849 are undergoing clinical evaluation with PD-1 and PD-L1 immunotherapies (see Table 5.2).

It also remains to be investigated what effect different inhibitor treatment strategies will have on therapeutic responses and whether the timing of drug administration can improve combination therapy, as well as reducing potential overlapping clinical toxicities [434]. Approaches such as sequential drug treatment or alternative dosing could yield major vulnerabilities within cancer cells or 'collateral sensitivities' as a result of evolutionary dynamics, that could then be targeted by a second treatment to selectively kill drug-resistant cells [235, 434]. This approach termed 'evolutionary herding' aims to exploit these weaknesses and control tumour cell growth by interrupting the growth of drug-dependent cells, enabling greater competition with drug-sensitive cells. For example, upfront anti-PD-1 therapy followed by BRAF/MEK targeted therapy was found to prolong anti-tumour responses in BRAF-mutant melanoma [435]. Moreover, prior resistance to EGFR inhibitors in EGFR-mutant lung cancer was associated with greater sensitivity to AUKORA kinase inhibition and is currently being clinically evaluated (NCT04085315) [436]. Intermittent dosing of RAF, MEK and ERK inhibitors in BRAF-mutant PDXs inhibited tumour growth with minimum toxicity [437]. In this study, pre-treatment with KRAS or MEK inhibitors generally rendered cells more resistant to a range of alternative targeted inhibitors, however there were exceptions such as increased sensitivity to FGFR1 and mTOR inhibition in AZD4785-treated resistant cells (Figure 5.1). Whether these drug responses are translated to complex preclinical and *in-vivo* models remains to be investigated, but subsequently it would also be informative to assess the timings of treatment to optimise combination approaches.

6.3 Challenges for the prediction of cancer drug resistance

The emergence of acquired drug resistance mechanisms is often described as an evolutionary process, supporting the survival of subpopulations of cells with favourable genetic alterations [263]. Branched evolutionary tumour growth supporting tumour heterogeneity provides the basis for the development of multiple parallel resistance mechanisms following treatment, which have been described both within tumours and across metastatic tumour sites [438]. Often these genetic alterations pre-exist treatment supporting clonal selection as an acquired resistance mechanism [439]. This heterogeneity represents a major challenge for recapitulating cancer evolutionary dynamics in preclinical models and for developing effective therapeutic strategies.

In this study gene and protein expression profiling using RNA-seq and RPPA was used to determine resistance signatures associated with KRAS inhibitor treatment. This highlighted clinically relevant pathways that were enriched as potential mechanisms of resistance. However, underlying tumour heterogeneity can be overlooked when analysing cell populations collectively. Subsequently it remains to be investigated whether the resistance mechanisms identified in this study are expressed collectively throughout the cell population or whether certain mechanisms can be attributed to distinct cell subpopulations, which may ultimately influence tumour evolution and implicate potential future treatment strategies. In recent years technologies such as single-cell genome profiling has provided higher resolution and coverage of the genetic heterogeneity of resistance mechanisms following treatment, enhancing precision medicine. Studies have used single cell RNA-seq on PDXs which identified distinct genomic characteristics of individual tumour cells in order to elucidate changes associated with drug resistance [440, 441]. Biomarkers of drug sensitive and drug tolerant populations could then be applied to identify tumours which would respond to combination therapy [441]. Whilst KRAS inhibitor combinations are evaluated in clinical trials, it will be important to assess the mechanisms and patterns of resistance that arise in

patients over time, to help assess disease progression and improve patient responses guided by the tumour's evolution.

As this study has highlighted, the identification of different gene and protein expression changes across acute and chronic treatments confirms that drug resistance to KRAS inhibitors is a continuous process whereby cells adapt accordingly. Currently the lung TRACERx clinical study is attempting to address the impact of tumour evolution and heterogeneity upon therapeutic outcomes and to define emerging genetic alterations following treatment relapse (NCT01888601)[442]. If the evolutionary trajectories of cancers following targeted treatments can be reasonably predicted, then it may be possible to optimise personalised treatment strategies for specific oncogene driven cancers in order to deliver better treatment outcomes and sustain relapse free survival. Other technologies that are being utilised to improve clinical prediction of treatment efficacy include artificial intelligence and mathematical predictive methods, which can help to understand cancer drug sensitivity and synergistic drug combinations by analysing gene-expression data [443, 444].

6.4 Conclusion

Recent progress in the development of direct KRAS inhibitors has provided hope for potential therapeutic treatments for this previously elusive cancer drug target. However as is the case with most targeted therapies, the development of acquired resistance often limits their efficacy and pre-clinical studies of KRAS-G12C inhibitors has provided evidence of this [425]. With KRAS-G12C inhibitors currently being tested in clinical trials and additional KRAS-mutant inhibitors in development, it is critical to be able to predict potential resistance mechanisms and develop suitable combination therapies. Relatively little is understood about the underlying mechanisms of this resistance, how this might change according to different mechanisms of KRAS inhibition as well as over the duration of treatment. This project aimed to identify resistance signatures associated with several KRAS inhibitors, including recently developed direct KRAS-G12C inhibitors, and to determine

potential combination strategies to prevent or delay the onset of acquired resistance (Figure 6.1).

To summarise, a novel panel of resistant cell lines using different KRAS inhibitors was generated. Transcriptomic and proteomic approaches were used to identify potential resistance mechanisms associated with these different approaches of KRASi, across both acute and chronic treatments. An extensive list of genes and proteins that were differentially regulated across the panel of inhibitors were identified, and those directly involved in RAS pathway and known cancer networks were shortlisted. Consistent upregulation of RTKs, RAS-GEFs, cell cycle and DNA damage repair pathways was observed. Further characterisation of RTK signalling and changes in RAS activity provided insight into potential signalling rewiring mechanisms that occurred in resistant cells. Resistance to KRAS-G12Ci was associated with increased ERBB2 expression and regained KRAS activity. Whereas resistance to pan-KRASi showed differential upregulation of alternative RTKs FGFR1 and PDGFRβ in chronically treated cells, coupled with KRAS independence, potential RAS isoform switching and a more mesenchymal phenotype. Consequently, this highlighted potential implications for overcoming resistance to different KRAS inhibitors which may require different therapeutic combination strategies.

Screening of 25 different compounds and inhibitor combinations identified 15 inhibitors which differentially mitigated resistance across the panel of resistant cells, with 3 inhibitors, flavopiridol - a broad CDK inhibitor and two mTOR inhibitors effective at re-sensitising all KRASi cells. Inhibitor combinations were also analysed alongside KRAS inhibitors in naïve parental cells to identify how well combinations prevented resistance from developing. The most effective included treatment with flavopiridol as well as inhibitor combinations targeting EGFR with either mTOR or SHP2.

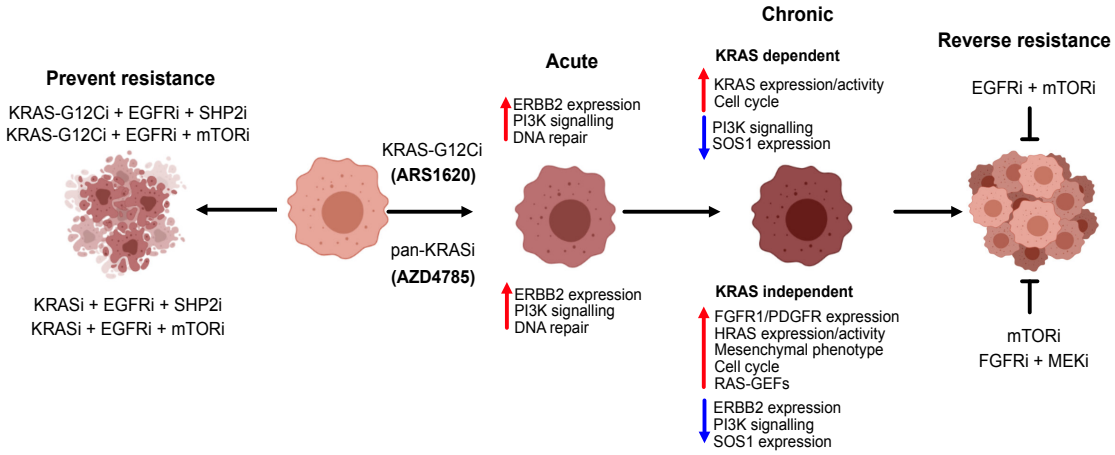

Figure 6.1: Acute and chronic acquired resistance mechanisms to KRAS inhibition and potential therapeutic combinations to overcome resistance

Summary of acute and chronic responses from gene and protein expression analysis following KRAS inhibition with ARS1620 and AZD4785. Inhibitor combination screening identified the most effective inhibitor combinations to reverse resistance to KRAS inhibitors as well as combinations that were most effective for preventing initial resistance from developing.

Thus, multi-omic analysis of resistant cells and screening of directed combinatorial therapeutics has been fundamental for advancing our understanding of resistance mechanisms to new direct classes of KRAS inhibitors. This data provides insightful approaches for effective KRAS inhibitor therapeutic combinations to overcome and slow the emergence of resistance, and represents exciting avenues to pursue for further preclinical and clinical studies.

References

1. Hoadley, K.A., et al., *Cell-of-Origin Patterns Dominate the Molecular Classification of 10,000 Tumors from 33 Types of Cancer.* Cell, 2018. **173**(2): p. 291-304.e6.
2. Dagogo-Jack, I. and A.T. Shaw, *Tumour heterogeneity and resistance to cancer therapies.* Nature Reviews Clinical Oncology, 2018. **15**(2): p. 81-94.
3. Fisher, R., L. Pusztai, and C. Swanton, *Cancer heterogeneity: implications for targeted therapeutics.* British journal of cancer, 2013. **108**(3): p. 479-485.
4. Hanahan, D. and R.A. Weinberg, *The hallmarks of cancer.* Cell, 2000. **100**(1): p. 57-70.
5. Hanahan, D. and R.A. Weinberg, *Hallmarks of cancer: the next generation.* Cell, 2011. **144**(5): p. 646-74.
6. Weinstein, I.B. and A.K. Joe, *Mechanisms of Disease: oncogene addiction—a rationale for molecular targeting in cancer therapy.* Nature Clinical Practice Oncology, 2006. **3**(8): p. 448-457.
7. Bailey, M.H., et al., *Comprehensive Characterization of Cancer Driver Genes and Mutations.* Cell, 2018. **173**(2): p. 371-385.e18.
8. Weinstein, I.B. and A. Joe, *Oncogene Addiction.* Cancer Research, 2008. **68**(9): p. 3077.
9. Pagliarini, R., W. Shao, and W.R. Sellers, *Oncogene addiction: pathways of therapeutic response, resistance, and road maps toward a cure.* EMBO reports, 2015. **16**(3): p. 280-296.
10. Piccart-Gebhart, M.J., et al., *Trastuzumab after adjuvant chemotherapy in HER2-positive breast cancer.* N Engl J Med, 2005. **353**(16): p. 1659-72.
11. O'Brien, S.G., et al., *Imatinib compared with interferon and low-dose cytarabine for newly diagnosed chronic-phase chronic myeloid leukemia.* N Engl J Med, 2003. **348**(11): p. 994-1004.
12. Lynch, T.J., et al., *Activating mutations in the epidermal growth factor receptor underlying responsiveness of non-small-cell lung cancer to gefitinib.* N Engl J Med, 2004. **350**(21): p. 2129-39.
13. Rosell, R., et al., *Erlotinib versus standard chemotherapy as first-line treatment for European patients with advanced EGFR mutation-positive non-small-cell lung cancer (EURTAC): a multicentre, open-label, randomised phase 3 trial.* Lancet Oncol, 2012. **13**(3): p. 239-46.
14. Chapman, P.B., et al., *Improved survival with vemurafenib in melanoma with BRAF V600E mutation.* N Engl J Med, 2011. **364**(26): p. 2507-16.
15. Harvey, J.J., *An Unidentified Virus which causes the Rapid Production of Tumours in Mice.* Nature, 1964. **204**(4963): p. 1104-1105.
16. Kirsten, W.H. and L.A. Mayer, *Morphologic responses to a murine erythroblastosis virus.* J Natl Cancer Inst, 1967. **39**(2): p. 311-35.
17. Ellis, R.W., et al., *The p21 src genes of Harvey and Kirsten sarcoma viruses originate from divergent members of a family of normal vertebrate genes.* Nature, 1981. **292**(5823): p. 506-511.

18. Chang, E.H., et al., *Human genome contains four genes homologous to transforming genes of Harvey and Kirsten murine sarcoma viruses.* Proceedings of the National Academy of Sciences, 1982. **79**(16): p. 4848.
19. Parada, L.F., et al., *Human EJ bladder carcinoma oncogene is homologue of Harvey sarcoma virus ras gene.* Nature, 1982. **297**(5866): p. 474-478.
20. Fernández-Medarde, A. and E. Santos, *Ras in Cancer and Developmental Diseases.* Genes & Cancer, 2011. **2**(3): p. 344-358.
21. Prior, I.A., P.D. Lewis, and C. Mattos, *A comprehensive survey of Ras mutations in cancer.* Cancer Res, 2012. **72**(10): p. 2457-67.
22. Omerovic, J., A.J. Laude, and I.A. Prior, *Ras proteins: paradigms for compartmentalised and isoform specific signalling.* Cellular and molecular life sciences : CMLS, 2007. **64**(19-20): p. 2575-2589.
23. Hobbs, G.A., C.J. Der, and K.L. Rossman, *RAS isoforms and mutations in cancer at a glance.* J Cell Sci, 2016. **129**(7): p. 1287-92.
24. Milburn, M.V., et al., *Molecular switch for signal transduction: structural differences between active and inactive forms of protooncogenic ras proteins.* Science, 1990. **247**(4945): p. 939-45.
25. Ma, J. and M. Karplus, *Molecular switch in signal transduction: reaction paths of the conformational changes in ras p21.* Proc Natl Acad Sci U S A, 1997. **94**(22): p. 11905-10.
26. Pai, E.F., et al., *Structure of the guanine-nucleotide-binding domain of the Ha-ras oncogene product p21 in the triphosphate conformation.* Nature, 1989. **341**(6239): p. 209-214.
27. Vetter, I.R. and A. Wittinghofer, *The guanine nucleotide-binding switch in three dimensions.* Science, 2001. **294**(5545): p. 1299-304.
28. Buhrman, G., et al., *Analysis of binding site hot spots on the surface of Ras GTPase.* Journal of molecular biology, 2011. **413**(4): p. 773-789.
29. Parker, J.A. and C. Mattos, *The Ras–Membrane Interface: Isoform-Specific Differences in the Catalytic Domain.* Molecular Cancer Research, 2015. **13**(4): p. 595.
30. Prior, I.A. and J.F. Hancock, *Ras trafficking, localization and compartmentalized signalling.* Seminars in cell & developmental biology, 2012. **23**(2): p. 145-153.
31. Hancock, John F. and Robert G. Parton, *Ras plasma membrane signalling platforms.* Biochemical Journal, 2005. **389**(Pt 1): p. 1-11.
32. Apolloni, A., et al., *H-ras but not K-ras traffics to the plasma membrane through the exocytic pathway.* Mol Cell Biol, 2000. **20**(7): p. 2475-87.
33. Roy, S., et al., *Individual palmitoyl residues serve distinct roles in H-ras trafficking, microlocalization, and signaling.* Mol Cell Biol, 2005. **25**(15): p. 6722-33.
34. Abankwa, D., et al., *Ras membrane orientation and nanodomain localization generate isoform diversity.* Proc Natl Acad Sci U S A, 2010. **107**(3): p. 1130-5.
35. Wright, L.P. and M.R. Philips, *Thematic review series: lipid posttranslational modifications. CAAX modification and membrane targeting of Ras.* J Lipid Res, 2006. **47**(5): p. 883-91.
36. Hancock, J.F., et al., *All ras proteins are polyisoprenylated but only some are palmitoylated.* Cell, 1989. **57**(7): p. 1167-77.

37. Gutierrez, L., et al., *Post-translational processing of p21ras is two-step and involves carboxyl-methylation and carboxy-terminal proteolysis.* Embo j, 1989. **8**(4): p. 1093-8.
38. Whyte, D.B., et al., *K- and N-Ras are geranylgeranylated in cells treated with farnesyl protein transferase inhibitors.* J Biol Chem, 1997. **272**(22): p. 14459-64.
39. Hancock, J.F., H. Paterson, and C.J. Marshall, *A polybasic domain or palmitoylation is required in addition to the CAAX motif to localize p21ras to the plasma membrane.* Cell, 1990. **63**(1): p. 133-9.
40. Hancock, J.F., et al., *A CAAX or a CAAL motif and a second signal are sufficient for plasma membrane targeting of ras proteins.* Embo j, 1991. **10**(13): p. 4033-9.
41. Zhou, Y. and J.F. Hancock, *Ras nanoclusters: Versatile lipid-based signaling platforms.* Biochimica et Biophysica Acta (BBA) - Molecular Cell Research, 2015. **1853**(4): p. 841-849.
42. Omerovic, J. and I.A. Prior, *Compartmentalized signalling: Ras proteins and signalling nanoclusters.* Febs j, 2009. **276**(7): p. 1817-25.
43. Simanshu, D.K., D.V. Nissley, and F. McCormick, *RAS Proteins and Their Regulators in Human Disease.* Cell, 2017. **170**(1): p. 17-33.
44. Margolis, B. and E.Y. Skolnik, *Activation of Ras by receptor tyrosine kinases.* Journal of the American Society of Nephrology, 1994. **5**(6): p. 1288.
45. Cherfils, J. and M. Zeghouf, *Regulation of small GTPases by GEFs, GAPs, and GDIs.* Physiol Rev, 2013. **93**(1): p. 269-309.
46. Vigil, D., et al., *Ras superfamily GEFs and GAPs: validated and tractable targets for cancer therapy?* Nat Rev Cancer, 2010. **10**(12): p. 842-57.
47. Downward, J., *Targeting RAS signalling pathways in cancer therapy.* Nature Reviews Cancer, 2003. **3**(1): p. 11-22.
48. Lowenstein, E.J., et al., *The SH2 and SH3 domain-containing protein GRB2 links receptor tyrosine kinases to ras signaling.* Cell, 1992. **70**(3): p. 431-42.
49. Buday, L. and J. Downward, *Epidermal growth factor regulates p21ras through the formation of a complex of receptor, Grb2 adapter protein, and Sos nucleotide exchange factor.* Cell, 1993. **73**(3): p. 611-20.
50. Aronheim, A., et al., *Membrane targeting of the nucleotide exchange factor Sos is sufficient for activating the Ras signaling pathway.* Cell, 1994. **78**(6): p. 949-61.
51. Mitin, N., K.L. Rossman, and C.J. Der, *Signaling interplay in Ras superfamily function.* Curr Biol, 2005. **15**(14): p. R563-74.
52. Farnsworth, C.L., et al., *Calcium activation of Ras mediated by neuronal exchange factor Ras-GRF.* Nature, 1995. **376**(6540): p. 524-7.
53. Fernández-Medarde, A. and E. Santos, *The RasGrf family of mammalian guanine nucleotide exchange factors.* Biochimica et Biophysica Acta (BBA) - Reviews on Cancer, 2011. **1815**(2): p. 170-188.
54. Ebinu, J.O., et al., *RasGRP, a Ras guanyl nucleotide- releasing protein with calcium- and diacylglycerol-binding motifs.* Science, 1998. **280**(5366): p. 1082-6.

55. Maertens, O. and K. Cichowski, *An expanding role for RAS GTPase activating proteins (RAS GAPs) in cancer.* Adv Biol Regul, 2014. **55**: p. 1-14.
56. Cichowski, K. and T. Jacks, *NF1 tumor suppressor gene function: narrowing the GAP.* Cell, 2001. **104**(4): p. 593-604.
57. Bollag, G., et al., *Loss of NF1 results in activation of the Ras signaling pathway and leads to aberrant growth in haematopoietic cells.* Nat Genet, 1996. **12**(2): p. 144-8.
58. Lau, N., et al., *Loss of Neurofibromin Is Associated with Activation of RAS/MAPK and PI3-K/AKT Signaling in a Neurofibromatosis 1 Astrocytoma.* Journal of Neuropathology & Experimental Neurology, 2000. **59**(9): p. 759-767.
59. Marais, R., et al., *Ras recruits Raf-1 to the plasma membrane for activation by tyrosine phosphorylation.* The EMBO journal, 1995. **14**(13): p. 3136-3145.
60. Matallanas, D., et al., *Raf family kinases: old dogs have learned new tricks.* Genes & cancer, 2011. **2**(3): p. 232-260.
61. Dhillon, A.S., et al., *Regulation of Raf-1 activation and signalling by dephosphorylation.* Embo j, 2002. **21**(1-2): p. 64-71.
62. Lavoie, H. and M. Therrien, *Regulation of RAF protein kinases in ERK signalling.* Nature Reviews Molecular Cell Biology, 2015. **16**(5): p. 281-298.
63. Tzivion, G., Z. Luo, and J. Avruch, *A dimeric 14-3-3 protein is an essential cofactor for Raf kinase activity.* Nature, 1998. **394**(6688): p. 88-92.
64. Williams, J.G., et al., *Elucidation of binding determinants and functional consequences of Ras/Raf-cysteine-rich domain interactions.* J Biol Chem, 2000. **275**(29): p. 22172-9.
65. Jaumot, M. and J.F. Hancock, *Protein phosphatases 1 and 2A promote Raf-1 activation by regulating 14-3-3 interactions.* Oncogene, 2001. **20**(30): p. 3949-58.
66. Thorson, J.A., et al., *14-3-3 Proteins Are Required for Maintenance of Raf-1 Phosphorylation and Kinase Activity.* Molecular and Cellular Biology, 1998. **18**(9): p. 5229.
67. Emuss, V., et al., *Mutations of C-RAF are rare in human cancer because C-RAF has a low basal kinase activity compared with B-RAF.* Cancer Res, 2005. **65**(21): p. 9719-26.
68. Luo, Z., et al., *Oligomerization activates c-Raf-1 through a Ras-dependent mechanism.* Nature, 1996. **383**(6596): p. 181-5.
69. Weber, C.K., et al., *Active Ras induces heterodimerization of cRaf and BRaf.* Cancer Res, 2001. **61**(9): p. 3595-8.
70. Rushworth, L.K., et al., *Regulation and role of Raf-1/B-Raf heterodimerization.* Mol Cell Biol, 2006. **26**(6): p. 2262-72.
71. Wan, P.T., et al., *Mechanism of activation of the RAF-ERK signaling pathway by oncogenic mutations of B-RAF.* Cell, 2004. **116**(6): p. 855-67.
72. Garnett, M.J., et al., *Wild-Type and Mutant B-RAF Activate C-RAF through Distinct Mechanisms Involving Heterodimerization.* Molecular Cell, 2005. **20**(6): p. 963-969.

73. Hatzivassiliou, G., et al., *RAF inhibitors prime wild-type RAF to activate the MAPK pathway and enhance growth.* Nature, 2010. **464**(7287): p. 431-5.
74. Porta, M., et al., *Cigarette smoking and K-ras mutations in pancreas, lung and colorectal adenocarcinomas: etiopathogenic similarities, differences and paradoxes.* Mutat Res, 2009. **682**(2-3): p. 83-93.
75. Caunt, C.J., et al., *MEK1 and MEK2 inhibitors and cancer therapy: the long and winding road.* Nat Rev Cancer, 2015. **15**(10): p. 577-92.
76. Eblen, S.T., *Extracellular-Regulated Kinases: Signaling From Ras to ERK Substrates to Control Biological Outcomes.* Advances in cancer research, 2018. **138**: p. 99-142.
77. Davis, R.J., *The mitogen-activated protein kinase signal transduction pathway.* Journal of Biological Chemistry, 1993. **268**(20): p. 14553-14556.
78. Roskoski, R., *Targeting ERK1/2 protein-serine/threonine kinases in human cancers.* Pharmacological Research, 2019. **142**: p. 151-168.
79. Jacobs, D., et al., *Multiple docking sites on substrate proteins form a modular system that mediates recognition by ERK MAP kinase.* Genes Dev, 1999. **13**(2): p. 163-75.
80. Lee, T., et al., *Docking motif interactions in MAP kinases revealed by hydrogen exchange mass spectrometry.* Mol Cell, 2004. **14**(1): p. 43-55.
81. Kosako, H., et al., *Phosphoproteomics reveals new ERK MAP kinase targets and links ERK to nucleoporin-mediated nuclear transport.* Nat Struct Mol Biol, 2009. **16**(10): p. 1026-35.
82. Lewis, T.S., et al., *Identification of novel MAP kinase pathway signaling targets by functional proteomics and mass spectrometry.* Mol Cell, 2000. **6**(6): p. 1343-54.
83. Courcelles, M., et al., *Phosphoproteome dynamics reveal novel ERK1/2 MAP kinase substrates with broad spectrum of functions.* Mol Syst Biol, 2013. **9**: p. 669.
84. Yoon, S. and R. Seger, *The extracellular signal-regulated kinase: multiple substrates regulate diverse cellular functions.* Growth Factors, 2006. **24**(1): p. 21-44.
85. Catalanotti, F., et al., *A Mek1-Mek2 heterodimer determines the strength and duration of the Erk signal.* Nat Struct Mol Biol, 2009. **16**(3): p. 294-303.
86. Dougherty, M.K., et al., *Regulation of Raf-1 by direct feedback phosphorylation.* Mol Cell, 2005. **17**(2): p. 215-24.
87. Ritt, D.A., et al., *Impact of feedback phosphorylation and Raf heterodimerization on normal and mutant B-Raf signaling.* Mol Cell Biol, 2010. **30**(3): p. 806-19.
88. Porfiri, E. and F. McCormick, *Regulation of epidermal growth factor receptor signaling by phosphorylation of the ras exchange factor hSOS1.* J Biol Chem, 1996. **271**(10): p. 5871-7.
89. Corbalan-Garcia, S., et al., *Identification of the mitogen-activated protein kinase phosphorylation sites on human Sos1 that regulate interaction with Grb2.* Mol Cell Biol, 1996. **16**(10): p. 5674-82.

90. Buday, L., P.H. Warne, and J. Downward, *Downregulation of the Ras activation pathway by MAP kinase phosphorylation of Sos.* Oncogene, 1995. **11**(7): p. 1327-31.
91. Owens, D.M. and S.M. Keyse, *Differential regulation of MAP kinase signalling by dual-specificity protein phosphatases.* Oncogene, 2007. **26**(22): p. 3203-3213.
92. Caunt, C.J. and S.M. Keyse, *Dual-specificity MAP kinase phosphatases (MKPs).* The FEBS Journal, 2013. **280**(2): p. 489-504.
93. Hanafusa, H., et al., *Sprouty1 and Sprouty2 provide a control mechanism for the Ras/MAPK signalling pathway.* Nat Cell Biol, 2002. **4**(11): p. 850-8.
94. Yusoff, P., et al., *Sprouty2 inhibits the Ras/MAP kinase pathway by inhibiting the activation of Raf.* J Biol Chem, 2002. **277**(5): p. 3195-201.
95. Burotto, M., et al., *The MAPK pathway across different malignancies: a new perspective.* Cancer, 2014. **120**(22): p. 3446-3456.
96. Zhang, M., H. Jang, and R. Nussinov, *The structural basis for Ras activation of PI3Kα lipid kinase.* Physical Chemistry Chemical Physics, 2019. **21**(22): p. 12021-12028.
97. Rodriguez-Viciana, P., et al., *Phosphatidylinositol-3-OH kinase as a direct target of Ras.* Nature, 1994. **370**(6490): p. 527-32.
98. Currie, R.A., et al., *Role of phosphatidylinositol 3,4,5-trisphosphate in regulating the activity and localization of 3-phosphoinositide-dependent protein kinase-1.* Biochem J, 1999. **337 (Pt 3)**(Pt 3): p. 575-83.
99. Alessi, D.R., et al., *Characterization of a 3-phosphoinositide-dependent protein kinase which phosphorylates and activates protein kinase Balpha.* Curr Biol, 1997. **7**(4): p. 261-9.
100. Downes, C.P., et al., *Stimulation of PI 3-kinase signaling via inhibition of the tumor suppressor phosphatase, PTEN.* Adv Enzyme Regul, 2007. **47**: p. 184-94.
101. Downward, J., *How BAD phosphorylation is good for survival.* Nature Cell Biology, 1999. **1**(2): p. E33-E35.
102. Datta, S.R., et al., *Akt phosphorylation of BAD couples survival signals to the cell-intrinsic death machinery.* Cell, 1997. **91**(2): p. 231-41.
103. Vivanco, I. and C.L. Sawyers, *The phosphatidylinositol 3-Kinase AKT pathway in human cancer.* Nat Rev Cancer, 2002. **2**(7): p. 489-501.
104. Pap, M. and G.M. Cooper, *Role of glycogen synthase kinase-3 in the phosphatidylinositol 3-Kinase/Akt cell survival pathway.* J Biol Chem, 1998. **273**(32): p. 19929-32.
105. Diehl, J.A., et al., *Glycogen synthase kinase-3beta regulates cyclin D1 proteolysis and subcellular localization.* Genes & development, 1998. **12**(22): p. 3499-3511.
106. Cohen, P. and S. Frame, *The renaissance of GSK3.* Nature Reviews Molecular Cell Biology, 2001. **2**(10): p. 769-776.
107. Inoki, K., et al., *TSC2 is phosphorylated and inhibited by Akt and suppresses mTOR signalling.* Nat Cell Biol, 2002. **4**(9): p. 648-57.
108. Richardson, C.J., S.S. Schalm, and J. Blenis, *PI3-kinase and TOR: PIKTORing cell growth.* Seminars in Cell & Developmental Biology, 2004. **15**(2): p. 147-159.

109. Engelman, J.A., J. Luo, and L.C. Cantley, *The evolution of phosphatidylinositol 3-kinases as regulators of growth and metabolism.* Nat Rev Genet, 2006. **7**(8): p. 606-19.
110. Matsubara, K., et al., *Plasma membrane recruitment of RalGDS is critical for Ras-dependent Ral activation.* Oncogene, 1999. **18**(6): p. 1303-1312.
111. Shirakawa, R. and H. Horiuchi, *Ral GTPases: crucial mediators of exocytosis and tumourigenesis.* The Journal of Biochemistry, 2015. **157**(5): p. 285-299.
112. Moskalenko, S., et al., *Ral GTPases regulate exocyst assembly through dual subunit interactions.* J Biol Chem, 2003. **278**(51): p. 51743-8.
113. Bodemann, B.O., et al., *RalB and the Exocyst Mediate the Cellular Starvation Response by Direct Activation of Autophagosome Assembly.* Cell, 2011. **144**(2): p. 253-267.
114. Chien, Y., et al., *RalB GTPase-mediated activation of the IkappaB family kinase TBK1 couples innate immune signaling to tumor cell survival.* Cell, 2006. **127**(1): p. 157-70.
115. De Ruiter, N.D., B.M. Burgering, and J.L. Bos, *Regulation of the Forkhead transcription factor AFX by Ral-dependent phosphorylation of threonines 447 and 451.* Mol Cell Biol, 2001. **21**(23): p. 8225-35.
116. Vigil, D., et al., *Aberrant overexpression of the Rgl2 Ral small GTPase-specific guanine nucleotide exchange factor promotes pancreatic cancer growth through Ral-dependent and Ral-independent mechanisms.* J Biol Chem, 2010. **285**(45): p. 34729-40.
117. Lim, K.H., et al., *Divergent roles for RalA and RalB in malignant growth of human pancreatic carcinoma cells.* Curr Biol, 2006. **16**(24): p. 2385-94.
118. Ward, Y., et al., *Signal Pathways Which Promote Invasion and Metastasis: Critical and Distinct Contributions of Extracellular Signal-Regulated Kinase and Ral-Specific Guanine Exchange Factor Pathways.* Molecular and Cellular Biology, 2001. **21**(17): p. 5958.
119. Mo, S.P., J.M. Coulson, and I.A. Prior, *RAS variant signalling.* Biochemical Society transactions, 2018. **46**(5): p. 1325-1332.
120. Der, C.J., T. Finkel, and G.M. Cooper, *Biological and biochemical properties of human rasH genes mutated at codon 61.* Cell, 1986. **44**(1): p. 167-76.
121. Seeburg, P.H., et al., *Biological properties of human c-Ha-ras1 genes mutated at codon 12.* Nature, 1984. **312**(5989): p. 71-75.
122. Trahey, M., et al., *Biochemical and biological properties of the human N-ras p21 protein.* Molecular and Cellular Biology, 1987. **7**(1): p. 541.
123. Hunter, J.C., et al., *Biochemical and Structural Analysis of Common Cancer-Associated KRAS Mutations.* Molecular Cancer Research, 2015. **13**(9): p. 1325.
124. Winters, I.P., et al., *Multiplexed in vivo homology-directed repair and tumor barcoding enables parallel quantification of Kras variant oncogenicity.* Nat Commun, 2017. **8**(1): p. 2053.
125. Guerrero, S., et al., *K-ras codon 12 mutation induces higher level of resistance to apoptosis and predisposition to anchorage-independent*

growth than codon 13 mutation or proto-oncogene overexpression. Cancer Res, 2000. **60**(23): p. 6750-6.
126. Hammond, D.E., et al., *Differential Reprogramming of Isogenic Colorectal Cancer Cells by Distinct Activating KRAS Mutations.* Journal of Proteome Research, 2015. **14**(3): p. 1535-1546.
127. Cox, A.D., et al., *Drugging the undruggable RAS: Mission possible?* Nat Rev Drug Discov, 2014. **13**(11): p. 828-51.
128. UK, C.R., *Half a million fewer deaths from lung cancer in 40 years*. 2019, Cancer Research UK.
129. Brown, K.F., et al., *The fraction of cancer attributable to modifiable risk factors in England, Wales, Scotland, Northern Ireland, and the United Kingdom in 2015.* British Journal of Cancer, 2018. **118**(8): p. 1130-1141.
130. Riely, G.J., et al., *Frequency and distinctive spectrum of KRAS mutations in never smokers with lung adenocarcinoma.* Clin Cancer Res, 2008. **14**(18): p. 5731-4.
131. Tate, J.G., et al., *COSMIC: the Catalogue Of Somatic Mutations In Cancer.* Nucleic Acids Res, 2019. **47**(D1): p. D941-d947.
132. Du, Z. and C.M. Lovly, *Mechanisms of receptor tyrosine kinase activation in cancer.* Molecular Cancer, 2018. **17**(1): p. 58.
133. Bethune, G., et al., *Epidermal growth factor receptor (EGFR) in lung cancer: an overview and update.* Journal of thoracic disease, 2010. **2**(1): p. 48-51.
134. Massarelli, E., et al., *KRAS Mutation Is an Important Predictor of Resistance to Therapy with Epidermal Growth Factor Receptor Tyrosine Kinase Inhibitors in Non–Small-Cell Lung Cancer.* Clinical Cancer Research, 2007. **13**(10): p. 2890.
135. Holderfield, M., et al., *Targeting RAF kinases for cancer therapy: BRAF-mutated melanoma and beyond.* Nature reviews. Cancer, 2014. **14**(7): p. 455-467.
136. Davies, H., et al., *Mutations of the BRAF gene in human cancer.* Nature, 2002. **417**(6892): p. 949-54.
137. Rajagopalan, H., et al., *RAF/RAS oncogenes and mismatch-repair status.* Nature, 2002. **418**(6901): p. 934-934.
138. Yaeger, R. and R.B. Corcoran, *Targeting Alterations in the RAF–MEK Pathway.* Cancer Discovery, 2019. **9**(3): p. 329.
139. Samatar, A.A. and P.I. Poulikakos, *Targeting RAS–ERK signalling in cancer: promises and challenges.* Nature Reviews Drug Discovery, 2014. **13**: p. 928.
140. Ordan, M., et al., *Intrinsically active MEK variants are differentially regulated by proteinases and phosphatases.* Scientific reports, 2018. **8**(1): p. 11830-11830.
141. Samuels, Y., et al., *High Frequency of Mutations of the PIK3CA Gene in Human Cancers.* Science, 2004. **304**(5670): p. 554.
142. Chalhoub, N. and S.J. Baker, *PTEN and the PI3-kinase pathway in cancer.* Annual review of pathology, 2009. **4**: p. 127-150.
143. End, D.W., et al., *Characterization of the Antitumor Effects of the Selective Farnesyl Protein Transferase Inhibitor R115777 in*

Vivo and <em>in Vitro</em&gt. Cancer Research, 2001. **61**(1): p. 131.
144. James, G., J.L. Goldstein, and M.S. Brown, *Resistance of K-RasBV12 proteins to farnesyltransferase inhibitors in Rat1 cells.* Proc Natl Acad Sci U S A, 1996. **93**(9): p. 4454-8.
145. Rowell, C.A., et al., *Direct demonstration of geranylgeranylation and farnesylation of Ki-Ras in vivo.* J Biol Chem, 1997. **272**(22): p. 14093-7.
146. Yang, C.H., et al., *A phase II study of lonafarnib (SCH66336) in patients with chemo-refractory advanced head and neck squamous cell carcinoma (HNSCC).* Journal of Clinical Oncology, 2005. **23**(16_suppl): p. 5565-5565.
147. Javaid, S., et al., *Abstract LB-276: Farnesyltransferase inhibitor (FTI)-induced growth inhibition of HRAS-mutant head and neck cancers is enhanced by concurrently inhibiting compensatory upregulation of the ERK-MAPK kinase cascade.* Cancer Research, 2019. **79**(13 Supplement): p. LB-276.
148. Lane, K.T. and L.S. Beese, *Thematic review series: lipid posttranslational modifications. Structural biology of protein farnesyltransferase and geranylgeranyltransferase type I.* J Lipid Res, 2006. **47**(4): p. 681-99.
149. Sjogren, A.K., et al., *Inactivating GGTase-I reduces disease phenotypes in a mouse model of K-RAS-induced myeloproliferative disease.* Leukemia, 2011. **25**(1): p. 186-9.
150. Liu, M., et al., *Targeting the protein prenyltransferases efficiently reduces tumor development in mice with K-RAS-induced lung cancer.* Proc Natl Acad Sci U S A, 2010. **107**(14): p. 6471-6.
151. Court, H., et al., *Isoprenylcysteine carboxylmethyltransferase deficiency exacerbates KRAS-driven pancreatic neoplasia via Notch suppression.* J Clin Invest, 2013. **123**(11): p. 4681-94.
152. Lin, D.T.S., N.G. Davis, and E. Conibear, *Targeting the Ras palmitoylation/depalmitoylation cycle in cancer.* Biochemical Society Transactions, 2017. **45**(4): p. 913-921.
153. Cox, A.D., C.J. Der, and M.R. Philips, *Targeting RAS Membrane Association: Back to the Future for Anti-RAS Drug Discovery?* Clinical cancer research : an official journal of the American Association for Cancer Research, 2015. **21**(8): p. 1819-1827.
154. Dharmaiah, S., et al., *Structural basis of recognition of farnesylated and methylated KRAS4b by PDEδ.* Proc Natl Acad Sci U S A, 2016. **113**(44): p. E6766-e6775.
155. Chandra, A., et al., *The GDI-like solubilizing factor PDEdelta sustains the spatial organization and signalling of Ras family proteins.* Nat Cell Biol, 2011. **14**(2): p. 148-58.
156. van der Hoeven, D., et al., *Fendiline inhibits K-Ras plasma membrane localization and blocks K-Ras signal transmission.* Mol Cell Biol, 2013. **33**(2): p. 237-51.
157. Cho, K.J., et al., *Staurosporines disrupt phosphatidylserine trafficking and mislocalize Ras proteins.* J Biol Chem, 2012. **287**(52): p. 43573-84.

158. Kisfalvi, K., et al., *Metformin inhibits the growth of human pancreatic cancer xenografts.* Pancreas, 2013. **42**(5): p. 781-785.
159. Cho, K.J., D. van der Hoeven, and J.F. Hancock, *Inhibitors of K-Ras plasma membrane localization.* Enzymes, 2013. **33 Pt A**: p. 249-65.
160. Pottier, C., et al., *Tyrosine Kinase Inhibitors in Cancer: Breakthrough and Challenges of Targeted Therapy.* Cancers, 2020. **12**(3): p. 731.
161. Tomasello, C., et al., *Resistance to EGFR inhibitors in non-small cell lung cancer: Clinical management and future perspectives.* Crit Rev Oncol Hematol, 2018. **123**: p. 149-161.
162. Ruess, D.A., et al., *Mutant KRAS-driven cancers depend on PTPN11/SHP2 phosphatase.* Nature Medicine, 2018. **24**(7): p. 954-960.
163. Mainardi, S., et al., *SHP2 is required for growth of KRAS-mutant non-small-cell lung cancer in vivo.* Nature Medicine, 2018. **24**(7): p. 961-967.
164. Ahmed, T.A., et al., *SHP2 Drives Adaptive Resistance to ERK Signaling Inhibition in Molecularly Defined Subsets of ERK-Dependent Tumors.* Cell Rep, 2019. **26**(1): p. 65-78.e5.
165. Sheridan, C., *Grail of RAS cancer drugs within reach.* Nature Biotechnology, 2020. **38**(1): p. 6-8.
166. Al-Lazikani, B., U. Banerji, and P. Workman, *Combinatorial drug therapy for cancer in the post-genomic era.* Nat Biotechnol, 2012. **30**(7): p. 679-92.
167. Poulikakos, P.I., et al., *RAF inhibitors transactivate RAF dimers and ERK signalling in cells with wild-type BRAF.* Nature, 2010. **464**(7287): p. 427-30.
168. Hatzivassiliou, G., et al., *RAF inhibitors prime wild-type RAF to activate the MAPK pathway and enhance growth.* Nature, 2010. **464**(7287): p. 431-435.
169. Oberholzer, P.A., et al., *RAS Mutations Are Associated With the Development of Cutaneous Squamous Cell Tumors in Patients Treated With RAF Inhibitors.* Journal of Clinical Oncology, 2011. **30**(3): p. 316-321.
170. Hauschild, A., et al., *Dabrafenib in BRAF-mutated metastatic melanoma: a multicentre, open-label, phase 3 randomised controlled trial.* Lancet, 2012. **380**(9839): p. 358-65.
171. Kim, T.W., et al., *Belvarafenib, a novel pan-RAF inhibitor, in solid tumor patients harboring BRAF, KRAS, or NRAS mutations: Phase I study.* Journal of Clinical Oncology, 2019. **37**(15_suppl): p. 3000-3000.
172. Ohren, J.F., et al., *Structures of human MAP kinase kinase 1 (MEK1) and MEK2 describe novel noncompetitive kinase inhibition.* Nat Struct Mol Biol, 2004. **11**(12): p. 1192-7.
173. Solit, D.B., et al., *BRAF mutation predicts sensitivity to MEK inhibition.* Nature, 2006. **439**(7074): p. 358-362.
174. Friday, B.B., et al., *BRAF V600E Disrupts AZD6244-Induced Abrogation of Negative Feedback Pathways between Extracellular Signal-Regulated Kinase and Raf Proteins.* Cancer Research, 2008. **68**(15): p. 6145.
175. Ascierto, P.A., et al., *Cobimetinib combined with vemurafenib in advanced BRAF(V600)-mutant melanoma (coBRIM): updated efficacy*

results from a randomised, double-blind, phase 3 trial. Lancet Oncol, 2016. **17**(9): p. 1248-60.
176. Robert, C., et al., *Five-year outcomes from a phase 3 METRIC study in patients with BRAF V600 E/K-mutant advanced or metastatic melanoma.* Eur J Cancer, 2019. **109**: p. 61-69.
177. Long, G.V., et al., *Adjuvant Dabrafenib plus Trametinib in Stage III BRAF-Mutated Melanoma.* New England Journal of Medicine, 2017. **377**(19): p. 1813-1823.
178. Ciombor, K.K. and T. Bekaii-Saab, *Selumetinib for the treatment of cancer.* Expert Opin Investig Drugs, 2015. **24**(1): p. 111-123.
179. Janne, P.A., et al., *Selumetinib plus docetaxel for KRAS-mutant advanced non-small-cell lung cancer: a randomised, multicentre, placebo-controlled, phase 2 study.* Lancet Oncol, 2013. **14**(1): p. 38-47.
180. Janne, P.A., H. Mann, and D. Ghiorghiu, *Study Design and Rationale for a Randomized, Placebo-Controlled, Double-Blind Study to Assess the Efficacy and Safety of Selumetinib in Combination With Docetaxel as Second-Line Treatment in Patients With KRAS-Mutant Advanced Non-Small Cell Lung Cancer (SELECT-1).* Clin Lung Cancer, 2016. **17**(2): p. e1-4.
181. Lito, P., et al., *Disruption of CRAF-mediated MEK activation is required for effective MEK inhibition in KRAS mutant tumors.* Cancer cell, 2014. **25**(5): p. 697-710.
182. Hatzivassiliou, G., et al., *Mechanism of MEK inhibition determines efficacy in mutant KRAS- versus BRAF-driven cancers.* Nature, 2013. **501**(7466): p. 232-6.
183. Lamba, S., et al., *RAF Suppression Synergizes with MEK Inhibition in KRAS Mutant Cancer Cells.* Cell Reports, 2014. **8**(5): p. 1475-1483.
184. Yen, I., et al., *Pharmacological Induction of RAS-GTP Confers RAF Inhibitor Sensitivity in KRAS Mutant Tumors.* Cancer Cell, 2018. **34**(4): p. 611-625.e7.
185. Moore, A.R., et al., *RAS-targeted therapies: is the undruggable drugged?* Nature Reviews Drug Discovery, 2020. **19**(8): p. 533-552.
186. Moschos, S.J., et al., *Development of MK-8353, an orally administered ERK1/2 inhibitor, in patients with advanced solid tumors.* JCI Insight, 2018. **3**(4).
187. Merchant, M., et al., *Combined MEK and ERK inhibition overcomes therapy-mediated pathway reactivation in RAS mutant tumors.* PloS one, 2017. **12**(10): p. e0185862-e0185862.
188. Weekes, C., et al., *A Phase Ib Study to Evaluate the MEK Inhibitor Cobimetinib in Combination with the ERK1/2 Inhibitor GDC-0994 in Patients with Advanced Solid Tumors.* The oncologist, 2020. **25**(10): p. 833-e1438.
189. Sullivan, R.J., et al., *First-in-Class ERK1/2 Inhibitor Ulixertinib (BVD-523) in Patients with MAPK Mutant Advanced Solid Tumors: Results of a Phase I Dose-Escalation and Expansion Study.* Cancer Discovery, 2018. **8**(2): p. 184.
190. Ozkan-Dagliyan, I., et al., *Low-Dose Vertical Inhibition of the RAF-MEK-ERK Cascade Causes Apoptotic Death of KRAS Mutant Cancers.* Cell Reports, 2020. **31**(11): p. 107764.

191. Gupta, S., et al., *Binding of Ras to Phosphoinositide 3-Kinase p110α Is Required for Ras- Driven Tumorigenesis in Mice.* Cell, 2007. **129**(5): p. 957-968.
192. Castellano, E., et al., *Requirement for Interaction of PI3-Kinase p110α with RAS in Lung Tumor Maintenance.* Cancer Cell, 2013. **24**(5): p. 617-630.
193. Engelman, J.A., et al., *Effective use of PI3K and MEK inhibitors to treat mutant Kras G12D and PIK3CA H1047R murine lung cancers.* Nature Medicine, 2008. **14**(12): p. 1351-1356.
194. Hoeflich, K.P., et al., *Intermittent administration of MEK inhibitor GDC-0973 plus PI3K inhibitor GDC-0941 triggers robust apoptosis and tumor growth inhibition.* Cancer Res, 2012. **72**(1): p. 210-9.
195. Jiang, Z.B., et al., *Combined use of PI3K and MEK inhibitors synergistically inhibits lung cancer with EGFR and KRAS mutations.* Oncol Rep, 2016. **36**(1): p. 365-75.
196. Bedard, P.L., et al., *A phase Ib dose-escalation study of the oral pan-PI3K inhibitor buparlisib (BKM120) in combination with the oral MEK1/2 inhibitor trametinib (GSK1120212) in patients with selected advanced solid tumors.* Clin Cancer Res, 2015. **21**(4): p. 730-8.
197. Shapiro, G.I., et al., *Phase Ib study of the MEK inhibitor cobimetinib (GDC-0973) in combination with the PI3K inhibitor pictilisib (GDC-0941) in patients with advanced solid tumors.* Invest New Drugs, 2020. **38**(2): p. 419-432.
198. Nitulescu, G.M., et al., *Akt inhibitors in cancer treatment: The long journey from drug discovery to clinical use (Review).* International journal of oncology, 2016. **48**(3): p. 869-885.
199. Tolcher, A.W., et al., *Phase I study of the MEK inhibitor trametinib in combination with the AKT inhibitor afuresertib in patients with solid tumors and multiple myeloma.* Cancer Chemotherapy and Pharmacology, 2015. **75**(1): p. 183-189.
200. Do, K., et al., *Biomarker-driven phase 2 study of MK-2206 and selumetinib (AZD6244, ARRY-142886) in patients with colorectal cancer.* Investigational New Drugs, 2015. **33**(3): p. 720-728.
201. Algazi, A.P., et al., *Phase II trial of trametinib in combination with the AKT inhibitor GSK 2141795 in BRAF wild-type melanoma.* Journal of Clinical Oncology, 2015. **33**(15_suppl): p. 9068-9068.
202. Tolcher, A.W., et al., *A phase IB trial of the oral MEK inhibitor trametinib (GSK1120212) in combination with everolimus in patients with advanced solid tumors.* Ann Oncol, 2015. **26**(1): p. 58-64.
203. Schram, A.M., et al., *A phase Ib dose-escalation and expansion study of the oral MEK inhibitor pimasertib and PI3K/MTOR inhibitor voxtalisib in patients with advanced solid tumours.* British Journal of Cancer, 2018. **119**(12): p. 1471-1476.
204. Ostrem, J.M., et al., *K-Ras(G12C) inhibitors allosterically control GTP affinity and effector interactions.* Nature, 2013. **503**(7477): p. 548-51.
205. Shima, F., et al., *Discovery of small-molecule Ras inhibitors that display antitumor activity by interfering with Ras.GTP-effector interaction.* Enzymes, 2013. **34 Pt. B**: p. 1-23.

206. Lim, S.M., et al., *Therapeutic Targeting of Oncogenic K-Ras by a Covalent Catalytic Site Inhibitor.* Angewandte Chemie International Edition, 2014. **53**(1): p. 199-204.
207. Patricelli, M.P., et al., *Selective Inhibition of Oncogenic KRAS Output with Small Molecules Targeting the Inactive State.* Cancer Discovery, 2016. **6**(3): p. 316-329.
208. Canon, J., et al., *The clinical KRAS(G12C) inhibitor AMG 510 drives anti-tumour immunity.* Nature, 2019. **575**(7781): p. 217-223.
209. Hallin, J., et al., *The KRAS^{G12C} Inhibitor MRTX849 Provides Insight toward Therapeutic Susceptibility of KRAS-Mutant Cancers in Mouse Models and Patients.* Cancer Discovery, 2020. **10**(1): p. 54-71.
210. Sakamoto, K., T. Masutani, and T. Hirokawa, *Generation of KS-58 as the first K-Ras(G12D)-inhibitory peptide presenting anti-cancer activity in vivo.* Scientific Reports, 2020. **10**(1): p. 21671.
211. Bery, N., A. Miller, and T. Rabbitts, *A potent KRAS macromolecule degrader specifically targeting tumours with mutant KRAS.* Nature Communications, 2020. **11**(1): p. 3233.
212. Kole, R., A.R. Krainer, and S. Altman, *RNA therapeutics: beyond RNA interference and antisense oligonucleotides.* Nature reviews. Drug discovery, 2012. **11**(2): p. 125-140.
213. Chan, J.H.P., S. Lim, and W.S.F. Wong, *ANTISENSE OLIGONUCLEOTIDES: FROM DESIGN TO THERAPEUTIC APPLICATION.* Clinical and Experimental Pharmacology and Physiology, 2006. **33**(5-6): p. 533-540.
214. Seth, P.P., et al., *Short Antisense Oligonucleotides with Novel 2'−4' Conformationaly Restricted Nucleoside Analogues Show Improved Potency without Increased Toxicity in Animals.* Journal of Medicinal Chemistry, 2009. **52**(1): p. 10-13.
215. Ross, S.J., et al., *Targeting KRAS-dependent tumors with AZD4785, a high-affinity therapeutic antisense oligonucleotide inhibitor of KRAS.* Science Translational Medicine, 2017. **9**(394): p. eaal5253.
216. Cunningham, C.C., et al., *A Phase I trial of H-ras antisense oligonucleotide ISIS 2503 administered as a continuous intravenous infusion in patients with advanced carcinoma.* Cancer, 2001. **92**(5): p. 1265-71.
217. Wang X, Z.H., Chen X, *Drug resistance and combating drug resistance in cancer.* Cancer Drug Resistance, 2019. **2**: p. 141-160.
218. Lippert, T.H., H.J. Ruoff, and M. Volm, *Intrinsic and acquired drug resistance in malignant tumors. The main reason for therapeutic failure.* Arzneimittelforschung, 2008. **58**(6): p. 261-4.
219. Hallin, J., et al., *The KRASG12C Inhibitor, MRTX849, Provides Insight Toward Therapeutic Susceptibility of KRAS Mutant Cancers in Mouse Models and Patients.* Cancer Discovery, 2019: p. CD-19-1167.
220. Ryan, M.B., et al., *Vertical Pathway Inhibition Overcomes Adaptive Feedback Resistance to KRAS(G12C) Inhibition.* Clin Cancer Res, 2020. **26**(7): p. 1633-1643.
221. Richman, S.D., et al., *Intra-tumoral heterogeneity of KRAS and BRAF mutation status in patients with advanced colorectal cancer (aCRC) and*

cost-effectiveness of multiple sample testing. Anal Cell Pathol (Amst), 2011. **34**(1-2): p. 61-6.
222. Kordiak, J., et al., *Intratumor heterogeneity and tissue distribution of KRAS mutation in non-small cell lung cancer: implications for detection of mutated KRAS oncogene in exhaled breath condensate.* J Cancer Res Clin Oncol, 2019. **145**(1): p. 241-251.
223. Lito, P., et al., *Allele-specific inhibitors inactivate mutant KRAS G12C by a trapping mechanism.* Science (New York, N.Y.), 2016. **351**(6273): p. 604-608.
224. Jiao, D. and S. Yang, *Overcoming Resistance to Drugs Targeting KRASG12C Mutation.* The Innovation, 2020. **1**(2): p. 100035.
225. Muzumdar, M.D., et al., *Survival of pancreatic cancer cells lacking KRAS function.* Nature Communications, 2017. **8**(1): p. 1090.
226. Facchinetti, F., et al., *Mechanisms of Resistance to Target Therapies in Non-small Cell Lung Cancer.* Handb Exp Pharmacol, 2018. **249**: p. 63-89.
227. Yu, H.A., et al., *Analysis of tumor specimens at the time of acquired resistance to EGFR-TKI therapy in 155 patients with EGFR-mutant lung cancers.* Clin Cancer Res, 2013. **19**(8): p. 2240-7.
228. Pao, W., et al., *Acquired resistance of lung adenocarcinomas to gefitinib or erlotinib is associated with a second mutation in the EGFR kinase domain.* PLoS Med, 2005. **2**(3): p. e73.
229. Emery, C.M., et al., *MEK1 mutations confer resistance to MEK and B-RAF inhibition.* Proc Natl Acad Sci U S A, 2009. **106**(48): p. 20411-6.
230. Hatzivassiliou, G., et al., *ERK Inhibition Overcomes Acquired Resistance to MEK Inhibitors.* Molecular Cancer Therapeutics, 2012. **11**(5): p. 1143.
231. Shi, H., et al., *Melanoma whole-exome sequencing identifies (V600E)B-RAF amplification-mediated acquired B-RAF inhibitor resistance.* Nat Commun, 2012. **3**: p. 724.
232. Long, G.V., et al., *Increased MAPK reactivation in early resistance to dabrafenib/trametinib combination therapy of BRAF-mutant metastatic melanoma.* Nat Commun, 2014. **5**: p. 5694.
233. Montagut, C., et al., *Elevated CRAF as a potential mechanism of acquired resistance to BRAF inhibition in melanoma.* Cancer research, 2008. **68**(12): p. 4853-4861.
234. Sun, C. and R. Bernards, *Feedback and redundancy in receptor tyrosine kinase signaling: relevance to cancer therapies.* Trends in Biochemical Sciences, 2014. **39**(10): p. 465-474.
235. Acar, A., et al., *Exploiting evolutionary herding to control drug resistance in cancer.* bioRxiv, 2019: p. 566950.
236. Nguyen, L.K. and B.N. Kholodenko, *Feedback regulation in cell signalling: Lessons for cancer therapeutics.* Seminars in Cell & Developmental Biology, 2016. **50**: p. 85-94.
237. Cremers, C.G. and L. Nguyen. *Network rewiring, adaptive resistance and combating strategies in breast cancer*. 2019.
238. Bean, J., et al., *MET amplification occurs with or without T790M mutations in EGFR mutant lung tumors with acquired resistance to gefitinib or erlotinib.* Proc Natl Acad Sci U S A, 2007. **104**(52): p. 20932-7.

239. Takezawa, K., et al., *HER2 amplification: a potential mechanism of acquired resistance to EGFR inhibition in EGFR-mutant lung cancers that lack the second-site EGFRT790M mutation.* Cancer Discov, 2012. **2**(10): p. 922-33.
240. Nazarian, R., et al., *Melanomas acquire resistance to B-RAF(V600E) inhibition by RTK or N-RAS upregulation.* Nature, 2010. **468**(7326): p. 973-7.
241. Wagle, N., et al., *Dissecting therapeutic resistance to RAF inhibition in melanoma by tumor genomic profiling.* J Clin Oncol, 2011. **29**(22): p. 3085-96.
242. Villanueva, J., et al., *Concurrent MEK2 mutation and BRAF amplification confer resistance to BRAF and MEK inhibitors in melanoma.* Cell Rep, 2013. **4**(6): p. 1090-9.
243. Shi, H., et al., *Acquired Resistance and Clonal Evolution in Melanoma during BRAF Inhibitor Therapy.* Cancer Discovery, 2014. **4**(1): p. 80.
244. Little, A.S., et al., *Amplification of the driving oncogene, KRAS or BRAF, underpins acquired resistance to MEK1/2 inhibitors in colorectal cancer cells.* Sci Signal, 2011. **4**(166): p. ra17.
245. Corcoran, R.B., et al., *BRAF gene amplification can promote acquired resistance to MEK inhibitors in cancer cells harboring the BRAF V600E mutation.* Science signaling, 2010. **3**(149): p. ra84-ra84.
246. de Bruin, E.C., et al., *Reduced NF1 expression confers resistance to EGFR inhibition in lung cancer.* Cancer Discov, 2014. **4**(5): p. 606-19.
247. Whittaker, S.R., et al., *A Genome-Scale RNA Interference Screen Implicates NF1 Loss in Resistance to RAF Inhibition.* Cancer Discovery, 2013. **3**(3): p. 350.
248. Sos, M.L., et al., *PTEN loss contributes to erlotinib resistance in EGFR-mutant lung cancer by activation of Akt and EGFR.* Cancer Res, 2009. **69**(8): p. 3256-61.
249. Arcila, M.E., et al., *Rebiopsy of lung cancer patients with acquired resistance to EGFR inhibitors and enhanced detection of the T790M mutation using a locked nucleic acid-based assay.* Clin Cancer Res, 2011. **17**(5): p. 1169-80.
250. Ohashi, K., et al., *Lung cancers with acquired resistance to EGFR inhibitors occasionally harbor BRAF gene mutations but lack mutations in KRAS, NRAS, or MEK1</em&gt.* Proceedings of the National Academy of Sciences, 2012. **109**(31): p. E2127.
251. Wagle, N., et al., *MAP Kinase Pathway Alterations in BRAF-Mutant Melanoma Patients with Acquired Resistance to Combined RAF/MEK Inhibition.* Cancer Discovery, 2014. **4**(1): p. 61.
252. Ahronian, L.G., et al., *Clinical Acquired Resistance to RAF Inhibitor Combinations in BRAF-Mutant Colorectal Cancer through MAPK Pathway Alterations.* Cancer Discovery, 2015. **5**(4): p. 358.
253. Jakobsen, K.R., et al., *The role of epithelial to mesenchymal transition in resistance to epidermal growth factor receptor tyrosine kinase inhibitors in non-small cell lung cancer.* Translational lung cancer research, 2016. **5**(2): p. 172-182.

254. Frederick, B.A., et al., *Epithelial to mesenchymal transition predicts gefitinib resistance in cell lines of head and neck squamous cell carcinoma and non–small cell lung carcinoma.* Molecular Cancer Therapeutics, 2007. **6**(6): p. 1683.
255. Thomson, S., et al., *Epithelial to mesenchymal transition is a determinant of sensitivity of non-small-cell lung carcinoma cell lines and xenografts to epidermal growth factor receptor inhibition.* Cancer Res, 2005. **65**(20): p. 9455-62.
256. Witta, S.E., et al., *Restoring E-cadherin expression increases sensitivity to epidermal growth factor receptor inhibitors in lung cancer cell lines.* Cancer Res, 2006. **66**(2): p. 944-50.
257. Richard, G., et al., *ZEB1-mediated melanoma cell plasticity enhances resistance to MAPK inhibitors.* EMBO Mol Med, 2016. **8**(10): p. 1143-1161.
258. Kitai, H., et al., *Epithelial-to-Mesenchymal Transition Defines Feedback Activation of Receptor Tyrosine Kinase Signaling Induced by MEK Inhibition in KRAS-Mutant Lung Cancer.* Cancer Discov, 2016. **6**(7): p. 754-69.
259. Adachi, Y., et al., *Epithelial-to-Mesenchymal Transition is a Cause of Both Intrinsic and Acquired Resistance to KRAS G12C Inhibitor in KRAS G12C–Mutant Non–Small Cell Lung Cancer.* Clinical Cancer Research, 2020. **26**(22): p. 5962.
260. Sequist, L.V., et al., *Genotypic and histological evolution of lung cancers acquiring resistance to EGFR inhibitors.* Sci Transl Med, 2011. **3**(75): p. 75ra26.
261. Sharma, S.V., et al., *A chromatin-mediated reversible drug-tolerant state in cancer cell subpopulations.* Cell, 2010. **141**(1): p. 69-80.
262. Hata, A.N., et al., *Tumor cells can follow distinct evolutionary paths to become resistant to epidermal growth factor receptor inhibition.* Nature Medicine, 2016. **22**(3): p. 262-269.
263. Amirouchene-Angelozzi, N., C. Swanton, and A. Bardelli, *Tumor Evolution as a Therapeutic Target.* Cancer Discov, 2017.
264. Ramirez, M., et al., *Diverse drug-resistance mechanisms can emerge from drug-tolerant cancer persister cells.* Nature Communications, 2016. **7**(1): p. 10690.
265. Kim, D., B. Langmead, and S.L. Salzberg, *HISAT: a fast spliced aligner with low memory requirements.* Nature Methods, 2015. **12**(4): p. 357-360.
266. Pertea, M., et al., *StringTie enables improved reconstruction of a transcriptome from RNA-seq reads.* Nature Biotechnology, 2015. **33**(3): p. 290-295.
267. Langmead, B. and S.L. Salzberg, *Fast gapped-read alignment with Bowtie 2.* Nature Methods, 2012. **9**(4): p. 357-359.
268. Li, B. and C.N. Dewey, *RSEM: accurate transcript quantification from RNA-Seq data with or without a reference genome.* BMC Bioinformatics, 2011. **12**(1): p. 323.
269. O'Bryan, J.P., *Pharmacological targeting of RAS: Recent success with direct inhibitors.* Pharmacol Res, 2019. **139**: p. 503-511.

270. Khan, I., J.M. Rhett, and J.P. O'Bryan, *Therapeutic targeting of RAS: New hope for drugging the "undruggable".* Biochim Biophys Acta Mol Cell Res, 2020. **1867**(2): p. 118570.
271. Janes, M.R., et al., *Targeting KRAS Mutant Cancers with a Covalent G12C-Specific Inhibitor.* Cell, 2018. **172**(3): p. 578-589.e17.
272. Chakraborty, A., E. Linnane, and S. Ross, *Ras proteins as therapeutic targets.* Biochemical Society Transactions, 2018. **46**(5): p. 1303-1311.
273. Ahearn, I.M., et al., *Regulating the regulator: post-translational modification of RAS.* Nature Reviews Molecular Cell Biology, 2012. **13**(1): p. 39-51.
274. Cho, K.-j., et al., *Inhibition of Acid Sphingomyelinase Depletes Cellular Phosphatidylserine and Mislocalizes K-Ras from the Plasma Membrane.* Molecular and Cellular Biology, 2016. **36**(2): p. 363-374.
275. Zimmermann, G., et al., *Small molecule inhibition of the KRAS-PDEdelta interaction impairs oncogenic KRAS signalling.* Nature, 2013. **497**(7451): p. 638-42.
276. Wong, K.K., J.A. Engelman, and L.C. Cantley, *Targeting the PI3K signaling pathway in cancer.* Curr Opin Genet Dev, 2010. **20**(1): p. 87-90.
277. Balmanno, K., et al., *Intrinsic resistance to the MEK1/2 inhibitor AZD6244 (ARRY-142886) is associated with weak ERK1/2 signalling and/or strong PI3K signalling in colorectal cancer cell lines.* Int J Cancer, 2009. **125**(10): p. 2332-41.
278. Sun, C., et al., *Intrinsic resistance to MEK inhibition in KRAS mutant lung and colon cancer through transcriptional induction of ERBB3.* Cell Rep, 2014. **7**(1): p. 86-93.
279. Kapoor, A., et al., *Yap1 activation enables bypass of oncogenic Kras addiction in pancreatic cancer.* Cell, 2014. **158**(1): p. 185-197.
280. Rosa, R., et al., *In vitro and in vivo models for analysis of resistance to anticancer molecular therapies.* Current medicinal chemistry, 2014. **21**(14): p. 1595-1606.
281. Garraway, L.A. and P.A. Jänne, *Circumventing Cancer Drug Resistance in the Era of Personalized Medicine.* Cancer Discovery, 2012. **2**(3): p. 214.
282. McDermott, M., et al., *In vitro Development of Chemotherapy and Targeted Therapy Drug-Resistant Cancer Cell Lines: A Practical Guide with Case Studies.* Frontiers in Oncology, 2014. **4**(40).
283. Tapias, L.F., et al., *Assessment of Proliferation and Cytotoxicity in a Biomimetic Three-Dimensional Model of Lung Cancer.* Ann Thorac Surg, 2015. **100**(2): p. 414-21.
284. Riedl, A., et al., *Comparison of cancer cells in 2D vs 3D culture reveals differences in AKT–mTOR–S6K signaling and drug responses.* Journal of Cell Science, 2017. **130**(1): p. 203.
285. Sarbassov, D.D., et al., *Phosphorylation and regulation of Akt/PKB by the rictor-mTOR complex.* Science, 2005. **307**(5712): p. 1098-101.
286. Buffet, C., et al., *DUSP5 and DUSP6, two ERK specific phosphatases, are markers of a higher MAPK signaling activation in BRAF mutated thyroid cancers.* PloS one, 2017. **12**(9): p. e0184861-e0184861.

287. Chen, H.-Y., et al., *A Five-Gene Signature and Clinical Outcome in Non–Small-Cell Lung Cancer.* New England Journal of Medicine, 2007. **356**(1): p. 11-20.
288. Zhang, Z., et al., *Dual specificity phosphatase 6 (DUSP6) is an ETS-regulated negative feedback mediator of oncogenic ERK signaling in lung cancer cells.* Carcinogenesis, 2010. **31**(4): p. 577-86.
289. Papke, B. and C.J. Der, *Drugging RAS: Know the enemy.* Science, 2017. **355**(6330): p. 1158-1163.
290. Philips, M.R., *Ras hitchhikes on PDE6δ.* Nature cell biology, 2012. **14**(2): p. 128-129.
291. Fujita-Sato, S., et al., *Enhanced MET Translation and Signaling Sustains K-Ras–Driven Proliferation under Anchorage-Independent Growth Conditions.* Cancer Research, 2015. **75**(14): p. 2851-2862.
292. Ravi, M., et al., *3D cell culture systems: advantages and applications.* J Cell Physiol, 2015. **230**(1): p. 16-26.
293. Pickl, M. and C.H. Ries, *Comparison of 3D and 2D tumor models reveals enhanced HER2 activation in 3D associated with an increased response to trastuzumab.* Oncogene, 2009. **28**(3): p. 461-468.
294. Han, K., et al., *CRISPR screens in cancer spheroids identify 3D growth-specific vulnerabilities.* Nature, 2020. **580**(7801): p. 136-141.
295. Edmondson, R., et al., *Three-Dimensional Cell Culture Systems and Their Applications in Drug Discovery and Cell-Based Biosensors.* Assay and Drug Development Technologies, 2014. **12**(4): p. 207-218.
296. Langhans, S.A., *Three-Dimensional in Vitro Cell Culture Models in Drug Discovery and Drug Repositioning.* Frontiers in pharmacology, 2018. **9**: p. 6-6.
297. Cross, D.A.E., et al., *AZD9291, an Irreversible EGFR TKI, Overcomes T790M-Mediated Resistance to EGFR Inhibitors in Lung Cancer.* Cancer Discovery, 2014. **4**(9): p. 1046.
298. Eberlein, C.A., et al., *Acquired Resistance to the Mutant-Selective EGFR Inhibitor AZD9291 Is Associated with Increased Dependence on RAS Signaling in Preclinical Models.* Cancer research, 2015. **75**(12): p. 2489-2500.
299. Mohr, L., et al., *Generation of Prostate Cancer Cell Models of Resistance to the Anti-mitotic Agent Docetaxel.* Journal of visualized experiments : JoVE, 2017(127): p. 56327.
300. Sale, M.J., et al., *MEK1/2 inhibitor withdrawal reverses acquired resistance driven by BRAFV600E amplification whereas KRASG13D amplification promotes EMT-chemoresistance.* Nature Communications, 2019. **10**(1): p. 2030.
301. Yuan, T.L., et al., *Cell-to-cell variability in PI3K protein level regulates PI3K-AKT pathway activity in cell populations.* Current biology : CB, 2011. **21**(3): p. 173-183.
302. Pavel, M., et al., *Contact inhibition controls cell survival and proliferation via YAP/TAZ-autophagy axis.* Nature Communications, 2018. **9**(1): p. 2961.
303. Wang, R., C. Jin, and X. Hu, *Evidence of drug-response heterogeneity rapidly generated from a single cancer cell.* Oncotarget, 2017. **8**(25): p. 41113-41124.

304. Basile, K.J. and A.E. Aplin, *Resistance to chemotherapy: short-term drug tolerance and stem cell-like subpopulations.* Advances in pharmacology (San Diego, Calif.), 2012. **65**: p. 315-334.
305. Wee, S., et al., *PI3K pathway activation mediates resistance to MEK inhibitors in KRAS mutant cancers.* Cancer Res, 2009. **69**(10): p. 4286-93.
306. Young, A., D. Lou, and F. McCormick, *Oncogenic and Wild-type Ras Play Divergent Roles in the Regulation of Mitogen-Activated Protein Kinase Signaling.* Cancer Discovery, 2013. **3**(1): p. 112.
307. Ryan, M.B. and R.B. Corcoran, *Therapeutic strategies to target RAS-mutant cancers.* Nature Reviews Clinical Oncology, 2018. **15**(11): p. 709-720.
308. Junttila, M.R., et al., *Modeling Targeted Inhibition of MEK and PI3 Kinase in Human Pancreatic Cancer.* Molecular Cancer Therapeutics, 2015. **14**(1): p. 40.
309. Holt, S.V., et al., *Enhanced Apoptosis and Tumor Growth Suppression Elicited by Combination of MEK (Selumetinib) and mTOR Kinase Inhibitors (AZD8055).* Cancer Research, 2012. **72**(7): p. 1804.
310. Tolcher, A.W., et al., *Antitumor activity in RAS-driven tumors by blocking AKT and MEK.* Clin Cancer Res, 2015. **21**(4): p. 739-48.
311. Manchado, E., et al., *A combinatorial strategy for treating KRAS-mutant lung cancer.* Nature, 2016. **534**(7609): p. 647-651.
312. Pek, M., et al., *Oncogenic KRAS-associated gene signature defines co-targeting of CDK4/6 and MEK as a viable therapeutic strategy in colorectal cancer.* Oncogene, 2017. **36**(35): p. 4975-4986.
313. Corcoran, R.B., et al., *Synthetic lethal interaction of combined BCL-XL and MEK inhibition promotes tumor regressions in KRAS mutant cancer models.* Cancer Cell, 2013. **23**(1): p. 121-8.
314. Ziemke, E.K., et al., *Sensitivity of KRAS-Mutant Colorectal Cancers to Combination Therapy That Cotargets MEK and CDK4/6.* Clin Cancer Res, 2016. **22**(2): p. 405-14.
315. Franco, J., A.K. Witkiewicz, and E.S. Knudsen, *CDK4/6 inhibitors have potent activity in combination with pathway selective therapeutic agents in models of pancreatic cancer.* Oncotarget, 2014. **5**(15): p. 6512-25.
316. Horn, T., et al., *High-Order Drug Combinations Are Required to Effectively Kill Colorectal Cancer Cells.* Cancer Research, 2016. **76**(23): p. 6950.
317. Hata, A.N., et al., *Failure to Induce Apoptosis via BCL-2 Family Proteins Underlies Lack of Efficacy of Combined MEK and PI3K Inhibitors for KRAS-Mutant Lung Cancers.* Cancer Research, 2014. **74**(11): p. 3146.
318. Yang, X., et al., *High-Throughput Transcriptome Profiling in Drug and Biomarker Discovery.* Frontiers in Genetics, 2020. **11**(19).
319. Shaheen, S., et al., *Differential Expression and Pathway Analysis in Drug-Resistant Triple-Negative Breast Cancer Cell Lines Using RNASeq Analysis.* International journal of molecular sciences, 2018. **19**(6): p. 1810.
320. Wang, Z., M. Gerstein, and M. Snyder, *RNA-Seq: a revolutionary tool for transcriptomics.* Nat Rev Genet, 2009. **10**(1): p. 57-63.

321. Huang, D.W., B.T. Sherman, and R.A. Lempicki, *Bioinformatics enrichment tools: paths toward the comprehensive functional analysis of large gene lists.* Nucleic acids research, 2009. **37**(1): p. 1-13.
322. Ashburner, M., et al., *Gene ontology: tool for the unification of biology. The Gene Ontology Consortium.* Nature genetics, 2000. **25**(1): p. 25-29.
323. Lu, M. and X. Zhan, *The crucial role of multiomic approach in cancer research and clinically relevant outcomes.* EPMA Journal, 2018. **9**(1): p. 77-102.
324. Waters, K.M., J.G. Pounds, and B.D. Thrall, *Data merging for integrated microarray and proteomic analysis.* Brief Funct Genomic Proteomic, 2006. **5**(4): p. 261-72.
325. Hanash, S., et al., *Integration of proteomics into systems biology of cancer.* Wiley interdisciplinary reviews. Systems biology and medicine, 2012. **4**(4): p. 327-337.
326. Boellner, S. and K.-F. Becker, *Reverse Phase Protein Arrays-Quantitative Assessment of Multiple Biomarkers in Biopsies for Clinical Use.* Microarrays (Basel, Switzerland), 2015. **4**(2): p. 98-114.
327. Creighton, C.J. and S. Huang, *Reverse phase protein arrays in signaling pathways: a data integration perspective.* Drug design, development and therapy, 2015. **9**: p. 3519-3527.
328. Briffa, R., et al., *Multi-Scale Genomic, Transcriptomic and Proteomic Analysis of Colorectal Cancer Cell Lines to Identify Novel Biomarkers.* PloS one, 2015. **10**(12): p. e0144708-e0144708.
329. Oyama, M., et al., *Integrated quantitative analysis of the phosphoproteome and transcriptome in tamoxifen-resistant breast cancer.* J Biol Chem, 2011. **286**(1): p. 818-29.
330. Yang, W., et al., *Integrating proteomics and transcriptomics for the identification of potential targets in early colorectal cancer.* International journal of oncology, 2019. **55**(2): p. 439-450.
331. Huang, D.W., et al., *The DAVID Gene Functional Classification Tool: a novel biological module-centric algorithm to functionally analyze large gene lists.* Genome biology, 2007. **8**(9): p. R183-R183.
332. Dennis, G., et al., *DAVID: Database for Annotation, Visualization, and Integrated Discovery.* Genome Biology, 2003. **4**(9): p. R60.
333. Sanchez-Vega, F., et al., *Oncogenic Signaling Pathways in The Cancer Genome Atlas.* Cell, 2018. **173**(2): p. 321-337.e10.
334. Waldman, T., K.W. Kinzler, and B. Vogelstein, *p21 is necessary for the p53-mediated G1 arrest in human cancer cells.* Cancer Res, 1995. **55**(22): p. 5187-90.
335. Song, K.-A. and A.C. Faber, *Epithelial-to-mesenchymal transition and drug resistance: transitioning away from death.* Journal of thoracic disease, 2019. **11**(6): p. E82-E85.
336. Du, B. and J.S. Shim, *Targeting Epithelial-Mesenchymal Transition (EMT) to Overcome Drug Resistance in Cancer.* Molecules (Basel, Switzerland), 2016. **21**(7): p. 965.
337. Wang, J., et al., *Transition to resistance: An unexpected role of the EMT in cancer chemoresistance.* Genes & Diseases, 2016. **3**(1): p. 3-6.

338. Lamouille, S., J. Xu, and R. Derynck, *Molecular mechanisms of epithelial-mesenchymal transition.* Nat Rev Mol Cell Biol, 2014. **15**(3): p. 178-96.
339. Hernández-de-Diego, R., et al., *PaintOmics 3: a web resource for the pathway analysis and visualization of multi-omics data.* Nucleic Acids Res, 2018. **46**(W1): p. W503-w509.
340. García-Alcalde, F., et al., *Paintomics: a web based tool for the joint visualization of transcriptomics and metabolomics data.* Bioinformatics, 2011. **27**(1): p. 137-9.
341. Montero-Conde, C., et al., *Relief of Feedback Inhibition of HER3 Transcription by RAF and MEK Inhibitors Attenuates Their Antitumor Effects in BRAF-Mutant Thyroid Carcinomas.* Cancer Discovery, 2013. **3**(5): p. 520.
342. Duncan, J.S., et al., *Dynamic reprogramming of the kinome in response to targeted MEK inhibition in triple-negative breast cancer.* Cell, 2012. **149**(2): p. 307-21.
343. Fedele, C., et al., *SHP2 Inhibition Prevents Adaptive Resistance to MEK Inhibitors in Multiple Cancer Models.* Cancer Discovery, 2018. **8**(10): p. 1237.
344. Fedele, C., et al., *SHP2 Inhibition Abrogates Adaptive Resistance to KRAS^{G12C}-Inhibition and Remodels the Tumor Microenvironment of KRAS-Mutant Tumors.* bioRxiv, 2020: p. 2020.05.30.125138.
345. Hillig, R.C., et al., *Discovery of potent SOS1 inhibitors that block RAS activation via disruption of the RAS-SOS1 interaction.* Proc Natl Acad Sci U S A, 2019. **116**(7): p. 2551-2560.
346. Xue, J.Y., et al., *Rapid non-uniform adaptation to conformation-specific KRAS(G12C) inhibition.* Nature, 2020. **577**(7790): p. 421-425.
347. Gatenby, R. and J. Brown, *The Evolution and Ecology of Resistance in Cancer Therapy.* Cold Spring Harbor perspectives in medicine, 2018. **8**(3): p. a033415.
348. Friedman, R., *Drug resistance in cancer: molecular evolution and compensatory proliferation.* Oncotarget, 2016. **7**(11): p. 11746-11755.
349. Foo, J. and F. Michor, *Evolution of acquired resistance to anti-cancer therapy.* Journal of theoretical biology, 2014. **355**: p. 10-20.
350. Abukhdeir, A.M. and B.H. Park, *P21 and p27: roles in carcinogenesis and drug resistance.* Expert Rev Mol Med, 2008. **10**: p. e19.
351. Schuster, K., et al., *Nullifying the CDKN2AB locus promotes mutant K-ras lung tumorigenesis.* Molecular cancer research : MCR, 2014. **12**(6): p. 912-923.
352. Young, R.J., et al., *Loss of CDKN2A expression is a frequent event in primary invasive melanoma and correlates with sensitivity to the CDK4/6 inhibitor PD0332991 in melanoma cell lines.* Pigment Cell Melanoma Res, 2014. **27**(4): p. 590-600.
353. Liu, W., et al., *Fanconi anemia pathway as a prospective target for cancer intervention.* Cell & Bioscience, 2020. **10**(1): p. 39.
354. Chen, P., et al., *The functional status of DNA repair pathways determines the sensitization effect to cisplatin in non-small cell lung cancer cells.* Cellular Oncology, 2016. **39**(6): p. 511-522.

355. Bryant, K.L., et al., *Combination of ERK and autophagy inhibition as a treatment approach for pancreatic cancer.* Nature Medicine, 2019. **25**(4): p. 628-640.
356. Viale, A., et al., *Oncogene ablation-resistant pancreatic cancer cells depend on mitochondrial function.* Nature, 2014. **514**(7524): p. 628-632.
357. Eroglu, Z. and A. Ribas, *Combination therapy with BRAF and MEK inhibitors for melanoma: latest evidence and place in therapy.* Therapeutic advances in medical oncology, 2016. **8**(1): p. 48-56.
358. Tabernero, J., et al., *Encorafenib Plus Cetuximab as a New Standard of Care for Previously Treated BRAF V600E-Mutant Metastatic Colorectal Cancer: Updated Survival Results and Subgroup Analyses from the BEACON Study.* J Clin Oncol, 2021. **39**(4): p. 273-284.
359. Kopetz, S., et al., *Encorafenib, Binimetinib, and Cetuximab in BRAF V600E-Mutated Colorectal Cancer.* N Engl J Med, 2019. **381**(17): p. 1632-1643.
360. Lou, K., et al., *KRAS(G12C) inhibition produces a driver-limited state revealing collateral dependencies.* Science signaling, 2019. **12**(583): p. eaaw9450.
361. Misale, S., et al., *KRAS G12C NSCLC Models Are Sensitive to Direct Targeting of KRAS in Combination with PI3K Inhibition.* Clinical Cancer Research, 2019. **25**(2): p. 796.
362. Kelsey, I. and B.D. Manning, *mTORC1 Status Dictates Tumor Response to Targeted Therapeutics.* Science Signaling, 2013. **6**(294): p. pe31.
363. Molina-Arcas, M., et al., *Development of combination therapies to maximize the impact of KRAS-G12C inhibitors in lung cancer.* Science Translational Medicine, 2019. **11**(510): p. eaaw7999.
364. Chen, Y.N., et al., *Allosteric inhibition of SHP2 phosphatase inhibits cancers driven by receptor tyrosine kinases.* Nature, 2016. **535**(7610): p. 148-52.
365. Nichols, R.J., et al., *RAS nucleotide cycling underlies the SHP2 phosphatase dependence of mutant BRAF-, NF1- and RAS-driven cancers.* Nat Cell Biol, 2018. **20**(9): p. 1064-1073.
366. Hofmann, M.H., et al., *Abstract PL06-01: Discovery of BI-3406: A potent and selective SOS1::KRAS inhibitor opens a new approach for treating KRAS-driven tumors.* Molecular Cancer Therapeutics, 2019. **18**(12 Supplement): p. PL06-01.
367. Guagnano, V., et al., *Discovery of 3-(2,6-Dichloro-3,5-dimethoxy-phenyl)-1-{6-[4-(4-ethyl-piperazin-1-yl)-phenylamino]-pyrimidin-4-yl}-1-methyl-urea (NVP-BGJ398), A Potent and Selective Inhibitor of the Fibroblast Growth Factor Receptor Family of Receptor Tyrosine Kinase.* Journal of Medicinal Chemistry, 2011. **54**(20): p. 7066-7083.
368. Gavine, P.R., et al., *AZD4547: an orally bioavailable, potent, and selective inhibitor of the fibroblast growth factor receptor tyrosine kinase family.* Cancer Res, 2012. **72**(8): p. 2045-56.
369. Wakeling, A.E., et al., *ZD1839 (Iressa): an orally active inhibitor of epidermal growth factor signaling with potential for cancer therapy.* Cancer Res, 2002. **62**(20): p. 5749-54.

370. Moyer, J.D., et al., *Induction of apoptosis and cell cycle arrest by CP-358,774, an inhibitor of epidermal growth factor receptor tyrosine kinase.* Cancer Res, 1997. **57**(21): p. 4838-48.
371. Rusnak, D.W., et al., *The effects of the novel, reversible epidermal growth factor receptor/ErbB-2 tyrosine kinase inhibitor, GW2016, on the growth of human normal and tumor-derived cell lines in vitro and in vivo.* Mol Cancer Ther, 2001. **1**(2): p. 85-94.
372. Xi, Y., et al., *CP-673451, a platelet-derived growth-factor receptor inhibitor, suppresses lung cancer cell proliferation and migration.* Onco Targets Ther, 2014. **7**: p. 1215-21.
373. Wang, P., et al., *Crenolanib, a PDGFR inhibitor, suppresses lung cancer cell proliferation and inhibits tumor growth in vivo.* Onco Targets Ther, 2014. **7**: p. 1761-8.
374. Mitsiades, C.S., et al., *Inhibition of the insulin-like growth factor receptor-1 tyrosine kinase activity as a therapeutic strategy for multiple myeloma, other hematologic malignancies, and solid tumors.* Cancer Cell, 2004. **5**(3): p. 221-30.
375. Shapiro, G.I., *Preclinical and Clinical Development of the Cyclin-Dependent Kinase Inhibitor Flavopiridol.* Clinical Cancer Research, 2004. **10**(12): p. 4270s.
376. Byth, K.F., et al., *AZD5438, a potent oral inhibitor of cyclin-dependent kinases 1, 2, and 9, leads to pharmacodynamic changes and potent antitumor effects in human tumor xenografts.* Mol Cancer Ther, 2009. **8**(7): p. 1856-66.
377. Meijer, L., et al., *Biochemical and cellular effects of roscovitine, a potent and selective inhibitor of the cyclin-dependent kinases cdc2, cdk2 and cdk5.* Eur J Biochem, 1997. **243**(1-2): p. 527-36.
378. Fry, D.W., et al., *Specific inhibition of cyclin-dependent kinase 4/6 by PD 0332991 and associated antitumor activity in human tumor xenografts.* Mol Cancer Ther, 2004. **3**(11): p. 1427-38.
379. VanArsdale, T., et al., *Molecular Pathways: Targeting the Cyclin D-CDK4/6 Axis for Cancer Treatment.* Clin Cancer Res, 2015. **21**(13): p. 2905-10.
380. Jiang, X., et al., *Current status and future prospects of PARP inhibitor clinical trials in ovarian cancer.* Cancer management and research, 2019. **11**: p. 4371-4390.
381. Shen, Y., et al., *BMN 673, a novel and highly potent PARP1/2 inhibitor for the treatment of human cancers with DNA repair deficiency.* Clin Cancer Res, 2013. **19**(18): p. 5003-15.
382. Jones, P., et al., *Discovery of 2-{4-[(3S)-piperidin-3-yl]phenyl}-2H-indazole-7-carboxamide (MK-4827): a novel oral poly(ADP-ribose)polymerase (PARP) inhibitor efficacious in BRCA-1 and -2 mutant tumors.* J Med Chem, 2009. **52**(22): p. 7170-85.
383. Riches, L.C., et al., *Pharmacology of the ATM Inhibitor AZD0156: Potentiation of Irradiation and Olaparib Responses Preclinically.* Molecular Cancer Therapeutics, 2020. **19**(1): p. 13.
384. Weber, A.M. and A.J. Ryan, *ATM and ATR as therapeutic targets in cancer.* Pharmacology & Therapeutics, 2015. **149**: p. 124-138.

385. Gorecki, L., et al., *Discovery of ATR kinase inhibitor berzosertib (VX-970, M6620): Clinical candidate for cancer therapy.* Pharmacol Ther, 2020. **210**: p. 107518.
386. Hirai, H., et al., *MK-1775, a small molecule Wee1 inhibitor, enhances anti-tumor efficacy of various DNA-damaging agents, including 5-fluorouracil.* Cancer Biol Ther, 2010. **9**(7): p. 514-22.
387. Saran, U., M. Foti, and J.F. Dufour, *Cellular and molecular effects of the mTOR inhibitor everolimus.* Clin Sci (Lond), 2015. **129**(10): p. 895-914.
388. Lane, H.A., et al., *mTOR inhibitor RAD001 (everolimus) has antiangiogenic/vascular properties distinct from a VEGFR tyrosine kinase inhibitor.* Clin Cancer Res, 2009. **15**(5): p. 1612-22.
389. Voss, M.H., et al., *Phase 1 study of mTORC1/2 inhibitor sapanisertib (TAK-228) in advanced solid tumours, with an expansion phase in renal, endometrial or bladder cancer.* British Journal of Cancer, 2020. **123**(11): p. 1590-1598.
390. Liu, Q., et al., *mTOR Mediated Anti-Cancer Drug Discovery.* Drug discovery today. Therapeutic strategies, 2009. **6**(2): p. 47-55.
391. Chresta, C.M., et al., *AZD8055 is a potent, selective, and orally bioavailable ATP-competitive mammalian target of rapamycin kinase inhibitor with in vitro and in vivo antitumor activity.* Cancer Res, 2010. **70**(1): p. 288-98.
392. Di Veroli, G.Y., et al., *Combenefit: an interactive platform for the analysis and visualization of drug combinations.* Bioinformatics, 2016. **32**(18): p. 2866-8.
393. Burgess, M.R., et al., *KRAS Allelic Imbalance Enhances Fitness and Modulates MAP Kinase Dependence in Cancer.* Cell, 2017. **168**(5): p. 817-829.e15.
394. Ambrogio, C., et al., *KRAS Dimerization Impacts MEK Inhibitor Sensitivity and Oncogenic Activity of Mutant KRAS.* Cell, 2018. **172**(4): p. 857-868.e15.
395. Sun, C., et al., *Rational combination therapy with PARP and MEK inhibitors capitalizes on therapeutic liabilities in RAS mutant cancers.* Science Translational Medicine, 2017. **9**(392): p. eaal5148.
396. Janysek, D.C., et al., *Clinical use and mechanisms of resistance for PARP inhibitors in homologous recombination-deficient cancers.* Translational Oncology, 2021. **14**(3): p. 101012.
397. Otto, T. and P. Sicinski, *Cell cycle proteins as promising targets in cancer therapy.* Nature Reviews Cancer, 2017. **17**(2): p. 93-115.
398. Ku, B.M., et al., *Mutational status of TP53 defines the efficacy of Wee1 inhibitor AZD1775 in KRAS-mutant non-small cell lung cancer.* Oncotarget, 2017. **8**(40): p. 67526-67537.
399. Puyol, M., et al., *A Synthetic Lethal Interaction between K-Ras Oncogenes and Cdk4 Unveils a Therapeutic Strategy for Non-small Cell Lung Carcinoma.* Cancer Cell, 2010. **18**(1): p. 63-73.
400. Goldman, J.W., et al., *A Randomized Phase III Study of Abemaciclib Versus Erlotinib in Patients with Stage IV Non-small Cell Lung Cancer With a Detectable KRAS Mutation Who Failed Prior Platinum-Based Therapy: JUNIPER.* Front Oncol, 2020. **10**: p. 578756.

401. Knudsen, E.S. and A.K. Witkiewicz, *The Strange Case of CDK4/6 Inhibitors: Mechanisms, Resistance, and Combination Strategies.* Trends in cancer, 2017. **3**(1): p. 39-55.
402. Bible, K.C. and S.H. Kaufmann, *Flavopiridol: A Cytotoxic Flavone That Induces Cell Death in Noncycling A549 Human Lung Carcinoma Cells.* Cancer Research, 1996. **56**(21): p. 4856.
403. Shapiro, G.I., et al., *Flavopiridol Induces Cell Cycle Arrest and p53-independent Apoptosis in Non-Small Cell Lung Cancer Cell Lines.* Clinical Cancer Research, 1999. **5**(10): p. 2925.
404. Burdette-Radoux, S., et al., *Phase II trial of flavopiridol, a cyclin dependent kinase inhibitor, in untreated metastatic malignant melanoma.* Invest New Drugs, 2004. **22**(3): p. 315-22.
405. Shapiro, G.I., et al., *A phase II trial of the cyclin-dependent kinase inhibitor flavopiridol in patients with previously untreated stage IV non-small cell lung cancer.* Clin Cancer Res, 2001. **7**(6): p. 1590-9.
406. Fekrazad, H.M., et al., *A phase I study of flavopiridol in combination with gemcitabine and irinotecan in patients with metastatic cancer.* Am J Clin Oncol, 2010. **33**(4): p. 393-7.
407. Bible, K.C., et al., *A phase 2 trial of flavopiridol (Alvocidib) and cisplatin in platin-resistant ovarian and primary peritoneal carcinoma: MC0261.* Gynecol Oncol, 2012. **127**(1): p. 55-62.
408. Lu, H., et al., *Resistance to allosteric SHP2 inhibition in FGFR-driven cancers through rapid feedback activation of FGFR.* Oncotarget, 2020. **11**(3): p. 265-281.
409. Ozkan-Dagliyan, I., et al., *Low-Dose Vertical Inhibition of the RAF-MEK-ERK Cascade Causes Apoptotic Death of KRAS Mutant Cancers.* Cell reports, 2020. **31**(11): p. 107764-107764.
410. Theard, P.L., et al., *Marked Synergy by Vertical Inhibition of EGFR signaling in NSCLC Spheroids: SOS1 as a therapeutic target in EGFR-mutated cancer.* bioRxiv, 2020: p. 2020.04.28.066241.
411. George, S., et al., *Phase I Study of Flavopiridol in Combination with Paclitaxel and Carboplatin in Patients with Non–Small-Cell Lung Cancer.* Clinical Lung Cancer, 2008. **9**(3): p. 160-165.
412. Chao, S.H. and D.H. Price, *Flavopiridol inactivates P-TEFb and blocks most RNA polymerase II transcription in vivo.* J Biol Chem, 2001. **276**(34): p. 31793-9.
413. Wang, S. and P.M. Fischer, *Cyclin-dependent kinase 9: a key transcriptional regulator and potential drug target in oncology, virology and cardiology.* Trends in Pharmacological Sciences, 2008. **29**(6): p. 302-313.
414. Yin, T., et al., *A novel CDK9 inhibitor shows potent antitumor efficacy in preclinical hematologic tumor models.* Mol Cancer Ther, 2014. **13**(6): p. 1442-56.
415. Cassandri, M., et al., *CDK9 as a Valuable Target in Cancer: From Natural Compounds Inhibitors to Current Treatment in Pediatric Soft Tissue Sarcomas.* Frontiers in pharmacology, 2020. **11**: p. 1230-1230.
416. Liu, X., et al., *CDKI-71, a novel CDK9 inhibitor, is preferentially cytotoxic to cancer cells compared to flavopiridol.* Int J Cancer, 2012. **130**(5): p. 1216-26.

417. Kessler, D., et al., *Drugging all RAS isoforms with one pocket.* Future Medicinal Chemistry, 2020. **12**(21): p. 1911-1923.
418. Ekert, J.E., et al., *Three-dimensional lung tumor microenvironment modulates therapeutic compound responsiveness in vitro--implication for drug development.* PLoS One, 2014. **9**(3): p. e92248.
419. Jacobi, N., et al., *Organotypic three-dimensional cancer cell cultures mirror drug responses in vivo: lessons learned from the inhibition of EGFR signaling.* Oncotarget, 2017. **8**(64): p. 107423-107440.
420. Tiriac, H., et al., *Organoid Profiling Identifies Common Responders to Chemotherapy in Pancreatic Cancer.* Cancer Discovery, 2018. **8**(9): p. 1112.
421. Driehuis, E., et al., *Pancreatic cancer organoids recapitulate disease and allow personalized drug screening.* Proceedings of the National Academy of Sciences, 2019. **116**(52): p. 26580.
422. Huo, K.-G., E. D'Arcangelo, and M.-S. Tsao, *Patient-derived cell line, xenograft and organoid models in lung cancer therapy.* Translational lung cancer research, 2020. **9**(5): p. 2214-2232.
423. Lopez, J.S. and U. Banerji, *Combine and conquer: challenges for targeted therapy combinations in early phase trials.* Nature reviews. Clinical oncology, 2017. **14**(1): p. 57-66.
424. Skoulidis, F., et al., *Sotorasib for Lung Cancers with KRAS p.G12C Mutation.* N Engl J Med, 2021. **384**(25): p. 2371-2381.
425. Govindan, R., et al., *446PD - Phase I study of AMG 510, a novel molecule targeting KRAS G12C mutant solid tumours.* Annals of Oncology, 2019. **30**: p. v163-v164.
426. Mageean, C.J., et al., *Absolute Quantification of Endogenous Ras Isoform Abundance.* PloS one, 2015. **10**(11): p. e0142674-e0142674.
427. Alcaide, M., et al., *A Novel Multiplex Droplet Digital PCR Assay to Identify and Quantify KRAS Mutations in Clinical Specimens.* The Journal of Molecular Diagnostics, 2019. **21**(2): p. 214-227.
428. Verissimo, C.S., et al., *Targeting mutant RAS in patient-derived colorectal cancer organoids by combinatorial drug screening.* eLife, 2016. **5**: p. e18489.
429. Yuan, T.L., et al., *Differential Effector Engagement by Oncogenic KRAS.* Cell Rep, 2018. **22**(7): p. 1889-1902.
430. Solanki, H.S., et al., *Cell Type–specific Adaptive Signaling Responses to KRAS^{G12C} Inhibition.* Clinical Cancer Research, 2021.
431. Garon, E.B., et al., *Pembrolizumab for the treatment of non-small-cell lung cancer.* N Engl J Med, 2015. **372**(21): p. 2018-28.
432. Borghaei, H., et al., *Nivolumab versus Docetaxel in Advanced Nonsquamous Non-Small-Cell Lung Cancer.* N Engl J Med, 2015. **373**(17): p. 1627-39.
433. Coelho, M.A., et al., *Oncogenic RAS Signaling Promotes Tumor Immunoresistance by Stabilizing PD-L1 mRNA.* Immunity, 2017. **47**(6): p. 1083-1099.e6.
434. Settleman, J., J.M.F. Neto, and R. Bernards, *Thinking Differently about Cancer Treatment Regimens.* Cancer Discovery, 2021.
435. Phadke, M.S., et al., *Targeted therapy given after anti-PD-1 leads to prolonged responses in mouse melanoma models through sustained*

antitumor immunity. Cancer Immunology Research, 2021: p. canimm.CIR-20-0905-A.2020.
436. Bertran-Alamillo, J., et al., *AURKB as a target in non-small cell lung cancer with acquired resistance to anti-EGFR therapy.* Nature communications, 2019. **10**(1): p. 1812-1812.
437. Xue, Y., et al., *An approach to suppress the evolution of resistance in BRAF(V600E)-mutant cancer.* Nature medicine, 2017. **23**(8): p. 929-937.
438. Swanton, C., *Intratumor heterogeneity: evolution through space and time.* Cancer research, 2012. **72**(19): p. 4875-4882.
439. Burrell, R.A. and C. Swanton, *Tumour heterogeneity and the evolution of polyclonal drug resistance.* Molecular Oncology, 2014. **8**(6): p. 1095-1111.
440. Kim, K.-T., et al., *Single-cell mRNA sequencing identifies subclonal heterogeneity in anti-cancer drug responses of lung adenocarcinoma cells.* Genome Biology, 2015. **16**(1): p. 127.
441. Aissa, A.F., et al., *Single-cell transcriptional changes associated with drug tolerance and response to combination therapies in cancer.* Nature Communications, 2021. **12**(1): p. 1628.
442. Jamal-Hanjani, M., et al., *Tracking genomic cancer evolution for precision medicine: the lung TRACERx study.* PLoS Biol, 2014. **12**(7): p. e1001906.
443. Li, X., et al., *Prediction of synergistic anti-cancer drug combinations based on drug target network and drug induced gene expression profiles.* Artif Intell Med, 2017. **83**: p. 35-43.
444. Menden, M.P., et al., *Machine learning prediction of cancer cell sensitivity to drugs based on genomic and chemical properties.* PLoS One, 2013. **8**(4): p. e61318.

Appendices

Appendix 1: Fold resistance between IC90 treated resistant cells and naïve cells.

Inhibitor	Day	Resistant cells IC50 (M)	Naïve cells IC50 (M)	Fold Resistance (%)
AZ6813 (Batch 1)	27	0.00001319	0.000004459	296
	38	0.000006087	0.000001254	485
	88	0.00001051	0.000009632	109
	75	0.000005613	0.000001675	335
	101	0.00001697	0.000003117	544
AZ6813 (Batch 2)	58	0.00001034	0.000003201	323
	72	0.00001132	0.000002089	541
ARS1620 (Batch 1)	66	0.000007191	0.000004435	162
	72	0.00001933	0.00001978	98
	79	0.000008954	0.000002789	321
AZD4785 (Batch 1)	30	0.00001122	0.000005799	193
	36	0.00007354	0.00001301	565
	88	0.00001455	0.00001467	99
	91	0.0000108	0.000003835	282
	97	0.0001315	0.0001315	1977
Selumetinib (Batch 1)	27	0.00005286	0.000002989	1768
	34	0.000005366	3.461E-07	1550
	75	0.000007521	0.000006867	110
	88	0.000004338	0.00000114	381
Selumetinib (Batch 2)	58	0.00003566	0.000001223	2916
	72	0.00002605	4.958E-07	5254
	86	0.00002485	0.000002781	894

Appendix 2: RPPA log_2fold protein expression levels which show the greatest change between acute and chronic treatment for each inhibitor.

Inhibitor	Antibody	Gene	Modification	H358-A log_2 fold change	H358-R log_2 fold change	Validation
AZ6813	Chk1_pS296	CHEK1	p	1.50860002	-0.2585704	V
	STING	STING1		1.21059002	0.34384956	V
	PAK_pT423_T402	PAK1-3	p	1.14189002	0.00933956	C
	NQO1	NQO1		1.10607002	-0.3635804	V
	p21	CDKN1A		0.96723002	-0.0997004	C
	Pdcd4	PDCD4		0.95650002	-0.0882904	C
	CRABP2	CRABP2		0.87381002	-0.2798704	V
	PKC-b-II_pS660	PRKCA/B/D/E/H/Q	p	0.85551002	-0.0106904	V
	Annexin-I	ANXA1		0.85389002	0.25309956	V
	INPP4b	INPP4B		0.82486002	0.21652956	C
	G6PD	G6PD		0.65129002	-1.0666104	V
	JNK_pT183_Y185	MAPK8	p	0.60614002	-0.3953204	C
	NF-kB-p65_pS536	RELA	p	0.46269002	-0.5670704	C
	EMA	MUC1		0.45768002	-0.6711904	C
	ACLY_pS455	ACLY	p	0.16265002	0.60337956	V
	Cdc6	CDC6		-0.75115	0.08992956	V
	EphA2	EPHA2		-1.00404	0.09434956	V
	Hif-1-alpha	HIF1A		-1.02464	-0.1124404	C
	S6_pS240_S244	RPS6	p	-1.04885	-0.1317604	V
	EphA2_pS897	EPHA2	p	-1.06784	0.03992956	C
	DUSP4	DUSP4		-1.12497	-0.4253104	V
ARS1620	p21	CDKN1A		1.24685002	0.05682425	V
	NQO1	NQO1		1.16227002	-0.2479657	V
	Pdcd4	PDCD4		0.98950002	0.16827425	C
	MTCO1	MT-CO1		0.87527002	-0.7753757	V
	PAI-1	SERPINE1		0.60533002	-0.3513257	C
	G6PD	G6PD		0.50934002	-0.9814157	C
	CRABP2	CRABP2		0.17143002	-0.6182957	V
	CDK1_pT14	CDK1-3	p	-0.63202	0.31330425	V
	Cyclin-B1	CCNB1		-0.68357	0.02257425	V
	S6_pS235_S236	RPS6	p	-0.69625	-0.0078957	V
	S6_pS240_S244	RPS6	p	-0.75796	-0.0680557	C
	Src_pY416	SRC	p	-0.81798	-0.1135257	V
Selumetinib	p21	CDKN1A		1.24091001	-0.28661	C
	STING	STING1		1.03068001	-0.04249	V
	Chk1_pS296	CHEK1	p	0.94054001	-0.41717	V
	NQO1	NQO1		0.84892001	-0.54041	V
	PAR	[PAR Modification]		0.55521001	-0.69821	C
	G6PD	G6PD		0.30228001	-1.16498	V
	Cdc6	CDC6		-0.90635	-0.20326	V
	CDK1_pT14	CDK1-3	p	-0.9254	-0.26334	C
	Aurora-B	AURKB		-1.00472	-0.26974	V
	EphA2	EPHA2		-1.08133	-0.12011	V
	Cyclin-B1	CCNB1		-1.16279	-0.21848	V
AZD4785 (ASO)	INPP4b	INPP4B		1.46289476	-0.8888217	C
	Tuberin_pT1462	TSC2	p	1.06431476	0.03074826	V
	STING	STING1		1.04071476	-1.3582317	V
	NQO1	NQO1		0.97038476	-2.0179717	V
	HER2	ERBB2		1.53644476	-0.3602917	V
	E-Cadherin	CDH1		0.62361476	-0.8015317	V
	P-Cadherin	CDH3		0.62035476	-0.3405017	C
	PAK1	PAK1		0.34876476	-1.2627417	V
	HMHA1	ARHGAP45		0.33192476	-0.9264617	V
	SHP2	PTPN11		0.00174476	-0.9807617	V
	Rab25	RAB25		0.47392476	-1.4541217	V
	Claudin-7	CLDN7		0.44588476	-1.5566717	V
	DRP1	DNM1L		0.36494476	1.00401826	V
	Bax	BAX		0.34076476	1.12806826	V
	Transglutaminase	TGM2		0.29777476	0.99099826	V
	PLC-gamma1_pS1248	PLCG1	p	0.28166476	1.01936826	V
	MMP14	MMP14		0.27548476	1.14071826	V
	p53	TP53		0.26072476	1.10379826	C

	IR-b	INSR		0.22777476	1.16075826	C
	Myosin-IIa_pS1943	MYH9	p	0.19875476	-1.3985917	V
	PAX6	PAX6		0.13676476	0.95544826	V
	DDR1	DDR1		0.12313476	-1.2947317	V
	LAD1	LAD1		0.04692476	-0.9422117	V
	PLC-gamma1	PLCG1		0.04347476	0.82404826	V
	Myosin-IIa	MYH9		0.04214476	-1.1792017	C
	Rb	RB1		0.03760476	0.86163826	Q
	Connexin-43	GJA1		0.00821476	2.06941826	C
	Tau	MAPT		-0.0041752	0.98907826	C
	Cyclophilin-F	PPIF		-0.0072852	0.87006826	V
	FGF-basic	FGF2		-0.0209452	2.84731826	C
	AceCS1	ACSS2		-0.0213052	1.04178826	V
	PKM2	PKM		-0.0752752	-1.4263417	C
	LC3A-B	MAP1LC3A/B		-0.2240652	1.57739826	C
	b-Catenin	CTNNB1		-0.2577952	-1.6715617	V
	Heregulin	NRG1		-0.3182752	0.96224826	V
	Enolase-1	ENO1		-0.3257352	-1.1067917	V
	CRABP2	CRABP2		-0.4589752	-2.4334617	V
	VHL-EPPK1	EPPK1		-0.5491652	-1.4552117	C
	JAB1	COPS5		-0.5616352	-1.2197517	C
	CDK1_pT14	CDK1-3	p	-1.0595752	0.83657826	C
	IGFBP2	IGFBP2		-1.0652852	-2.5723017	V
	MCT4	SLC16A3		-1.0825152	-3.2263717	V
	Cyclin-B1	CCNB1		-1.2232252	0.26762826	V
	Rb_pS807_S811	RB1	p	-1.5226952	0.49924826	V
	S6_pS240_S244	RPS6	p	-0.3672852	0.69354826	V
	eEF2	EEF2		-0.3694252	0.69709826	C
	PKA-a	PRKAR1A		-0.4797652	0.62633826	V
	SLC1A5	SLC1A5		-0.5858952	0.79197826	C
	Cdc6	CDC6		-1.0609452	0.26993826	
	Caveolin-1	CAV1		-0.9412352	0.13097826	V
	Cyclin-D3	CCND3		-0.1685652	0.69808826	V
	Wee1	WEE1		0.03130476	-0.5701717	C

Appendix 3: Ras Network Expression for H358-R AZ6813, H358-R AR1620 and H358-R Selumetinib

Heat maps illustrating RNA-Seq differential gene expression in Ras pathway genes. Red indicates positive log fold change and represents increased expression in inhibitor treated cells compared to the corresponding vehicle control, whilst blue indicates negative log fold change and a decrease in expression. (Figure continued on next page).

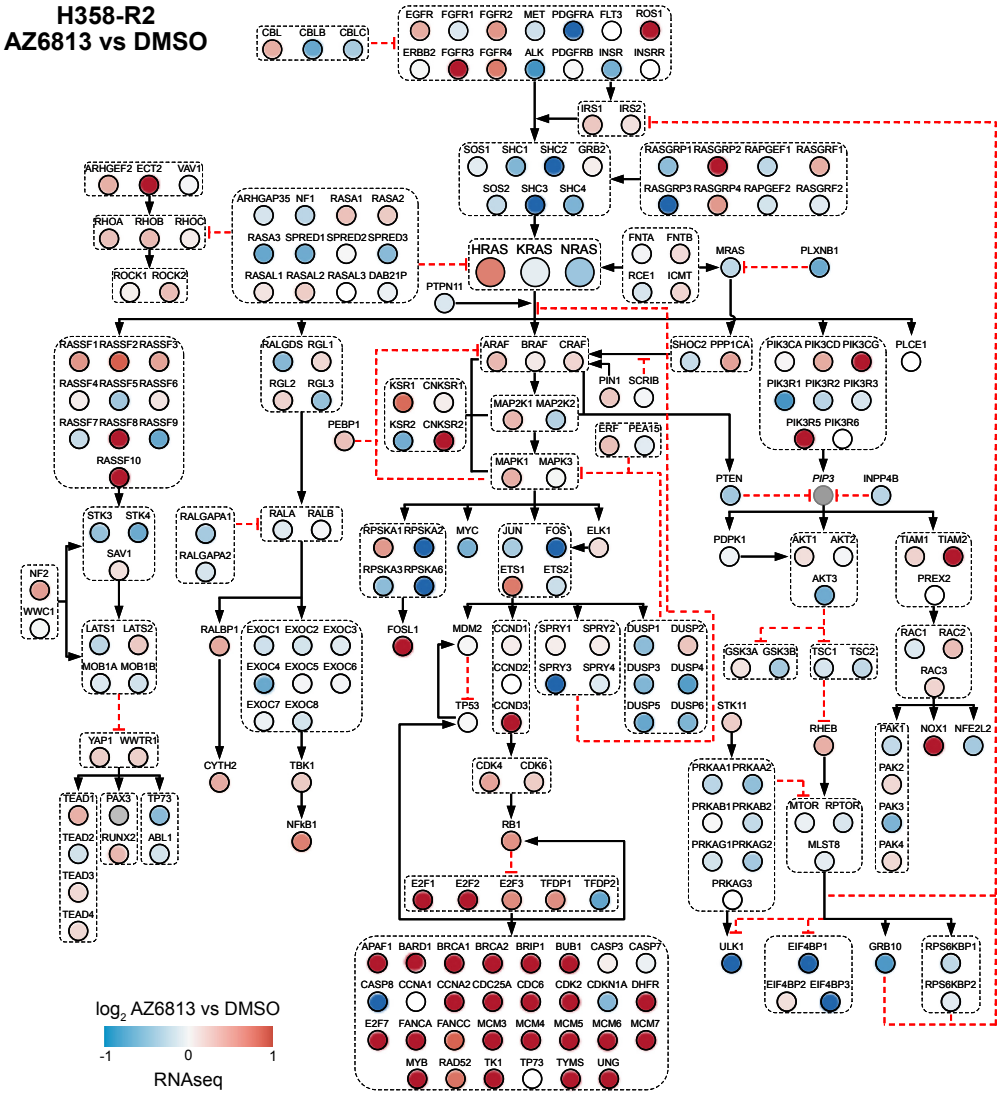

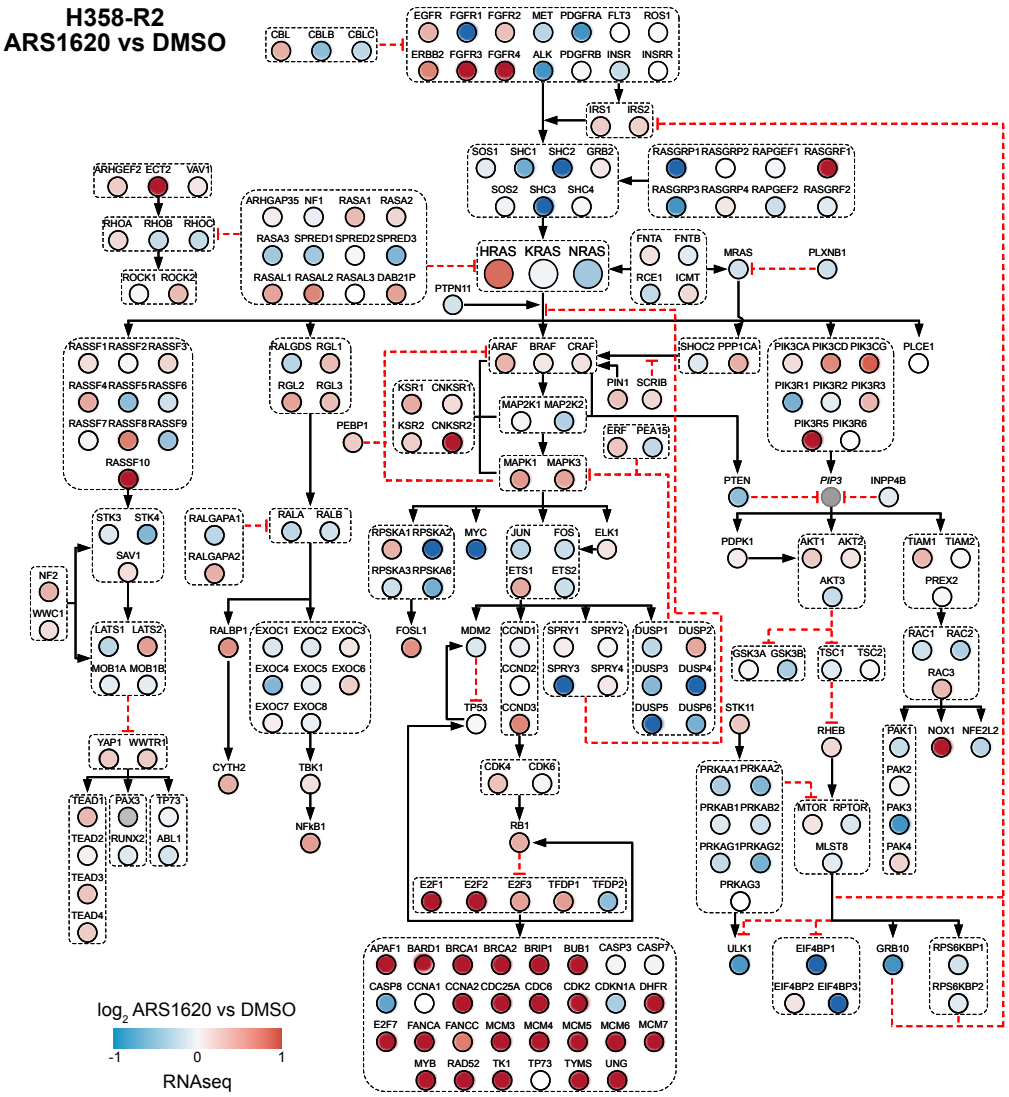
H358-R2
ARS1620 vs DMSO
CBL CBLB CBLC
EGFR FGFR1 FGFR2 MET PDGFRA FLT3 ROS1
ERBB2 FGFR3 FGFR4 ALK PDGFRB INSR INSRR
IRS1 IRS2
SOS1 SHC1 SHC2 GRB2
SOS2 SHC3 SHC4
RASGRP1 RASGRP2 RAPGEF1 RASGRF1
RASGRP3 RASGRP4 RAPGEF2 RASGRF2
ARHGEF2 ECT2 VAV1
RHOA RHOB RHOC
ROCK1 ROCK2
ARHGAP35 NF1 RASA1 RASA2
RASA3 SPRED1 SPRED2 SPRED3
RASAL1 RASAL2 RASAL3 DAB21P
HRAS KRAS NRAS
FNTA FNTB
RCE1 ICMT
MRAS
PLXNB1
PTPN11
RASSF1 RASSF2 RASSF3
RASSF4 RASSF5 RASSF6
RASSF7 RASSF8 RASSF9
RASSF10
RALGDS RGL1
RGL2 RGL3
PEBP1
ARAF BRAF CRAF
KSR1 CNKSR1
KSR2 CNKSR2
MAP2K1 MAP2K2
MAPK1 MAPK3
PIN1 SCRIB
ERF PEA15
SHOC2 PPP1CA
PIK3CA PIK3CD PIK3CG
PIK3R1 PIK3R2 PIK3R3
PIK3R5 PIK3R6
PLCE1
PTEN
PIP3
INPP4B
PDPK1
AKT1 AKT2
AKT3
TIAM1 TIAM2
PREX2
STK3 STK4
SAV1
NF2
WWC1
LATS1 LATS2
MOB1A MOB1B
YAP1 WWTR1
TEAD1
TEAD2
TEAD3
TEAD4
PAX3
RUNX2
TP73
ABL1
RALGAPA1
RALGAPA2
RALA RALB
RALBP1
CYTH2
EXOC1 EXOC2 EXOC3
EXOC4 EXOC5 EXOC6
EXOC7 EXOC8
TBK1
NFkB1
RPSKA1 RPSKA2
RPSKA3 RPSKA6
MYC
JUN FOS ELK1
ETS1 ETS2
FOSL1
MDM2
TP53
CCND1
CCND2
CCND3
SPRY1 SPRY2
SPRY3 SPRY4
DUSP1 DUSP2
DUSP3 DUSP4
DUSP5 DUSP6
CDK4 CDK6
RB1
E2F1 E2F2 E2F3 TFDP1 TFDP2
APAF1 BARD1 BRCA1 BRCA2 BRIP1 BUB1 CASP3 CASP7
CASP8 CCNA1 CCNA2 CDC25A CDC6 CDK2 CDKN1A DHFR
E2F7 FANCA FANCC MCM3 MCM4 MCM5 MCM6 MCM7
MYB RAD52 TK1 TP73 TYMS UNG
GSK3A GSK3B
TSC1 TSC2
RHEB
STK11
PRKAA1 PRKAA2
PRKAB1 PRKAB2
PRKAG1 PRKAG2
PRKAG3
MTOR RPTOR
MLST8
ULK1
RAC1 RAC2
RAC3
PAK1
PAK2
PAK3
PAK4
NOX1 NFE2L2
EIF4BP1
EIF4BP2 EIF4BP3
GRB10
RPS6KBP1
RPS6KBP2
log2 ARS1620 vs DMSO
-1 0 1
RNAseq

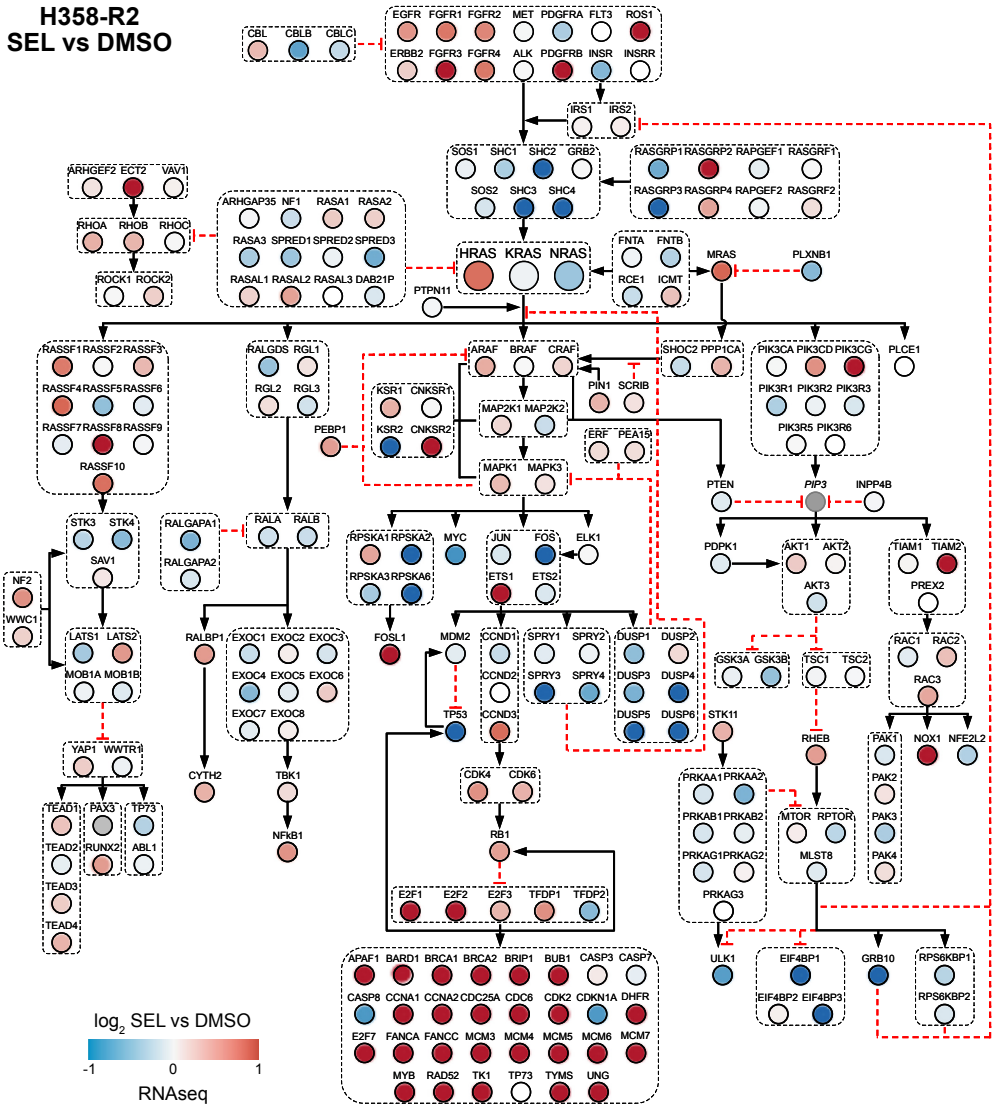
H358-R2
SEL vs DMSO
CBL CBLB CBLC
EGFR FGFR1 FGFR2 MET PDGFRA FLT3 ROS1
ERBB2 FGFR3 FGFR4 ALK PDGFRB INSR INSRR
IRS1 IRS2
SOS1 SHC1 SHC2 GRB2
SOS2 SHC3 SHC4
RASGRP1 RASGRP2 RAPGEF1 RASGRF1
RASGRP3 RASGRP4 RAPGEF2 RASGRF2
ARHGEF2 ECT2 VAV1
RHOA RHOB RHOC
ROCK1 ROCK2
ARHGAP35 NF1 RASA1 RASA2
RASA3 SPRED1 SPRED2 SPRED3
RASAL1 RASAL2 RASAL3 DAB21P
HRAS KRAS NRAS
FNTA FNTB
RCE1 ICMT
MRAS
PLXNB1
PTPN11
RASSF1 RASSF2 RASSF3
RASSF4 RASSF5 RASSF6
RASSF7 RASSF8 RASSF9
RASSF10
RALGDS RGL1
RGL2 RGL3
ARAF BRAF CRAF
SHOC2 PPP1CA
PIN1 SCRIB
PIK3CA PIK3CD PIK3CG PLCE1
PIK3R1 PIK3R2 PIK3R3
PIK3R5 PIK3R6
KSR1 CNKSR1
KSR2 CNKSR2
PEBP1
MAP2K1 MAP2K2
ERF PEA15
MAPK1 MAPK3
PTEN
PIP3
INPP4B
PDPK1
AKT1 AKT2
AKT3
TIAM1 TIAM2
PREX2
STK3 STK4
SAV1
NF2
WWC1
LATS1 LATS2
MOB1A MOB1B
RALGAPA1
RALGAPA2
RALA RALB
RPSKA1 RPSKA2
RPSKA3 RPSKA6
MYC
JUN FOS
ETS1 ETS2
ELK1
RALBP1
EXOC1 EXOC2 EXOC3
EXOC4 EXOC5 EXOC6
EXOC7 EXOC8
FOSL1
MDM2
TP53
CCND1
CCND2 CCND3
SPRY1 SPRY2
SPRY3 SPRY4
DUSP1 DUSP2
DUSP3 DUSP4
DUSP5 DUSP6
GSK3A GSK3B
TSC1 TSC2
RAC1 RAC2
RAC3
PAK1 PAK2 PAK3 PAK4
NOX1 NFE2L2
STK11
RHEB
MTOR RPTOR
MLST8
YAP1 WWTR1
TEAD1 TEAD2 TEAD3 TEAD4
PAX3 RUNX2
TP73 ABL1
CYTH2
TBK1
NFkB1
CDK4 CDK6
RB1
E2F1 E2F2 E2F3 TFDP1 TFDP2
PRKAA1 PRKAA2
PRKAB1 PRKAB2
PRKAG1 PRKAG2
PRKAG3
ULK1
EIF4BP1
EIF4BP2 EIF4BP3
GRB10
RPS6KBP1
RPS6KBP2
APAF1 BARD1 BRCA1 BRCA2 BRIP1 BUB1 CASP3 CASP7
CASP8 CCNA1 CCNA2 CDC25A CDC6 CDK2 CDKN1A DHFR
E2F7 FANCA FANCC MCM3 MCM4 MCM5 MCM6 MCM7
MYB RAD52 TK1 TP73 TYMS UNG
log2 SEL vs DMSO
-1 0 1
RNAseq

Appendix 4: Immunofluorescence of acutely treated H358 cells (H358-A)

H358 cells were seeded onto coverslips and treated with vehicle or inhibitor for a total period of 8 days. Cells were re-dosed every 48hrs. Cells were stained with E-cadherin (red) or N-cadherin (green) primary antibodies and immunofluorescence was imaged using the 40X lens on a Nickon Ti-E microscope. Scale bar represents 20uM.

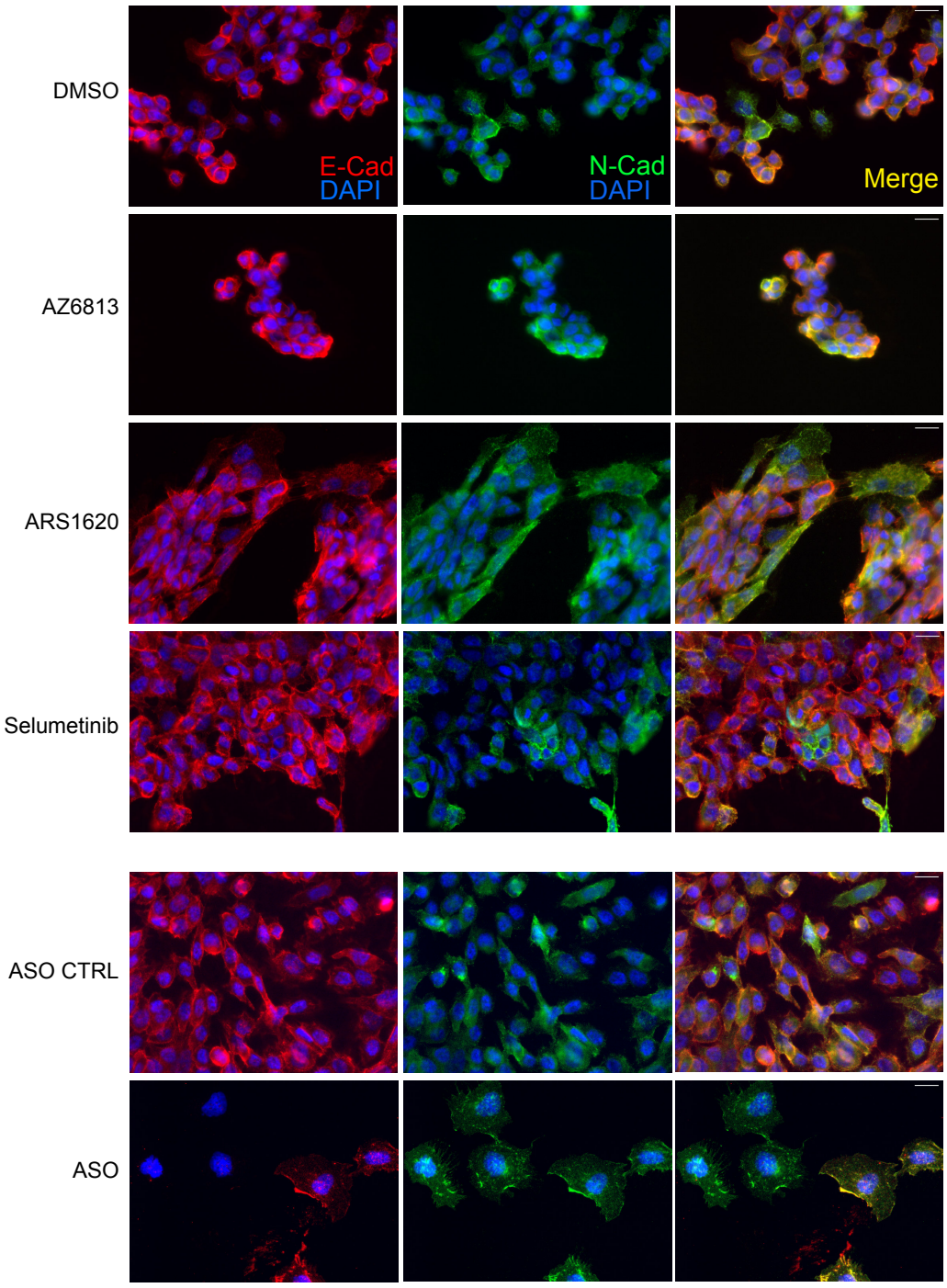

Appendix 5: Immunofluorescence of resistant H358 cells (H358-R)

H358-R cells were seeded onto coverslips and treated with corresponding vehicle or inhibitor until cells were confluent. Cells were re-dosed with fresh media containing inhibitor every 48hrs. Cells were stained with E-cadherin (red) or N-cadherin (green) primary antibodies and immunofluorescence was imaged using the 40X lens on a Nickon Ti-E microscope. Scale bar represents 20uM.

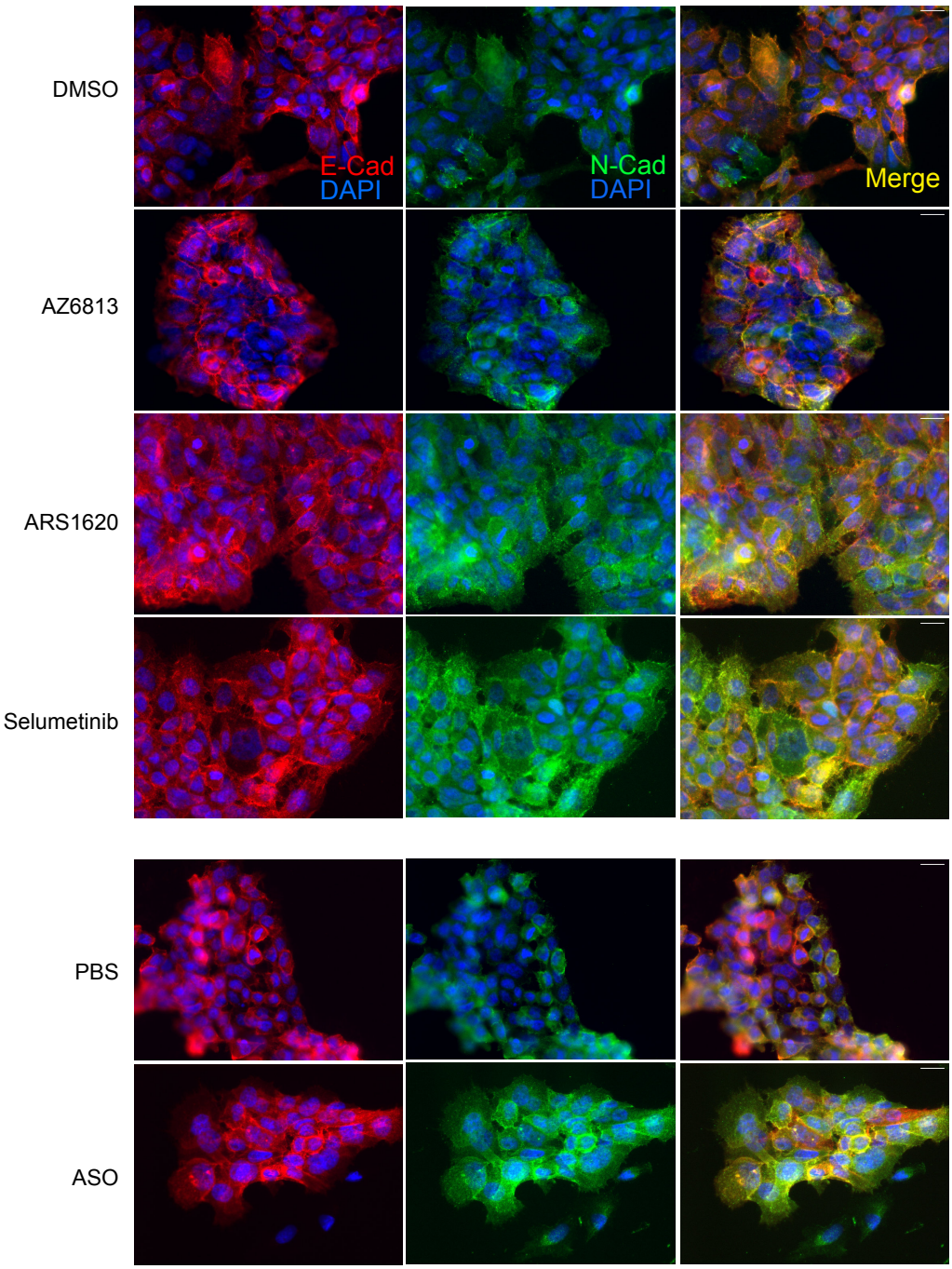

Appendix 6: Dose responses of combination therapeutics in resistant cells (cytotoxicity) Resistant H358 cell lines treated with ARS1620 (R-ARS), selumetinib (R-Sel) and AZD4785 (R-ASO), alongside naïve parental H358 cells treated with DMSO (R-DMSO) were treated with their previous IC90 inhibitor treatments (ARS1620, Selumetinib, AZD4785 and DMSO respectively) in combination with dose responses of additional targeted inhibitors (see table 5.1). The change in IncuCyte Cytotox Green fluorescence was recorded following 4 days of inhibitor treatment. Graphs are presented as mean percentages of vehicle controls ±SEM from triplicates of one-three independent experiments. Figure continued on next page.

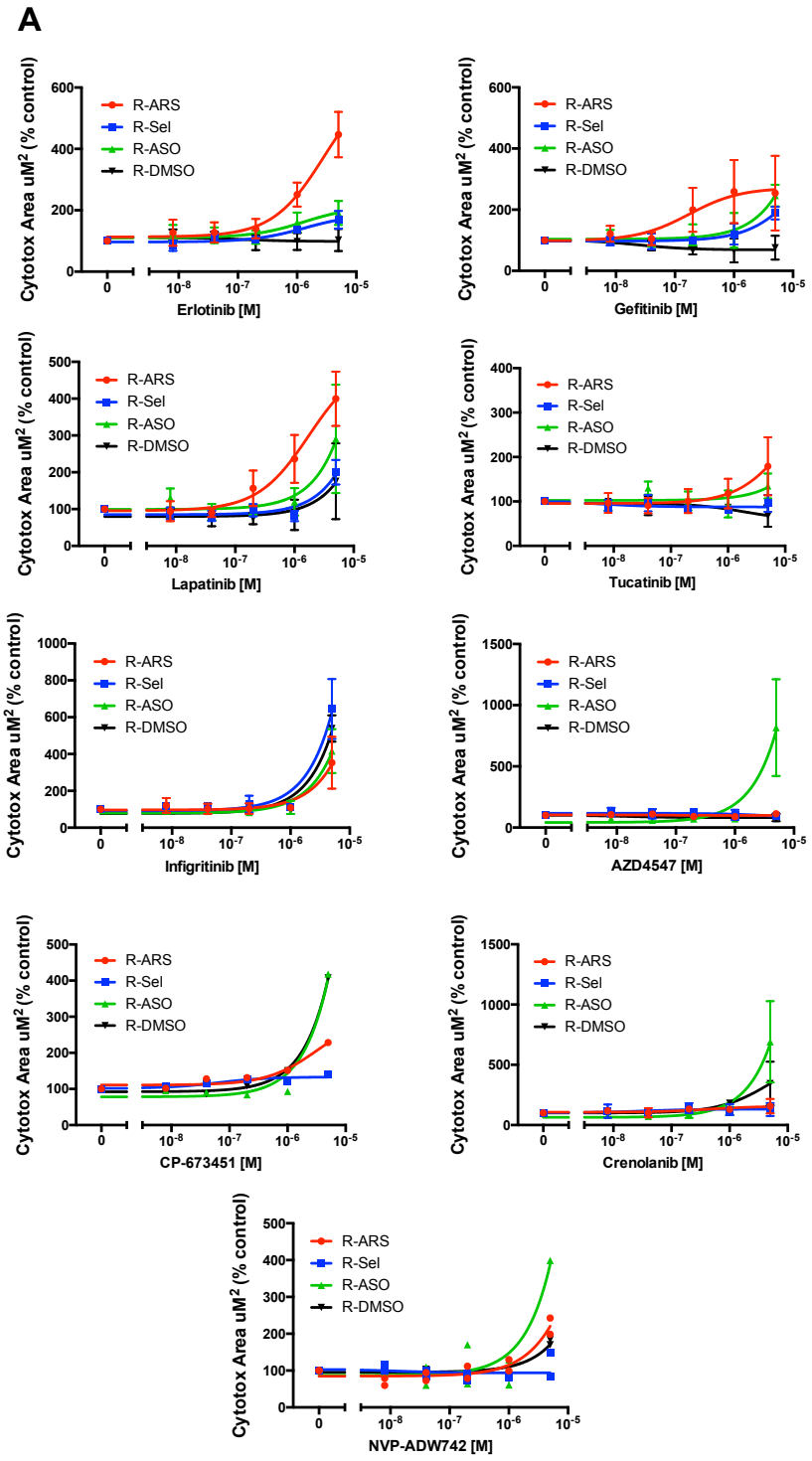

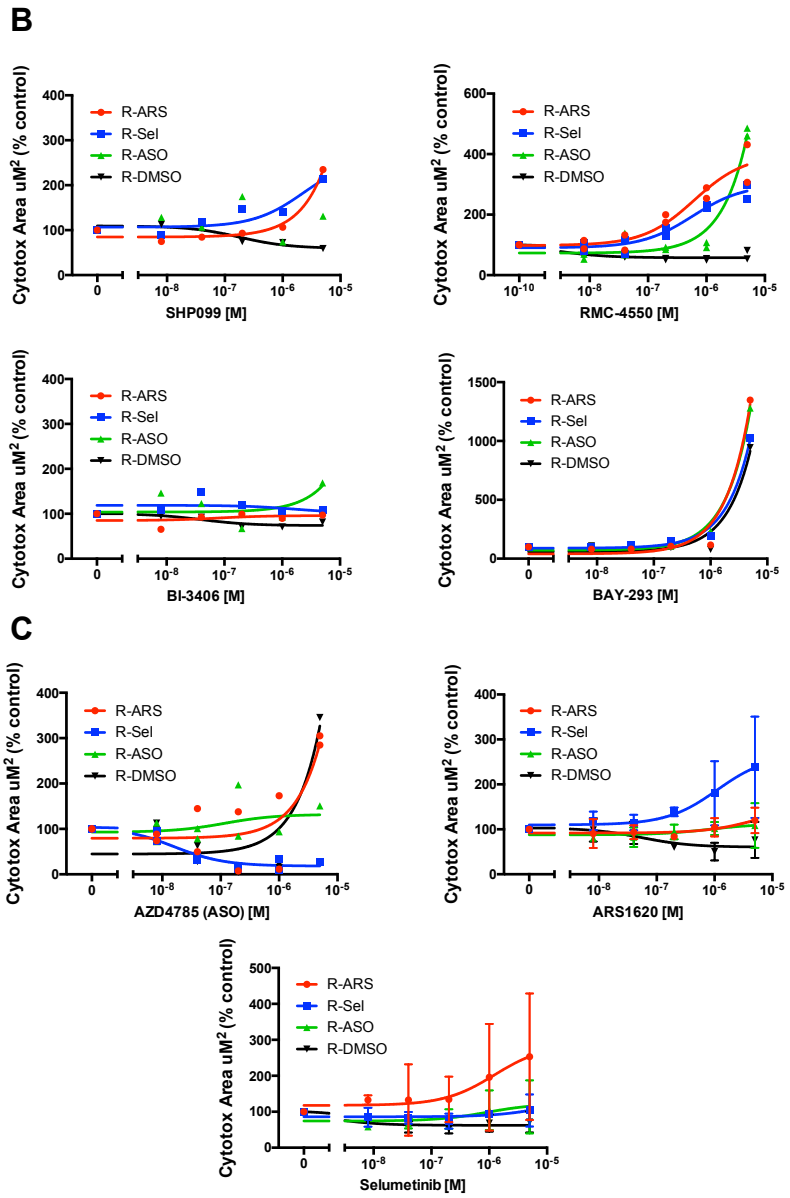
B
Cytotox Area uM2 (% control)
R-ARS
R-Sel
R-ASO
R-DMSO
SHP099 [M]
RMC-4550 [M]
BI-3406 [M]
BAY-293 [M]
C
AZD4785 (ASO) [M]
ARS1620 [M]
Selumetinib [M]

D

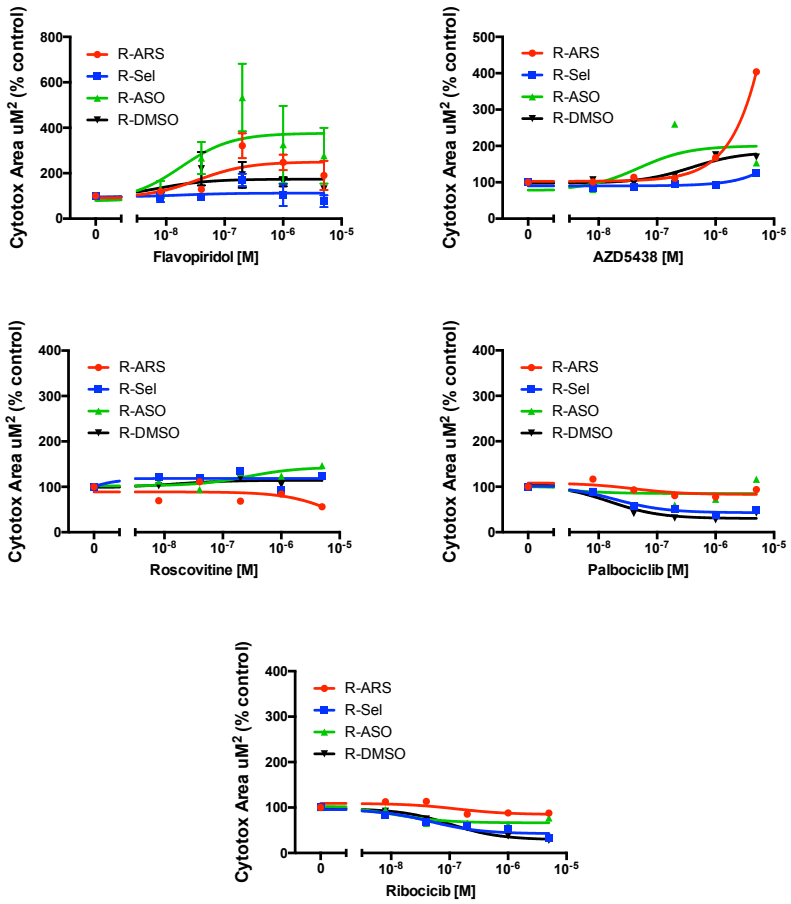
Cytotox Area uM2 (% control)
R-ARS
R-Sel
R-ASO
R-DMSO
Flavopiridol [M]
AZD5438 [M]
Roscovitine [M]
Palbociclib [M]
Ribocicib [M]

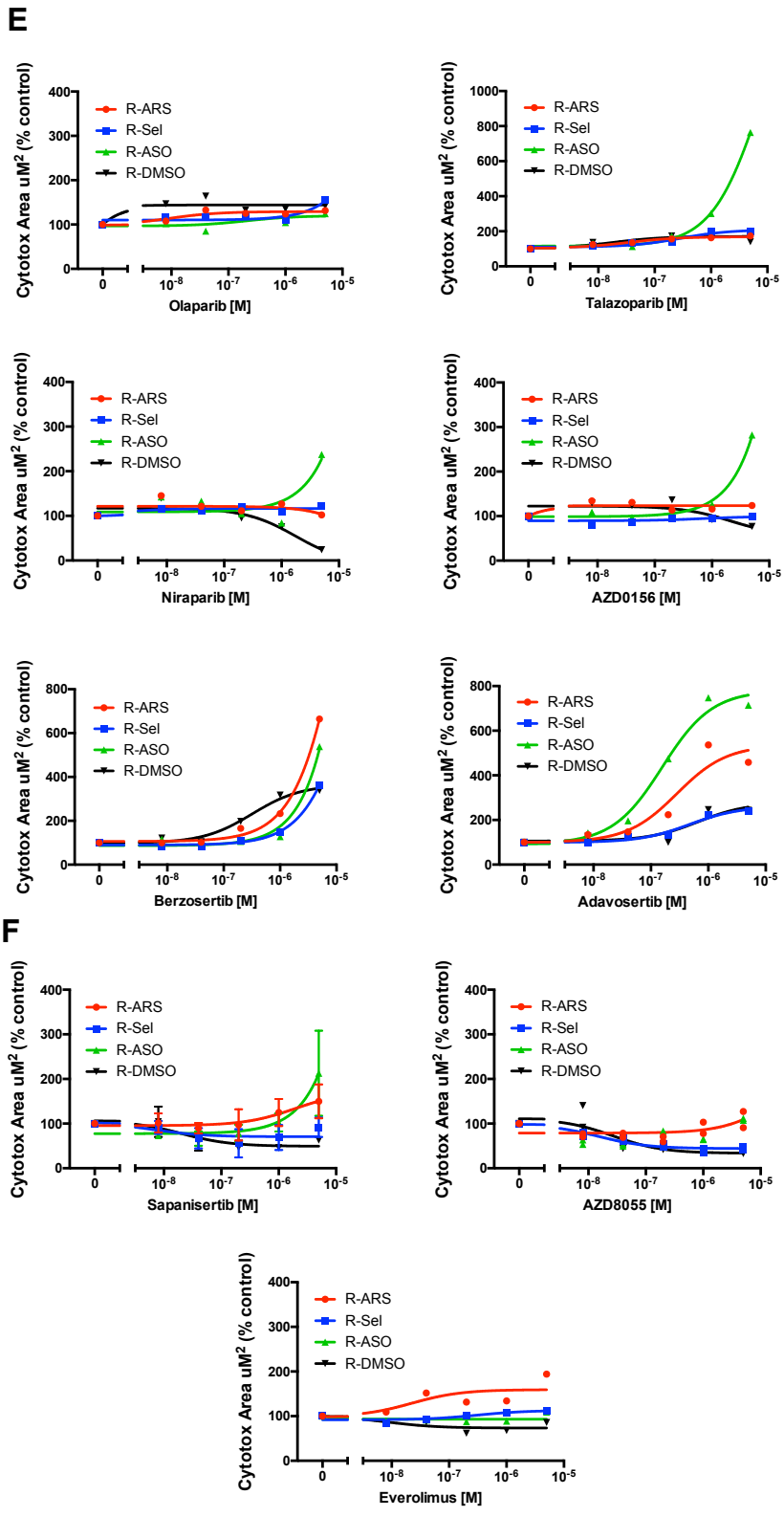
E
Cytotox Area uM2 (% control)
R-ARS
R-Sel
R-ASO
R-DMSO
Olaparib [M]
Talazoparib [M]
Niraparib [M]
AZD0156 [M]
Berzosertib [M]
Adavosertib [M]
F
Sapanisertib [M]
AZD8055 [M]
Everolimus [M]

Appendix 7: Dose responses of combination therapeutics in resistant cells (proliferation) Resistant H358 cell lines treated with ARS1620 (R-ARS), selumetinib (R-Sel) and AZD4785 (R-ASO), alongside naïve parental H358 cells treated with DMSO (R-DMSO) were treated with their previous IC90 inhibitor treatments (ARS1620, Selumetinib, AZD4785 and DMSO respectively) in combination with dose responses of additional targeted inhibitors (see table 5.1). The change in IncuCyte Nuclight Rapid Red staining was recorded following 4 days of inhibitor treatment. Graphs are presented as mean percentages of vehicle controls ±SEM from triplicates of one-three independent experiments. Figure continued on next page.

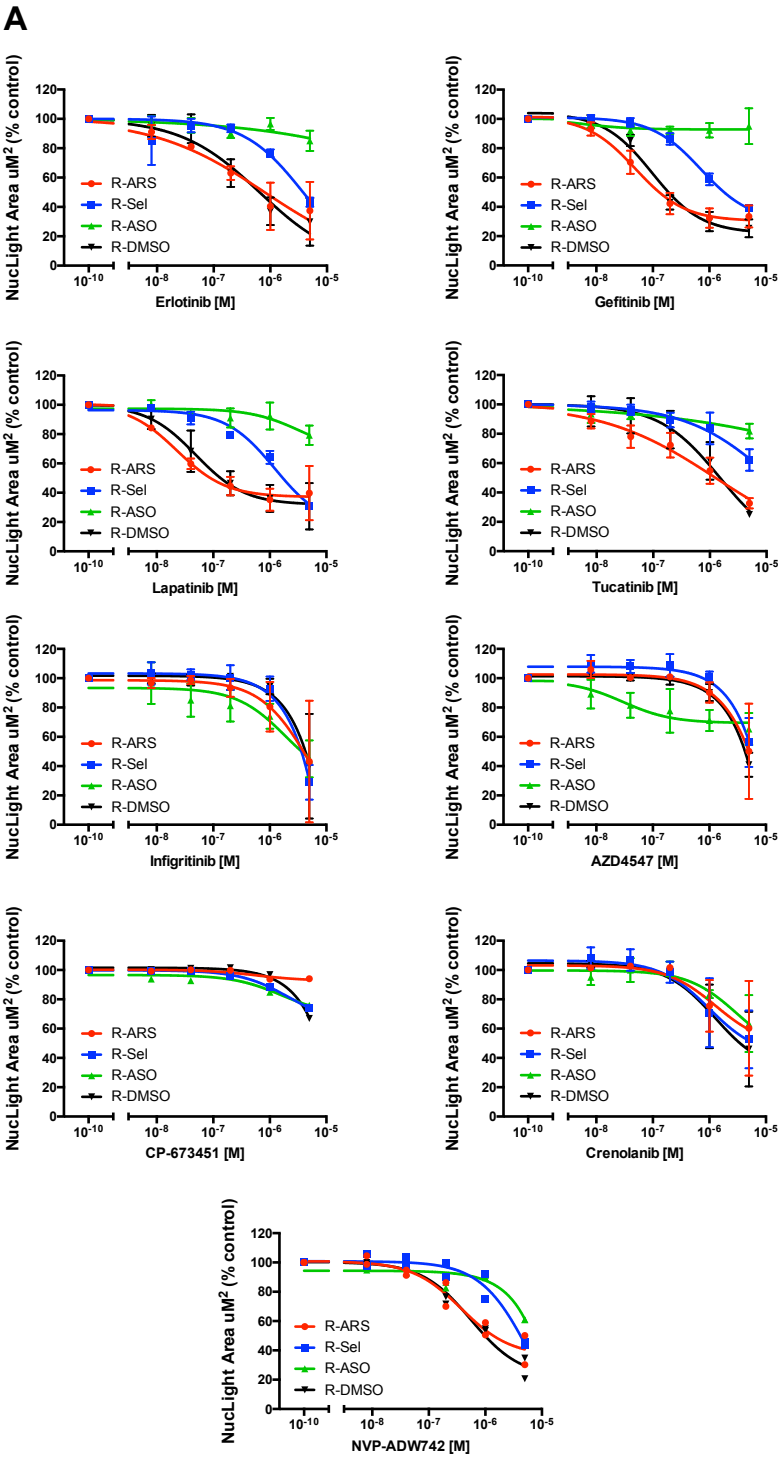

B

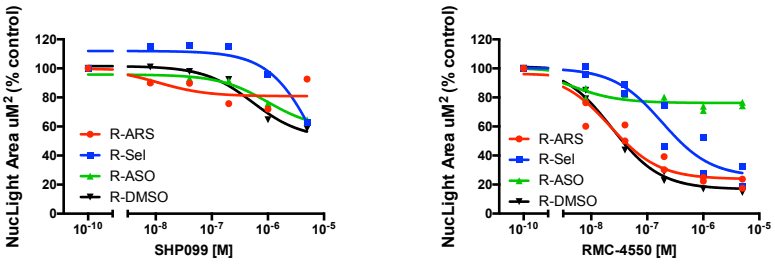
NucLight Area uM2 (% control)
R-ARS
R-Sel
R-ASO
R-DMSO
SHP099 [M]
RMC-4550 [M]

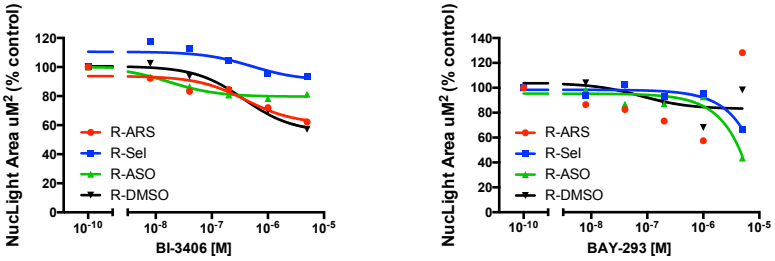
NucLight Area uM2 (% control)
R-ARS
R-Sel
R-ASO
R-DMSO
BI-3406 [M]
BAY-293 [M]

C

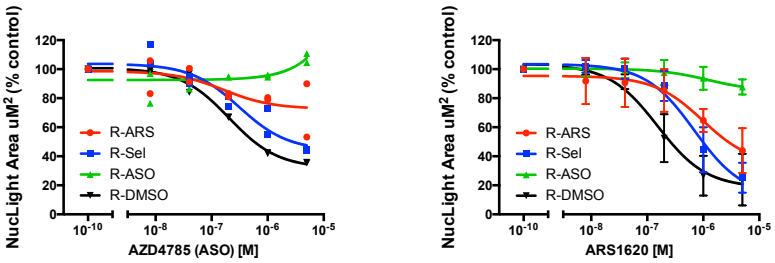
NucLight Area uM2 (% control)
R-ARS
R-Sel
R-ASO
R-DMSO
AZD4785 (ASO) [M]
ARS1620 [M]

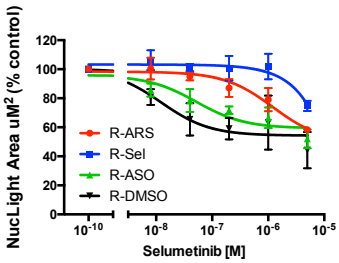
NucLight Area uM2 (% control)
R-ARS
R-Sel
R-ASO
R-DMSO
Selumetinib [M]

D

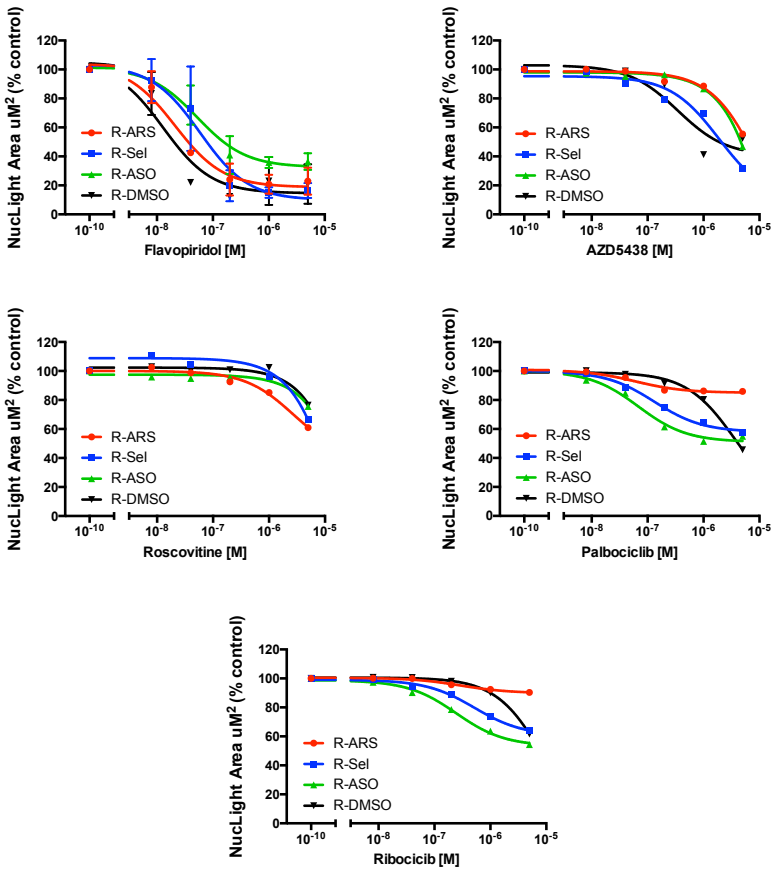
NucLight Area uM2 (% control)
R-ARS
R-Sel
R-ASO
R-DMSO
Flavopiridol [M]
AZD5438 [M]
Roscovitine [M]
Palbociclib [M]
Ribocicib [M]

E

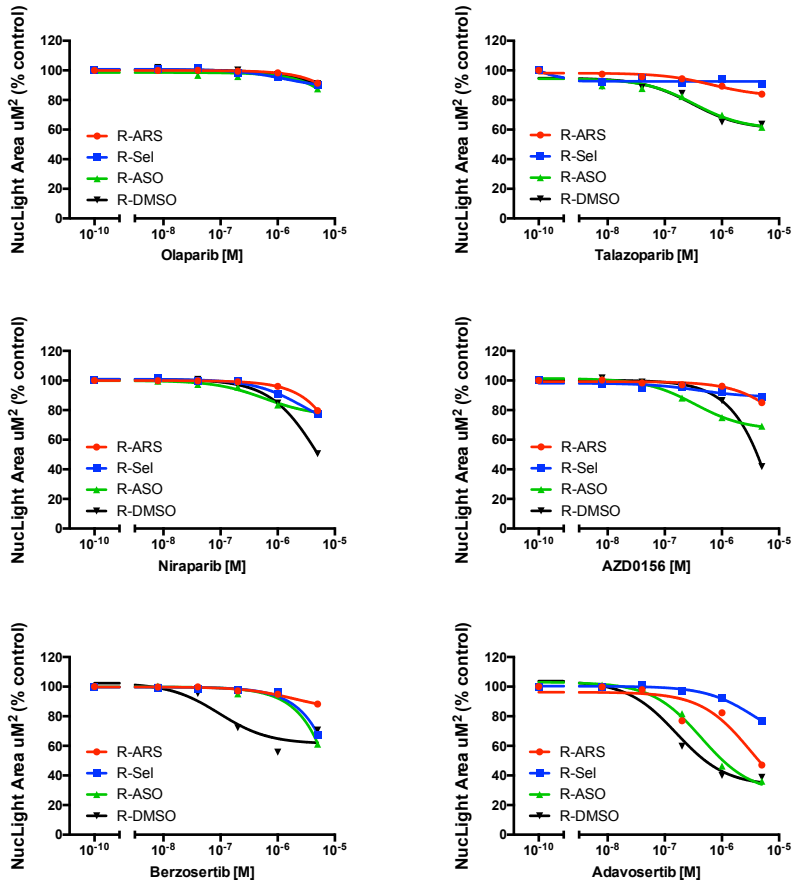
NucLight Area uM2 (% control)
R-ARS
R-Sel
R-ASO
R-DMSO
Olaparib [M]
Talazoparib [M]
Niraparib [M]
AZD0156 [M]
Berzosertib [M]
Adavosertib [M]

F

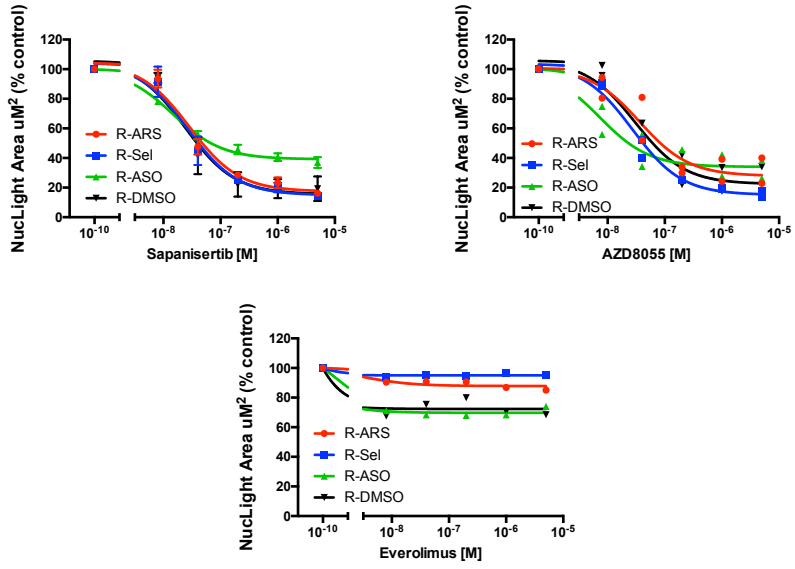
NucLight Area uM2 (% control)
R-ARS
R-Sel
R-ASO
R-DMSO
Sapanisertib [M]
AZD8055 [M]
Everolimus [M]

Appendix 8: Synergy matrixes of triple combination therapeutics in resistant cells

Synergy scores from double inhibitor combination assays were calculated using the Loewe model in Combenefit [392]. Areas coloured blue indicate drug combinations that are synergistic. Figure continued on next page.

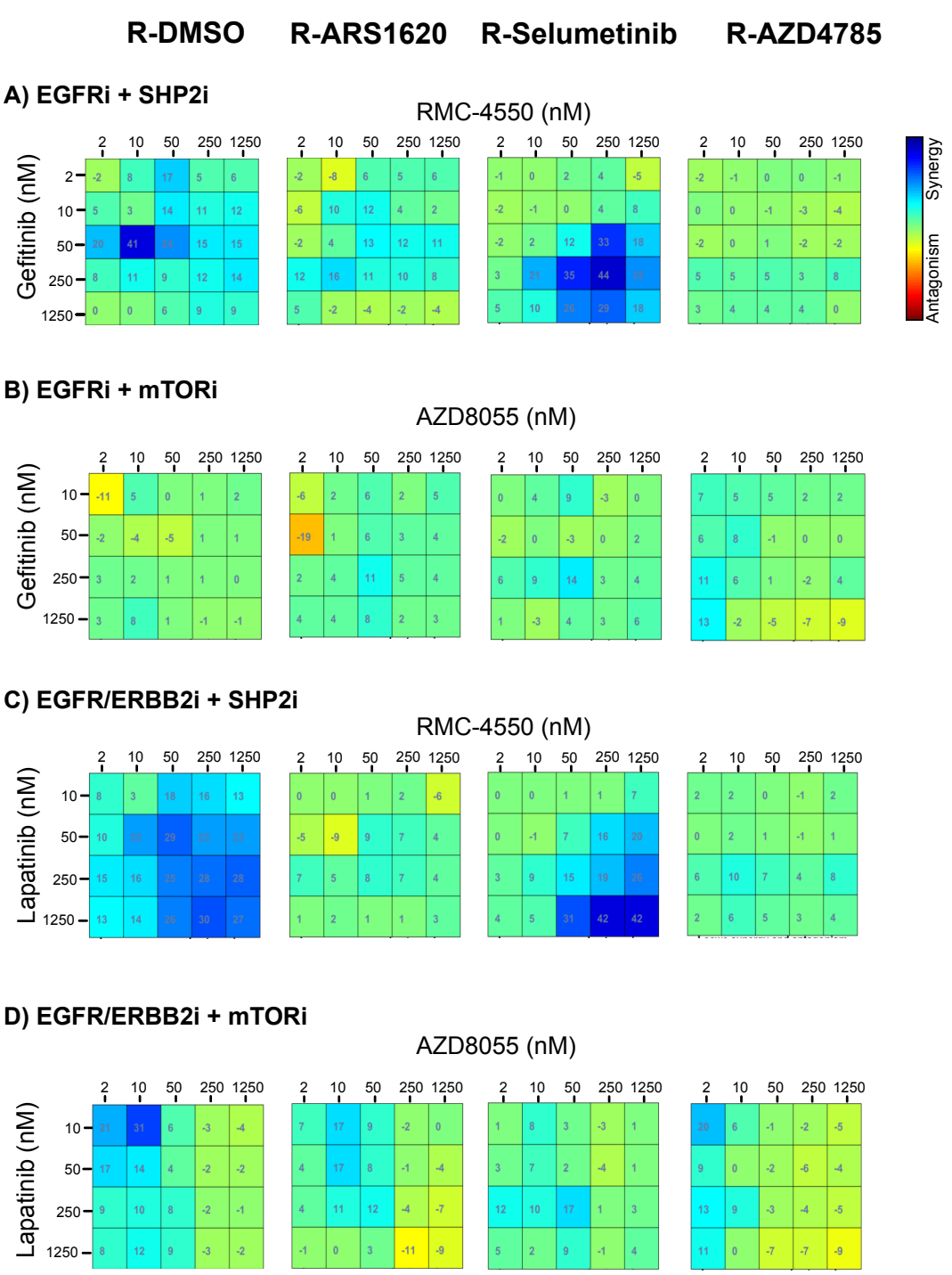

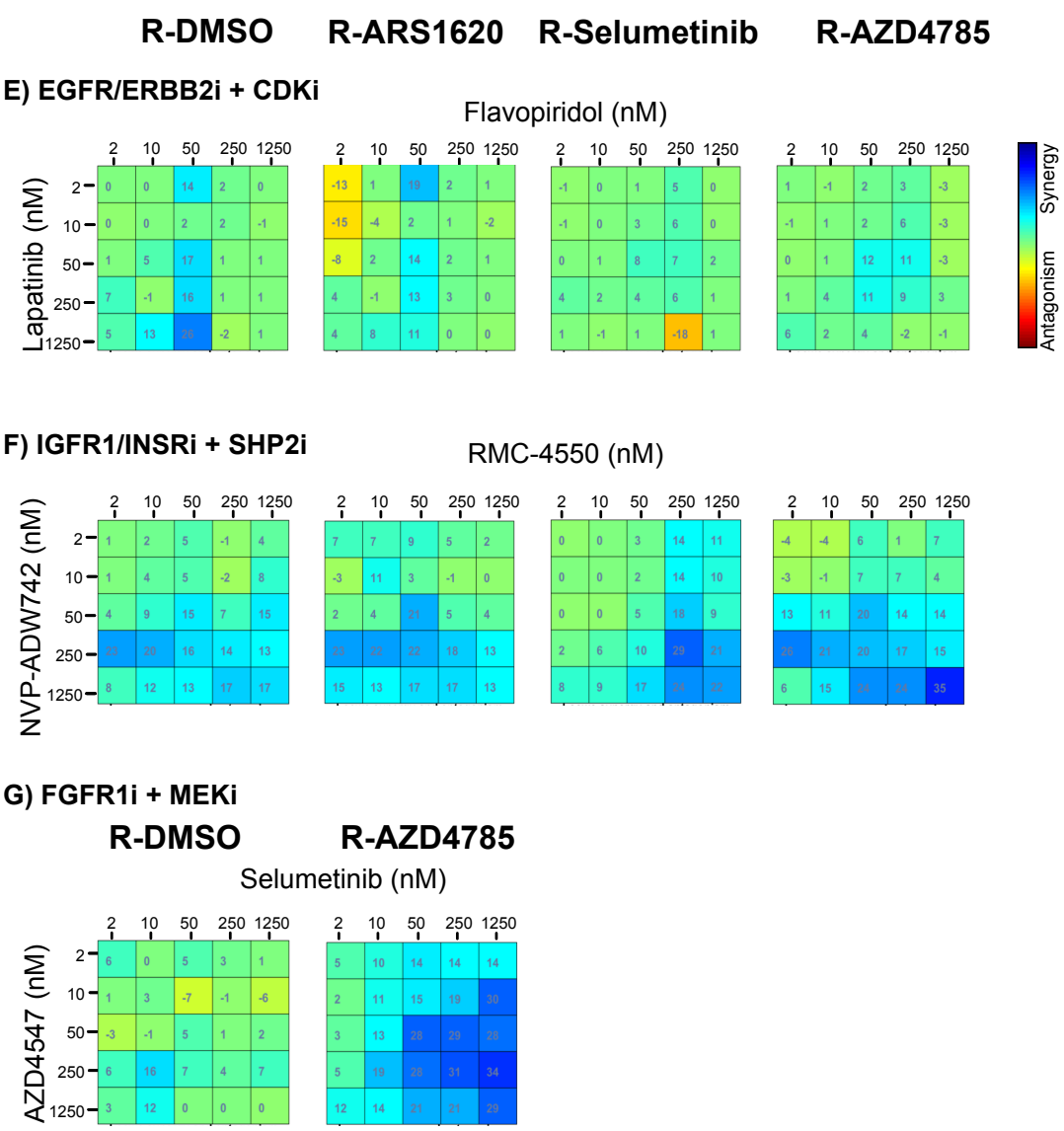
R-DMSO
R-ARS1620
R-Selumetinib
R-AZD4785
E) EGFR/ERBB2i + CDKi
Flavopiridol (nM)
Lapatinib (nM)
2 10 50 250 1250
Synergy
Antagonism
F) IGFR1/INSRi + SHP2i
RMC-4550 (nM)
NVP-ADW742 (nM)
G) FGFR1i + MEKi
R-DMSO
R-AZD4785
Selumetinib (nM)
AZD4547 (nM)